CERN 64-6

Nuclear Physics Division
31st January, 1964.

ORGANISATION EUROPÉENNE POUR LA RECHERCHE NUCLÉAIRE
CERN EUROPEAN ORGANIZATION FOR NUCLEAR RESEARCH

1963 EASTER SCHOOL FOR PHYSICISTS

Using the Nuclear Emulsion Technique in Conjunction with the CERN Proton Synchrotron and Synchro-Cyclotron

held at St. Cergue, March 20-27, 1963

PROCEEDINGS
edited by

D. Evans
W.O. Lock

G E N E V A
1964

SCIENTIFIC ORGANIZING COMMITTEE:

From CERN:	Dr. J.C. Combe Dr. D. Evans Dr. L. Hoffmann Dr. G. Vanderhaeghe
From Outside Groups:	Prof. C. O'Ceallaigh (Dublin) Prof. G. Ekspong (Stockholm) Dr. M. Gailloud (Lausanne) Dr. A. Manfredini (Rome)
Organizing Secretary:	Miss E.W.D. Steel (CERN)

* * *

5666/NP/smg

CONTENTS

5666/NP/smg

PREFACE

The 1963 Easter School for emulsion physicists devoted its main attention to physics rather than to matters of technique, which were discussed in detail at the 1962 School.

These Proceedings contain all except two of the lectures that were given. The talks on Hyperfragment Physics were also given at the Hyperfragment Conference and appear in the Proceedings of that conference (Report 64 - 1) as well as here; since the same stencils were used, the text which is printed here does not carry page numbers. We trust that this will not be a serious inconvenience to the reader.

We are grateful to the speakers who kindly provided us with the manuscripts of their talks. Almost all of the students (who are listed in the Appendix) acted as Scientific Secretaries for one or more sessions which has enabled us to report the substance of the discussions following each talk. We thank them for their hard work.

We must also thank the following people who contributed to the success of the School and to the production of these Proceedings: Mr. E. Bissa, Mr. M.A. Roberts, Mr. P. de Vautibault and Mr. P. Vannier for the technical arrangements at St. Cergue; Mr. A. Bondi and the Scientific Information Service for the diagrams; our colleagues in the Emulsion Group for assistance with the proof reading; Miss S. Merrens for transcribing some of the talks from the tape recordings; Miss A. Sanders for translating the paper of Prof. G.B. Zhdanov from the original Russian text; and Miss S. Greenstreet and Mrs. K. Wakley for the patient typing of the many stencils.

D. Evans
W.O. Lock

Geneva, January, 1964.

5666/NP/smg

I. ELASTIC SCATTERING

PART I.1

HIGH-ENERGY SCATTERING AND REGGE POLES*)

R. Hagedorn,
Theory Division, CERN.

I. INTRODUCTION

In the last year a rather unexpected phenomenon was found in elastic pp scattering at high energies ($\gtrsim 5$ GeV): the diffraction peak shrinks logarithmically with the c.m. energy squared. To be definite: the angular opening of the diffraction peak - namely the width of $d\sigma/d\Omega$ - naturally becomes smaller when the incident energy increases. What happens, is that $d\sigma/dt$ (t = squared momentum transfer) becomes narrower. The uncertainty relation shows roughly what that means:

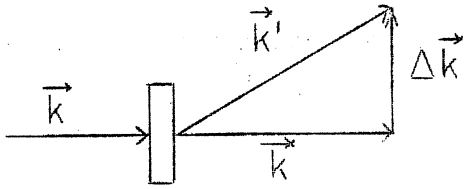

Fig 1

If a particle is scattered on an obstacle of diameter 2R, then, roughly speaking, either it is not scattered at all or it has been inside the scattering region of diameter 2R. This being equivalent to a position measurement, we expect an uncertainty in momentum

$$|\Delta k| \sim \frac{1}{2R}$$

*) Part of this lecture has been given already at the II Internationale Universitätswoche für Kernphysik, February 1963, Schladming (Austria), organized by the Institute of Theoretical Physics, University of Graz, Austria, the proceedings of which will be published in Acta Physica Austriaca, Vol. XVII/1-2 (Springer-Verlag, Vienna).

perpendicular to $\vec{k}$. Thus the width of the diffraction pattern should be given by

$$\gtrsim \frac{1}{2R}$$

independently of the primary momentum. In this talk the experimental fact, that for pp scattering this is not so, will be analysed in terms of Regge poles.

II. KINEMATICS

We consider the process $p + k \to p' + k'$ where all particles are assumed to have equal masses m. We neglect spin and isospin. Notation:

$$p = (p_o, \vec{p}); \quad p^2 = p_o^2 - \vec{p}^2 = m^2; \quad \hbar = c = 1.$$

We describe the general process (Fig. 2) in the centre-of-momentum system ($\vec{p} + \vec{k} = 0$) [Fig. 3].

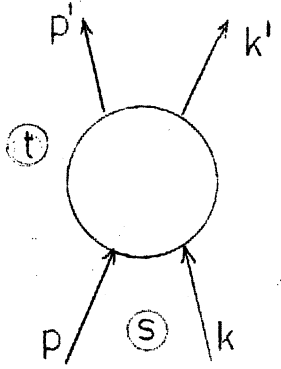

Fig. 2

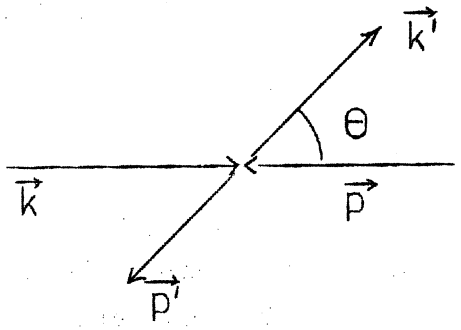

Fig. 3

If the S-matrix is defined

$$\langle f|S|i\rangle = \langle f|i\rangle + \frac{i}{(2\pi)^2} \frac{\delta^4(p+k-p'-k')}{\sqrt{16 p_o k_o p_o' k_o'}} A(pkp'k'); \qquad (1)$$

then $A(p'k'pk)$ is an invariant function of the four four-vectors. Applied to our case it follows from four-momentum conservation

$$p + k - p' - k' = 0 \qquad (2)$$

that

$$p_o = p_o' = k_o = k_o' = \frac{1}{2} E_{cm} \tag{3}$$

and that the momenta

$$|\vec{p}| = |\vec{k}| = |\vec{p}'| = |\vec{k}'| = K. \tag{4}$$

The scattering amplitude $A(p'k'pk)$, being a relativistic invariant, can depend only on the invariants one can construct with $p'k'pk$. There are altogether ten such invariants (and functions thereof):

$$\begin{gathered} p'^2;\ k'^2;\ p^2;\ k^2 \\ p'k';\ p'p;\ p'k;\ k'p;\ k'k;\ pK. \end{gathered} \tag{5}$$

Now, the first four are all equal m^2 and hence constant and uninteresting. Remaining are the six in the second line. They cannot be independent, since four-momentum conservation (2) yields four equations. This reduces the six to two. One has to be careful to select two which really are independent of each other (e.g. <u>not</u> pk' and kp' because, on account of (2), they are equal).

We select two independent invariants

$$\begin{aligned} s &= (p+k)^2 = (p'+k')^2 \\ t &= (k-k')^2 = (p-p')^2 . \end{aligned} \tag{6}$$

In the c.m.s. we have

$$\begin{aligned} p &= (\tfrac{1}{2}E,\ \vec{p}) \\ k &= (\tfrac{1}{2}E,\ -\vec{p}) \\ p' &= (\tfrac{1}{2}E,\ \vec{p}'), \end{aligned}$$

hence

$$\begin{aligned} s &= (E,\ \vec{0})^2 = E^2 = 4(K^2 + m^2) \\ t &= (0,\ \vec{p} - \vec{p}')^2 = -2K^2 + 2K^2 \cos\Theta = -2K^2\ (1 - \cos\Theta_s). \end{aligned} \tag{7}$$

We have then

$$A(p'k'pk) = A(st) . \tag{8}$$

If one calculates the differential elastic cross-section in the c.m.s. using Eqs. (1) and (8) one finds

$$\frac{d\sigma}{d\Omega} = \frac{K^2}{\pi} \frac{d\sigma}{dt} = |f(E,\Theta)|^2$$

$$f(E,\Theta) = \frac{1}{8\pi\sqrt{s}} A(st) . \tag{9}$$

Here $f(E,\Theta)$ is the usual scattering amplitude in the asymptotic expression

$$\psi^{(+)} \sim e^{ikz} + \frac{e^{ikr}}{r} f(E,\Theta) . \tag{10}$$

III. CROSSING SYMMETRY, ANALYTICITY

It can be shown by discussing the scattering amplitude in a more explicit form, that it has, besides the relativistic invariance, two more important properties:

A(st) is an analytic function of the complex variables s and t. That means: A(st) can be continued from the real, physical values of s and t into the complex s- and t-space. The physical values are then the boundary values of this function. We do not know what the singularities of A(st) are - remember: an analytic function can by means of Cauchy's integral be represented by its singularities (up to an entire function). Suggestions like those of Mandelstam have not been proved and are, in spite of their practical value, very probably not true.

$A(s,t)$ is crossing symmetric. That means: if we invert the momenta p' and k, then they become momenta of anti-particles and p' goes in, whereas k goes out. This new process, nucleon-antinucleon elastic scattering, is described by the same analytic function $A(st)$, only s and t have now a different physical interpretation and other values.

Since crossing symmetry is crucial to our problem, I wish to make this more clear.

Let us introduce a third relativistic invariant

$$u = (k - p')^2 , \tag{11}$$

which is not independent of s and t. Indeed:

$$s + t + u = \underbrace{p^2 + k^2 + k^2 + k'^2 + k^2 + p'^2}_{6m^2} + \underbrace{2k(\underbrace{p - k' - p'}_{-k})}_{-2m^2} = 4m^2$$

hence

$$s + t + u = 4m^2 . \tag{12}$$

We remember from elementary geometry a theorem on triangles, (see Fig. 4).
$ag_a + bg_b + cg_c = 2F$, where F is the area of the triangle. On the other hand $2F = ah_a = bh_b = ch_c$ where h_a, h_b and h_c are the corresponding heights of the triangle with the sides of lengths a, b and c respectively considered as the base.
Hence,

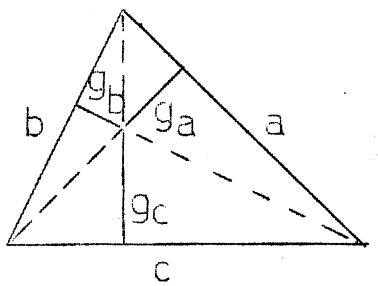

Fig. 4

$$\frac{a}{c} g_a + \frac{b}{c} g_b + g_c = h_c$$

$$\text{c.f.} \quad s + t + u = 4m^2 .$$

These two equations suggest to choose $a = b = c$; $h_c = 4m^2$ and identify g_a, g_b, g_c with s, t, u.

The result is shown in Fig. 5 (Mandelstam diagram)

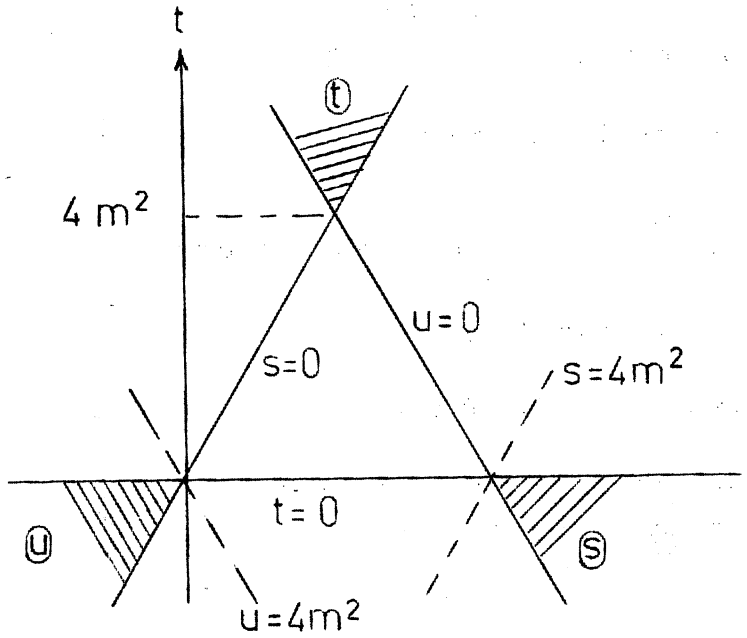

Fig. 5

We now discuss the processes nucleon-nucleon and nucleon-antinucleon scattering.

For nucleon-nucleon scattering we see from Eq. (7) that

$$s \geq 4m^2; \quad -4K^2 = 4m^2 - s \leq t \leq 0 \tag{13}$$

(see also CERN 62-18 Yellow Report, p. 89). We call this "scattering in the s-channel". The shaded region (s) in Fig. 5 indicates the "physical region" for the s-channel. For nucleon-antinucleon scattering p′ is reversed and goes in, k goes out.

We have, under these circumstances,

$$\begin{aligned} s &= (p-k)^2 = -2K^2(1-\cos\Theta_t) \leq 0 \\ t &= (p+p')^2 = 4(K^2+m^2) \geq 4m^2 . \end{aligned} \tag{13′}$$

Hence the physical region in the "t-channel" is now the shaded area (t) in Fig. 5. Similarly a "u-channel" can be defined. As one sees, the only difference is, s and t assume other values if one goes from the s- to the t-channel, that is from nucleon-nucleon to antinucleon-nucleon scattering. The meaning of crossing symmetry and analyticity of A(st) is then, that one single function

$$\begin{aligned} &A(s,t) \quad \text{describes nucleon-nucleon scattering} \\ &\qquad\quad \text{in the s-channel:} \quad s \geq 4m^2; \quad t \leq 0 \\ &A(s,t) \quad \text{describes nucleon-antinucleon scattering} \\ &\qquad\quad \text{in the t-channel:} \quad t \geq 4m^2; \quad s \leq 0. \end{aligned} \tag{14}$$

IV. PARTIAL WAVE EXPANSION OF A(st)

We have defined the scattering amplitude by Eq. (9). Unitarity requires the "optical theorem"

$$\text{Im } f(E,\Theta) = \frac{K}{4\pi} \sigma_{tot} . \tag{15}$$

We shall express $E = \sqrt{s}$ and Θ by s and t and simply write f(st) instead of $f(E,\Theta)$.

Using the common partial wave expansion of f we have

$$A(st) = 8\pi\sqrt{s}\, f(st) = -4\pi i \frac{\sqrt{s}}{K} \Sigma(2\ell+1)\, P_\ell\left(1+\frac{t}{2K^2}\right) a_\ell(s)$$

$$a_\ell(s) = e^{2i\delta_\ell} - 1 = 2i \sin\delta_\ell\, e^{i\delta_\ell} \tag{16}$$

$\delta_\ell(s)$ is complex in general.

In this notation we obtain:

$$\frac{d\sigma_{el}}{dt} = \frac{1}{64\pi K^2 s} |A(st)|^2 = \frac{\pi}{4K^2} \left|\Sigma(2\ell+1)\ P_\ell\left(1+\frac{t}{2K^2}\right)\ a_\ell(s)\right|^2$$

$$\sigma_{el} = \int \frac{d\sigma_{el}}{dt}\, dt = \frac{\pi}{K^2} \Sigma(2\ell+1) |a_\ell(s)|^2 \qquad (17)$$

$$\sigma_{tot} = \frac{1}{2K\sqrt{s}} \operatorname{Im} A(s0) = -\frac{2\pi}{K^2} \Sigma(2\ell+1) \operatorname{Re} a_\ell(s)$$

V. THE BLACK SPHERE

1. In high-energy collisions, pp collision at $\geq$ 10 GeV, the majority of reactions are inelastic and the elastic cross-section becomes more and more the minimum required to fulfil unitarity. The phase shifts in Eq. (16), which are real below the threshold for inelastic processes, become more and more imaginary. Then the a_ℓ becomes more and more real and the extreme situation of a totally absorbing sphere of radius R would give

$$a_\ell = -1 \quad \text{for all} \quad \ell < KR$$

$$a_\ell = 0 \quad \text{for all} \quad \ell > KR\,.$$

This very primitive model leads to the direct evaluation of Eq. (17) if KR is very large:

$$\sigma_{tot} = \frac{2\pi}{K^2} \sum_0^{KR} 2\ell+1 \approx \frac{2\pi}{K^2} \int_0^{KR} 2\ell\, d\ell = 2\pi R^2 = \text{const (independent of E)}$$

$$\sigma_{el} = \frac{\pi}{K^2} \sum_0^{KR} 2\ell+1 = \pi R^2 = \frac{1}{2}\sigma_{tot}$$

$$\frac{d\sigma_{el}}{dt} = \frac{\pi}{4K^2} \left[\sum_0^{KR} (2\ell+1)\ P_\ell\left(1+\frac{t}{2K^2}\right)\right]^2 .$$

Here we use the formula

$$\lim_{\ell\to\infty} P_\ell(\cos\tfrac{x}{\ell}) = J_0(x)\,.$$

As we see, for $KR \to \infty$ the main contribution comes from large ℓ, hence we may write

$$P_\ell(\cos\tfrac{x}{\ell}) = P_\ell(1 - \tfrac{x^2}{2\ell^2}) = J_0(x)\,,$$

putting

$$\frac{x^2}{2\ell^2} = -\frac{t}{2K^2}$$

we have

$$x = \frac{\ell}{K}\sqrt{-t}$$

and the sum becomes

$$\sum (2\ell+1)\,P_\ell(1+\tfrac{t}{2K^2}) \approx \sum_0^{KR} (2\ell+1)\,J_0(\tfrac{\ell}{K}\sqrt{-t}) \approx \int_0^{KR} (2\ell+1)\,J_0(\tfrac{\ell}{K}\sqrt{-t})\,d\ell$$

$$= 2K^2\int_0^R \rho\,J_0(\rho\sqrt{-t})\,d\rho\,.$$

We then obtain for $KR \to \infty$

$$\frac{d\sigma_{el}}{dt} \approx 2\pi R^2 \cdot \frac{J_1^2(R\sqrt{-t})}{-2t} = \frac{\sigma_{tot}}{2}\left[\frac{J_1^2(R\sqrt{-t})}{-t}\right] = \sigma_{tot}\cdot F(t)\,. \qquad (18)$$

As a function of t this gives the well-known optical diffraction pattern (Fig. 6)

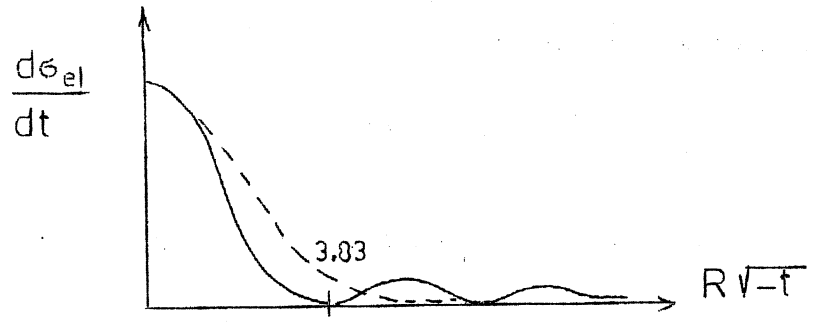

Fig. 6

Of course, the nucleon is not a black sphere with a sharp surface. We should therefore not expect diffraction minima and maxima but something like the dotted line in Fig. 6. However, the form of the curve should be roughly $\sigma \cdot F(t)$, hence independent of the energy. This is in agreement with the uncertainty principle: $\sqrt{-t} = |\Delta\vec{k}| \approx 4/R$ is our present result, where as the uncertainty principle yielded $|\Delta\vec{k}| \geq \frac{1}{2R}$.

2. The condition for minimum elastic scattering [see Rarita and Schwed Phys.Rev. 112, 271 (1958)]. The authors proceed to make the general substitution:

$$a_\ell(s) = \alpha_\ell + i\beta_\ell ,$$

then with Eq. (17)

$$\sigma_{el} = \frac{\pi}{K^2} \Sigma(2\ell+1)(\alpha_\ell^2 + \beta_\ell^2)$$

$$\sigma_{tot} = -\frac{2\pi}{K^2} \Sigma(2\ell+1)\ \alpha_\ell .$$

The following assumptions are then made:

i) $0 \leq \ell < L$ (that is: a value of L exists, such that $a_\ell = 0$ for $\ell > L$);

ii) σ_{tot} is given.

We find out the minimum value of σ_{el} which is possible under these conditions.

One sees at once that $\beta_\ell = 0$ is necessary. Thus

$$\sigma_{el} = \frac{\pi}{K^2} \sum_{0}^{L} (2\ell + 1)\alpha_\ell^2 = \text{minimum}$$

$$\sigma_{tot} = - \frac{2\pi}{K^2} \sum (2\ell + 1)\, \alpha_\ell \text{ is given.}$$

Using the method of Lagrange multipliers we can rewrite the last two equations as:

$$F(\alpha_0\ \alpha_1\ \ldots\ \alpha_L) = \min$$

$$G(\alpha_0\ \alpha_1\ \ldots\ \alpha_L) = \text{const.}$$

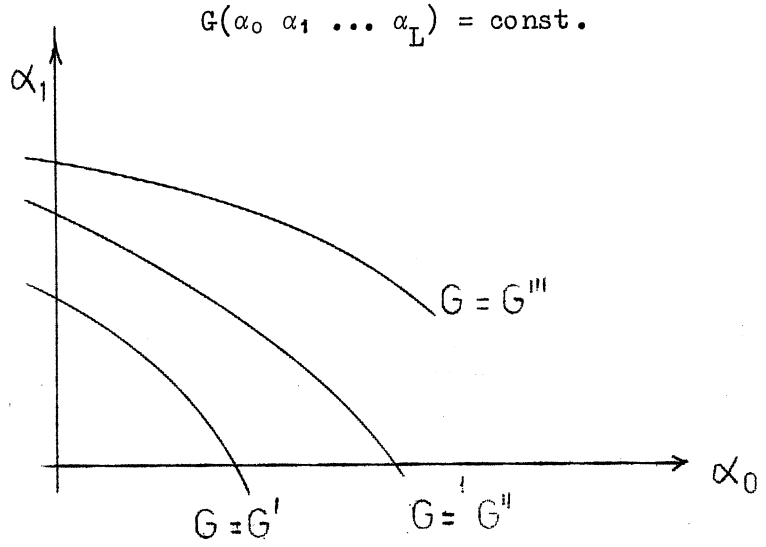

Fig. 6a

We have to find a stationary value of F when going along the curve G = const (see Fig. 6a). Thus the gradient of F and that of G must be proportional, since grad F must have no component tangential to the surface G = const, and grad G has, by definition, no component tangential to the plane G = const. Hence,

$$\text{grad } F = \lambda \text{ grad } G.$$

This gives:

$$\frac{\partial F}{\partial \alpha_\ell} = \frac{\pi}{K^2} 2(2\ell+1)\ \alpha_\ell = -\lambda \frac{2\pi}{K^2} (2\ell+1)\ (\ell = 0 \ldots L),$$

hence:

$$\alpha_0 = \alpha_1 = \ldots \alpha_\ell = \ldots \alpha_L = -\lambda .$$

Since

$$\sigma_{tot} = -\frac{2\pi}{K^2} \sum_{\ell=0}^{L} (2\ell+1)\ \alpha_\ell = \lambda \cdot \frac{2\pi}{K^2} \sum_{0}^{L} (2\ell+1)$$

is given, we have with

$$\sum_{0}^{L} (2\ell+1) = 2 \sum_{0}^{L} \ell + L + 1 = 2 \cdot \frac{L(L+1)}{2} + L + 1 = (L+1)^2 ,$$

$$\lambda = \frac{K^2 \sigma_{tot}}{2\pi} \left(\frac{1}{L+1}\right)^2$$

$$\min \sigma_{el} = \frac{\pi}{K^2} \lambda^2 \cdot \sum (2\ell+1) = \frac{\pi}{K^2} \frac{K^4 \sigma_{tot}^2}{4\pi^2} \left(\frac{1}{L+1}\right)^4 \cdot (L+1)^2$$

$$\min \sigma_{el} = \frac{K^2 \sigma_{tot}^2}{4\pi (L+1)^2} .$$

This is the minimum elastic cross-section compatible with a given total cross-section and the assumption of an upper bound L (which will depend on "range of force" and momentum) above which the $a_\ell(s)$ are negligible.

This minimum elastic cross-section turns out to be exactly that of the black sphere. Namely if we put L = KR and neglect 1 << KR, then

$$\lambda = -\alpha_\ell = -\mathrm{Re}\ a_\ell(s) = \frac{K^2 \sigma_{tot}}{2\pi K^2 R^2} = \frac{\sigma_{tot}}{2\pi R^2} = 1$$

since for the black sphere $\sigma_{tot} = 2\pi R^2$. Hence the black sphere gives the minimum possible elastic scattering. In particular the minimum possible elastic scattering is obtained for a black sphere with a sharp edge; namely our result was:

$$\alpha_0 = \alpha_1 = \ldots \alpha_L = -1$$

$$\alpha_\ell = 0 \text{ for } \ell > L.$$

In other words, for all $\ell < L = KR$ the scattering is as inelastic and as strong as possible and all phase shifts are equal. Consider σ_{react} for fixed ℓ and $\alpha_\ell = -1$:

$$\sigma_{react,\ell} \equiv \sigma_{tot,\ell} - \sigma_{el,\ell} = \frac{2\pi}{K^2}(2\ell+1) - \frac{\pi}{K^2}(2\ell+1) = \frac{\pi}{K^2}(2\ell+1).$$

We obtain, neglecting the $1 << 2\ell$ and putting $Kr = \ell$:

$$\sigma_{react,\ell} = \frac{2\pi r}{K}.$$

Now $r = \ell/K$ gives $\Delta r = \Delta\ell/K$
and for $\Delta\ell = 1$ one has
$\sigma_{react,\ell} = 2\pi r \cdot \Delta r$.

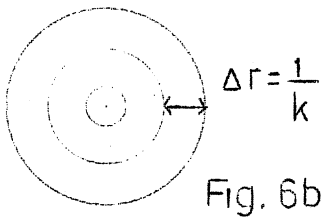

Fig. 6b

A nucleon certainly does not look like this. If the assumption of the existence of L(s) is kept (and this may be very large but finite), the elastic cross-section must become larger than the minimum one, because if we (artificially) select any very large L, the phase shifts cannot stay constant and hence $\sigma_{el} \geq \sigma_{el,min}$. Hence,

$$\sigma_{el} \geq \frac{K^2\sigma_{tot}^2}{4\pi(L+1)^2}$$

or, given σ_{el} and σ_{tot}, then

$$(L+1)^2 \geq \frac{K^2}{4\pi}\frac{\sigma_{tot}^2}{\sigma_{el}} \text{ gives } (L+1)^2 \geq (L_{min}+1)^2$$

where up to L_{min} is to be included in a phase shift analysis.

Put $L_{min} = KR_{min}$ and neglect the 1

$$\frac{K^2}{4\pi}\frac{\sigma_{tot}^2}{\sigma_{el}} = K^2 R_{min}^2$$

defines the minimum range of interaction compatible with σ_{tot} and σ_{el}:

$$R \geq R_{min}$$

where R_{min} is the value for the black sphere.

$$\left[\begin{array}{l}\text{remember for}\\ \text{black sphere:}\end{array}\quad \begin{array}{l}\sigma_{tot} = 2\pi R^2\\ \sigma_{el} = \pi R^2\end{array}\quad ;\quad \frac{\sigma_{tot}^2}{\sigma_{el}} = 4\pi R^2\right].$$

With L = KR we have then

$$R^2 \geq \frac{\sigma_{tot}^2}{4\pi\sigma_{el}} = R_{min}^2$$

or

$$\sigma_{el} \geq \frac{\sigma_{tot}^2}{4\pi R^2} = \sigma_{el} \cdot \frac{R_{min}^2}{R^2}.$$

VI. RECENT EXPERIMENTS

Of all the above features only one seems to be true: the total cross-section becomes energy independent for high energies; but the width of the diffraction peak becomes apparently smaller with increasing energy.

A.N. Diddens, E. Lillethun, G. Manning, A.E. Taylor, T.G. Walker and A.M. Wetherell [Phys.Rev.Letters 9, 111 (1962)] describe their result in a form which takes into account the optical theorem:

$$\left.\frac{d\sigma_{el}}{dt}\right|_{t=0} = \frac{1}{64\pi K^2 s}\,|A(s,0)|^2 \approx \frac{1}{64\pi K^2 s}\,|\mathrm{Im}\,A(s,0)|^2 = \frac{\sigma_{tot}^2}{16\pi}. \qquad (19)$$

They plot then

$$\left(\frac{d\sigma_{el}}{dt}\right) \Big/ \left(\frac{d\sigma_{el}}{dt}\right)_{t=o},$$

in other words

$$\frac{16\pi}{\sigma_{tot}^2} \frac{d\sigma_{el}}{dt} = \frac{16\pi^2}{\sigma_{tot}^2 K^2} \frac{d\sigma_{el}}{d\Omega}$$

against

$$s/(2m^2)$$

and find the behaviour which is sketched in Fig. 7. (The complete data are shown in Fig. 10 of the following paper by Dr. Wetherell.) This behaviour can be written:

$$\frac{d\sigma_{el}}{dt} = \left(\frac{d\sigma_{el}}{dt}\right)_{t=o} \cdot F(t) \cdot s^{2[\alpha(t)-1]}. \tag{20}$$

In order that the total cross-section becomes constant, Eq. (19) requires, together with Eq. (20), that

$$F(0) = \alpha(0) = 1, \tag{21}$$

which agrees with the experiment.

These findings mean that the width of the diffraction peak is not energy independent.

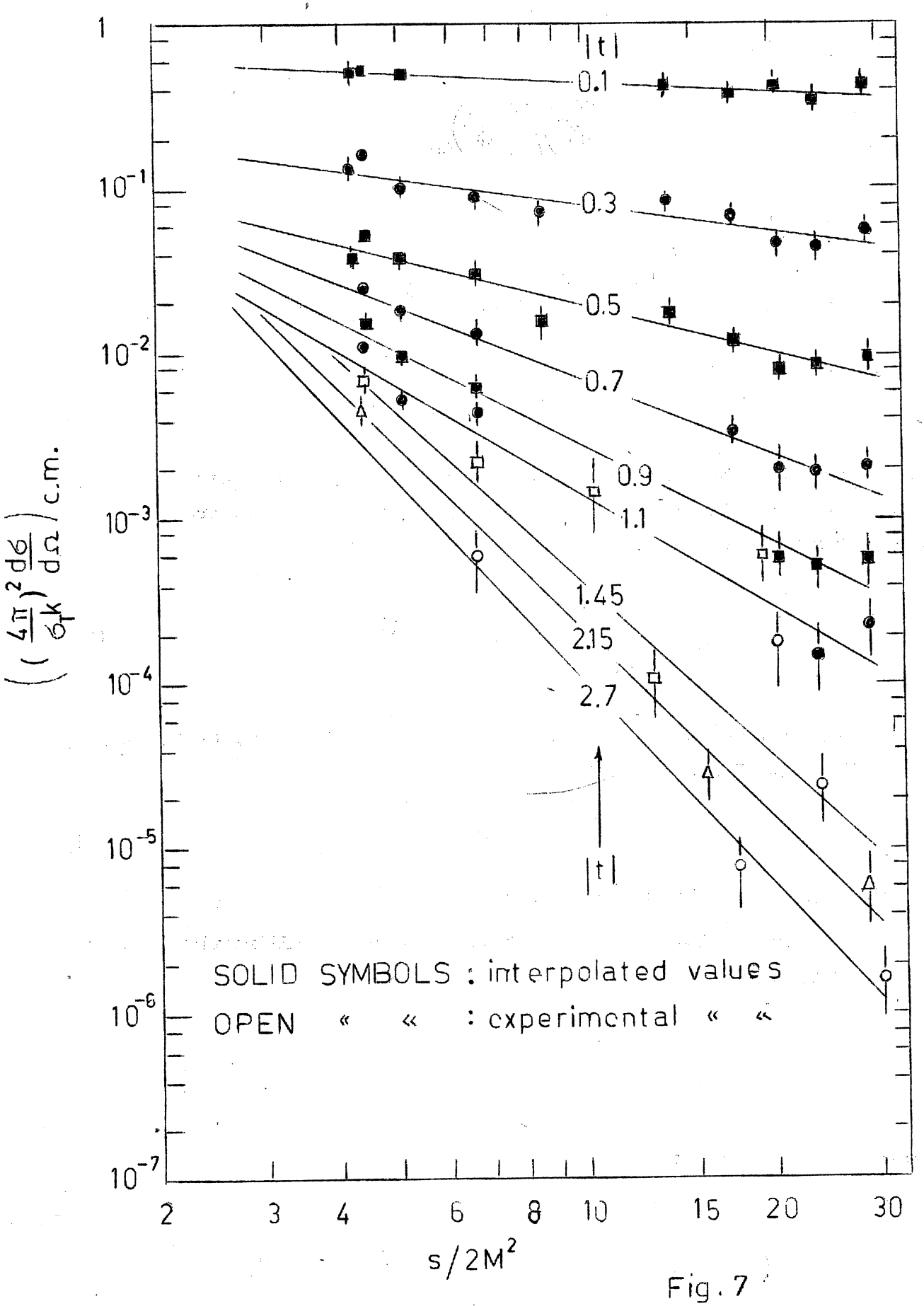
1
10^{-1}
10^{-2}
10^{-3}
10^{-4}
10^{-5}
10^{-6}
10^{-7}
$\left(\left(\frac{4\pi}{\sigma_t k}\right)^2 \frac{d\sigma}{d\Omega}\right)_{c.m.}$
|t|
0.1
0.3
0.5
0.7
0.9
1.1
1.45
2.15
2.7
|t|
SOLID SYMBOLS : interpolated values
OPEN « « : experimental « «
2
3
4
6
8
10
15
20
30
$s/2M^2$

Fig. 7

We may define the half-width by means of Eq. (20) and Fig. 8.

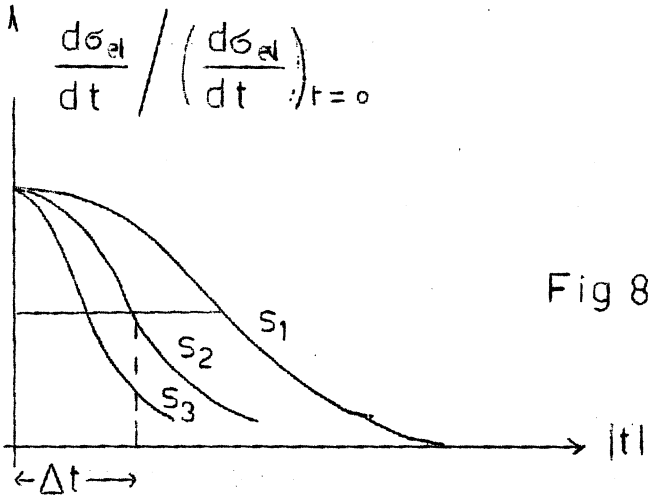

Fig 8

$$F(t)\, s^{2[\alpha(t)-1]} = \tfrac{1}{2}$$

putting

$$\alpha(t) = 1 + \alpha'(0)\, \Delta t + \ldots$$

gives

$$F(t) = e^{\gamma(t)} = e^{\Delta t \cdot \gamma'(0)}.$$

Hence,

$$e^{\Delta t \gamma'(0)}\, s^{2\Delta t \alpha'(0)} = \tfrac{1}{2}$$

$$e^{\Delta t[\gamma'(0) + 2\alpha'(0) \log s]} = \tfrac{1}{2}$$

i.e. $$\Delta t \approx \frac{\text{const}}{\gamma'(0) + 2\alpha'(0) \log s} \approx \frac{\text{const}}{\log s} \text{ for } s \to \infty.$$

If we force this into our black sphere picture, we have:

$$\sqrt{\Delta t} \approx \frac{2}{R} \approx \frac{\text{const}}{\sqrt{\log s}} \text{ or } R \approx \text{const} \sqrt{\log s}. \qquad (22)$$

Our black sphere would increase in radius if the energy raises! On the other hand the total cross-section of the black sphere is $2\pi R^2$, thus it should increase as const $\cdot$ log s. Experimentally it stays constant. This would mean that we had to consider the sphere to become more and more

transparent as it grows. Eq. (17) suggests to write

$$\sigma_{tot} \approx \frac{2\pi}{K^2} \sum_{0}^{KR} (2\ell+1) \mathrm{Re}\ a_\ell(s) \approx \overline{|\mathrm{Re}\ a_\ell(s)|} \cdot \frac{2\pi}{K^2} \sum_{0}^{KR} (2\ell+1) = 2\pi R_0^2 \log s \cdot \overline{|\mathrm{Re}\ a_\ell(s)|}$$

where the average $|\mathrm{Re}\ a_\ell(s)|$ is over all $\ell = 0 \ldots KR$; $R = R_0\sqrt{\log s}$. In order to have σ_{tot} constant, we should have

$$\overline{|\mathrm{Re}\ a_\ell(s)|} \approx \frac{\sigma_{tot}}{2\pi R_0^2} \cdot \frac{1}{\log s} . \qquad (23)$$

Our sphere has therefore a radius growing with $\sqrt{\log s}$ and its "blackness" goes proportional to 1/log s. This may be a way of speaking, but has nothing to do with any understanding. It simply shows that the absorbing sphere is no longer acceptable as a model of high-energy scattering.

The elastic cross-section is given from Eq. (17)

$$\sigma_{el} = \frac{\pi}{K^2} \sum (2\ell+1) |a_\ell|^2 \approx \overline{|\mathrm{Re}\ a_\ell|}^2 \frac{\pi}{K^2} \sum_{0}^{KR} (2\ell+1).$$

Using the treatment of Rarita and Schwed (Section V.2)

$$\sum_{0}^{KR} 2\ell+1 = K^2R^2$$

which gives with Eq. (23) for $\overline{|\mathrm{Re}\ a_\ell|}$:

$$\sigma_{el} \approx \frac{\sigma_{tot}^2}{4\pi^2 R^4} \cdot \frac{\pi}{K^2} K^2R^2 = \frac{\sigma_{tot}^2}{4\pi R_0^2 \log s} .$$

The elastic cross-section goes to zero as 1/log s which is no contradiction to the results of Rarita and Schwed.

The increase of R and the decrease of blackness has a consequence on the scattering of protons by heavy nuclei. If the individual nucleons would be black, then the total cross-section of a nucleus of A nucleons would be "geometric", that is

$$\sigma(A) \cong \sigma_0 \cdot A^{2/3}$$

because the primary protons are absorbed on the surface. However, if the individual nucleons become more and more transparent with increasing energy, then the primary protons penetrate through the nucleus and the individual cross-sections of the A nucleons would add; hence

$$\sigma(A) \cong \sigma_0 A \text{ for } s \to \infty .$$

This might be tested experimentally. [B.M. Udgaonkar and M. Gell-Mann, Phys.Rev.Letters 8, 346 (1962).]

VII. THE REGGE POLES

A possible explanation of the behaviour of high-energy elastic scattering might come from Regge's analysis of the analytic properties of the scattering amplitude in the complex $\lambda = \ell + i\ell_1$ plane.

We shall first outline the idea*) and apply it without hesitation to the given situation - afterwards we shall point to the difficulties.

The essentials are the following. One considers the elastic scattering first in the t-channel, that is nucleon-antinucleon scattering. There we shall use Regge's representation of the scattering amplitude as a sum over residues of the poles in the complex λ plane of the partial wave amplitudes. This leads to a simple asymptotic behaviour in the highly unphysical region where the cosine of the scattering angle tends to infinity. By means of the crossing symmetry this is at the same time a physical region in the s-channel; namely it describes nucleon-nucleon scattering for very large energies. Since A(st) is the one function which describes both processes according to in which region (see Fig. 5) the variables s and t lie, we obtain the asymptotic behaviour of A(st) for $s \to \infty$ in the physical region for nucleon-nucleon scattering.

In the t-channel we have from Eq. (13):

$$\cos \Theta_t = 1 + \frac{2s}{t - 4m^2} \qquad (24)$$

*) In this part we follow closely a lecture by W. Kummer, CERN 62-13.

and the partial wave expansion of the scattering amplitude becomes, according to Eq. (16):

$$A(st) = -4\pi i \frac{\sqrt{t}}{K_t} \sum (2\ell + 1)\, P_\ell\left(1 + \frac{2s}{t - 4m^2}\right) a_\ell^{(t)}(t) . \qquad (25)$$

Regge [Nuovo Cimento 14, 195 (1959)] proved that in the case of potential scattering (superposition of Yukawa potentials) the following transformation can be carried out. We introduce the complex $\lambda = \ell + i\ell_1$ plane and write the sum as an integral (see Fig. 9a):

$$A(st) = \frac{2\pi\sqrt{t}}{K_t} \int_{C_0} \frac{2\lambda + 1}{\sin \pi\lambda} P_\lambda(-\cos \Theta_t)\, a_\lambda^{(t)}\, d\lambda . \qquad (26)$$

Calculating this integral by the Cauchy formula gives back Eq. (25).

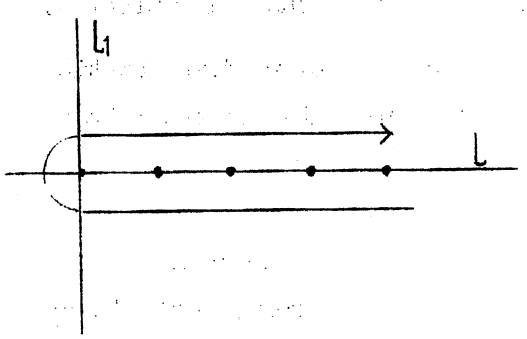

Fig. 9a

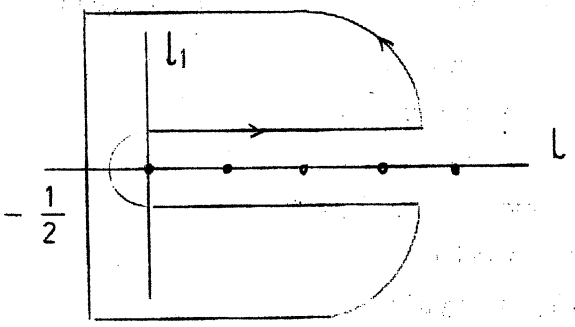

Fig. 9b

Since

$$\int_{C_0} = -2\pi i \sum \text{Res at the poles}$$

$$\sin \pi\lambda = \sin \pi\ell \cos \pi\lambda' + \cos \pi\ell \sin \pi\lambda' \text{ if } \lambda = \ell + \lambda'$$

$$= (-)^\ell \cdot \pi\lambda' \text{ (when } \sin \pi\lambda \to 0)$$

$$\text{Res}(\ell) = \frac{(2\ell + 1)\,(-)^\ell\,(-)^\ell\, P_\ell(\cos \Theta)\, a_\ell^{(t)}(t)}{\pi}$$

giving

$$\int_{C_0} = -\frac{4\pi i\sqrt{t}}{K} \sum (2\ell+1)\, P_\ell(\cos\Theta)\, a_\ell(t)\,.$$

We now complete the integration path by adding a half circle and a straight line as shown in Fig. 9b, where we assume the radius of the half circle to go to infinity. This path is called C_1 and the integral along C_1 with the integrand of Eq. (26) is then:

$$\int_{C_1} = \int_{C_0} + \int_{\text{half circle}} + \int_{-\frac{1}{2}+i\infty}^{-\frac{1}{2}-i\infty} = 2\pi i \times \Sigma \text{ (residues in } C_1). \qquad (27)$$

Regge proved that (for superposed Yukawa potentials) the contribution of the infinite half circles vanishes and that the integrand has a finite number of simple poles inside C_1. These poles come from the $a_\lambda^{(t)}(t)$ since all the rest of the integrand is regular inside C_1. We call the locations of these poles $\lambda_i \equiv \alpha_i(t)$; thus in the neighbourhood of such a pole

$$a_\lambda^{(t)}(t) = \frac{R_{\alpha j}(t)}{\lambda - \alpha_j(t)} + \ldots \qquad (28)$$

where $R_{\alpha j}(t)$ is the residue. With this notation one obtains from Eq. (27):

$$A(st) = \frac{2\pi\sqrt{t}}{K_t} \int_{C_0} = \frac{2\pi\sqrt{t}}{K_t}\, 2\pi i \sum_{j=1}^{N} \frac{2\alpha_j + 1}{\sin \pi\alpha_j}\, R_{\alpha j}(t)\, P_{\alpha j}(-\cos\Theta_t) \qquad (29)$$

$$- \int_{-\frac{1}{2}+i\infty}^{-\frac{1}{2}-i\infty} (\ldots)\, d\lambda\,.$$

The locations $\alpha_j(t)$ and residues $R_{\alpha j}(t)$ are of course functions of t; that is, the Regge-poles move in the λ-plane.

However, now let us keep t fixed and ≤ 0 and let s become very large and positive. We leave then the t-channel and arrive in the s-channel. Under these circumstances the contribution of the remaining integral can be shown to vanish, namely:

$$-\cos\Theta_t \to \text{const} \cdot s \quad \text{(see below)}$$

$$\left|P_{-1/2+i\ell_1}(\text{const} \cdot s)\right| \approx \left|(\text{const} \cdot s)^{-1/2+i\ell_1}\right| \approx \frac{1}{\sqrt{s}}$$

and the scattering amplitude is given by the sum in Eq. (29). Now, if s becomes sufficiently large, only one single term of the sum is important because:

i) with $s \to \infty$ and $t < 1$

$$-\cos\Theta_t \to -\frac{2s}{t-4m^2} = \frac{2s}{|t|+4m^2} \to +\infty ; \tag{30}$$

ii)

$$P_{\alpha_j}(-\cos\Theta_t) \to (-\cos\Theta_t)^{\alpha_j} = \left(\frac{2s}{|t|+4m^2}\right)^{\alpha_j(t)} ; \tag{31}$$

iii) only a finite number of such poles exist and therefore one of them has the largest real part; it gives the highest power of s in the asymptotic form (31) of the P_{α_j}. This special pole is at $\alpha_j(t) = \alpha_{1j}(t) + i\alpha_{2j}(t)$.

Hence, if we retain only this term and combine all t-dependence in a factor g(t) (remember that K_t does not depend on s), we arrive at

$$A(st) \to g(t)\, s^{\alpha_1(t)+i\alpha_2(t)} . \tag{32}$$

The differential cross-section becomes, with Eq. (17),

$$\frac{d\sigma_{el}}{dt} = \frac{1}{64\pi K_s^2 s}\left|A(st)\right|^2 \to \frac{\left|g(t)\right|^2}{16\pi s^2}\, s^{2\alpha_1(t)} = G(t)\, s^{2[\alpha_1(t)-1} \tag{33}$$

which is the form found experimentally [Eq. (20)].

VIII. THE DIFFICULTIES

All this looks rather promising. It should not be forgotten, however, that we have made two assumptions which may seem to get some support by the success, but which in fact are very doubtful and probably wrong.

i) We assumed that the results from potential scattering can be applied to relativistic situations. There are strong indications that this cannot be done and that in addition to poles there might be cuts in the λ-plane.

ii) We assumed that in the present experimental situation the asymptotic region, in which only the "highest" Regge pole dominates, is actually reached. This is probably not true, because if it would be true, then this one pole should dominate not only nucleon-nucleon scattering. In fact it should be the leading contribution to antinucleon-nucleon scattering and to pion-nucleon scattering as well. One should expect then that all corresponding total cross-sections should be equal and constant*). This not being the case we must admit that the behaviour at 25 GeV is not yet asymptotic and that a rather improbable cancellation of contributions from different Regge poles (if anything like that exists) might have taken place in such a way that the "one-Regge-pole-behaviour" is simulated. Recent experiments, carried out by Lindenbaum and co-workers at Brookhaven (to be published) seem to confirm this point of view: there is no shrinking of the pion-nucleon diffraction peak and the shrinkage of the nucleon-nucleon diffraction peak follows the Regge-pole-behaviour at lower energies better than at the highest available values - contrary to what one would expect. However, this direction of research seems to be promising; but we are certainly not yet near to the truth.

---

*) Corresponding means for particles a,b and antiparticles $\bar{a},\bar{b}$ that $\sigma_{ab} \approx \sigma_{\bar{a}\bar{b}}$ etc.

IX. REGGE POLES AND PERIPHERAL MODEL

We shall look at the analogies between Regge-behaviour and peripheral-model-behaviour of scattering amplitudes in the high-energy limit $s \to \infty$.

We cannot go into detail. Further information may be taken from the following papers:

i) S.C. Frautschi, M. Gell-Mann and F. Zachariasen, Phys.Rev. 126, 2204 (1962);

ii) M. Gell-Mann, Phys.Rev.Letters 8, 263 (1962);

iii) S.D. Drell, 1962 Int.Conf.on High-Energy Physics, CERN, Geneva, p. 897.

Let us consider the Regge-pole contribution of Eq. (29)

$$A(st) \underset{s\to\infty}{\approx} \sum_{..j} \beta_j(t) \frac{P_{\alpha_j}(-\cos\Theta_t)}{\sin \pi\alpha_j(t)} = \sum_j a_j(st). \tag{34}$$

Here we have combined all t-dependence [except for the $\sin \pi\alpha_j(t)$] in $\beta_j(t)$.

Consider one single term and omit the subscript j. We observe that

$$a(st) = i\beta(t) \frac{P_{\alpha(t)}(-\cos\Theta_t)}{\sin \pi\alpha(t)} \tag{35}$$

may have a singularity or resonance in t coming from $\sin \pi\alpha(t) \simeq 0$. Let us call

$$\alpha(t) = \alpha_1(t) + i\alpha_2(t) \qquad \alpha_1 \text{ and } \alpha_2 \text{ real}. \tag{36}$$

Obviously $\sin \pi\alpha(t) = 0$ for $\alpha(t) = \ell$.

If $\alpha_2(t) = 0$, we have a genuine pole; if $\alpha_2(t) \neq 0$ we have a resonance behaviour. Let $t = t_\ell$ be the value where $\alpha_1(t_\ell) = \ell$.

Then

$$\alpha(t) = \alpha(t_\ell) + \left.\frac{d\alpha}{dt}\right|_{t_\ell} (t - t_\ell) = \ell + i\alpha_2(t_\ell) + \left[\left.\frac{d\alpha_1}{dt}\right|_{t_\ell} + i \left.\frac{d\alpha_2}{dt}\right|_{t_\ell}\right] \times (t - t_\ell). \quad (37)$$

Since the Regge poles move first along the real ℓ-axis and then start off from $i\ell$ (Fig. 10), it is clear that for $\alpha_2(t)$ small, the trajectory moves still nearly parallel to the real ℓ-axis, giving thus a family of resonances at $\ell = 1, 2, 3, \ldots$.

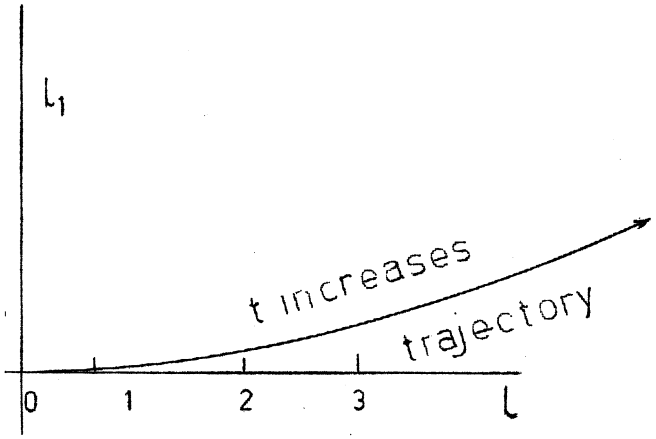

Fig. 10

Hence

$$\left|\frac{d\alpha_2}{dt}\right|_{t=t_\ell} \ll \left|\frac{d\alpha_1}{dt}\right|_{t=t_\ell}$$

and Eq. (37) becomes, with

$$\alpha_1'(t_\ell) \equiv \left.\frac{d\alpha_1}{dt}\right|_{t=t_\ell},$$

$$\alpha(t) = \ell + i\alpha_2(t_\ell) + \alpha_1'(t_\ell) \cdot (t - t_\ell) \equiv \ell + \epsilon$$

where ϵ is small. We can then expand the sin $\pi\alpha(t)$:

$$\sin \pi(\ell + \epsilon) \cong (-)^\ell \cdot \pi\epsilon = \pi(-)^\ell \cdot \alpha_1'(t_\ell) \left[t - t_\ell + i \frac{\alpha_2(t_\ell)}{\alpha_1'(t_\ell)} \right]. \quad (38)$$

We introduce this into Eq. (35) and obtain

$$a(st) \sim \frac{\beta(t_\ell)}{\pi\alpha_1'(t_\ell)} \frac{(-)^\ell (P_\ell(+\cos\Theta_t)}{t - \left(t_\ell \; i \frac{\alpha_2(t_\ell)}{\alpha_1'(t_\ell)}\right)} + \ldots . \qquad (39)$$

The factor $(-)^\ell$ cancels the - sign in the argument of P_ℓ. Looking at this, we see a striking similarity to a one-particle-exchange contribution of Fig. 11.

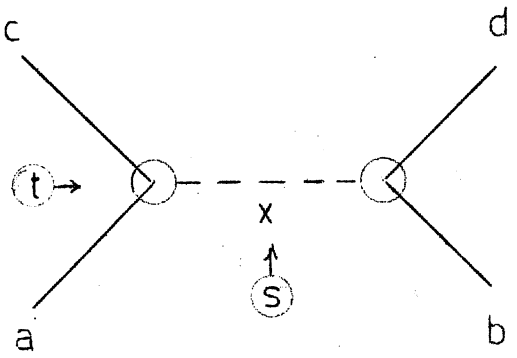

Fig. 11

Namely, comparing this to the pole term in dispersion theory one sees the following correspondences. The "exchanged" particle x has

$$\text{mass } m_x^2 \;\langle=\rangle\; t_\ell - i \frac{\alpha_2(t_\ell)}{\alpha_1'(t_\ell)} \qquad \left[\begin{array}{l}\text{it is a "resonance" if } \alpha_2 > 0 \\ \text{it is stable if } \alpha_2 = 0\end{array}\right]$$

$$\text{coupling } g_{axc}(t_\ell)\, g_{bxd}(t_\ell) \;\langle=\rangle\; \frac{\beta(t_\ell)}{\pi\alpha_1'(t_\ell)} \qquad (40)$$

$$\text{propagator } \frac{1}{t - m_x^2} \;\langle=\rangle\; \frac{\pi\alpha_1'(t_\ell)}{\sin \pi\alpha(t_\ell)}$$

$$\text{angular momentum } \ell \;\langle=\rangle\; \alpha_1(t_\ell) .$$

This correspondence gives, however, a different high-energy behaviour of the amplitude depending on whether one writes down a graph like in Fig. 11 using

i) the left-hand side (mass, coupling, propagator, fixed ℓ) or

ii) the right-hand side (the Reggeized" particle x)

in order to construct its contribution to the scattering amplitude. In the first case ("peripheral model") ℓ is a fixed integer and the scattering amplitude for $s \to \infty$ (in the s-channel) behaves asymptotically as

$$a(st) \sim \frac{g_{axc}\, g_{bxd}}{t - m_x^2} P_\ell(\cos \Theta_t) \sim F(t) \cdot s^\ell \,. \qquad (41a)$$

If one uses the right-hand side of the correspondence one arrives back at Eq. (35) [use Eq. (31) for $s \to \infty$]

$$a(st) \sim \frac{\beta(t)}{\sin \pi\alpha(t)} \left(\frac{2s}{|t| + 4m^2}\right)^{\alpha(t)} = G(t)\, s^{\alpha(t)} \qquad (41b)$$

so that the high-energy behaviour may rapidly change, because ℓ is replaced by $\alpha(t)$.

X. THE FACTORIZATION OF CROSS-SECTIONS

The analogies (40) have a very interesting consequence. Let us admit that a "leading Regge pole" - that is the one with the largest real part $\alpha_1(t)$ - exists.

Froissart has shown that $\alpha_1(0) \leq 1$ is necessary. Assume then that there is a pole with $\alpha_1(0) = 1$ [which is strongly suggested by experiment: Eq. (21) and Fig. 7]. It is then this trajectory $\alpha(t)$ which would govern the limiting behaviour of elastic two-body amplitudes (and elastic cross-sections) as well as the total cross-sections, via the optical theorem (17).

Looking at the elastic amplitude, which is a special case of Fig. 11 and is shown in Fig. 12, we see that the exchanged Regge-particle x should have the quantum numbers of the vacuum - except for angular momentum - since $a \to a$ and $b \to b$. Therefore one should associate the quantum numbers of the vacuum to the whole leading Regge trajectory $\alpha(t)$.

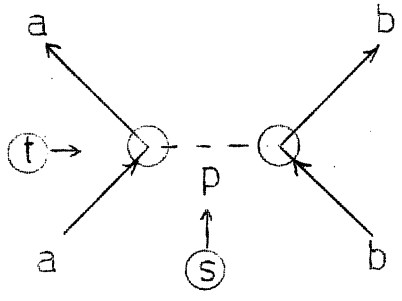

Fig. 12

This is then the so-called Pomeranchuk trajectory $\alpha_P(t)$, since its property $\alpha_P(0) = 1$ would guarantee the constancy of the total cross-section σ_{ab} for $s \to \infty$ [see Eqs. (19), (20), (21)], which is one statement of the Pomeranchuk-theorem. We call the particle x from now on P.

In the same way, considering reactions $a + b \to c + d$ will lead to the "exchange" of a particle x with quantum numbers equal to those of a "bound state" of a and $\bar{c}$ (or $\bar{b}$ and d). This particle x will then be associated with a Regge-trajectory with just these quantum numbers. This means that each Regge-trajectory has a definite set of quantum numbers (strangeness, nucleon number, isospin etc.) attached to it. One may then conjecture that all "elementary" particles are just coming from Regge-trajectories passing at an integer ℓ. Prof. Van Hove will say more about this.

Consider now the total cross-sections σ_{aa}, σ_{ab}, σ_{bb} in the limit $s \to \infty$. From Eq. (17) follows

$$\sigma_{jk}(s \to \infty) = \frac{1}{s} \operatorname{Im} A_{jk}(s,0) = \frac{1}{is} A_{jk}(s,0) \qquad (42)$$

$$(j = a,b)$$
$$(k = a,b)$$

since $A_{jk}(s,0) \to$ purely imaginary for $s \to \infty$.

Before going on, we have to make one correction on what has been said so far. The form of Eq. (35) must actually be rewritten as

$$a(st) = i\beta(t) \frac{P_{\alpha(t)}(-\cos \Theta_t) \pm P_{\alpha(t)}(\cos \Theta_t)}{\sin \pi\alpha(t)}, \qquad (35')$$

which is required by crossing symmetry in relativistic scattering and by exchange potentials in non-relativistic scattering. The + sign applies to those trajectories where for $\alpha = \ell$, a physical state of odd ℓ exists (- sign for those leading to even ℓ). Since $\alpha(0) = 1$ means $\ell = 1$, we have to assign + to the Pomeranchuk trajectory. We have then for $t \to 0$ and $\alpha(t) \to 1$ a cancellation of the singularity, since the numerator

goes to zero as sin $\pi\alpha$ does. What essentially remains is

$$\sigma_{jk}(s \to \infty) = \beta_{jk}(0) .$$

Now from Eq. (40) we know that $\beta_{jk}(0)$ must factorize into a factor depending on particles j and P and another one depending on particles k and P. Hence, if we compare the graphs for aa, ab, bb scattering with one P exchanged, we find (Fig. 13)

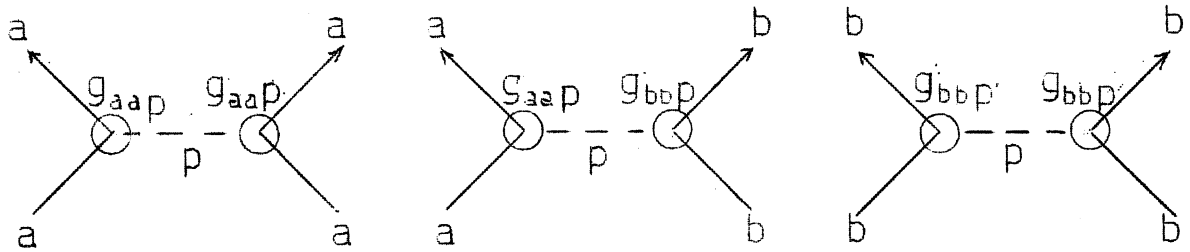

Fig 13

$$\sigma_{aa} = g_{aaP} \cdot g_{aaP}$$

$$\sigma_{ab} = g_{aaP} \cdot g_{bbP} \qquad (\sigma_{ab})^2_{tot} = (\sigma_{aa})_{tot} (\sigma_{bb})_{tot} \qquad (43)$$

$$\sigma_{bb} = g_{bbP} \cdot g_{bbP} \qquad \text{for } s \to \infty .$$

This is Gell-Mann's factorization theorem. It leads - if the presently used accelerator energies ~ 30 GeV are considered as "asymptotic" - to

$$\sigma_{\pi\pi} = (\sigma_{N\pi})^2/(\sigma_{NN}) = (25)^2/40 \approx 15 \text{ mb},$$

which is a quite reasonable figure.

Taking $a = \bar{b}$ we obtain Pomeranchuk's theorem, namely:

$$(\sigma_{aa}^{-})^2 = \sigma_{aa} \cdot \sigma_{aa}^{--} = (\sigma_{aa})^2$$

since $\sigma_{aa} = \sigma_{aa}^{--}$ is equal from C-invariance. Hence

$$\lim_{s\to\infty}(\sigma_{aa} - \sigma_{aa}^{-}) = 0 .$$

Of course, the difficulties and doubts expressed in Section VIII apply also to the considerations in the last two sections.

* * *

PART I.2

EXPERIMENTAL TECHNIQUES FOR MEASURING ELASTIC SCATTERING AT VERY HIGH ENERGY

A.M. Wetherell,
Nuclear Physics Division, CERN.

I. INTRODUCTION

In this talk I shall discuss experimental techniques which have been used for measuring the elastic scattering of strongly interacting particles in the momentum range of about 8-28 GeV/c. The range covers work done at the proton synchrotrons operating at Brookhaven, CERN and Dubna. Accelerator experiments on multi-GeV electron and muon scattering have only just begun and will not be discussed; some of the methods which I shall describe are directly applicable to these problems, however.

Before proceeding to descriptions of experimental methods I shall outline, qualitatively, the general features which are found in the high-energy elastic scattering of the strongly interacting particles. These features are important with respect to the choice of an experimental technique.

II. GENERAL FEATURES OF ELASTIC SCATTERING

In discussing scattering processes, it is often convenient to use the invariants s, equal to the square of the total centre-of-mass energy and t, equal to the square of the four-momentum transfer, as variables.

The energy variable is given by

$$s = M_1^2 + M_2^2 + 2E_1 M_2 \approx 2M_2 E_1 \qquad (1)$$

where the subscripts 1 and 2 refer to projectile and target particles respectively. For very high energies the approximate relation is useful.

The angle variable is given by

$$t = -2\bar{p}^2 (1 - \cos \bar{\Theta}) \approx -2p_1 p_3 (1 - \cos \Theta_3). \qquad (2)$$

In the approximate equation, which is useful when $\gamma_1, \gamma_3 >> 1$, the subscript 3 refers to the outgoing scattered particle.

At the energies which we are discussing, elastic scattering angular distributions are dominated by a large peak in the forward direction. This sharply falling peak is compatible with most of the scattering being due to diffraction, resulting from the absorption of the incident wave by the many inelastic channels open in the collision process. An optical Fraunhofer diffraction type of description[1] has been used for many years in discussing the shadow scattering in nuclear physics and it is still useful, for an orientation, in elementary particle physics. The familiar optical formula is

$$\frac{1}{\bar{K}^2} \frac{d\sigma}{d\bar{\Omega}} = \left(\frac{\sigma_{tot}}{2\pi}\right)^2 \left(\frac{J_1(\bar{K}R \sin \bar{\Theta})}{\bar{K}R \sin \bar{\Theta}}\right)^2 , \qquad (3)$$

$\bar{K}$ being the c.m. wave number and R the radius of the black diffracting sphere. This angular distribution has a forward peak within an angle (ℓ.s)

$$\Theta \approx \frac{3.8}{KR} \qquad (4)$$

and a succession of subsidiary peaks. It is only the main peak which concerns us, the others arise from the artificiality of the model, namely a black absorbing sphere.

To obtain a feeling for the diffraction pattern, let us take proton-proton scattering at 24 GeV/c. Putting $R \approx 1/M_\pi$ for the radius

of the strongly interacting matter in a proton, the optical model gives a diffraction angular distribution lying within a lab angle of about 30 mrad ($\approx 2°$).

The value of t corresponding to Eq. (4) and for $R \approx 1/M_\pi$ is

$$t \approx -25\, M_\pi^2 \approx -0.5\ \text{GeV}^2. \tag{5}$$

A good approximation to the Bessel function in Eq. (3), within the angle defined by Eq. (4) is a Gaussian

$$\left(\frac{J_1(x)}{x}\right)^2 \approx \frac{1}{4} \exp - \left(\frac{x}{2}\right)^2. \tag{6}$$

Using this approximation and going over to the variable t rather than momentum and angle, one obtains

$$\frac{d\sigma}{dt}(s,t) = \left(\frac{d\sigma}{dt}\right)_0 \exp \frac{1}{4} R^2 t \tag{7}$$

where

$$\left(\frac{d\sigma}{dt}\right)_0 = \frac{d\sigma}{dt}(s,0) = -\pi \left(\frac{\sigma_{tot}(s)}{4\pi}\right)^2. \tag{8}$$

Equation (7) leads one to expect that the diffraction distribution as a function of t should be exponential, the rate of fall characterized by the parameter R which is a constant. This behaviour, we shall see, is quite a good representation of experimental results. It turns out, however, that a better description of the data, in the diffraction region, is obtained if R is allowed to vary with energy, in fact it increases very slowly. Theoretically such a behaviour is expected from more sophisticated approaches, such as the Regge pole model.

Another point of great current interest concerns elastic scattering at very small angles. A general quantum mechanical theorem, the Optical Theorem [also Wick's inequality[2]] gives a relation between

the total cross-section and the forward differential elastic scattering cross-section. This is

$$\left(\frac{d\sigma}{d\Omega}\right)_0 \geq \left(\frac{\bar{K}\sigma_{tot}}{4\pi}\right)^2 . \qquad (9)$$

The equality holds for a pure imaginary scattering amplitude without spin dependence and one sees it for a specific case in Eq. (8) for the black absorbing sphere model. If the scattering amplitude is not pure imaginary and/or has a spin dependence then the forward scattering cross-section is greater than the optical value, as the quantity in relation Eq. (9) [or Eq. (8)] is called.

A real part to the scattering amplitude will interfere either constructively or destructively with the Coulomb scattering amplitude and, as the phase of the latter is known, observation of interference can lead to a determination of the phase of the real part of the nuclear amplitude and of course its magnitude. Observation of possible deviations from the optical limit and of Coulomb interference entail experiments at very small angles. An example of p-p scattering at 10 GeV/c, which will be discussed later, indicates that good measurements have to be done in the range of about 4 to 10 mrad.

The narrow, approximately exponential, forward diffraction peak accounts for practically all the elastic scattering total cross-section, nevertheless there is great interest in data on the small amount of elastic scattering outside the forward peak. This scattering at larger angles might, qualitatively, be called potential or hard-core scattering. The momentum transfers attainable with the particles from the proton synchrotrons are very large. As an example consider 24 GeV/c p-p scattering at 90° c.m.s. (about 16° symmetrically in the lab). Equation (2) gives $-t \approx 23$ GeV^2 and the corresponding distance probed by the strong interaction is of the order of 0.04 fermi. For backward scattering of non identical particles even higher momentum transfers can be attained.

The experimental technique chosen to measure a particular elastic process will therefore depend strongly on the angular region of interest. In the diffraction peak, very good angular precision from point to point on the angular distribution is needed. The cross-sections are large, in the order of barns/sterad. Outside the diffraction region, approaching 90° to 180° c.m., the technique has to cope with extremely small cross-sections, of the order of fractions of micro-barns/sterad. In all cases the momentum resolution has to be such as to discard events in which a single low energy pion has been created. In the light of these foregoing general points we shall discuss the various particle detectors available and their applications.

III. NUCLEAR EMULSION EXPERIMENTS

The nuclear emulsion technique has so far been used at multi-GeV energies only for measurements in the diffraction region where the cross-sections are very large and where good precision in angle measurements are needed. Three types of experiment can be discussed.

1. Forward camera experiments

The classic experiment of this type is that of Preston et al.[3] performed for proton-proton scattering at 3 GeV. A very narrow, well collimated, beam of momentum analysed particles enters a target (liquid hydrogen) and after a further momentum analysis the fast scattered particles are detected in nuclear emulsions in the horizontal scattering plane. At the high energies we are considering, the main problem seems to be in preparing a beam with the required optical properties, and reasonable intensity, only 2-3 mm in diameter. This has been attempted with rather high intensity proton beams and long, narrow collimators but the inelastic background from the defining slit generally seems to be severe. If this could be overcome by using very refined optics and an intense parallel beam, for example an extracted proton beam, then the method would offer

very good momentum (< 1%) and angular resolution (~ $\frac{1}{10}$ mrad). It would be suitable for an attack on the very small angle p-p scattering[4].

2. Perpendicular plate method

The perpendicular exposure method was described by Lyubimov et al.[5] and has been much used in the high-energy range. In this type of experiment a well collimated and momentum analysed beam bombards an emulsion stack (often water loaded to increase the free proton content) placed accurately perpendicular (to < 2 mrad) to it. The emulsions are area scanned for recoil protons from elastic scattering events. For small angle scattering the recoils lie almost in the plane of the emulsions. The candidates for elastic scattering events can be separated from inelastic and quasi-elastic events by satisfying the elastic kinematics with respect to:

a) the recoil proton range and fast scattered particle angle;
b) the recoil proton range and recoil proton angle;
c) the recoil proton and fast scattered particle must be coplanar.

Bull and Garbutt[6] have reported work on 24 GeV/c and 19.8 GeV/c p-p scattering using this technique. They were able to obtain a precision of a few tenths of an mrad on the angle of the scattered particle, in the range of 3-10 mrad, and for a few per cent on the angle of the recoil. A criticism noted in this experiment is the low scanning speed required and subsequent slow rate of accumulation of data. As a result, this type of experiment is very limited in statistical accuracy, which seems to be so vital in looking at the probably subtle energy and angle variations of the small angle scattering.

Figure 1 shows a collection of data[7] from small angle p-p experiments at various energies. Most of the points come from work done with perpendicular plates. The Coulomb cross-section has been subtracted. There appears to be a tendency for the points to fall above the optical limit. Clearly, greater statistical weight and more points at each energy are needed. The result obtained by Bull and Garbutt at 19.8 GeV/c[7] is

$$\frac{\sigma_{el}(0)}{\sigma_{optical}} = 1.60^{+0.34}_{-0.28} .$$

It is interesting to look, now, at the result of a Regge pole calculation by Phillips[8,9] for 10 GeV/c p-p scattering. This model uses three Regge poles, the Pomeranchuk pole P, the ω pole and a second vacuum pole P'. The two latter poles give an appreciable real part to the scattering amplitude and Figure 2 shows the nuclear cross-section and also the nuclear plus Coulomb plus interference cross-sections. The two possibilities, namely destructive and constructive interference, depending on the sign of the real part, are given. The deviation of the nuclear cross-section from the optical limit is about 20%. Figure 2 makes the need for good statistics and angular resolution very clear.

3. Recoil proton method

An experiment of this type for 6 and 10 GeV p-p elastic scattering has been described by Bekker et al.[10]. Figure 3 shows the experimental arrangement. Recoil protons from elastic scatters of the internal beam of the Dubna synchro-phasotron in a CH_2 target were detected in nuclear emulsions placed at essentially 90° from the beam. About 10^4 elastic p-p events were collected and precise range and angle measurements made on the recoils. It is worth noting, at this point, some kinematics for the recoil nucleon. The kinetic energy of the recoil is given by

$$T_r = \frac{-t}{2M_N} \approx \frac{p^2\Theta^2}{2M_N} . \qquad (10)$$

The approximate relation holds for high energies and small angles. As an example, let us take 10 GeV/c p-p collisions and a scattering angle of 10 mrad, then T_r = 5.3 MeV and the recoil angle is close to 90°. A 1½% change in the momentum of the fast scattered particle changes T_r by 3%, or 160 keV. For p-p experiments this method seems to have much to commend it and can probably be extended to much higher energies. A disadvantage in the Dubna measurement was the lack of an absolute cross-section scale as it was not known how many incident protons had passed through the target. This could probably be measured by a radiochemical method using a spallation activity in the carbon contained in the CH_2 target.

IV. BUBBLE CHAMBER EXPERIMENTS

The large liquid hydrogen bubble chambers (~ 1 m) seem to be very suitable instruments for obtaining data with good statistical accuracy on elastic scattering in the diffraction peak and also significant data very much outside, in special cases[11].

An experiment on $\pi^- p$ scattering at 10 GeV/c has been carried out at CERN by Brandt et al.[12] using pictures from the Ecole Polytechnique 80 cm liquid hydrogen bubble chamber. From 45,000 pictures 1706 elastic events up to $t = -1.4$ GeV^2 were obtained, 55 being outside $|t| = 0.5$ GeV^2 (70 mrad lab angle). Usable data exists in the range of $-t = 0.008$ to 0.02 i.e. about 9-14 mrad pion angle, corresponding to a recoil proton range of 3-10 mm. Measurements of the scattered pion momentum, the recoil proton energy and the two angles were made on two prong candidates and a kinematic least squares fit programme applied to select the elastic events. Some numbers with respect to resolving power are as follows: for a 40 cm long track the momentum resolution on a 10 GeV/c pion was $\approx 8\%$; for a stopping proton the energy resolution was $\approx \frac{1}{2} - 1\%$ and for a curvature measurement on a fast recoil proton about 2-5%.

Unfortunately I cannot show any data from this experiment as it has only just been completed. The physical points emerging will be the shape of the diffraction peak and a good extrapolation to the forward direction for an optical limit comparison.

It appears that the main difficulty with this type of experiment lies in the precise measurements which have to be made, the scanning is no problem.

V. COUNTER EXPERIMENTS

Counter techniques applied to high-energy elastic scattering appear, so far, to be useful over all parts of the angular distribution except in the region of very small angles, namely < 10 mrad.

The experiments I shall discuss have been done mainly at CERN and have studied p-p scattering both in the diffraction[13] and rather large momentum transfer regions[14,15].

Figure 4 shows the two types of CERN experiments. In the internal beam experiments the momentum spectra of protons scattered from alternating CH_2 and C targets were measured using 2 × 2 m magnets and five counter telescopes. Employing a radio-chemical method (Be^7 activity), a difference could be taken and p-p momentum spectra obtained together with an absolute cross-section normalization. These measurements were done for momenta between 8.94 and 27.83 GeV/c and at scattering angles of about 20, 60 and 110 mrad. The momentum resolution turned out to be about 1½% and the elastic scattering was well resolved.

The scattered out external beam measurements were done using a 20 cm liquid hydrogen target and counter telescopes placed at about 10, 20, 30, 40 and 50 mrad scattering angles. 2 × 2 m magnets were used for momentum analysis. The momentum resolution in this case was about 6% and an unfolding procedure was used to separate the elastic scattering momentum peak from the continuous inelastic contributions.

Figure 5 gives a 110 mrad proton momentum spectrum and shows the best resolution achieved. The inelastic bumps correspond to excitation of the second and third isotopic spin ½ nucleon resonances, the cross-sections for these excitations are very valuable data. Figure 6 shows how the detection of the elastic scattering momentum spike degenerates as the cross-section falls with increasing momentum transfer and energy.

Figure 7 contains two momentum spectra from the external beam measurements. Using the known resolution functions for the spectrometer, the experimental points were fitted by varying the inelastic scattering contributions close to the elastic peak. The procedure gave both the elastic cross-sections and estimates of cross-sections at small inelasticities.

Another type of high momentum transfer p-p experiment, using an internal proton beam, has been performed by Baker et al.[16] at Brookhaven. In these measurements both scattered and recoil protons were momentum

analysed and detected. Data only on elastic scattering were then obtained. It was possible to measure rather small cross-sections confidently, as only events from p-p collisions were recorded due to the tight constraints imposed by the geometry and momentum selection. Figure 8 shows the layout of the Brookhaven experiment, the c.m. scattering angle was 68.5°, the incident momentum 11.2 GeV/c and $t = -6.15\ \text{GeV}^2$.

The experimental data from these p-p experiments are shown in Figures 9 and 10. Figure 9 presents the cross-sections normalized to the optical value and plotted as a function of t. The range of cross-section covered is enormous $\sim 10^7$; at $t = -0.5\ \text{GeV}^2$, the end of the diffraction region [Eq. (5)], the cross-section has fallen to $\sim 10^{-2}$ of its forward value. Another way of presenting the data is shown in Figure 10 where the normalized cross-sections are plotted as a function of s at fixed values of t. This figure shows a slow shrinking of the elastic angular distribution with increasing energy. The data have been analysed[15] in terms of a single Pomeranchuk Regge pole using the formula

$$\left(\frac{d\sigma}{dt}\right) = \left(\frac{d\sigma}{dt}\right)_0 F(t) \left(\frac{s}{2M^2}\right)^{2\alpha(t)-2} . \qquad (11)$$

A possible approximation for $\alpha(t)$ and $F(t)$ was found to be (for $0 < -t < 0.5\ \text{GeV}^2$)

$$\alpha(t) = 1 + \alpha'(0)t \qquad (12)$$

$$F(t) = e^{\gamma t} . \qquad (13)$$

Substituting Eq. (12) and Eq. (13) in Eq. (11) one obtains

$$\left(\frac{d\sigma}{dt}\right) = \left(\frac{d\sigma}{dt}\right)_0 \exp\left[\gamma + 2\alpha'(0)\ln\left(\frac{s}{2M^2}\right)\right] t . \qquad (14)$$

Equation (14) shows an exponential behaviour in t with an energy dependent, exponent, as distinct from the constant parameter R of the optical model [Eq. (7)].

There are serious current doubts as to whether this analysis is valid.

The smallest angle cross-sections from the external beam measurements (down to angles of 10 mrad) were extrapolated exponentially in t to t = 0 and gave, relative to the optical value, 1.2 ± 0.2, a not highly significant result.

An elaborate counter experiment has very recently been performed at Brookhaven by Lindenbaum et al.[17]. The scattering distributions of $\pi^{\pm}$, p, $\bar{p}$ and $K^{\pm}$ have been measured at several energies in the diffraction region. The incident particles were identified using differential gas Čerenkov counters and their directions and momenta measured with counter hodoscopes and magnets. Both scattered and recoil particles were measured in direction and also the momentum of the fast scattered particle by a spectrometer and hodoscope. The information from the detectors and logic circuits was put directly into an on-line computer, which both monitored the correct operation of the experimental apparatus and also provided computed cross-sections rapidly.

Preliminary results from an experiment on backward $\pi^{+}p$ scattering at 3.14 and 4.6 GeV/c have been reported by Kulakov et al[18]. The method employed was to measure the direction and velocity of the knock-on proton and to detect in coincidence the low energy wide angle pions. A similar experiment is planned[19] at CERN for higher energies and with better momentum resolution (≈ 2%) on the knock-on proton.

VI. SPARK CHAMBER EXPERIMENTS

The spark chamber technique offers very versatile systems for measuring elastic scattering over all angular ranges. The spatial resolution of spark chambers is better than 1 mm, about a factor 10 down on most scintillation counter arrangements. The chambers can be made so as to interpose very little superfluous scattering material in beams. A defect is the limitation in beam intensities which can be passed through them; as their time resolution is ~ 1 μsec, it is necessary to limit

the number of particles passing through during an accelerator pulse of say 100 ms to something like 10^4.

I shall immediately describe an experiment recently performed at CERN on $\pi^{\pm}$p and p-p scattering at 8, 12 and 18 GeV/c in the range of lab angles 21-150 mrad. Some of the names connected with this work are G. Giacomelli, D. Harting, L.W. Jones and W.C. Middelkoop. Figure 11 shows the experimental arrangement in which, after velocity selection, the beam scatters on a liquid hydrogen target and both the scattered and recoil particles are detected. The separations between all the direction defining spark chambers was 1 m, the pion directions were found to ± 0.7 mrad (s.d.) compatible with a location accuracy of about 1 mm. The recoil proton direction was measured to ± 2 mrad, its cut-off energy was about 60 MeV equivalent to a pion scattering angle of about 20 mrad at 18 GeV/c.

The method of analysis of the events has proceeded variously but one method has been to subject the measured quantities p_π (in), Θ_π, Θ_p and p_π (out) to a kinematic least squares fit programme, the events with large χ^2 coming out have been proved to be inelastic and a "reasonable" cut is made in the χ^2 distribution. This method is supposed to be very safe with respect to rejecting inelastic events or throwing out real elastic ones.

A disturbing feature about this type of experiment is the time and effort needed for the analysis and measurement of the pictures obtained, in this case about 500,000.

Another type of spark chamber experiment has been begun by Cocconi et al.[20]. In this experiment the spark positions are recorded by a measurement of the time of flight of the sonic shock wave from them, using a method of Maglić and Kirsten[21]. No pictures are taken.

Figure 12 shows the schematic layout of this experiment which is to measure high-energy p-p scattering in the interval 10-27 GeV/c and in the angular range of about 2-20 mrad. Only the scattered particle

is detected. The aim is to obtain the cross-section at about 10 angles in this range to a statistical accuracy of 3% and with small systematic errors.

An angular resolution of 0.35 mrad is obtained from the geometry shown in Fig. 12, assuming a spark location accuracy of 1 mm. The momentum resolution is, geometrically, about 0.6%; it should be noted that the experimental arrangement is very long, extending over about 40 m.

So far only tests have been made with beam particles passing through the whole system. The sonic detection system using four detectors in each gap of the six two gap chambers gives spark locations to about ± ¼ mm. It is hoped to perform the experiment before the end of the year, using an IBM 7090 computer to store and analyse the data from each event as it comes.

VII. THE HIGH ENERGIES OF THE FUTURE

Proton synchrotrons in the range of 100-300 GeV (giving ≈ 13.7 - 23.7 GeV in the c.m.s.) are now being discussed. It is interesting to look at some of the magnitudes which will be involved in working on elastic scattering problems with particle beams in this range of energies. Figure 13 shows an extrapolation of the CERN 12-26 GeV/c p-p results [using essentially the dependence in Eq. (14)] to 300 GeV. The angular range of the diffraction peak becomes extremely small and experiments aiming to measure the fast scattered particle will have to become rather long, spatially, to obtain any significant separation between scattered and unscattered particles. It should also be noted that the magnitude of the energy resolution needed, namely, the pion mass divided by the incident momentum, becomes very small, for example ≈ 0.14% at 100 GeV.

It would appear possible to extend counter hodoscope experiments in a reasonably straight forward way to these energies. For spark chambers the long flight paths involved will provide difficulties with respect to the time needed (~ several μsec) to form trigger signals.

The highest machine energy of all realistically planned for the future is provided by the CERN proton synchrotron storage ring project. In this two 25 GeV/c proton beams collide head on providing 50 GeV in the c.m.s. In order to obtain this in a stationary target collision, the incident projectile would need to have a momentum of 1330 GeV/c. Experiments with colliding beams have not yet been done and probably radical new methods will have to be used; nevertheless de Raad[22] has looked at the possibilities for elastic scattering experiments at 50 GeV c.m.s. using the proposed proton storage rings. The idea is attractive as the scattered particles have manageable energies.

Figure 14 gives an idea of the scale of this experiment. Magnets B_1 and B_1' could be extended to provide momentum analysis for the scattered particles. Detection would be by spark chamber and counter hodoscope systems. The counting rates estimated do not seem impossibly low for small scattering angles. A circulating beam current of 20 A (3.6×10^{14} protons stacked) is specified. An example worked out for 30 mrad gives about one elastic event per second in the solid angle of the detection system ($\approx 3.10^{-5}$ sterad). This high-energy scattering experiment would seem to be the most challenging, both technically and theoretically, yet discussed.

* * *

REFERENCES

1. S. Fernbach, R. Serber and T.B. Taylor, Phys.Rev. 75, 1352 (1949).

2. G.C. Wick, Phys.Rev. 75, 1459 (1949).

3. W.M. Preston, R. Wilson and J.C. Street, Phys.Rev. 118, 579 (1959).

4. G. Cvijanovich, J. Pahl and H. Winzeler, EmC 62/4.

5. V.G. Lyubimov, P.K. Markov, E.N. Tsyganov, Chen Pu-ing and M.G. Shafranova, Soviet Phys. JETP 10, 651 (1961).

6. V.A. Bull and D.A. Garbutt, Proc. Aix-en-Provence International Conference, 1961, Vol.I, page 85.

7. V.A. Bull and D.A. Garbutt, private communication.

8. R.J.N. Phillips, Phys.Letters 3, 184 (1963).

9. F. Hadjioannou, R.J.N. Phillips and W. Rarita, Phys.Rev.Letters 9, 183 (1962).

10. B. Bekker, L. Kirillova, A. Nomofilov, V. Nikitin, V. Pantuev, V. Sviridov, L. Strunov, M. Khachaturian and M. Shafranova, Proc. International Conference on High-Energy Physics, CERN 1962, p. 582.

11. Y. Goldschmidt-Clermont, M. Guinea, T. Hofmokl, R. Lewisch, D.R.O. Morrison, M. Schneeberger and S. Unamuno, Proc. International Conference on High-Energy Physics, CERN 1962, p. 84.

12. S. Brandt, V.T. Cocconi, D.R.O. Morrison, A. Wroblewski, P. Fleury, G. Kayas, F. Muller and C. Pelletier, private communication.

13. A.N. Diddens, E. Lillethun, G. Manning, A.E. Taylor, T.G. Walker and A.M. Wetherell, Phys.Rev.Letters 9, 108 (1962).

14. G. Cocconi, A.N. Diddens, E. Lillethun, G. Manning, A.E. Taylor, T.G. Walker and A.M. Wetherell, Phys.Rev.Letters 7, 450 (1961).

15. A.N. Diddens, E. Lillethun, G. Manning, A.E. Taylor, T.G. Walker and A.M. Wetherell, Phys.Rev.Letters 9, 111 (1962).

16. W.F. Baker, E.W. Jenkins, A.L. Read, G. Cocconi, V.T. Cocconi and J. Orear, Phys.Rev.Letters 9, 221 (1962).

17. S. Lindenbaum et al., private communication*).

*) This work has been published, since the present lecture was given, by K.J. Foley, S.J. Lindenbaum, W.A. Love, S. Ozaki, J.J. Russell and L.C.L. Yuan, Phys.Rev.Letters 10, 376 (1963)

18. B.A. Kulakov, M.F. Lykhachev, A.L. Lyubimov, Yu.A. Matulenko, I.A. Savin and V.S. Stavinski, Proc. International Conference on High-Energy Physics, CERN 1962, p. 584.

19. G. Weber, private communication.

20. G. Cocconi, E. Lillethun, B. Maglić, G. Manning, A.E. Taylor, T.G. Walker and A.M. Wetherell, private communication.

21. B.C. Maglić and F.A. Kirsten, Nucl.Instr. and Meth. 17, 49 (1962).

22. B. de Raad, AR/Int. S.G./62-2, Sept. 1962.

23. S.A. Azimov, Do In Seb, L.F. Kirillova, E.M. Khabibullina, E.N. Tsyganov, M.G. Shafranova, B.A. Shakhbazyan and A.A. Yuldashev, Joint Institute for Nuclear Research, Preprint R-797, Dubna (1961).

24. E.N. Tsyganov, Joint Institute for Nuclear Research, Preprint D-882

25. A.I. Zlateva, P.K. Markov, A.T. Peeva, L.G. Khristov and Kh.M. Chernov, Doklady Bolgarskoi Akademii Nauk 14, 443 (1961).

26. Do In Seb, L.F. Kirillova, P.K. Markov, L.G. Popova, I.N. Silin, E.N. Tsyganov, M.G. Shafranova, B.A. Shakhbazyan and A.A. Yuldashev, JETP 14, 1243 (1962).

27. E. Marquit, University of Warsaw, private communication.

28. G. Czapek, G. Kellner and G. Otter, private communication.

29. D.R.O. Morrison, International Conference on Theoretical Aspects of Very High-Energy Phenomena, CERN 1961, p. 153.

30. B. Cork, W.A. Wenzel and C.W. Causey, Jr., Phys.Rev. 107, 859 (1957).

* * *

DISCUSSION

Hoogland : I heard about a very recent experiment on p-p scattering that also in the case of p-p scattering there were difficulties with the narrowing of the diffraction peak; in fact that this narrowing was smaller than in the CERN experiment. Is that true?

Wetherell : This is true. There has been a recent experiment at Brookhaven by Lindenbaum et al. on p-p and π-p scattering at high energies up to 20 GeV. In these experiments they did rather better measurements on the p-p than we were able to do and what they found is shown in Fig. 1.

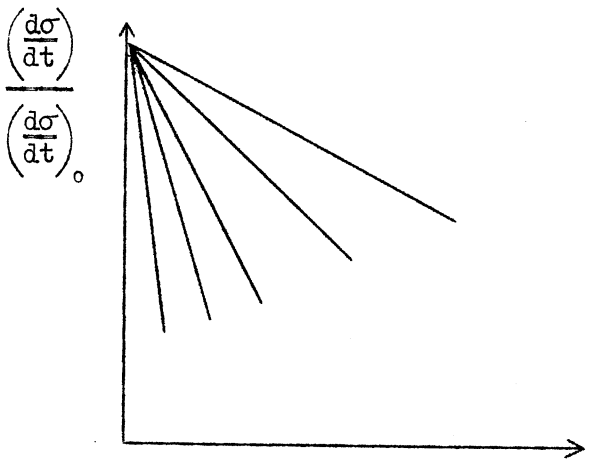

Fig. 1

One found here a family of curves certainly going down as we did at CERN. However, as they went to high energies they had better measurements, better accuracy on their points. They found that the rate of change of the curves was getting slower, that is to say they were crowding together at highest energies. One can say then that perhaps the single Regge-pole approach, which is this $s^{2\alpha(t)-2}$ business, does not work. It might even be that none of it works at all because one may find if one goes to high enough energy they do not shrink any more. We had a glimmer of this in our measurements at CERN but the error was too large really to say anything about the gradient across these curves.

Wetherell (cont.) : Another result from Lindenbaum et al. is that all curves for π-p scattering lie together (Fig. 2).

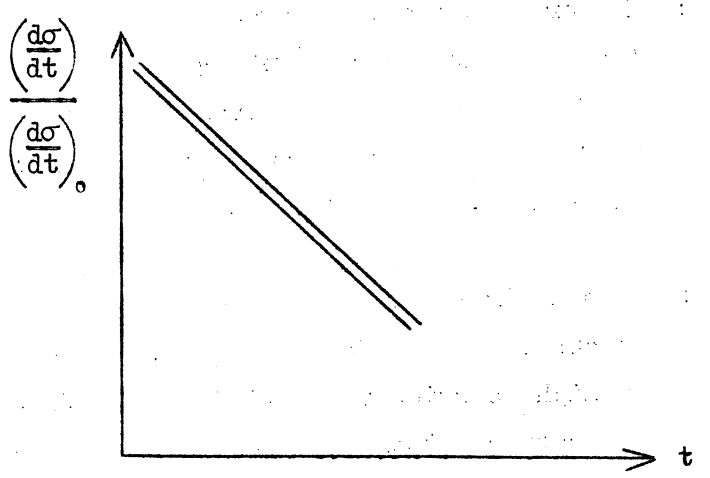

Fig. 2

There is no shrinking which is very interesting.

* * *

66/NP/smg

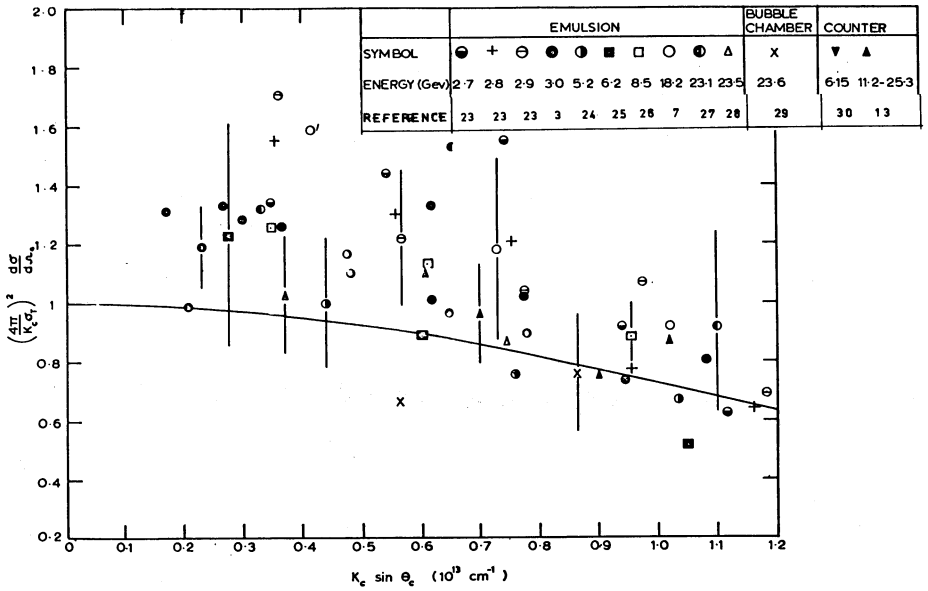

Fig. 1 Data from very small angle p-p elastic scattering experiments.

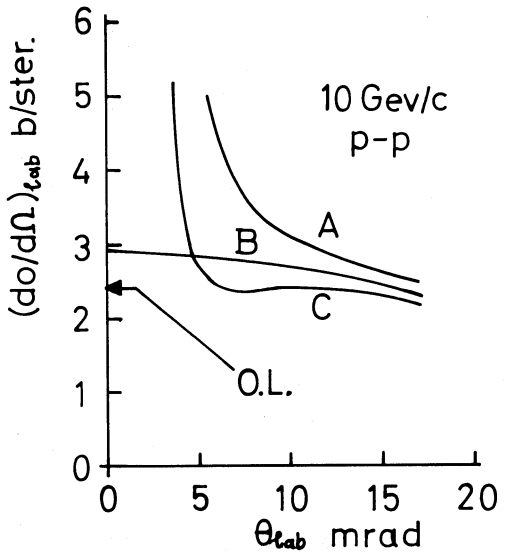

Fig. 2 Small angle p-p scattering at 10 GeV/c according to a three-Regge-Pole model of Phillips[8),9)]. Curve B is the pure nuclear scattering, A nuclear and Coulomb with constructive interference and C with destructive interference. The Optical Limit is marked O. L.

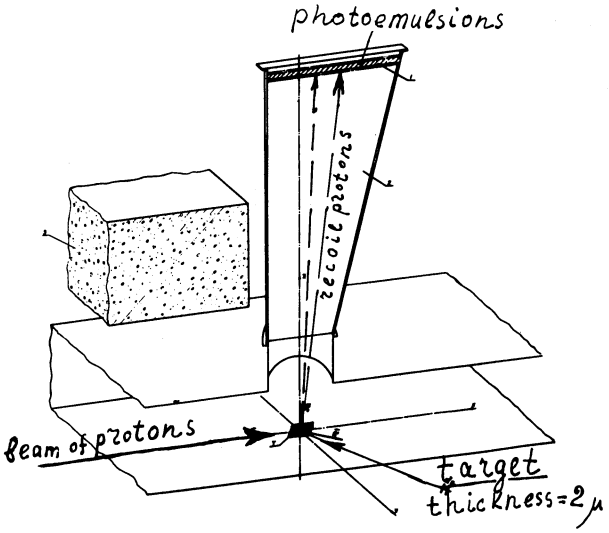

Fig. 3 Experimental arrangement in Dubna proton recoil measurements.

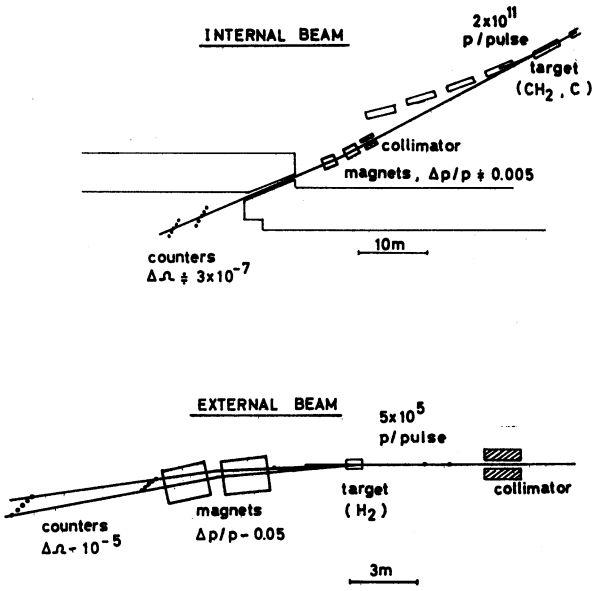

Fig. 4 Experimental layouts for CERN elastic p-p scattering experiments.

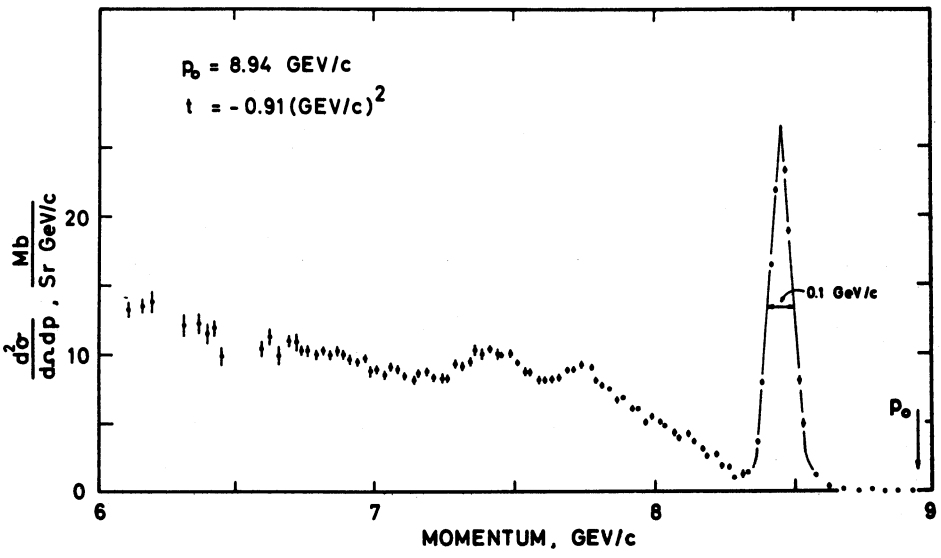

Fig. 5 Momentum spectrum from internal beam p-p measurements. The scattering angle was 110 mrad and the incident momentum was 8.94 GeV/c.

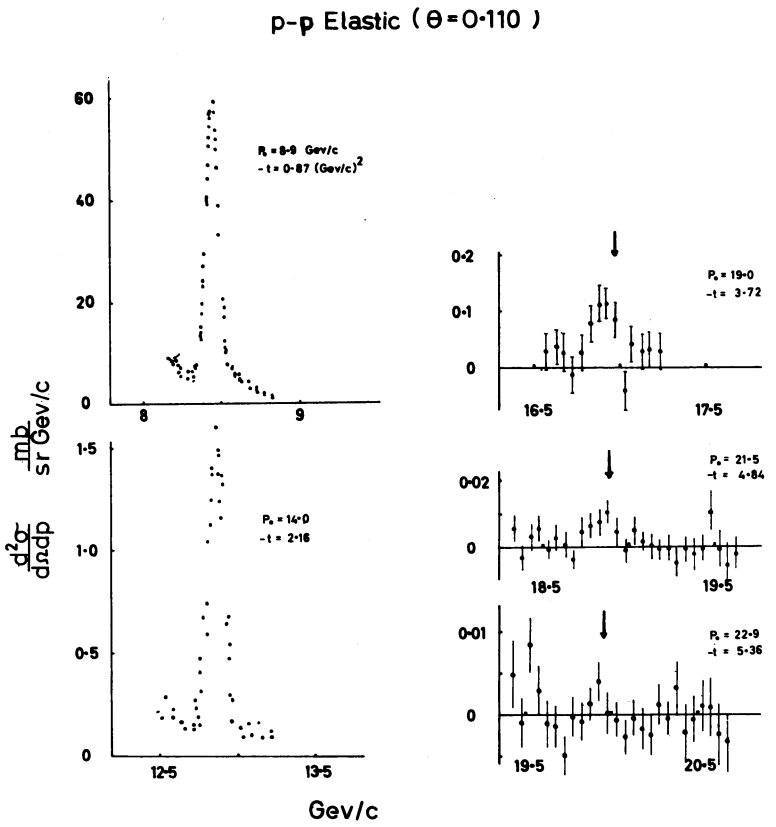

Fig. 6 p-p scattering momentum spectra measured at 110 mrad and various momenta using the CERN proton synchrotron internal beam. The arrows mark the expected positions of the elastic peaks.

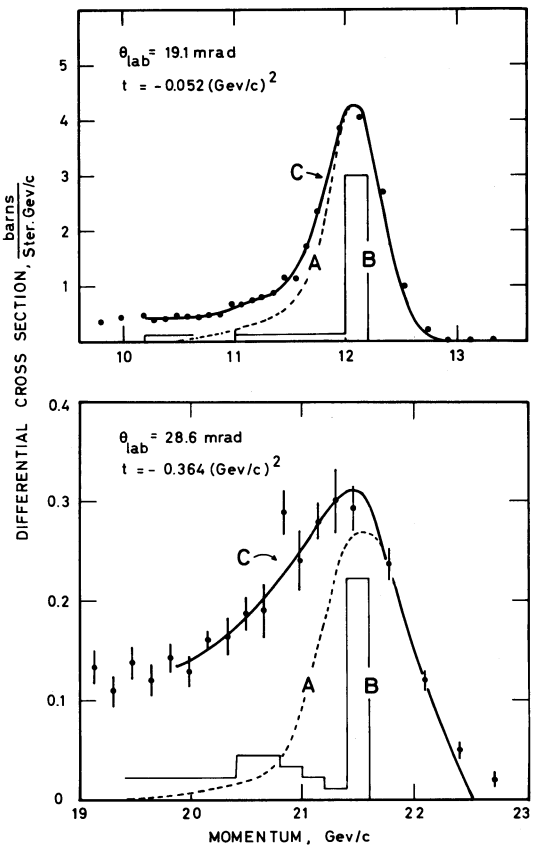

Fig. 7 Proton momentum spectra from the external beam CERN measurements.

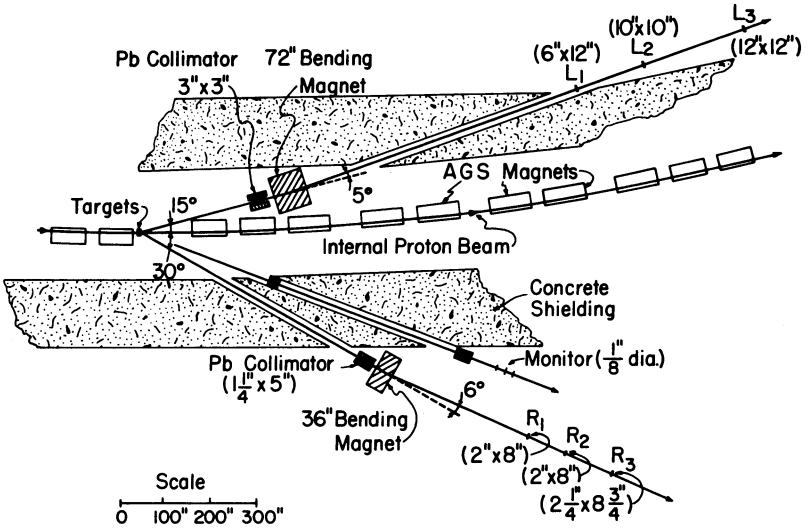

Fig. 8 Experimental layout for the Brookhaven measurement of p-p scattering at 11.2 GeV/c and $t = -6.15$ GeV^2 ($\theta_{cm} = 68.5^o$).

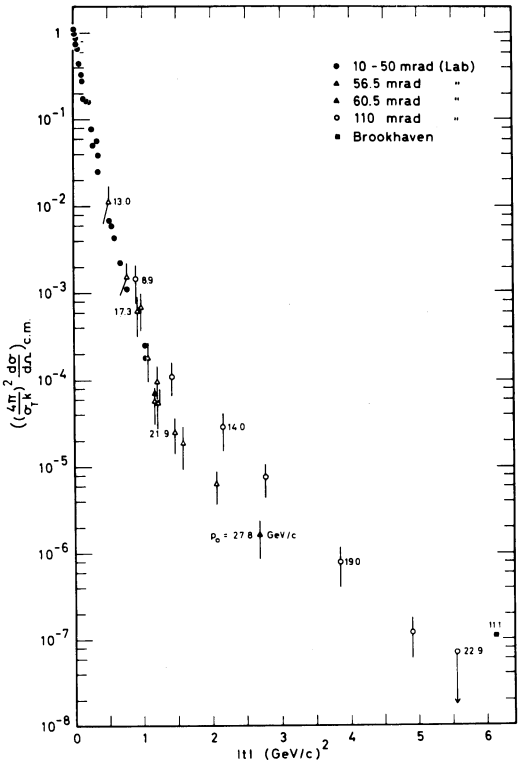

Fig. 9 p-p elastic differential cross sections normalized to the optical value for forward scattering and plotted as a function of t.

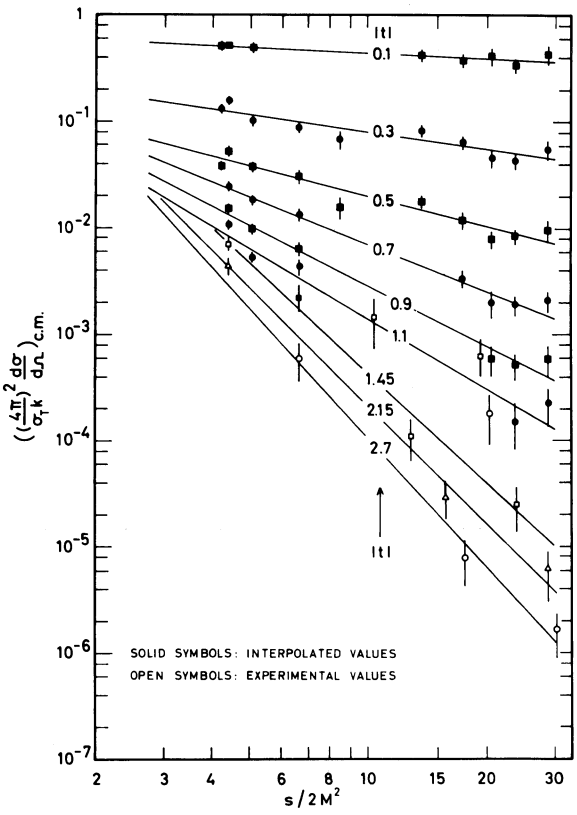

Fig. 10 p-p elastic differential cross sections normalized to the optical value for forward scattering and plotted as a function of s at fixed t values.

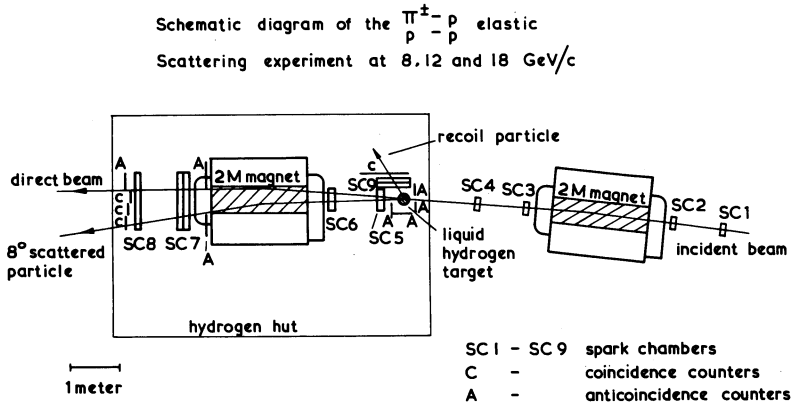

Fig. 11 Layout of high-energy π^- p and p-p elastic scattering experiment done at the CERN proton synchrotron using spark chambers.

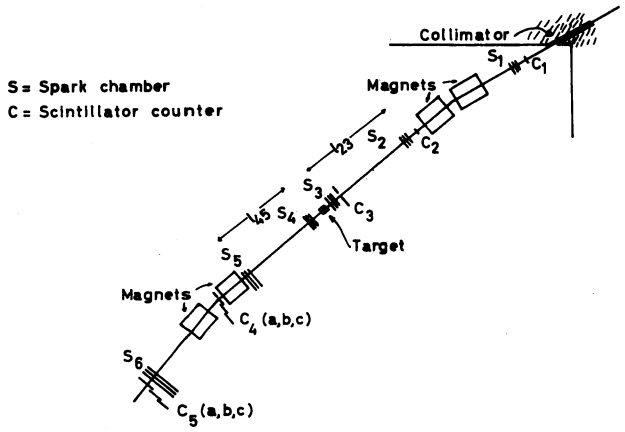

Fig. 12 Layout of sonic spark chamber experiment for small angle p-p scattering measurements at CERN.

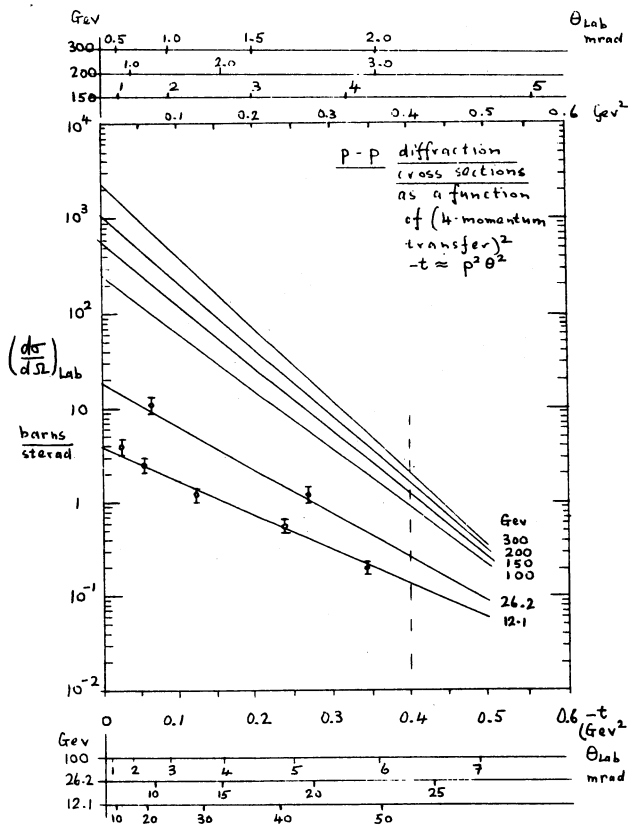

Fig. 13 p-p diffraction cross sections extrapolated to 300 GeV.

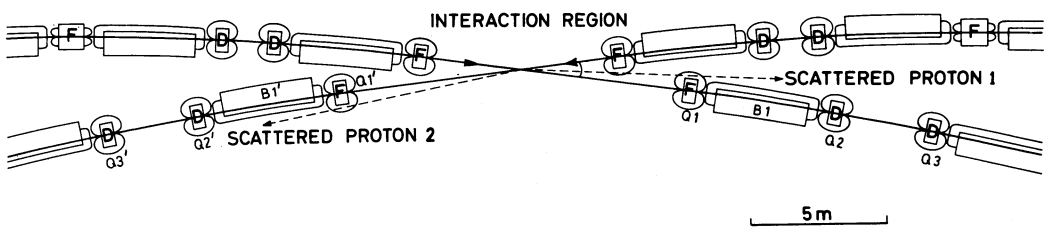

Fig. 14 Proton-proton scattering by colliding beams in storage rings.

II. ELEMENTARY PARTICLES

PART II.1

THE CLASSIFICATION OF ELEMENTARY PARTICLES

L. Van Hove,
Theory Division, CERN.

I. INTRODUCTION

I will deal with two principles of classification of elementary particles which in recent times seem to have had some success and are of great use for the discussion of experimental results on new resonances and particles, as well as for the possible discovery of new resonances or particles.

The first of these principles of classification is based on Regge poles and is closely connected with the discussion of Regge poles in scattering that was given to you by Dr. Hagedorn. It is a principle of classification according to angular momentum. One puts together particles in angular momentum series, i.e. in series where within the same series only the spin changes.

The second principle of classification is completely different and can be regarded as complementary to the first one. It is based on the so-called unitary symmetry, which is an extention of the isotopic spin symmetry and which classifies particles by putting them in groups with the same spin.

My first topic is the classification of particles in angular momentum series. I shall introduce this subject by taking first a topic in atomic theory, then an example in low-energy nuclear physics, and then go over to the proposal of Chew and Frautschi to classify elementary particles and resonances according to this principle. In the course of this discussion we shall meet with the concept of Regge poles.

II. CLASSIFICATION OF ELEMENTARY PARTICLES ON REGGE TRAJECTORIES

1. Regge trajectories of the excited states of the hydrogen atom

Suppose that one were given by the experimentalists the atomic levels of the hydrogen atom and that one plotted them as shown in Fig. 1. Horizontally one plots the energy made dimensionless by using the usual unit $me^4/2\hbar^2$, where m and e are the mass and charge, respectively, of the electron, and the ordinate is the orbital angular momentum ℓ for each of the atomic states. For each value of ℓ ($\ell = 0,1,2...$) the energy levels are $-1/n^2$ with $n = \ell+1, \ell+2, \ldots$. The principle of classification which we discuss corresponds to grouping levels into families lying on the curves in the (E,ℓ) plane which are defined by the equation

$$\sqrt{-\frac{me^4}{2E\hbar^2}} = \ell + \nu \,, \qquad (1)$$

with ν a parameter of values $\nu = 1,2,3...$ (see Fig. 1).

To study the hydrogen atom one starts from the Schrödinger equation:

$$\left(-\frac{\hbar^2}{2m}\nabla + V\right)\Psi = E\,\Psi \,, \qquad (2)$$

where V is the potential and m is the mass of the electron. One separates the radial and the angular parts of the wave function in the usual way, using the quantum numbers ℓ and m for the angular part,

$$\Psi = \frac{R(r)}{r} P_\ell^m(\cos\Theta)e^{im\varphi}$$

$$\frac{d^2R}{dr^2} + \left(\frac{2m(E-V)}{\hbar^2} - \frac{\ell(\ell+1)}{r^2}\right)R = 0 \,. \qquad (3)$$

The latter is the radial wave equation where $\ell(\ell+1)/r^2$ can be regarded as describing the centrifugal potential.

Then one determines the eigenfunctions of this equation satisfying the proper boundary conditions, which requires that the function R is regular at the origin and that it drops rapidly to 0 at infinity as is required for a bound state. One thereby finds the relation (1) between E and ℓ. Now if we keep ν fixed in Eq. (1) we can treat ℓ as a continuous parameter. This gives the curves of Fig. 1. The physical states, however, only correspond to the points on these curves for which the orbital angular momentum ℓ takes integral values.

This is an example of how one can classify levels in families by a mathematical procedure allowing one to establish some kind of continuity between the allowed values of the angular momentum.

2. Regge trajectories for bound states of a general potential

Let us now discuss the case of a general potential. One can consider for every potential V the radial Schrödinger equation for continuous values of the parameter ℓ and thereby define quite generally trajectories, analogous to those in Fig. 1. Let me illustrate this by assuming an attractive potential V(r) (curve I of Fig. 2). I combine it with the centrifugal potential and obtain

$$W = V + \frac{\hbar^2}{2m} \frac{\ell(\ell+1)}{r^2} . \qquad (4)$$

The shape of W for $\ell > 0$ is shown by curve II of Fig. 2. I now consider a bound state of the radial Schrödinger equation for a given arbitrary value of ℓ. This gives a level at a certain energy E. I then let the parameter ℓ vary slowly in a continuous fashion, thereby deforming the potential W. If ℓ increases, the potential will go up, and if ℓ decreases it will go down. It is clear that the level will move up and down in the course of this variation. Unless ℓ is increased so much that the level becomes unstable we have a level energy E which is a real continuous function of ℓ:

$$E = E_r(\ell)$$

or, by inverting this relation,

$$\ell = \ell_r(E)$$

where the index r labels the level (there may be several such levels). Whenever ℓ is 0, 1, 2,... the level is physically significant; it is a real bound state of the particle. When ℓ has a non-integral value it has only a mathematical significance. This is the kind of consideration which classifies levels in series of angular momentum states. The quantity $\ell_r(E)$ is called a Regge pole at energy E, because it turns out to be a pole of the S-matrix corresponding to the scattering problem at energy E (see Hagedorn's lectures). The curve described by $\ell = \ell_r(E)$ when E varies is called a Regge trajectory and is schematically shown in Fig. 3. The meaning of $\ell = \ell_r(E)$ as a function of E is the following. Up to now we took a particular ℓ, looked for the corresponding levels $E_r(\ell)$, and saw how they varied with ℓ. For a particular value of ℓ one will not, in general, have any bound state corresponding to a given value E. But by changing the angular momentum ℓ, thereby changing the shape of the W potential, one will find a potential W that accommodates a level at E. This will be found for $\ell = \ell_r(E)$. What one does is to find the centrifugal force which is necessary in order to get exactly a bound state at the energy E. So the physical significance of $\ell_r(E)$ in the region of bound states (E negative), is that $\ell_r(E)$ is the value of the angular momentum which would be just strong enough to give a bound state with energy E. Up to now we have discussed only the bound state region $E < 0$. Positive values of E will be discussed presently.

3. Trajectories in the scattering region E > 0 for a general potential

For positive values of the energy E the main phenomenon that occurs is scattering of the particle by the potential. However, there may still be something left which is very analogous to the bound states

discussed above, namely metastable states (they are states which are approximately stationary, but only for a limited lifetime, after which they decay). They allow us to continue the curve I of Fig. 3 to positive values of E. Let me go back to the consideration of one particular level $E = E_r(\ell)$. Let me increase the centrifugal force, thereby moving the potential and the level upward. Eventually I may have a situation as depicted in Fig. 4. The level has reached a position where E is above zero and it has a possibility to leak out through the potential barrier formed by the centrifugal potential. It is a metastable state, the instability of which is mathematically described by the fact that the energy E has a small positive imaginary part. Such a metastable state manifests itself in scattering as a resonance. At this stage, in the equation $E = E_r(\ell)$, E has become complex for real ℓ, hence the inverse relation $\ell = \ell_r(E)$ will give complex ℓ for E real positive. This complex function $\ell_r(E)$ of real E is the continuation of the Regge trajectory for $E > 0$ (see Fig. 3).

How can the complex angular momentum $\ell_r(E)$ be interpreted physically? ℓ enters into the expression for the potential W through the centrifugal barrier term. Hence ℓ becoming imaginary implies that W acquires an imaginary part. Remember, now, the significance of an imaginary part to a potential, e.g. in the optical model for the scattering of neutrons by nuclei: when the neutrons are elastically scattered from nuclei which at the same time absorb them, this can be formally represented by an imaginary part to the so-called optical potential which describes elastic scattering. The sign of the imaginary part must be chosen correctly to represent absorption (it must be negative when the Schrödinger equation is written $i\,\partial\psi/\partial t = H\psi$). If the opposite sign were chosen, it would represent creation of particles.

In our present case, if ℓ is real, we have a metastable state for our particle, i.e. there is a finite probability for the particle to leak through the potential barrier shown in Fig. 4. The imaginary part of ℓ needed to make E real is formally equivalent to

introducing just the right amount of imaginary potential to create particles at a rate compensating for this leakage through the barrier. It must have the correct sign to correspond to the creation of particles inside the potential well (i.e. positive under the above convention).

The extension of a Regge trajectory to positive E is shown in Fig. 3. Points with integral ℓ and $E > 0$ have physical meaning as metastable states if the corresponding value of $\mathrm{Im}\ \ell_r(E)$ is small (for large $\mathrm{Im}\ \ell_r(E)$ the lifetime would be too short for the state to have meaning).

In the Coulomb force case, all the trajectories go to infinity for $E \to 0$ from the negative side. They have no extension to $E > 0$. If, however, one takes $V = V_0\, e^{-Kr}/r$ with $V_0 < 0$, one can have the case shown by Fig. 3, if at least $|V_0|$ is big enough. The behaviour of Regge trajectories for strong or weak potentials is illustrated in Fig. 5 by curves I and II, respectively.

We will now investigate the order of magnitude of $\partial E_r/\partial \ell$, i.e. of the shift in energy of a level $E_r(\ell)$ for a small change in ℓ. The potential W is related to ℓ by Eq. (4):

$$W = V + \frac{\hbar^2}{2m}\,\frac{\ell(\ell+1)}{r^2}\ . \qquad (4)$$

$R(r)/r = \chi$ being the normalized radial wave function and H the Hamiltonian, we have

$$\begin{aligned}\delta E_r &= \delta \langle \chi | H | \chi \rangle = \langle \delta\chi | H | \chi \rangle + \langle \chi | H | \delta\chi \rangle \\ &\quad + \langle \chi | \delta H | \chi \rangle = E_r \delta \langle \chi | \chi \rangle + \langle \chi | \delta W | \chi \rangle \\ &= \langle \chi | \delta W | \chi \rangle\ .\end{aligned}$$

This gives

$$\delta E_r = \frac{\hbar^2}{2m}\,\frac{\delta[\ell(\ell+1)]}{\rho^2} \qquad (5)$$

where we put $\rho^{-2} = \langle\chi|r^{-2}|\chi\rangle$. Hence for the Regge trajectory $\ell = \ell_r(E)$

$$\frac{\delta[\ell_r(\ell_r+1)]}{\delta E} = \frac{2m}{\hbar^2}\rho^2 . \qquad (6)$$

The length ρ is of order of the range of the potential, so that Eq. (6) gives an order of magnitude estimate of the slope of the Regge trajectory.

To extend these considerations from atomic physics to both nuclear physics and elementary particles physics we must take into account the fact that one has, in general, different forms for states of opposite parities. In the above examples I have used one potential for all the states, whether they have odd or even parity (i.e. odd or even ℓ's). In nuclear or elementary particles physics the states of even ℓ are usually subject to different forces from the states of odd ℓ. This is due to the fact that there are strong exchange forces between particles. Consequently, to classify states in angular momentum series, we shall have to do it separately for the even ℓ-states and for the odd ℓ-states, and Regge trajectories of two types will be required. One will have Regge trajectories $\ell = \ell_r^+(E)$ carrying the even states $\ell = 0, 2, 4\ldots$, and different trajectories $\ell = \ell_r^-(E)$ for the odd states $\ell = 1, 3, \ldots$. The even or odd parity of ℓ associated with a trajectory is called its signature.

4. Rotational series in nuclei

The existence of rotational bands among the excited states of nuclei was first discussed by Bohr and Mottelson. It occurs for nuclei which have a non-spherical ground state, the so-called deformed nuclei. These excited states correspond to a rotation of the deformed shape of the nucleus. The various states in such a rotational family have the following energy spectrum

$$E = \frac{\hbar^2}{2M} J(J+1) \qquad (7)$$

where J is the total angular momentum (analogous to the ℓ we used previously) and M is equivalent to a moment of inertia.

This is exactly the formula valid for a rigid rotator. The value of M, however, is smaller for nuclei than for a rigid rotator. Considering even-even nuclei, J takes the values 0, 2, 4..., so that, using the terminology of Regge pology, the rotational levels of nuclei lie on a Regge trajectory of even signature. One knows from experimental data that the number of such levels in a given series is small -- perhaps three or four levels but never much more. So the trajectory bends down for increasing E as indicated for curve I on Fig. 3. As to Eq. (6) for the slope of the trajectory, one finds that it holds order of magnitude-wise for the levels in a rotational series.

It is amusing that even for very light nuclei we have situations of the same type as are described above, and I want to give here an example which was noticed some time ago by Iwas and Viano and which they discussed in a Genoa University preprint. They have found evidence of a rotational series for the simple system composed of two α particles. This system of two spin zero particles has three metastable states, which are the ground state and two excited states of Be^8. Figure 6 gives the energy spectrum, taking the ground state of Be^8 as zero of energy. These three states have values of J = 0, 2, 4, respectively; all have even parity and isotopic spin zero. One finds that the Regge trajectory obtained by plotting the energy of the levels against values of J(J + 1) is close to linear, in reasonable agreement with Eq. (7).

5. Classification of the elementary particles

The idea of using Regge trajectories to classify elementary particles and resonances stems from Chew and Frautschi[1]. Its success up to now, however, is very limited. All one can say is that it seems

to make some sense to use for elementary particles this same principle of classification according to angular momentum. The very attractive feature of the original suggestion was the proposal that Regge trajectories be also used for describing high-energy scattering, and the great hope was to get a link between very high energy scattering at small momentum transfer and the mass spectrum of particles and resonances. The Regge trajectory approach to high-energy scattering has unfortunately not been supported by the experimental data. (See lectures given by Drs. Hagedorn and Wetherell). While there is some measure of agreement between theoretical prediction and experiment with regard to the shrinking of the diffraction peak for high-energy proton-proton scattering, the results on pion-proton scattering do not show the predicted shrinking. More experimental results are needed, and higher energy machines than are now available, before one will know completely how profound is the difference between prediction and experiment in the field of scattering, but the Regge trajectory approach seems at present to be at a dead end for this phenomenon. We are left then with the partial and rather trivial suggestion of using the concept of Regge trajectory or angular momentum series to classify particles. This, of course, makes some sense. Much in the same way as beryllium shows some rotational structure, it may very well be that elementary particles show also such a structure.

We have then to ask ourselves whether the known particles show some tendency to fall onto smooth lines in a mass-versus-spin plot, and if so whether Eq. (6) gives a reasonable value for the range of forces involved. There are at present very few particles which put themselves onto Regge trajectories with a reasonable slope. However, it is much too early to speak of any definite success or failure of the idea. It is just a conjecture which is helpful in trying to analyse data and trying to find places where one has to look for new resonances.

For elementary particles one has to keep in mind that all fermions have a spin J which is half integral. The classification will then be naturally in series with half integral values of J, either

the series ½, 5/2, 9/2, etc., or the series 3/2, 7/2, ½, etc. For bosons (integral values of spin) one would have 0, 2, 4... or 1, 3, 5... .

On the subject of bosons I can be extremely brief, because one has never found two bosons to put in the same series. Still, one boson has been much discussed in this context: the f^0 particle. This is a resonance between two pions at a mass of 1250 MeV which at first sight seems a very good candidate for being on the Regge trajectory used to describe the shrinking elastic scattering of protons on protons (the so-called Pomeranchuk trajectory). If extended into the region of particles, this trajectory suggests that one would find a boson of spin 2 with about the same mass as the f^0 particle. However, a more extensive study of elastic scattering has not confirmed the existence of the Pomeranchuk trajectory and, consequently, the conjecture that the f^0 particle falls on this trajectory may well be entirely meaningless.

For fermions, on the other hand, there is some indication of a few particles grouping themselves on what might be possible trajectories. Chew found two particles which could be put in the same series, and it appears since then that more groupings may be possible. The two particles first considered are the nucleon and one of its excited states (the latter are known experimentally as pion-nucleon resonances). These are two particles with isotopic spin ½. The nucleon has a mass of 940 MeV and spin ½. One gives it parity + by definition, i.e. the nucleon is a (½ +) state. There are several resonances found in pion-nucleon scattering. The first, of mass 1238 MeV, has isotopic spin 3/2, spin and parity (3/2 +). Then there are two resonances of isotopic spin ½ and masses 1512 MeV and 1688 MeV. It is the second of these which seems to fall on a trajectory with the nucleon. Its spin and parity are (5/2 +). One can regard it as a proton and a pion bound in metastable f state ($\ell = 3$, parity -). The negative parity of the orbital motion combines with the negative parity of the pion to give a resultant positive parity. From the masses of the two particles and the formula

$$\frac{\delta[J(J+1)]}{\delta E} = \frac{2m}{\hbar^2}\rho^2 \qquad \text{[see Eq. (6)]}$$

in which we simply put $\delta E = \delta m$, one finds

$$\rho \sim \frac{\hbar c}{2m\pi} ,$$

i.e. $\frac{1}{2}\ 10^{-13}$ cm, typical of the range of strong interactions. This is, of course, only an order of magnitude argument, but the result is satisfactory. If it had been $\leq 10^{-14}$ or $\geq 10^{-12}$ cm, one would certainly reject the attempt to put these particles on the same trajectory. To predict the next member of the family, Chew suggested the rather arbitrary rule of a linear relationship between J and m^2. This would give a resonance $(\frac{9}{2}+)$ of isotopic spin $\frac{1}{2}$ at a mass around 2200 MeV. A π resonance of isotopic spin $\frac{1}{2}$ has been found at 2190 MeV, and if it would turn out to be $(\frac{9}{2}+)$ it would give a beautiful example of rotational series of elementary particles.

For isotopic spin $\frac{3}{2}$ we have the well-known first resonance (N*) of the pion-nucleon system which is a $(\frac{3}{2}+)$ state, and has a mass of 1238 MeV. Adopting again a linear relationship between J and m^2, and taking the slope to be the same as for the trajectory of the nucleon described above, one finds that the resonances of masses 1920 and 2360 are good candidates to be put on the trajectory of N*. Unfortunately none of these resonances has the spin well determined yet. The prediction would be that the resonance of mass 1920 would be a $(\frac{7}{2}+)$ state and that at 2360 would be $(\frac{11}{2}+)$. When the spin and parity of these resonances will all be known we will have a severe test of out classification scheme.

Very little can be said at present for the hyperon resonances, and I shall refer to Glashow and Rosenfeld[2] for an indication of possible rotational series.

III. CLASSIFICATION OF ELEMENTARY PARTICLES ACCORDING TO THE OCTET SYMMETRY

1. General discussion of octet symmetry

In the previous sections we have been considering a classification based on families of particles which have the same quantum numbers except for the angular momentum. Now we classify the strongly interacting particles in families where the angular momentum is the same, but where other quantum numbers are different for the various members of the family.

The ideas behind this classification scheme are similar to those underlying the classification in isotopic spin multiplets. Heisenberg first suggested the use of an isospin formalism just after the discovery of the neutron in 1932; it described the proton and the neutron as members of a doublet called the nucleon. Since then all the strongly interacting particles have been classified with success in isospin multiplets, and the strong interactions have been verified to obey isospin symmetry quite generally. Clearly, from the beginning, violation of the symmetry principle was expected and found in electromagnetic as well as in weak interactions.

I now want to discuss an attempt at a more extensive classification of elementary particles by placing them in larger families than is done in the isospin formalism. Many forms of classification based on so-called "higher symmetries" have been suggested, the most significant being the schemes based on:

i) global symmetry;
ii) the Sakata model of unitary symmetry;
iii) the octet model of unitary symmetry.

Only the third one is supported by the facts, although it is far from being well established. The octet model is only a slight modification of the Sakata model, conceptually, but has very different conclusions capable of experimental test. The model was first proposed by Gell-Mann[3])

and Ne'eman[4], although other people had considered modifying the Sakata model of 1956 in an octet version (Yamaguchi). The reason for making this modification (to be described in the next paragraph) is that there seem to be several families of eight particles, each member in a family having the same spin and parity. Table 1 shows these families.

Table 1

Family type	Spin parity	Members of family with isospin (I) and hypercharge (Y)† assignment			
		I = ½; Y = 1	I = 0; Y = 0	I = 1; Y = 0	I = ½; Y = 1
Baryons	$\frac{1}{2}^+$	p^+ n^0	Λ	Σ^+ Σ^0 Σ^-	Ξ^0 Ξ^-
Antibaryons	$\frac{1}{2}^+$	$\bar{p}$ $\bar{n}$	$\bar{\Lambda}$	$\bar{\Sigma}^+$ $\bar{\Sigma}^0$ $\bar{\Sigma}^-$	$\bar{\Xi}^0$ $\bar{\Xi}^-$
Pseudo-scalar mesons	0^-	K^+ K^0	η	π^+ π^0 π^-	$\bar{K}^0$ $\bar{K}^-$
Vector bosons	1^-	K^{*+} K^{*0}	ω	ρ^+ ρ^0 ρ^-	$\bar{K}^{*0}$ $\bar{K}^{*-}$

†) Y = N + S; N is baryon number, S is strangeness.

It has recently been found that the relative parity of the Λ and Σ is even and this is the main argument to put the eight baryons together (although spin and parity of Ξ are not measured yet). If it had turned out that the relative Λ-Σ parity were odd, we would have put p n Λ in one family of three members and this would have been the Sakata model.

The octet model also proposes multiplets in which to accommodate the other strongly interacting particles. In particular, various multiplets are proposed for the baryon resonances[2]. Such assignments are tentative and all of them have to await further experimental support.

2. Some consequences of the octet classification

We must expect one important difference between the predictions of classification schemes based on higher symmetries and the results obtained using isospin symmetry: the effects of violation of conservation of isospin are small, being due only to electromagnetic and weak interactions (they are of the order of a few %); the effects of violation of a higher symmetry are certainly larger.

We can see this immediately in the mass differences between members of the same multiplet. When the proton and neutron are considered as being an isospin doublet, one has put together two particles with nearly equal masses; similarly for the pions, kaons and hyperons, where masses of the members of each isospin multiplet are very close to each other. Now, when we use a more extensive symmetry principle for putting more particles in the same family, we are bound to put together particles with large mass differences. However, the differences in the masses cannot be entirely arbitrary; they must result from certain symmetry violating terms, the form of which is not arbitrary. Using such considerations Gell-Mann and Okubo have deduced a formula for the mass splittings within any multiplet of the octet model. If we write

$$M_r = M_0 + \Delta M_r$$

where M_r is the mass of a member of the multiplet, M_0 a constant for the multiplet, and ΔM_r the term due to the violation of the symmetry, we have

$$\left.\begin{array}{ll} \text{for fermions} & \Delta M_r \\ \text{for bosons} & (\Delta M_r)^2 \end{array}\right\} = a + bY + c[Y^2 - 4I(I+1)]$$

where a, b, c are constants, Y is the hypercharge (nucleon number plus strangeness) and I the isotopic spin.

For the octets in Table 1 this result implies the following identity between masses:

i) fermions : $\frac{1}{2}(M_N + M_\Xi) = \frac{1}{4}(3M_\Lambda + M_\Sigma)$

Experiment : 1127 MeV 1134 MeV

ii) pseudoscalar mesons : $(M_K)^2 = \frac{1}{4}(3M_\eta^2 + M_\pi^2)$

Experiment : $(495\ \text{MeV})^2$ $(480\ \text{MeV})^2$

iii) vector mesons : $(M_{K^*})^2 = \frac{1}{4}(3M_\omega^2 + M_\beta^2)$

Experiment : $(888\ \text{MeV})^2$ $(775\ \text{MeV})^2$.

One can see remarkable agreement between prediction and experiment for cases (i) and (ii), but it seems that for the vector mesons one needs a mass of 920 MeV for the ω instead of 780 MeV found experimentally. One should perhaps look for another meson of spin 1, odd parity and isospin zero, with a higher mass*).

The above example illustrates the kind of predictions that a classification based on higher symmetries can make: one can calculate the effects of symmetry violations, always with the proviso that the violating terms are small perturbations.

Other predictions are relations between the magnetic moments of baryons (μ) [5]:

$$\mu(p) = \mu(\Sigma^+)$$
$$\mu(\Xi^0) = \mu(n)$$
$$\mu(\Xi^-) = \mu(\Sigma^-)$$
$$\mu(\Lambda) = \tfrac{1}{6}[\mu(p) + \mu(\Sigma^-) + 4\mu(n)]$$
$$\mu(\Sigma^0) = \tfrac{1}{2}[\mu(\Sigma^+) + \mu(\Sigma^-)] .$$

---

*) Such a meson, the φ particle of mass 1020 MeV, has been found since, and it seems that in Table 1 ω must be replaced by a linear combination of ω and φ such that its mass should be 920 MeV.

These relations are, of course, only approximate (perhaps to 10 or 20%). One also has relations for the total cross-section as the energy gets very large[6]:

$$\sigma(\pi^{\pm}p) = \sigma(K^{\pm}p) \ .$$

For comparison, one finds experimentally at 20 GeV

$$\sigma(\pi^{-}p) = 27 \pm \sim 1 \text{ mb} \qquad \sigma(K^{-}p) = 23 \pm 2 \text{ mb}$$
$$\sigma(\pi^{+}p) = 25 \pm \sim 1 \text{ mb} \qquad \sigma(K^{+}p) = 18 \pm 2 \text{ mb} \ .$$

As more experimental data becomes available we shall be able to test more stringently the requirements of the scheme. We now give a brief introduction to the mathematical contents of the octet model.

3. Formal description of the octet model

First let me stress very emphatically that unitary symmetry is up to now not established with any certainty comparable to isospin symmetry. In the case of isospin we have a great deal of evidence with regard to its utility in discussing elementary particle interactions; for unitary symmetry we only have the very suggestive grouping in octets shown in Table 1 with the predictions about masses discussed in the last section, but we are left with many other consequences which have not yet been tested experimentally, and many resonances which have not been grouped in multiplets.

I first want to recall the mathematical formalism of spinor calculus which is the calculus of complex vectors in two dimensions. One can write down two kinds of vectors:

a) a covariant vector u_μ with components u_1 and u_2;

b) a contravariant vector v^μ with components v^1 and v^2.

One considers on these vectors the group SU(2) of linear transformations $S_{\mu\nu}$ which are unitary and unimodular. These transformations act as follows on the vectors:

a) covariant : $u'_\mu = \sum_\nu S_{\mu\nu}\, u_\nu$

b) contravariant : $\sum_\mu v'^\mu\, S_{\mu\nu} = v^\nu$

where (b) follows from (a) and the requirement

$$\sum_\mu u'_\mu\, v'^\mu = \sum_\mu u_\mu\, v^\mu \ .$$

The condition that S should be unitary means that

$$\sum_\nu S_{\mu\nu}\, S^\dagger_{\nu\mu'} = S_{\mu\mu'} \qquad \text{(the unity matrix)}$$

where $S^\dagger_{\nu\mu'} = S^*_{\mu'\nu}$ (the + denotes the Hermitian conjugate, the star the complex conjugate). The statement that S is unimodular means that its determinant is unity. Because of unitarity the transformation law for a contravariant vector can also be written

$$v'\mu = \sum_\nu S^*_{\mu\nu}\, v^\nu \ .$$

It is the above group of transformations which provides the basis for the formal description of isotopic spin. One describes the nucleon with the two components, the neutron and proton, by means of a covariant vector

$$\begin{pmatrix} u_1 \\ u_2 \end{pmatrix} = \begin{pmatrix} p \\ n \end{pmatrix},$$

the antinucleon by means of a contravariant vector

$$(v'v^2) = (\bar{p}\ \bar{n}).$$

This is the formal description of the particles of isotopic spin ½, and isospin symmetry means that all interactions are invariant under the group SU(2) defined above.

To extend this to particles of isospin 1 like the pions or the Σ hyperons, one uses tensors of second rank.

Consider the mixed tensor:

$$t^{\mu}_{\nu} = \begin{pmatrix} t^1_1 & t^2_1 \\ t^1_2 & t^2_2 \end{pmatrix}$$

where the components as far as the lower index is concerned behave as a covariant vector, while they behave as a contravariant vector with respect to the upper index. The transformation law under SU(2) will now be

$$t'^{\mu}_{\nu} = \sum_{\mu'\nu'} S_{\nu\nu'}\, S^*_{\mu\mu'}\, t^{\mu'}_{\nu'} \,.$$

The tensor, which has four independent components $(t^1_1, t^2_1, t^1_2, t^2_2)$, can be decomposed in a part which is invariant under the transformations of the group and another tensor which has only three independent components.

The invariant part is the trace $T = t^1_1 + t^2_2$, and if I subtract $\frac{1}{2} T\, \delta^{\mu}_{\nu}$ from the mixed tensor I obtain the traceless tensor

$$\begin{pmatrix} \frac{t^1_1 - t^2_2}{2} & t^2_1 \\ t^1_2 & -\frac{(t^1_1 - t^2_2)}{2} \end{pmatrix}$$

i.e. a tensor with only three independent components. This can be used to describe the three charge states of the pion:

$$(t^1_1 - t^2_2)/2 = \pi^0/\sqrt{2} \;; \quad t^2_1 = \pi^+ \;; \quad t^1_2 = \pi^- \,.$$

It is also possible to give some kind of physical meaning to the mathematical construction of the traceless tensor. Suppose I have two objects of isospin $\frac{1}{2}$, similar to nucleons,

$$\begin{pmatrix} a^+ \\ a^0 \end{pmatrix} \text{ and } \begin{pmatrix} \alpha^+ \\ \alpha^0 \end{pmatrix} .$$

I can construct with them the following mixed tensor:

$$\begin{pmatrix} \bar{a}^+ \alpha^+ & \bar{a}^o \alpha^+ \\ \bar{a}^+ \alpha^o & \bar{a}^o \alpha^o \end{pmatrix}.$$

The α^+, α^o are the components of a covariant vector. The $\bar{a}^+$ and $\bar{a}^o$ are complex conjugates of the components of a covariant vector and are thus the components of a contravariant vector. Physically, the α^+, α^o are similar to the proton and neutron, while the $\bar{a}^+$ and $\bar{a}^o$ are the two components of the antinucleon.

I then take out the trace divided by 2:

$$\tfrac{1}{2} T = \tfrac{1}{2}(\bar{a}^+ \alpha^+ + \bar{a}^o \alpha^o)$$

which is an isospin invariant (i.e. an isospin singlet) and obtain the traceless tensor composed of the three components of an isospin triplet

$$\begin{pmatrix} \dfrac{\bar{a}^+\alpha^+ - \bar{a}^o\alpha^o}{2} & \bar{a}^o \alpha^+ \\ \bar{a}^+ \alpha^o & \dfrac{\bar{a}^o\alpha^o - \bar{a}^+\alpha^+}{2} \end{pmatrix}$$

the component of which I identify with

$$\begin{pmatrix} \dfrac{\pi^o}{\sqrt{2}} & \pi^+ \\ \pi^- & -\dfrac{\pi^o}{\sqrt{2}} \end{pmatrix}.$$

Assuming the original states a, α to be normalized to 1, it then follows that $\pi^\pm$ and π^o are also normalized to 1. This construction of pions out of nucleon-antinucleon pairs may have more significance than a simple mathematical analogy. It might actually be true that pions are bound states of nucleons and antinucleons. The trace may similarly be regarded as an I = 0 meson like the η meson:

$$\bar{a}^+\alpha^+ + \bar{a}^o\alpha^o = \sqrt{2}\,\eta\,.$$

A similar construction would yield the Λ and Σ hyperons if I took, for example, $\begin{pmatrix} a^+ \\ a^o \end{pmatrix}$ as $\begin{pmatrix} p \\ n \end{pmatrix}$ and $\begin{pmatrix} \alpha^+ \\ \alpha^o \end{pmatrix}$ as $\begin{pmatrix} K^+ \\ K^o \end{pmatrix}$.

The group of transformations which described isotopic spin symmetry is called SU(2): S refers to the unimodular property, U to unitarity, and (2) to the number of components of the vectors. Unitary symmetry, both in the Sakata model and in the octet model, is based on the SU(3) group, i.e. the group of unimodular, unitary transformations of three-dimensional complex vectors.

Our basic vectors now are

(a) covariant $\begin{pmatrix} u_1 \\ u_2 \\ u_3 \end{pmatrix} = \begin{pmatrix} \alpha^+ \\ \alpha^o \\ \beta^o \end{pmatrix}$

(b) contravariant $(v^1 v^2 v^3) = (\bar{a}^+ \bar{a}^o \bar{b}^o)$.

In the Sakata model p, n and Λ are taken as the components of a covariant vector; however, the resulting scheme gives difficulties with recent experiments [7]. In the octet model, all particles are identified with tensors. To achieve this identification one can imagine that $\begin{pmatrix} a^+ \\ a^o \end{pmatrix}$, $\begin{pmatrix} \alpha^+ \\ \alpha^o \end{pmatrix}$ are unknown objects of isospin $I = \frac{1}{2}$ and hypercharge $Y = 1$, while b^o and β^o are $I = 0$, $Y = 0$ elements. Then we can construct the traceless tensor

$$t^\mu_\nu = v^\mu u_\nu - \tfrac{1}{3} \delta^\mu_\nu (v^\rho u_\rho)$$

which has eight independent components. In terms of a, b, α, β it is

$$t^\mu_\nu = \begin{pmatrix} \frac{1}{3}(2\bar{a}^+ a^+ - \bar{a}^o \alpha^o - \bar{b}^o \beta^o) & \bar{\alpha}^o \alpha^+ & \bar{b}^o \alpha^+ \\ \bar{\alpha}^+ \alpha^o & \frac{1}{3}(-\bar{a}^+ \alpha^+ + 2\bar{a}^o \alpha^o - \bar{b}^o \beta^o) & \bar{b}^o \alpha^o \\ \bar{\alpha}^+ \beta^o & \bar{a}^o \beta^o & \frac{1}{3}(-\bar{a}^+ \alpha^+ - \bar{a}^o \alpha^o + 2\bar{b}^o \beta^o) \end{pmatrix}.$$

By looking at the value of Y and I for each of the elements, the following identifications can then be made:

$$\left.\begin{aligned} \bar{b}^{o}\alpha^{+} &\equiv P,\ \bar{\Xi}^{o},\ K^{+},\ K^{*+} \\ \bar{b}^{o}\alpha^{o} &\equiv n,\ \bar{\Xi}^{o},\ K^{o},\ K^{*o} \end{aligned}\right\} \text{because } \begin{matrix} Y = 1 \\ I = \tfrac{1}{2} \end{matrix}$$

$$\left.\begin{aligned} \bar{a}^{+}\beta^{o} &\equiv \Xi^{-},\ \bar{p},\ \bar{K}^{-},\ \bar{K}^{*-} \\ \bar{a}^{o}\beta^{o} &\equiv \Xi^{o},\ \bar{n},\ \bar{K}^{o},\ \bar{K}^{*o} \end{aligned}\right\} \text{because } \begin{matrix} Y = -1 \\ I = \tfrac{1}{2} \end{matrix}$$

$$\left.\begin{aligned} \bar{a}^{o}\alpha^{+} &\equiv \Sigma^{+},\ \bar{\Sigma}^{-},\ \pi^{+},\ \rho^{+} \\ \bar{a}^{+}\alpha^{o} &\equiv \Sigma^{-},\ \bar{\Sigma}^{+},\ \pi^{-},\ \rho^{-} \\ \frac{\bar{a}^{+}\alpha^{+} - \bar{a}^{o}\alpha^{o}}{\sqrt{2}} &\equiv \Sigma^{o},\ \bar{\Sigma}^{o},\ \pi^{o},\ \rho^{o} \end{aligned}\right\} \text{because } \begin{matrix} Y = 0 \\ I = 1\ . \end{matrix}$$

There remains $\bar{a}^{+}\alpha^{+} + \bar{a}^{o}\alpha^{o}/\sqrt{2}$ and $\bar{b}^{o}\beta^{o}$, both being combinations having having Y = 0, I = 0. In the matrix they occur as $-2\bar{b}^{o}\beta^{o} + \bar{a}^{+}\alpha^{+} + \bar{a}^{o}\alpha^{o}/\sqrt{6}$ and can be identified with Λ, $\bar{\Lambda}$, η, ω.

The coefficient like $1/\sqrt{2}$, $1/\sqrt{6}$ are selected so as to have norm 1 for each state, assuming a, b, α, β all to have norm 1. For the baryons the traceless tensor now has the form

$$t^{\mu}_{\nu} = \begin{pmatrix} \frac{\Sigma^{o}}{\sqrt{2}} + \frac{\Lambda}{\sqrt{6}}, & \Sigma^{+}, & P \\ \Sigma^{-}, & -\frac{\Sigma^{o}}{\sqrt{2}} + \frac{\Lambda}{\sqrt{6}}, & n \\ \Xi^{-}, & \Xi^{o}, & -\frac{2}{\sqrt{6}}\Lambda \end{pmatrix}$$

and similar forms hold for antibaryons, pseudoscalar mesons, and vector mesons.

When our problem was to generate triplets in the triplets in the isotopic spin symmetry, we could start with basic spinors which themselves could immediately be identified with the isospin ½ particles (nucleon or kaon), and from them we constructed traceless tensors, the elements of which were identified with particles of isospin 1. In the

octet model, however, we have no known particles forming the basic triplet (called $a^+a^0b^0$, or $\alpha^+\alpha^0\beta^0$ above), and this is rather unsatisfactory. If the validity of the model is established, one should look for these particles, which may be of high mass.

The further use of the formalism to study interactions is, in principle, very simple. Invariant interactions are built by constructing invariants with the tensors describing the particles involved. For example, the baryon-baryon-pseudoscalar interaction will be of the following type

$$\sum_{\mu\nu\lambda} \left[f\, \bar{B}^{\mu}_{\nu} \gamma^5 B^{\nu}_{\lambda} P^{\lambda} + f' \bar{B}^{\mu}_{\nu} \gamma^5 B^{\lambda}_{\mu} P^{\nu}_{\lambda} \right]$$

where B^{μ}_{ν}, $\bar{B}^{\mu}_{\nu}$, P^{μ}_{ν} are the tensors representing baryons, antibaryons, and mesons, respectively, and where f, f' are two coupling constants. The consequence of such formulae will not be worked out here, but it is clear that they will give many identities among matrix elements.

* * *

REFERENCES

1. G.F. Chew and S.C. Frautschi, Phys.Rev.Letters 7, 394 (1961); and Phys.Rev.Letters 8, 41 (1962).

2. S.L. Glashow and A.H. Rosenfeld, Phys.Rev.Letters 10, 192 (1963).

3. M. Gell-Mann, Caltech Report (1961) (unpublished); and Phys.Rev. 125, 1067 (1962).

4. Y. Ne'eman, Nucl.Phys. 26, 222 (1961).

5. S. Okubo, Progr.Theor.Phys. 27, 949 (1962).

6. P.G.O. Freund, H. Ruegg, D. Speiser and A. Morales, Nuovo Cimento 25, 307 (1962).

7. B. d'Espagnat, Proc. International Conf. on High-Energy Physics, CERN (1962), p. 917.

* * *

Fig.1

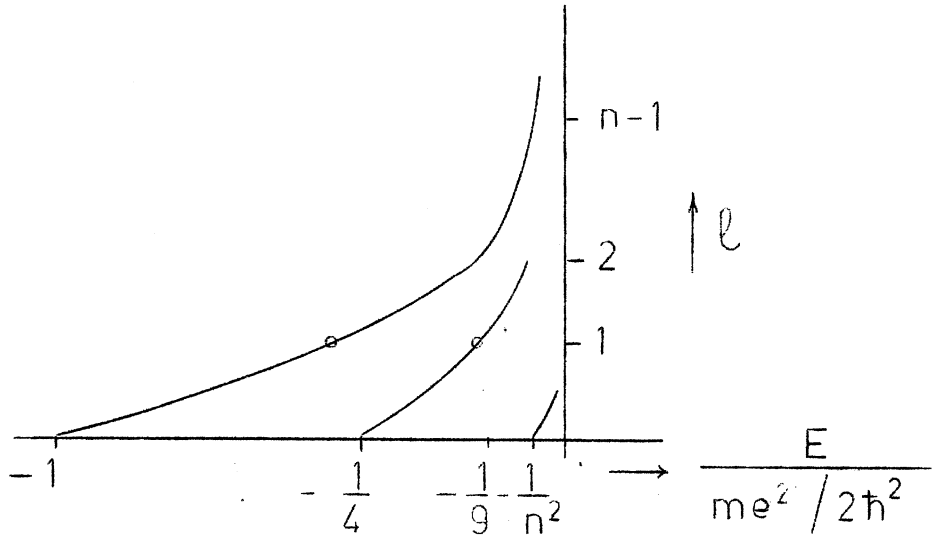

Regge trajectories for the hydrogen atom.

$$W = V + \frac{\hbar^2}{2m}\,\frac{\ell(\ell+1)}{r^2}$$

Fig.2

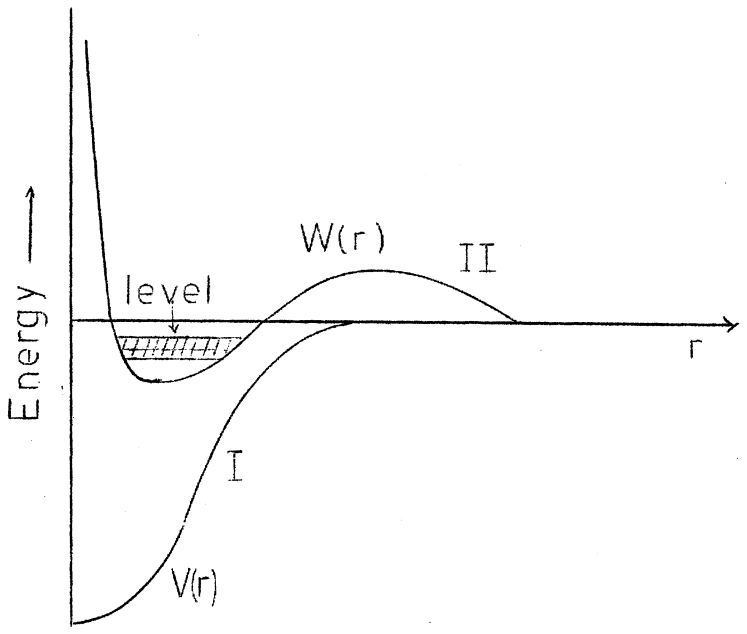

Effect of centrifugal potential on form of a general potential V(r).

Schematic Regge trajectory for general potential.

Fig. 3

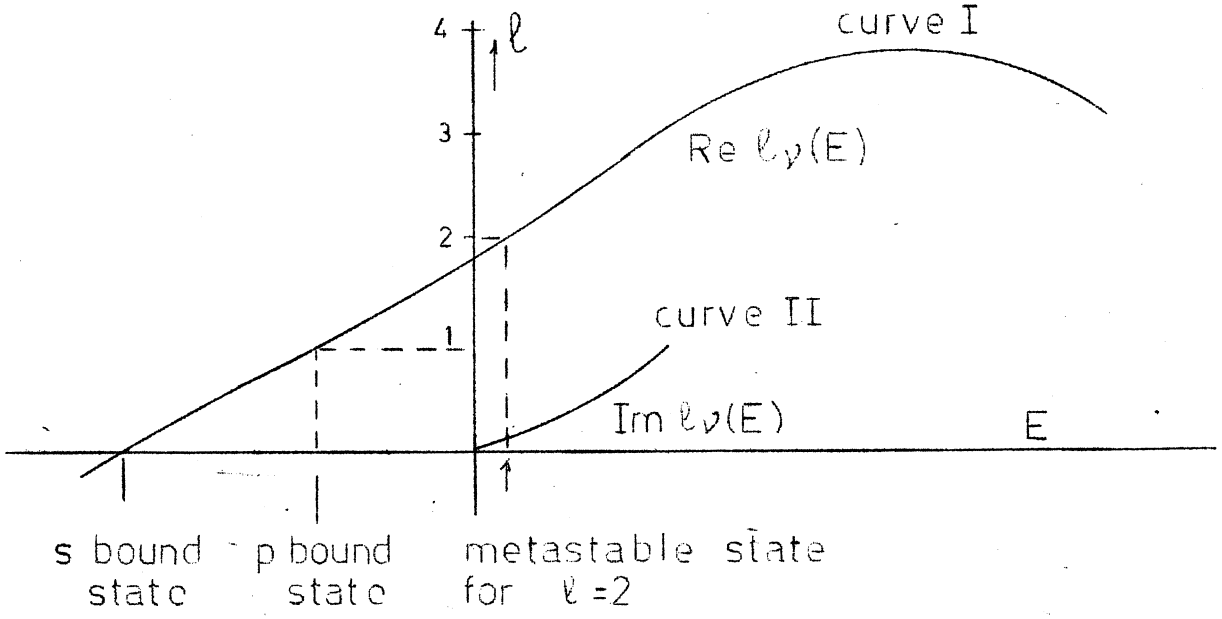

Fig. 4

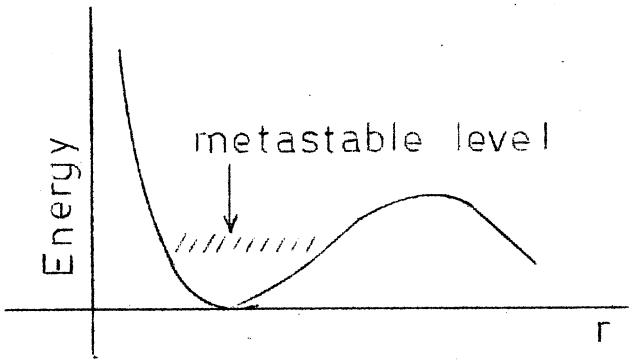

The effect of a centrifugal barrier giving a metastable state.

Fig. 5

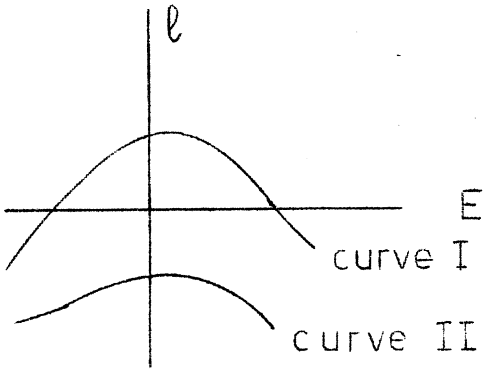

Regge trajectory for strong and weak potentials

Fig. 6

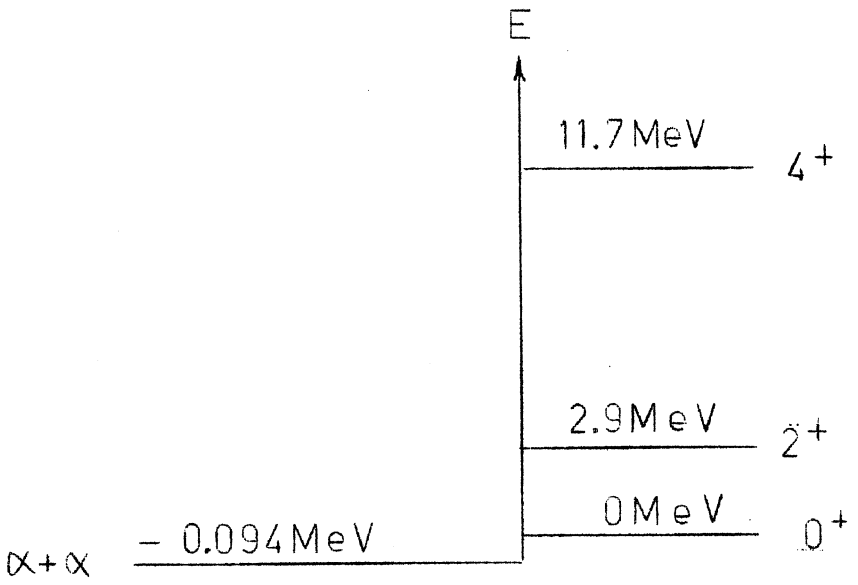

Lowest lying levels of Be^8

PART II.2

EXPERIMENTAL OBSERVATIONS ON RESONANCES

G. Ekspong,
Department of Physics, University of Stockholm.

I. ESTABLISHING THE EXISTENCE OF NEW PARTICLES

1. Remarks on lifetimes

Until about three years ago, all particles which were identified had the property of a relatively long life. By long I mean a lifetime order of magnitude longer than 10^{-24} sec, which is about the time it takes a light signal to transverse a nucleon. Most particles have an extremely long lifetime, in the range $10^{-7} - 10^{-10}$ sec. Our instruments are sensitive only to times in a limited range, the lowest limit reached is about 10^{-16} sec. We have been rather blind - and in a certain sense still are - to the region between 10^{-16} and 10^{-22} sec. Below about 10^{-22} we use the relation $\Gamma \cdot \tau = \hbar$. If we can measure widths $\Gamma \gtrsim 1$ MeV we can reach times $\tau \lesssim \hbar/\Gamma \simeq 6 \cdot 10^{-22}$ sec. Below $\tau = 10^{-24}$ sec the width would be > 600 MeV, i.e. of the order of the mass itself. Here it makes no sense to speak of particles. Figure 1 summarizes the experimental situation.

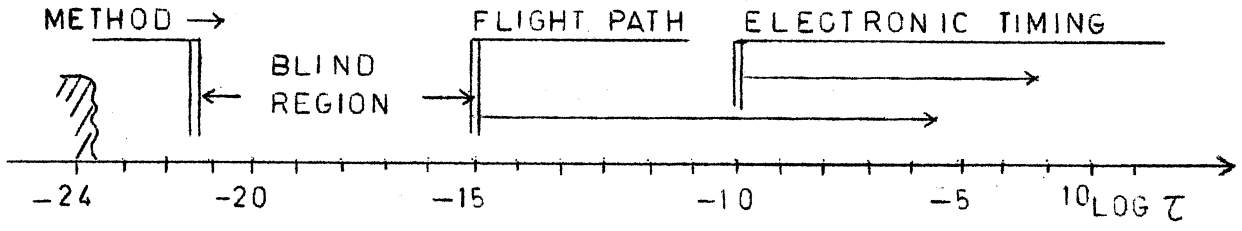

FIG. 1

The neutral pion is an example of a particle just about measurable by the flight path method. The Σ^0 is an example of a particle, probably lying in the blind region. Some of the new particles, called resonances [ρ, K*, Y* (1385)] are in the Γ region; some are probably at present in the blind region: η, ω, Y* (1405). The blind region may be opened to some extent by cross-section measurements like the Primakoff method for π^0.

The old particles (pions, K mesons, hyperons and muons) decay by weak or electromagnetic interactions. The new particles (resonances) decay by strong or electromagnetic interactions and are thus in general faster. Strangeness and parity are conserved in the last-mentioned interactions.

2. Peakology

Although the lifetimes of particles may be too short for direct measurements, their existence is revealed by a peak in the variation of a total cross-section with energy (e.g. some of the nucleon resonances or isobars) or by detecting the decay products (e.g. the pion resonances). In the latter case the final state of the interaction will contain particles other than the decay products of the resonance, e.g.

$$\left.\begin{array}{l} \bar{P} + P \rightarrow \omega^0 + \pi^+ + \pi^- \\ \qquad\quad \hookrightarrow \pi^+ + \pi^- + \pi^0 \end{array}\right\} \rightarrow \pi^+ + \underbrace{\pi^- + \pi^0 + \pi^+}_{\omega^0} + \pi^- \ .$$

If in this case one always chose the three pions from the ω decay and plotted the distribution of their invariant mass (M*):

$$M^{*2} = (\Sigma E_i)^2 - (\Sigma p_i)^2 \ ,$$

one would obtain a clustering around a central value for the M* corresponding to the mass of the ω. In practice one does not know which charged pions to include in the triplet decay and therefore one has to plot the M* distribution for all combinations of π^+, π^-, π^0 in the five particle final state. If there were no resonance involved in the final state of this reaction one would expect the M* distribution to be smoothly

distributed between a lowest limit (the sum of the masses of three pions) and the upper limit set by the total energy available. In the example taken, one gets such a distribution for pion triplets that do not come from the ω meson. The presence of the ω is seen as a peak superimposed on this background. The individual values of the energy in the peak due to the resonance are spread around the central value for two reasons; one is due to the errors of measurement, the other to the natural line width of the parent particle mass. One thinks here in terms of a Breit-Wigner distribution:

$$P(E)\,dE = \frac{\text{const}}{(E - E_0)^2 + \frac{\Gamma^2}{4}}\,dE\,,$$

where Γ is the full width at half maximum, E_0 and E the mass, and our energy (M*) variable respectively. The time dependence of a quantum mechanical decaying state may be described:

$$\psi_t = \psi_0\, e^{-\gamma \frac{t}{2}}\, e^{-iE_0 t/\hbar}$$

where E_0 is the energy. Here γ is the decay constant, because the probability of the state at time t is

$$|\psi_t|^2 = |\psi_0|^2\, e^{-\gamma t} \quad \text{(exponential decay)}.$$

The mean lifetime τ is related to γ in the usual way, $\gamma \cdot \tau = 1$. The state can be written as a superposition of stationary states of various energies E, i.e.

$$\psi_t = \int_{-\infty}^{\infty} A(E)\, e^{-iEt/\hbar}\, dE\,.$$

The amplitude A(E) is obtained by Fourier's integral theorem and its square gives the probability of the energy E

$$P(E) = |A(E)|^2 = \frac{\text{const}}{(E - E_0)^2 + \frac{\Gamma^2}{4}} \quad \text{(Breit-Wigner formula)},$$

where Γ has been introduced instead of γ; the relation being $\Gamma = \hbar \cdot \gamma = \hbar/\tau$. This shows that the relation $\Gamma \cdot \tau = \hbar = 6.58 \cdot 10^{-22}$ MeV sec is exact and not an inequality of the type derivable from the uncertainty principle.

In general, in a reaction producing a resonance in the final state one sees the decay products of the resonance and the particles directly produced as in the above example. This results in a smooth invariant mass distribution with a peak superimposed. In the energy histograms everybody now looks for peaks, signalling the existence of a parent or resonance particle. I would like to mention a danger at this stage, namely the risk of seeing too many peaks or peaks too often and also the risk of missing a peak that might be there. In some papers one reads unclear statements saying that the observed peak is statistically significant. The problem is in its simplest form of the following type. We have a histogram (ideograms should be avoided) as in Fig. 2.

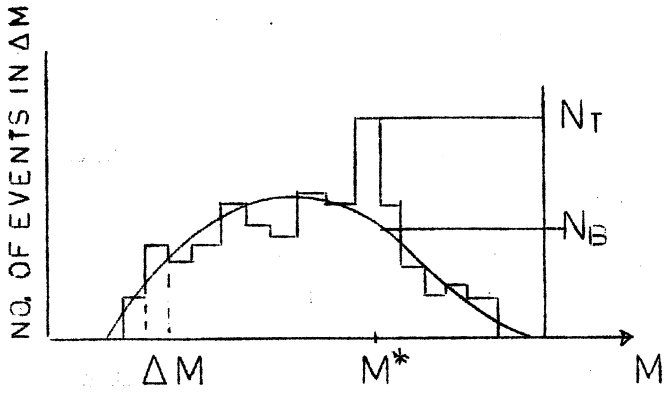

FIG 2

We wish to test if there is a significant peak above the background at M* or if it is merely a fluctuation of the background. First of all, significance is a question of judgement. From Cramér's statistical textbooks the following useful rules are suggested:

i) if the probability for $N \geq N_T$ is $\leq 0.1\%$, based on the hypothesis that the expected value is N_B, the peak is said to be highly significant;

ii) if $0.1\% < P(N \geq N_T) \leq 1\%$, the peak is significant;

iii) if $1\% < P(N \geq N_T) \leq 5\%$, the peak is almost significant;

iv) if $P(N \geq N_T) > 5\%$, the peak is not significant.

Note: Cramér actually deals with fluctuations both ways. In conformity with that we could require even stricter rules, e.g. only for $P(N \geq N_T) \leq 0.05\%$ is the peak highly significant.

One important thing is that the experimenter should decide for himself before the experiment on these levels of significance, or others if he so prefers. The concept of statistical risk is also important. If one decides to publish discoveries of peaks based on the significance level of 10%, then one may find that too many "discoveries" disappear in the long run. It is safer, less risky, to stick to a level of 1% or less. Nowadays, when we have hundreds of histograms published every year, we are not to be surprised if a few objects which were significant one year turn out not to be so the next year. I have been told that the T = 2 meson at about 600 MeV ($\pi^+ \pi^+$ and $\pi^- \pi^-$) recently disappeared when the experiment in which it was found was continued.

One more thing is important. Even in one single histogram there are many bins; 10 is a low number, but let us use it for convenience. If we do not know a priory where the peak is expected, we have 10 chances to find a fluctuation. To get a level of significance of 1% for the whole histogram, we must set our standard as high as 0.1% for each bin. If we know the expected position, this is not necessary. The latter case applies, for instance, to a situation where we look for η^0 production (or any other already known state) in a new reaction. We then know where to look for a peak.

I now come to the question of how to test the significance. Some people take the $\sqrt{N_T}$ and test whether $N_T - N_B > 3\sqrt{N_T}$ or generally $> \alpha\sqrt{N_T}$. Others use $\sqrt{N_B}$ and test whether $N_T - N_B > 3\sqrt{N_B}$. Still others compute the

strength of the line $S = N_T - N_B$ and its compounded error $\Delta S = \sqrt{N_T + N_B}$ and test whether S is significantly different from zero, i.e. $S \geq 3\sqrt{N_T + N_B}$. All three cannot be correct as they might lead to different results. Let me exemplify. I decide first on which probability level, I will regard a peak as significant. Let me choose the rules just stated. If the background is $N_B = 16$ events and on top of that 10 events, one reaches 26 events ($= N_T$). The observed difference of 10 is equal to $2.5\sqrt{N_B}$; the probability of a background fluctuation ≥ 10 is 0.6%. The peak is thus significant but not highly significant. This is the correct treatment, because it is based on the hypothesis that there is no peak on top of the background. If we test on the basis of $\sqrt{N_T} = \sqrt{26}$ we get P = 3% and on the basis of $\sqrt{N_T + N_B} = \sqrt{42}$, we get P = 6%, which is not significant, but not correct treatment either. Many difficulties arise when determining the background level in the region of the peak when it is wide. The sure thing is to get peaks well above the background as in Fig. 3 (ω production; cf. Fig. 4, the basis for ω discovery).

II. DETERMINATION OF PROPERTIES OF RESONANCE PARTICLES

1. Mass

The most used method already introduced in the last section is very general and consists of a calculation of the invariant mass (M^*) of the decay products in their rest system. Note:

$$M^{*2} = (\Sigma E_i)^2 - (\Sigma \bar{p}_i)^2 .$$

If the final state contains only one other particle (numbered 3) apart from the resonance particle under study, we have a two-body reaction which can be treated as follows:

$$M^{*2} = (\Sigma E_i)^2 - (\Sigma \bar{p}_i)^2$$

$$= (E_0 - E_3)^2 - (\bar{p}_0 - \bar{p}_3)^2 ,$$

where E_0 and p_0 are the energy and momentum of the initial state.

If we work in the rest system of the initial state (or discuss a reaction at rest in the lab) then $\bar{p}_0 = 0$ and $M^{*2} = E_0^2 + m_3^2 - 2E_0E_3$ so that M^* varies with E_3, the energy of the third particle (all other things being constant). This means that a sharp value of M^* is reflected into a constant value of E_3 and of course also its momentum p_3. This was how the first excited hyperon $Y_1^*(1385)$ was discovered in the reaction

$$K^- + P \rightarrow Y_1^* + \pi \rightarrow \Lambda^0 + \pi^\pm + \pi^\mp$$

at 1.15 GeV/c (K beam) by the Berkeley group.

Similarly Frisk (Stockholm) has observed a sharp line of $|\bar{p}_1 + \bar{p}_2|$ $(= p_3)$ in a reaction of K^- with emulsion nuclei, interpreted as

$$K^- + C^{12} \rightarrow Y^* + B^{11}$$
$$\hookrightarrow \Sigma^\pm + \pi^\mp \ .$$

I will return later to this case, since if the results are borne out when higher statistics are available, it appears to be the resonance best suited for a detailed study by the nuclear emulsion technique. For neutral states and also more general situations, the missing mass computation is of great value.

2. The lifetime τ (or width Γ)

This quantity is known only for a few of the new resonance particles. In bubble chamber experiments, which dominate this field of research, the widths obtained have varied rather widely. What this means is difficult to say; one can think of measurement errors or, if these are not sufficient, final state effects. In two cases, the η^0 (548 MeV) and the ω^0 (782 MeV), the width seems to be too small to measure with available techniques. In a third case, Y* (1405), the situation is unclear. With bubble chambers, a width of about 50 MeV (resolution claimed 5 MeV) was obtained by several groups. Using nuclear emulsions, the sharp peak observed at Stockholm mentioned in Section II.1, for the momentum of the Y* from K^- absorption on C^{12}, would imply a width of 2 MeV for the Y* (1405). The emulsion work requires confirmation based on much higher

statistics before discussing the possibility of, e.g. two resonant states, etc. For the π-nucleon resonances, the behaviour with energy of the π nucleon total cross-section gives the width.

3. Quantum numbers

The quantum numbers are listed below:

B = baryon number (baryon B = + 1, antibaryon B = - 1, meson and lepton B = 0);

S = strangeness (restricted at present to S = 0, ± 1, - 2);

T = isobaric spin (T = 0 charge singlet, T = ½ doublet, T = 1 triplet);

J = spin;

P = parity;

G = G parity.

The first three are obtained most easily. The production or decay channels give B and S immediately from the fact that these numbers are separately conserved in the strong interaction processes. In several cases the T (isobaric spin) has been determined by search for states with the same mass but different charge. Thus the ω mass of 782 MeV is obtained only in the neutral combination $\pi^+ \pi^- \pi^0$ not in any charged combination; thus ω is a T = 0 particle. Also the use of Clebsch-Gordan coefficients in comparing the observed intensities in various decay channels has been used. This is exemplified for the ρ meson. The reaction studied by Erwin et al.[1] was as follows.

Table 1

	T = 0	T = 1	T = 2	Exper.
$\pi^- + P \rightarrow P\ \pi^-\ \pi^0$	0	1	1	1
$\hookrightarrow n\ \pi^+\ \pi^-$	2	2	2/9	1.7 ± 0.3
$\hookrightarrow n\ \pi^0\ \pi^0$	1	0	4/9	$\leq$ 0.25 ± 0.25

Table 1 shows the expected branching ratios for T = 0, 1 and 2. The experimental result points to T = 1 for the ρ meson. It should be mentioned that the data refer to peripheral π-p reactions (in essence π-π scattering).

The assignment of spin and parity is of great importance for the classification of the particles and for a deeper understanding of their structure. These quantum numbers are still not known for some resonances, especially not for the hyperon states (like Y_0^*, etc.). However, we recall that only recently has the Σ-Λ parity been established (by a CERN group) with greater confidence as positive and that the spin of the Ξ is only very recently fixed with such confidence to be $\frac{1}{2}$.

The situation is much better for the mesonic states (Table 2) where K* (888 MeV) is 1^- (vector), K is 0^- (pseudoscalar).

Table 2

J^{PG} for non-strange mesons

0^{--} π T = 1	0^{-+} η T = 0	pseudoscalar mesons
1^{--} ω T = 0	1^{-+} ρ T = 1	vector mesons

Here the π has been included to make the symmetry evident. In fixing the values of spin and parity for ω and η, the Dalitz diagram, once invented for the K meson (τ decay), is useful. The procedure is roughly as follows.

a) A Dalitz diagram is a two-dimensional plot of events for three-body reactions, e.g. $\omega \to \pi^+ + \pi^- + \pi^0$. In the c.m.s. of the parent particle the energy sum is $T_1 + T_2 + T_3 = Q$ = constant. So each event can be represented by a dot in a two-dimensional diagram (only two energies are independent). Figure 5 shows three ways of making such a diagram.

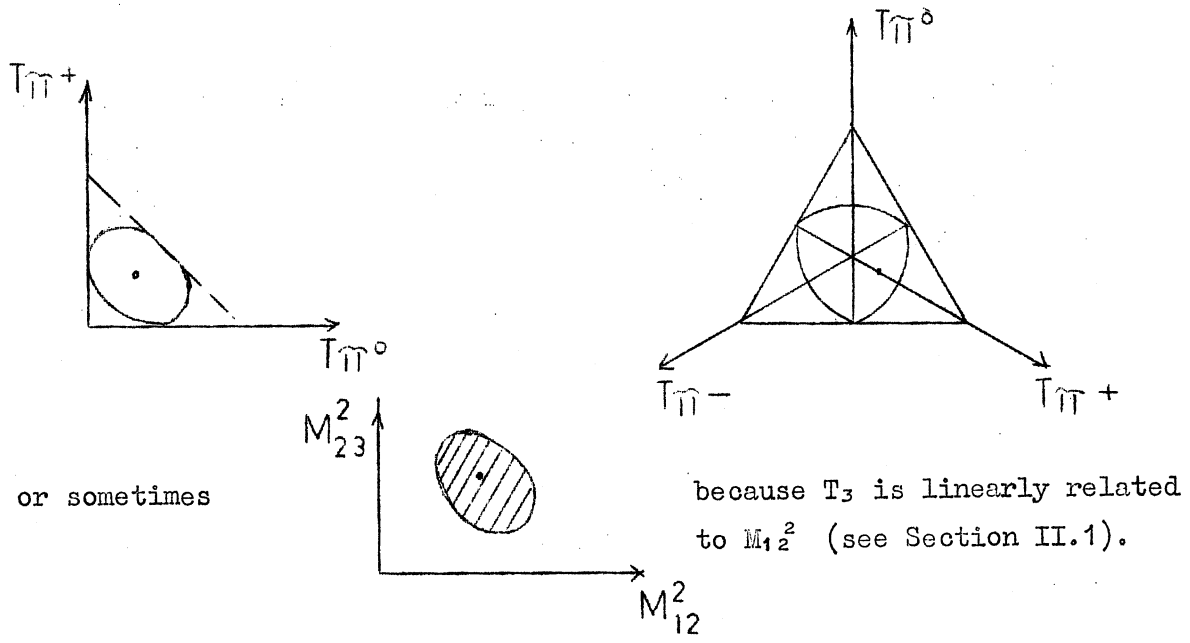

FIG. 5

b) Each event is represented by a dot in the diagram. Only a certain area of the diagram is allowed by energy-momentum conservation.

c) The density of points is the important thing to study, because it is proportional to the square of the matrix element for the transition. The reason that this is so is that the phase space volume is proportional to $dT_1\ dT_2$, the elementary area in the diagrams. Figure 6 shows how the density may vary with spin and parity. Figure 7 is the Dalitz diagram for ω and Fig. 8 a radial plot for ω.

4. Particle systematics

The systematization of the particles, resonance particles and old particles together, is based on the quantum numbers. We leave the leptons ($e\ \mu\ \nu_e\ \nu_\mu$) out and also the photon (γ) and study only the strongly interacting particles. The start is made with the baryon number B, which is strictly conserved, then the strangeness S, the isobaric spin T and finally spin J and parity P. Table 3 shows isospin multiplets.

Table 3

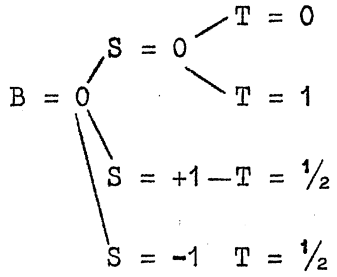

J^P				
0^+	0^-	1^-	1^+	unknown
	$\eta^0(548)$	$\omega^0(782)$		$f^0(1250$
	$\pi(140)$	$\rho(750)$		$\xi(560)$
	$K(494)$	$K^*(890)$		
	$\bar{K}(494)$	$\bar{K}^*(890)$		

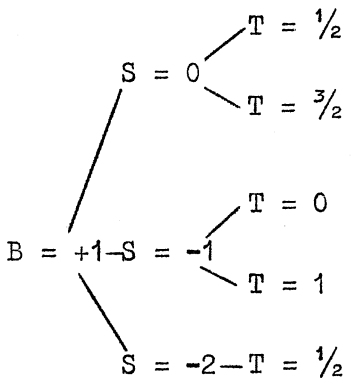

$\frac{1}{2}^+$	$\frac{1}{2}^-$	$\frac{3}{2}^-$	$\frac{3}{2}^+$	unknown
N(938)		N*(1512)		**N*(2190)**
			N*(1238)	N*(1920) N*(2360)
$\Lambda^0(1115)$		$Y_0^*(1520)$		Y*(1405)
$\Sigma(1190)$		$Y_1^*(1660)$		$Y_1^*(1385)$
$\Xi(1321)$				$\Xi^*(1530)$

Note how well filled are the meson columns (0^-), (1^-), leaving 0^+, 1^+ empty. The octets (see Van Hove's lecture) are found in these columns and in the one containing the nucleon. One new octet may be formed in the $\frac{3}{2}^-$ column. This new octet should then consist of the doublet N*(1512), the singlet Y*(1520), the triplet $Y_1^*(1660)$ and a yet to be discovered doublet with strangeness S = -2.

5. Production channels

A large variety of reactions have been studied in which the resonances occur. In a few cases, the threshold is below the masses of the particles in the initial state, such as in the production of pion resonances (ω, ρ, K^*) in $P\bar{P}$. Also η is below the threshold, of course, but has not been observed. This fact might not exclude it being produced in the reaction because of two factors:

i) the phase space is low in the η region;

ii) the η is decaying to charged pions in only about 25% of the events.

The η has been observed in the following reactions.

		Threshold kinetic energy
a)	$\gamma + P \rightarrow \eta + P$	710 MeV
b)	$\pi^+ + P \rightarrow \eta + P + \pi^+$	790 MeV
c)	$\pi^- + P \rightarrow \eta + n$	560 MeV
d)	$\pi^+ + d \rightarrow \eta + P + P$	480 MeV
e)	$K^- + P \rightarrow \eta + \Lambda$	380 MeV
f)	$P + P \rightarrow \eta + P + P$	1260 MeV
	a similar list for ω contains:	
g)	$\pi^- + P \rightarrow \omega +$ neutrals	960 MeV
h)	$\rightarrow \omega + \pi^- + P$	1220 MeV
i)	$\pi^+ + P \rightarrow \omega + \pi^+ + P$	1220 MeV
j)	$\pi^+ + d \rightarrow \omega + P + P$	802 MeV
k)	$K^- + P \rightarrow \omega + \Lambda^\circ$	825 MeV
l)	$P + P \rightarrow \omega + P + P$	1890 MeV
m)	$P + \bar{P} \rightarrow \omega + \pi^- + \pi^+ + i\pi^\circ \quad i \geq 0$	< 0 MeV
n)	$\rightarrow \omega + 2\pi^+ + 2\pi^-$	< 0 MeV
o)	$\rightarrow \omega + K^+ + K^-$	< 0 MeV
p)	$\rightarrow \omega + K^\circ + \bar{K}^\circ$	< 0 MeV.

Figure 9 shows results of reactions (d) and (j). Figure 10 on reaction (o) shows how free from background ω is produced, e.g. nearly all pions produced come via ω(~ 90%).

Nature seems to favour the production of a few particles, which then decay to a few particles giving a final state of larger multiplicity. A striking example is the following reaction reported by W. Chinowsky et al.[2)]

$$K^+ + P \to (K^*)^0 + (N^*)^{++} \to K^+ + P + \pi^+ + \pi^-$$

$$(N^*)^{++} \to P + \pi^+$$

$$(K^*)^0 \to K^+ + \pi^-.$$

The total cross-section for K^+P is at the energy of this experiment 18 ± 3 mb. The channel with $K^+P\ \pi^+\ \pi^-$ corresponds to about 2 mb and of this about 80% goes through the double resonance K^*N^*. In addition some cases correspond to $K^*P\ \pi^+$ and some to $K^+\ \pi^-\ N^*$. Thus only a few per cent of the cases proceed without involving a resonance particle (Fig. 11).

Another example of interest is the reaction $\pi^+ + P \to P +$ several π as studied by Alff et al.[3)]. Here the three pionic resonances ρ, η and ω were all found and with considerable intensities for the ρ and ω. Also the cross-section is appreciable for

$$\pi^+ + P \to N^* + \rho \text{ (double resonances)}$$

$$\to N^* + \omega \text{ (double resonances)},$$

where N^* is the pion-nucleon first resonance $(3/2, 3/2)$. The intensities for ω are impressive. Thus ω is produced in 50% of the sample with $\pi^+\ \pi^-\ \pi^0$ present. Of this sample 10-15% seems to go via $N^* + \omega$.

About ten years ago the multiple production of particles, mainly pions, was thought of as a statistical mechanics problem. The Fermi theory for evaporation of many pions from the heated interaction volume of two colliding high-energy particles was used during the 1950's. The situation has now changed and the multiple particle states are far more interesting than anybody could dream of ten years ago.

The observed production dynamics of the resonances can be used to determine their intrinsic properties. As an example we can take the reaction mentioned above:

$$K^+ + P \rightarrow K^* + N^* .$$

In condensed form the following holds:

i) the K* is emitted strongly forward;

ii) an Adair analysis was made on the forward events to obtain information on the spin of K*;

iii) the angle α is the angle between K^+ outgoing in the c.m.s. of K* and the incident K^+ direction. The distribution of α was found to be $\cos^2 \alpha$;

iv) the anisotropy rules cut $J(K^*) = 0$;

v) spin of K* is from $\cos^2 \alpha$ evidence $J(K^*) \geq 1$.

Alston et al.[4] have evidence that $J(K^*) < 2$ from which it is concluded that

$$J(K^*) = 1 .$$

As for the parity, it is odd on the basis of $P(K^*)$ is odd and spin $J(K) = 0$, because then $K + \pi$ is in a p-state which is odd (the odd intrinsic parities of K and π cancel). K* is thus $J^P = 1^-$, nicely fitting in the octet of vector mesons with ω and ρ and $\overline{K^*}$. The CERN study [Armenteros et al.[5]] of $\bar{P} + P \rightarrow K^* + K$ together with arguments by M. Schwarz also is evidence for the assignment of vector character to the K*.

6. Decay channels

A new state of resonance (particle) is discovered by the study of a particular combination of decay products. The next important question that arises is whether there are other decay modes of the same state. The identification of these presents new difficulties. The branching ratios are of great importance for the understanding of their properties. The following discusses what is at present known in this field.

η (548) For the η meson several groups have reported a large amount of neutral decays of unidentified nature. Thus in the reaction $K^- + P \to \Lambda +$ neutrals, the missing mass of η occurred[6]. Likewise in $P + P \to P + P +$ neutrals[7], in $\pi^+ + d \to P + P +$ neutrals[8] and $\pi^+ + P \to \pi^+ + P +$ neutrals[3]. Events with η mass were found in such quantity that the branching ratio is

$$\frac{\eta \to \text{neutrals}}{\eta \to \pi^+ \pi^- \pi^0} = 3 \pm 0.5 \ .$$

The nature of the neutral modes are important as can be seen from the following Table 4.

Table 4

J^{PG} of η	Expected dominant decay mode
1^{--}	$\pi^0 + \gamma$
0^{-+}	2γ and $3\pi^0$
1^{++}	$\pi^0 + 2\gamma$ and $3\pi^0$

If the 2γ mode is observed it fixes $J = 0$ for the η. It has been observed by Chrétien et al.[9] and more recently by Behr et al. at the Ecole Polytechnique[10]. The last-mentioned group worked with a heavy liquid bubble chamber at "Saturne". In such a chamber the photons have a good chance to produce electron pairs. The reaction was:

$\pi^- + P \to n + 2\gamma$ (or 3γ), the γ's producing pairs.
(1.15 GeV/c)

The mass of the parent of 2γ is found from

$$M^2 = (E_1 + E_2)^2 - (\bar{p}_1 + \bar{p}_2)^2 = 2E_1E_2 - 2p_1p_2 \cos \Phi$$

$$= 2E_1E_2(1 - \cos \Phi) = 4E_1E_2 \sin^2 \Phi/2 \ (\text{note } E = p \text{ for photons}).$$

The background caused by unrelated γ's from two π^0 in $\pi^- + P \to n + \pi^0 + \pi^0$ could be subtracted and what remained was as

shown in Fig. 12. They also find no evidence for $\eta \to \pi^0 + \gamma$ $(\to \gamma + \gamma + \gamma)$.
A further study of η by Fowler et al.[11] has shown that $\eta \to \pi^+ + \pi^- + \gamma$ occurs (Figs. 13 and 14). The branching ratio they obtain is:

$$\frac{\Gamma(\eta \to \pi^+ \pi^- \gamma)}{\Gamma(\eta \to \pi^+ \pi^- \pi^0)} = 0.26 \pm 0.08 \ .$$

The branching ratio for $\eta \to 3\pi^0$ is not experimentally known and is more difficult to study. Wali[21] predicts that the ratio depends on the π^0 energy spectrum in $\eta \to \pi^+ \pi^- \pi^0$. This spectrum is now known (Dalitz plot of η) and in the paper by Fowler et al.[11] the predicted value is

$$\frac{\Gamma(\eta \to 3\pi^0)}{\Gamma(\eta \to \pi^+ \pi^- \pi^0)} = 1.68 \pm 0.05 \ .$$

If no other neutral modes occur apart from $3\pi^0$ and 2γ we have

$$\Gamma(\eta \to 3\pi^0) = 1.68 \cdot \Gamma(\pi^+ \pi^- \pi^0) \text{ (predicted)}$$

$$\Gamma(\eta \to 2\gamma) = 1.33 \cdot \Gamma(\pi^+ \pi^- \pi^0) \text{ (if } 2\gamma \text{ and } 3\pi^0 \text{ only)}$$

$$\Gamma(\eta \to \pi^+ \pi^- \gamma) = 0.26 \cdot \Gamma(\pi^+ \pi^- \pi^0) \text{ (directly measured)}.$$

The total width of η is not known (the present experimental limit of a few MeV is set by errors of measurement). From a theoretical estimate of $\Gamma(\eta \to 2\gamma)$, made with the same method as that used for $\pi^0 \to 2\gamma$, a total width of about 190 eV is deduced and a lifetime of $4 \cdot 10^{-18}$ sec, indeed in a difficult time region. This lifetime of η is entirely a theoretical value.

ρ (750) For this state only 2π decays are known. A search for $\rho^0 \to \pi^+ \pi^+ \pi^- \pi^-$ in antiproton-proton reactions [Chadwick et al.[12]] gave the limit of less than 2.5%. The ρ mass distribution is very wide and the corresponding peak in histograms like a jelly. A splitting of ρ into two peaks (ρ_1 ρ_2) has been discussed but the evidence is not yet convincing.

ω (782) The dominant mode is 3π, namely $\omega^0 \to \pi^+ \pi^- \pi^0$. The mode $\omega \to 3\pi^0$ is forbidden. The other modes possible for ω violate G parity. The neutral mode expected to dominate is $\omega \to \pi^0 + \gamma$ and here the branching ratio from several experiments [Pevsner et al.[13], Alff et al.[5] and Armenteros et al.[17]] seem to point to about 10%. The $\omega \to 2\pi$ is interesting, but difficult because of the nearby $\rho^0 \to 2\pi$ and interference between the two. Of the order of at the most a few per cent has been reported; but the situation is not at all clear.

K*(888 MeV)goes 100% to $K + \pi$.

Y_1^* (1385) is dominated by the decay $Y_1^* \to \Lambda + \pi$. The expected $Y_1^* \to \Sigma + \pi$ is weak or absent; < 4%.

Y_0^* (1405) is observed as $Y_0^* \to \Sigma^{\pm\,0} + \pi^{\mp\,0}$. No other decay is known.

III. STUDY OF Y* (1405 MeV) BY NUCLEAR EMULSIONS

The rest of my lecture will be devoted to what has been done on Y* (1405) in nuclear emulsion studies. Besides the research on nucleon isobars by the Copenhagen group, this resonance is the only one studied by the emulsion technique. If the resonance is very narrow as some available results indicate, it is well suited to such studies.

We note that the mass of Y_0^* reported by the bubble chamber groups M(Y*) = 1405(± 5) MeV is below the sum of masses of the particles that can produce it (K^- and proton), $M(K^-) + M(P)$ = 1432 MeV. The difference is 27 MeV. With free protons only the reaction $K^- + P \to Y^* + \gamma$ is energetically possible. It has, however, not been observed, but, as far as I know, has not been seriously searched for either. The energy of the γ ray and the width of the γ ray line would give the mass of Y*, respectively its width (Γ). The many competing reactions $K^- + P \to \Sigma\pi$, $\Lambda\pi$, its small phase space and the electromagnetic coupling constant, will together make it a rare reaction, unfortunately.

On bound protons, the residual nucleus can take up the recoil momentum so one would get

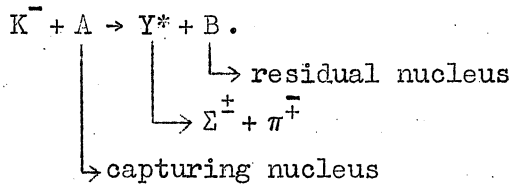

The first study of this type was undertaken by Eisenberg et al.[16] with K^- stopping in nuclear emulsions. From the measured energies of the Σ and the π they obtained a distribution of the energy sum $E = (E_\Sigma + E_\pi)$ and of the invariant mass

$$M = \sqrt{(E_\Sigma + E_\pi)^2 - (\bar{p}_\Sigma + \bar{p}_\pi)^2} .$$

Their M distribution was somewhat narrower than the E distribution, which they claimed was evidence for Y* production. This argument was questioned by Burhop at the Aix-en-Provence Conference (1961). He claimed that this could happen even if Y* is not produced. Burhop's argument is apparently based on an infinitely large nucleus. For a light nucleus where you have well defined energy states of the residual nucleus

$$K^- + A \rightarrow \Sigma + \pi + B^* ,$$

the E distribution consists of fairly sharp lines, broadened only by the kinetic energy variation of B (0-4 MeV) [one line for each excited state of B]. On the other hand the distribution of $\bar{p}_\Sigma + \bar{p}_\pi$, which reflects the internal momentum distribution of the protons in the capturing nucleus is rather wide. So, contrary to Burhop's argument, the expected M distribution should be wider than the E distribution (provided Y* is not produced). The findings of Eisenberg et al.[16] are, however, not confirmed by Frisk[14] who finds that the M distribution is - if anything - wider than the E distribution. This can be seen in Figs. 15 and 16. Both the experimental situation and the theoretical arguments on this point are therefore somewhat confused. However, in what follows, the whole point may be forgotten. As I just said, the distribution in $|\bar{p}_\Sigma + \bar{p}_\pi|$ expected, if

the Σ and the π are directly produced by $K^- + P \to \Sigma + \pi$ on a bound proton, reflects the internal momentum distribution of the bound protons (modified by phase space, by surface absorption of the K and by angular momentum conservation).

If a Y* is formed this is not so any longer. Let us consider a two-body process

$$K^- + A \to Y^* + B$$

where the residual nucleus is in a certain state (ground state or excited state). Let p be the momentum of Y*, energy-momentum conservation gives

$$m_K + m_A - B_{\text{Atomic K}} = M(Y^*) + M_B + \frac{p^2}{2M_{Y^*}} + \frac{p^2}{2M_B}$$

$$\therefore\ p^2 \left(\frac{1}{2M_Y} + \frac{1}{2M_B}\right) = 27 - B_{\text{proton}} - B_A - E_{\text{exc.}}\ (B) + [1405 - M(Y^*)]\ .$$

For a given capturing nucleus, the proton binding energy B_{proton} and B_A are fixed. Therefore p is constant (a line) widened only by the variation of the mass of Y*.

The effect of a wide Y*-mass distribution has now to be worked out. According to bubble chamber results on Y* (1405), it has been reported that $\Gamma(Y_0^*) \simeq 50$ MeV[20]. This means that in our formula the term (1405-M) is often at least 25 MeV, which has a large effect on p. It spreads p from its central value down to 0 and up to 300 MeV/c with a tail even higher up. Many such curves will overlap, one curve for each capturing nucleus and each final state nuclide. Qualitatively, the expected distribution in p is like the one expected for direct production of Σ and π; so it would seem as if nothing could be learned from a p plot.

It was, therefore, very surprising when Frisk (1962) found a sharp line in the momentum distribution. He studied events in nuclear emulsion of the type $K^- + A \to \Sigma^{\pm} + \pi^{\mp} + B +$ (ev. neutrals) [Fig. 17]. The peak in the region 160-180 MeV/c is highly significant. A search for systematic errors has not led to any explanation, nor has a search for nuclear physics effects.

The peak has been identified with the existence of a $Y_o^* \to \Sigma^{\mp} + \pi^{\pm}$. From the foregoing arguments, the narrowness of the momentum line requires the Y* to have a width much smaller than the 50 MeV reported from bubble chamber experiments. The observed width of the line at 170 MeV/c is ± 5 MeV/c (standard error) which corresponds to the computed errors of measurements from $p^2 = p_\pi^2 + p_\Sigma^2 + 2p_\pi p_\Sigma \cos \Phi$, where Φ is the space angle between $\bar{p}_\pi$ and $\bar{p}_\Sigma$.

$$\frac{p\delta p}{M_{red}} = \delta M(Y^*),$$

where M_{red} is the reduced mass of Y* and the residual nucleus B;

$$\frac{p}{M_{red}} = \frac{1}{7}$$

is the relative velocity, β, of Y* and residual nucleus,

$$\therefore \delta M = \frac{1}{7} \cdot \delta p = \pm \frac{1}{7} \cdot 5 = \pm 0.7 \text{ MeV}.$$

Thus $\Gamma < 1.4$ is the result.

In a later work by Frisk and myself[15] we could make a more detailed study of the line and confirm the suggestion made by Frisk that the line corresponds to captures in carbon.

If the line is caused by captures in light elements (C,N,O), the momentum of 170 MeV/c is sufficient to render the recoil track of the residual nucleus visible (2 - 3 μm). Captures in Ag, Br would not make the recoil visible. The events were divided into two subsamples:

i) those with no recoil and no Auger electron;
ii) those with a possible recoil.

The graphs Figs. 18 and 19 show that the peak at 170 MeV/c fell into the second sample, but is absent from the no-recoil sample. In the second sample a further subdivision of events was undertaken. This time we required the recoil to be measurable and not obscured by other tracks, be it the K meson track or Auger electron or the outgoing Σ or π tracks.

This procedure introduces a bias, corresponding so that:

i) no heavy recoil nucleus can be included (no captures in Ag and Br);

ii) light nuclei with momenta below about 100 MeV/c are absent.

For the region of interest, around momenta of 170 MeV/c of light nuclei, the bias is thus not serious. In the sample so selected we measured the angle between $\overline{p_{Y^*}} = \overline{P_\Sigma} + \overline{p_\pi}$ and the recoil track. The plane angle was in nearly all cases 180° (± 20°) and in dip angle we only could require that they were approximately opposite.

The momentum distribution of this highly selected sample is shown in Fig. 20. The peak is still in the same position sitting on a low background. The position of this peak (172 MeV/c) was used to compute the Y* mass from the formula

$$m(Y^*) = m_K + m_p - B_{proton} - B_\Lambda - E_{exc.}\ (B) - p^2 \left(\frac{1}{2m_{Y^*}} + \frac{1}{2m_B}\right)$$

or the equivalent relativistic expression for the kinetic energy.

The mass one obtains depends on the nature of the capturing nucleus (B_{proton}) and the state of excitation ($E_{exc.}$) of the final nucleus. To help in fixing these things we did the following:

i) computed the invariant mass for the peak events with the result $\langle M_{inv} \rangle = 1404 \pm 1$ MeV where ± 1 is the standard error in the weighted mean;

ii) measured the ranges of the recoil tracks. The mean range is (after correction for dip) only consistent with the lightest possible recoil nucleus, ^{11}B (from Barkas range energy relation for heavy nuclei, extrapolated down to our region). One would like to have ranges for light nuclei down to about 1 MeV kinetic energy (the present limit is 4 MeV). We, finally, find all evidence points to the reaction

$$K^- + {}^{12}C \rightarrow Y^* + {}^{11}B \text{ (gr. state)}$$

as <u>mainly</u> responsible for the line. The results are: mass of Y* = 1404.2 ± 0.4 MeV [invariant mass of Y* = 1404 ± 1 MeV], width (Y*) is $\Gamma < 1.4$ MeV.

The line has been reported also by Eisenberg[18]. In a study of S. White and C. Gilbert (unpublished) it was not seen in the overall ($\Sigma\pi$) sample, but was clear in the sample with recoils. They obtained two lines one at the position expected for carbon captures, the other (weaker line) corresponding to oxygen captures. The Brussels group has also reported the line, whereas still others are working on it. (Note added in proof Recently at Berkeley A. Barbaro-Galtieri, F.M. Smith and J.W. Patrick, Phys.Letters 5, 63 (1963), reported results which do not confirm the existence of a line in the momentum spectrum. The reason for this situation with conflicting results is not at present known.) Frisk measured the pion energies mostly by grain-counting, by range only for pions that stopped in his rather small stack. In order to get better resolution range measurements are preferable; but then, one must have a large stack as the pion ranges go up to 8 cm. If one selects only stopping pions in a small stack, a bias is introduced.

Another systematic error which may wash out a sharp peak is emulsion distortion which has an effect on p(Y*) because of the error it introduces in the angle Φ

$$p^2 = p_{\pi}{}^2 + p_{\Sigma}{}^2 + 2p_{\pi}p_{\Sigma} \cos \Phi$$

$$\frac{\partial p}{\partial \Phi} = - \frac{p_{\pi}p_{\Sigma}}{p} \sin \Phi \, d\Phi .$$

The distortion error in Φ comes in via errors in dip angles and the plane angle between the π and the Σ. A Monte Carlo calculation of the expected broadening of an initially sharp peak has been carried out by P. Carlson (unpublished). The full width at half maximum of the line is about $60 \cdot K$ MeV, where K is the distortion vector. So if K = 20 μm/600 μm = 1/30, only 2 MeV/c broadening is expected. The calculation was made only for a simple combination of first and second order distortion.

Future lines of research have obviously first to deal with the problem of whether there is a line as reported by Frisk or not. With a large enough sample one should be able to find lines at other momenta,

corresponding to captures in other nuclei than carbon and to reactions with the final nucleus left in an excited state. The finding of such lines would constitute strong evidence in favour of the existence of a Y* with a narrow width. The existence or non-existence of a line in the momentum plot of the $\Sigma\pi$ system is always based on statistical tests and it seems now as if more data are needed.

* * *

REFERENCES

1. A.R. Erwin, R. March, W.D. Walker and E. West, Phys.Rev.Letters 6, 628 (1961).

2. W. Chinowsky, G. Goldhaber, S. Goldhaber, W. Lee and T. O'Halloran, Proc.of Int.Conf.on High-Energy Phys., CERN 1962, p. 380 and Phys.Rev.Letters 9, 330 (1962).

3. C. Alff, D. Berley, D. Colley, N. Getfand, U. Nauenberg, D. Miller, J. Schultz, J. Steinberger, T.H. Tan, H. Brugger, P. Kramer and R. Plano, Phys.Rev.Letters 9, 322 (1962).

4. M. Alston, L.W. Alvarez, P. Eberhard, M.L. Good, W. Graziano, H.K. Ticho and S.G. Wojcicki, Phys.Rev.Letters 6, 300 (1961).

5. R. Armenteros, L. Montanet, D.R.O. Morrison, S. Nilsson, A. Shapira, J. Vandermeulen, Ch. d'Andlau, A. Astier, C. Ghesquière, B.P. Gregory, D. Rahm, P. Rivet and F. Solmitz, Proc.of Int.Conf.on High-Energy Phys., CERN 1962, p. 295.

6. P.L. Bastien, J.P. Berge, O.I. Dahl, M. Ferro-Luzzi, D.H. Miller, J.J. Murray, A.H. Rosenfeld and M.B. Watson, Phys.Rev.Letters 8, 114 (1962).

7. E. Pickup, D.K. Robinson and E.O. Salant, Phys.Rev.Letters 8, 329 (1962).

8. M. Meer, R. Strand, R. Kraemer, L. Madansky, M. Nussbaum, A. Pevsner, C. Richardson, T. Toohig, M. Block, S. Orenstein and T. Fields, Proc.of Int.Conf.on High-Energy Phys., CERN 1962, p. 103.

5666/NP/smg

9. M. Chrétien, F. Bulos, H.R. Crouch, R.E. Lanou, J.T. Massimo, A.M. Shapiro, J.A. Averell, C.A. Bordner, A.E. Brenner, D.R. Firth, M.E. Law, E.E. Ronat, K. Strauch, J.C. Street, J.J. Szymanski, A. Weinberg, B. Nelson, I.A. Pless, L. Rosenson, G.A. Salandin, R.K. Yamamoto, L. Guerriero and F. Waldner, Phys.Rev.Letters 9, 127 (1963).

10. L. Behr, P. Mittner and P. Musset, Phys.Letters 4, 22 (1963).

11. E.C. Fowler, F.S. Crawford, L.J. Lloyd, R.A. Grossman and LeRoy Price, Phys.Rev.Letters 10, 110 (1963).

12. G.B. Chadwick, W.T. Davies, M. Derrick, C.J.B. Hawkins, P.B. Jones, J.H. Mulvey, D. Radojicic, C.A. Wilkinson, M. Cresti, A. Grigoletto, S. Limentani, A. Loria, L. Peruzzo and R. Santangelo, Proc.of Int. Conf.on High-Energy Phys., CERN 1962, p. 73.

13. A. Pevsner, R. Kraemer, M. Nussbaum, C. Richardson, P. Schlein, R. Strand, T. Toohig, M. Block, A. Engler, R. Gessaroli and C. Meltzer, Phys.Rev.Letters 7, 421 (1961).

14. Å. Frisk, Ark.Fys. 24, 221 (1963).

15. Å. Frisk and G. Ekspong, Phys.Letters 3, 27 (1962).

16. Y. Eisenberg, G. Yekutieli, P. Abrahamsson and D. Kessler, Nuovo Cimento 21, 563 (1961) and The Aix-en-Provence Conf.Proc., Vol. I, 389 (1961).

17. R. Armenteros, R. Budde, L. Montanet, D.R.O. Morrison, S. Nilsson, A. Shapira, J. Vandermeulen, C. d'Andlau, A. Astier, C. Ghesquière, B. Gregory, D. Rahm, P. Rivet and F. Solmitz, Proc.of Int.Conf.on High-Energy Phys., CERN 1962, p. 90.

18. Y. Eisenberg, Proc.of Int.Conf.on High-Energy Phys., CERN 1962, p. 791.

19. B.C. Maglić, L.W. Alvarez, A.H. Rosenfeld and M.L. Stevenson, Phys.Rev.Letters 7, 178 (1961).

20. M.H. Alston, L.W. Alvarez, M. Ferro-Luzzi, A.H. Rosenfeld, H.K. Ticho and S.G. Wojcicki, Proc.of Int.Conf.on High-Energy Phys., CERN 1962, p. 311.

21. K.C. Wali, Phys.Rev.Letters 9, 120 (1962).

* * *

DISCUSSION

Harmsen : How large is the error in the extrapolation of the range-energy-relation which you have used for the mass determination of the recoils?

Ekspong : The error is hard to estimate. Barkas and his collaborators have made a universal curve for the ranges of slow heavy particles (carbon, oxygen etc. up to argon). Their actual measurements for light nuclei (carbon) go down to about 4 MeV and we need ranges for 1 - 2 MeV particles. We used their data for heavier atoms for this extrapolation, thus assuming the universal curve of Barkas et al. to hold. The actual average range for our boron atoms are about 0.5 microns longer than expected from the extrapolation. When we first started to study the recoil ranges we did not know how good a job one can do. It seems, however, that the ranges come out rather constant, but as I said about 0.5 microns too long (the range is 2.9 μm). In the future we hope to be able to use the range measurements in the analysis to separate captures in carbon from captures in oxygen. Therefore, one would like to know the range-energy curves for light nuclei in the region 1 - 2 MeV from calibration experiments.

Hoogland : Do you know why in your emulsion experiment the Y* is produced mostly in ^{12}C?

Ekspong : I think it is only that carbon is very favourable, so when you first see the thing it is in carbon. I think it should be produced in all the elements including oxygen unless angular momentum conservation prevents it from going to the groundstate of ^{15}N from ^{16}O.

Key : Wouldn't the uncertainties in momentum in those cases which had to be grain-counted, swamp the 170 MeV/c peak?

Ekspong : I don't think so. By using checks on the grain density-range curve, counting as much as 1000 grains, you will end up with a standard error of about 9% in the pion energy. How large an error you get in the $(\Sigma\pi)$ momentum from this depends on the configuration of the event. You have to compute the error event by event. Frisk put everything in a computer which calculated the momentum with its errors and also the invariant mass and its errors. He fed the computer with all information from the measurements including errors of measurements. Most of the time the error on the momentum of the $(\Sigma\pi)$ system around 170 MeV/c was ± 5 MeV/c, but sometimes larger, up to about ± 15 MeV/c. If one could get the pion energy by range in all cases and also the Σ energy and have accurate angles, then one would certainly measure better, say ± 3 MeV/c; but the present method does not swamp the peak.

Hoogland : You spoke about the fact that interference could be an explanation for the differences in the width of resonances in different experiments with bubble chambers. Is it also possible that these interferences can give rise to different masses?

Ekspong : Well, in the case of the ω and the ρ, the closeness of their masses together with the large width of the ρ, can give rise to interference between $\omega^0 \to \pi^+ \pi^-$ and $\rho^0 \to \pi^+ \pi^-$. Such an interference could change the observed distribution of the $\pi^+ \pi^-$ masses in the neighbourhood of the ω mass to one with fluctuations up and down there. As for final-state interactions they might broaden the observed mass distributions or change their shapes.

Hoogland : I thought there was some indication that in a special case of experiment the mass of the resonance was lower than that hitherto found.

Ekspong : I don't know of any clear experiment on this.

Hoogland : Can you give an explanation for the value of the branching ratio

$$\frac{\eta \to \pi^+ \pi^- \gamma}{\eta \to \pi^- \pi^+ \pi^0} = \frac{1}{4} ?$$

Ekspong : I haven't done any calculation on that at all; I don't know if anybody else has done it. Of course, one could try the simple thing with an energy independent matrix element to see whether it comes close or not to the experimental value, which is 0.26 ± 0.08. The only thing which I know has been theoretically predicted by Wali is the ratio of $3\pi^0$ mode versus the $\pi^+ \pi^- \pi^0$. The prediction has not been experimentally confirmed as the $3\pi^0$ mode has not been measured.

* * *

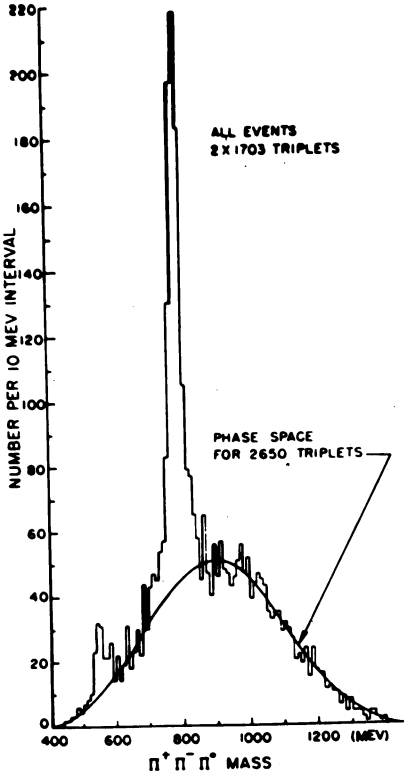

Fig. 3 Histogram with very strong evidence for ω -production. The data are from an experiment by C. Alff et al. (ref. 5), on the reaction $\pi^+ + p \rightarrow \pi^+ + p + \pi^+ + \pi^- + \pi^0$. Besides the strong ω-peak at 780 MeV, another peak at 550 MeV corresponding to η -production, is evident.

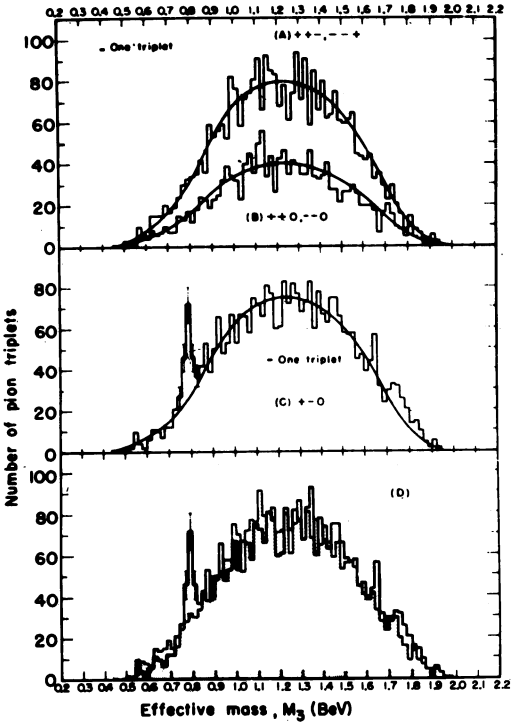

Fig. 4 Original evidence for ω -production in antiproton-proton annihilation by Maglic et al. (ref. 19).

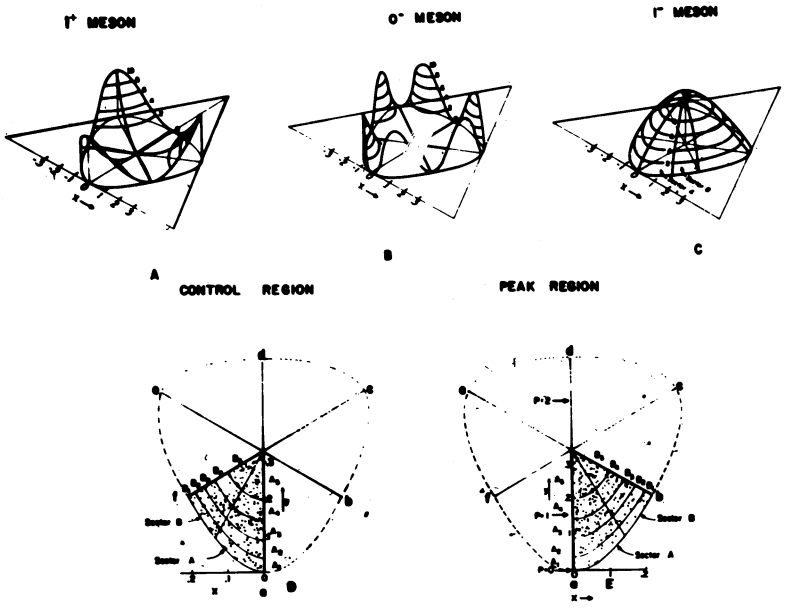

Fig. 6 Three-dimensional diagrams showing expected intensity distribution in Dalitz plots for 3 π-decay of mesons with spin-parity 1^+, 0^- and 1^-.

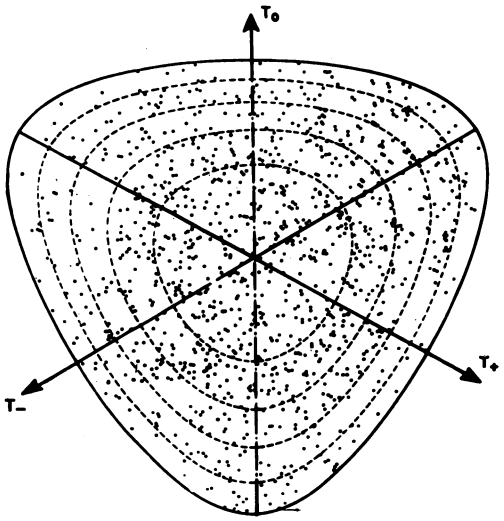

Fig. 7 Dalitz-diagram for ω -decay (1100 events) showing higher point density near the center region with a fall of intensity towards the outer sides, typical for a meson with spin parity assignments 1^-.

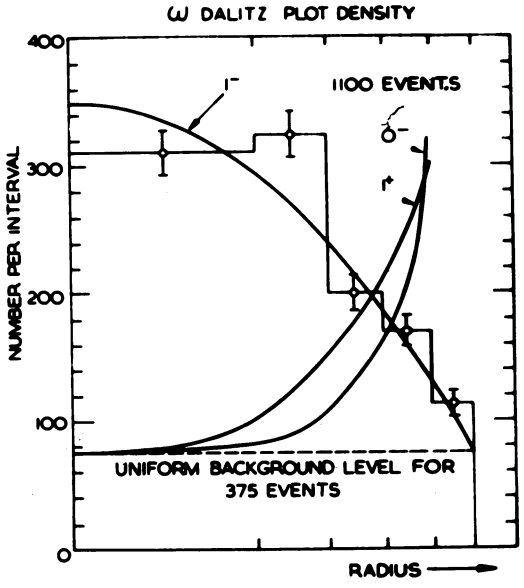

Fig. 8 Intensity of ω -decay as a function of the "radius" of the Dalitz plot (fig. 7). Solid lines show prediction for mesons 1^-, 0^- and 1^+. Experimental histogram does not fit 0^- and 1^+ mesons.

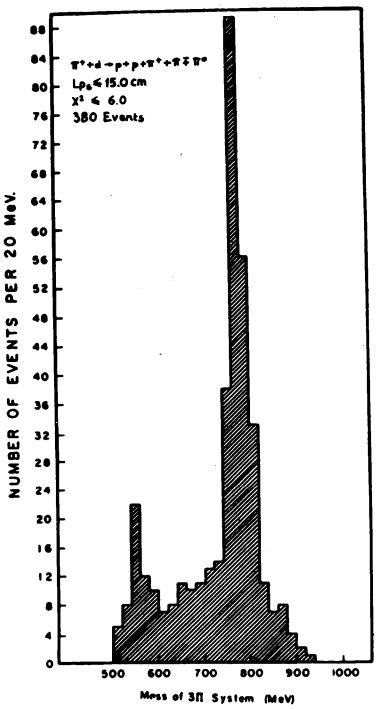

Fig. 9 The reaction $\pi^+ + d \rightarrow p + p + \pi^+ + \pi^- + \pi^0$ shows strong evidence for both ω (780 MeV) and η (550 MeV) production (ref. 13).

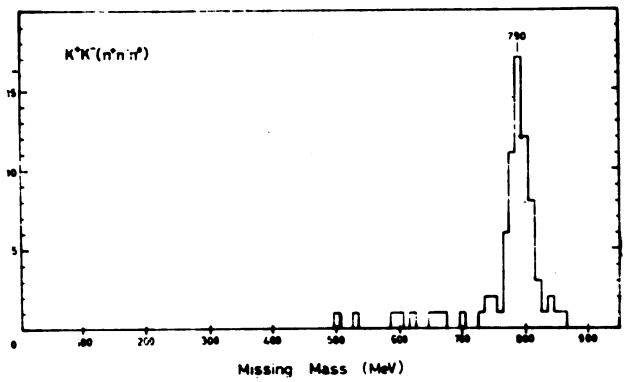

Fig. 10 In antiproton proton annihilations at rest into a pair of K mesons and three pions the pions are to a high proportion (> 90%) produced via the ω particle. The sample of ω is unusually free from background events (data by Armenteros et al. ref. 17).

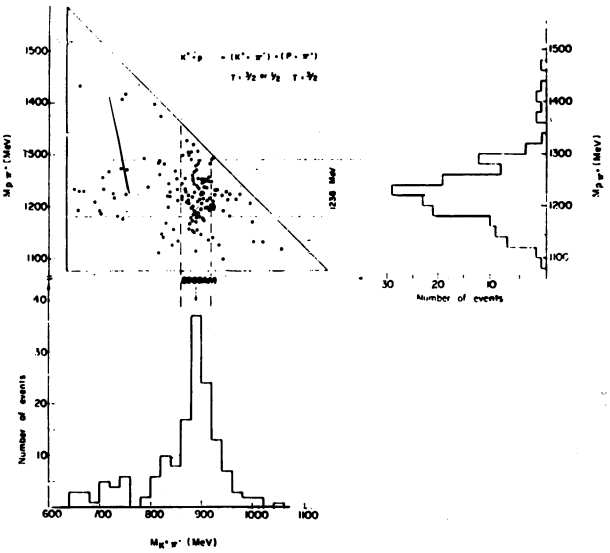

Fig. 11 Simultaneous production of both K^* (890 MeV) and N^*(1238 MeV) in the reaction by 2.6 GeV/c K^+ mesons

$$K^+ + p \rightarrow K + \pi + \pi + p$$

data by W. Chinowsky et al. (ref. 2).

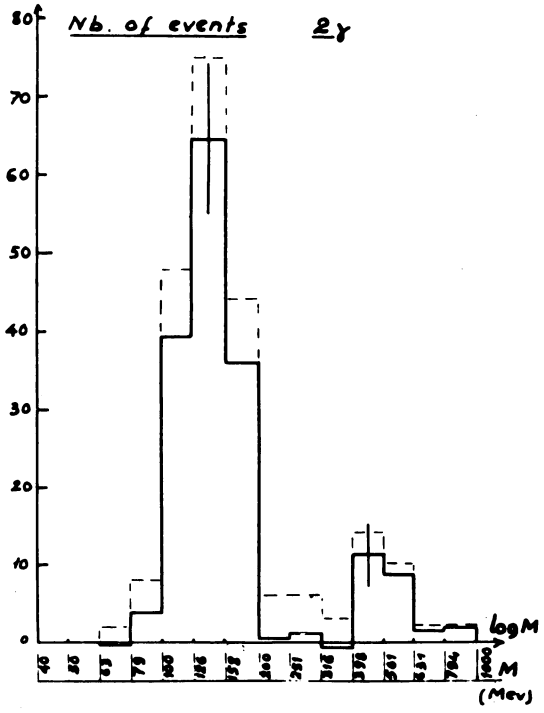

Fig. 12 Observations of two simultaneous γ-rays in a heavy liquid chamber (L. Behr et al., Saclay, ref. 10) give two peaks, one for π^0 the other corresponding to η^0(550 MeV). Gives direct evidence that the decay $\eta \rightarrow 2\gamma$ exists, implying spin 0 for η .

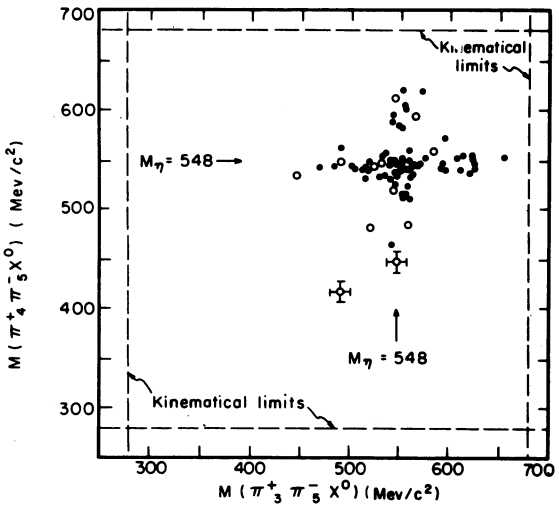

Fig. 13 Data by E. C. Fowler et al. (ref. 11) shows that the decay $\eta^0 \to \pi^+ \pi^- \gamma$ exists (open circles) besides $\eta \to \pi^+ \pi^- \pi^0$ (black dots).

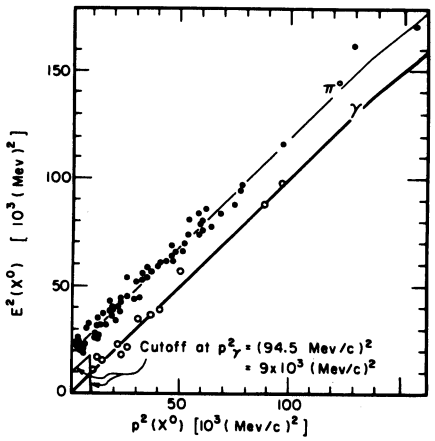

Fig. 14 Identification of neutral particle in η -decay by its mass as either π^0 (full circles) or γ (open circles). The relation $E^2 = p^2 + m^2$ (c=1) plotted. Same data as in fig. 13.

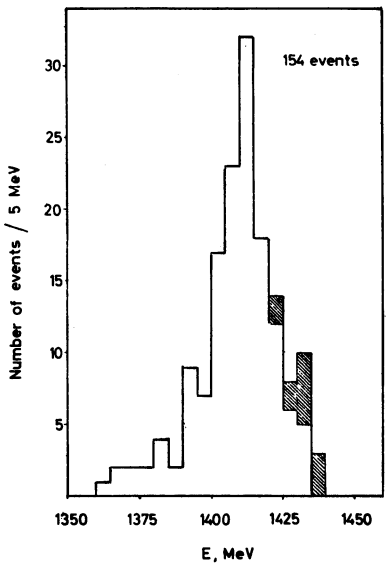

Fig. 15 Distribution of energy sum for Σ and π emitted in nuclear absorption reactions by K^- (A. Frisk, ref. 14). Shaded events correspond to reactions with free protons in nuclear emulsions.

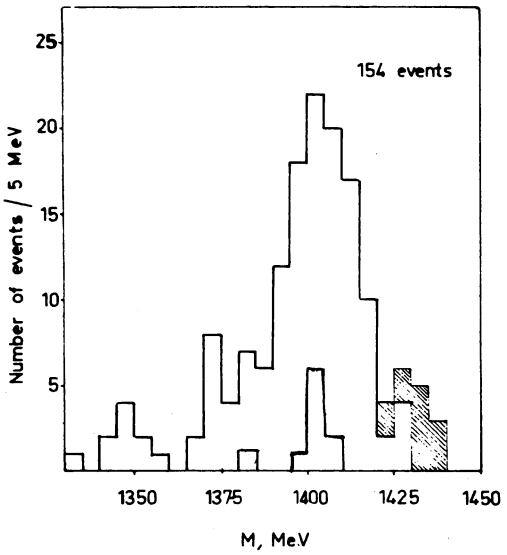

Fig. 16 Distribution of the invariant mass of 154 $\Sigma\pi$ events. Same data as in fig. 15. The 9 events close to 1405 MeV are interpreted as being examples of the reaction ^{12}C (K^-, Y^*) ^{11}B.

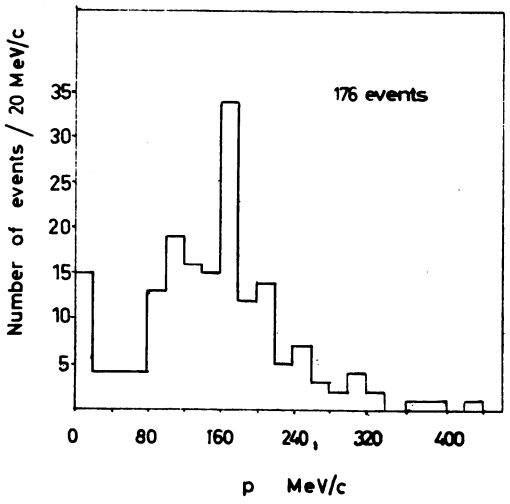

Fig. 17 Distribution of momentum of the $\Sigma\pi$ system (same data as figs. 15 & 16 showing unexpected sharp peak close to 170 MeV/c.

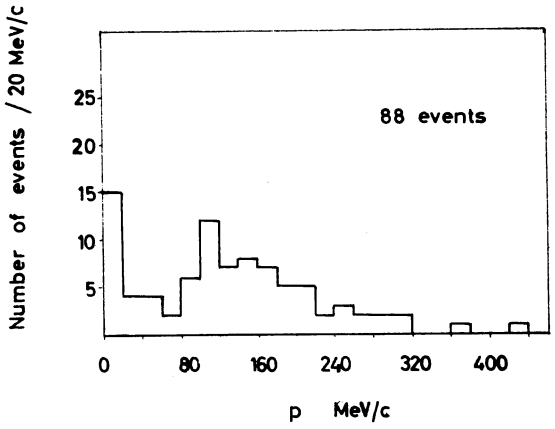

Fig. 18 Subsample of data in fig. 17 consisting of events of the type $K^- + A \rightarrow \Sigma + \pi + B$ where the residual nucleus (B) does not show any visible recoil track. Line at 170 MeV/c is absent.

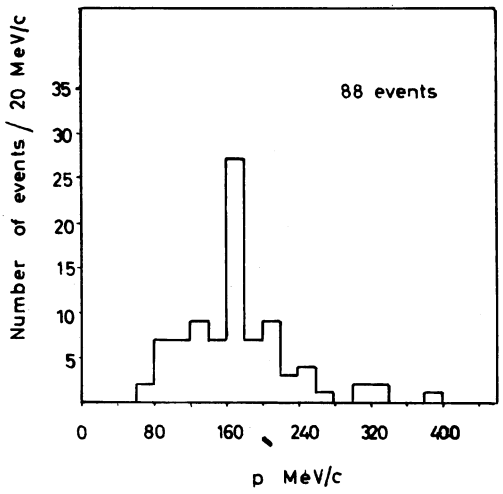

Fig. 19 Remaining subsample consisting of events enriched in visible recoils of nucleus B in reactions $K^- + A \rightarrow \Sigma + \pi + B$. Line at 170 MeV/c as strong as in the total sample of events; background reduced to about 50% of that in fig. 17.

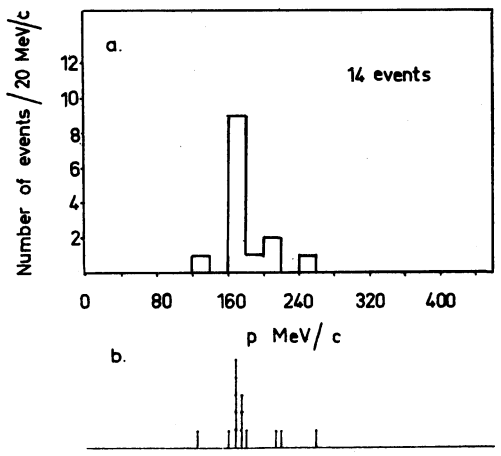

Fig. 20 Events of the type $K^- + A \rightarrow \Sigma + \pi + B$ with a measurable recoil track attributed to nucleus B. In (b) individual events are plotted, showing close grouping of events at 172 MeV/c.

III. NEUTRINO PHYSICS

PART III.1

NEUTRINO EXPERIMENTS

G. von Dardel,
Nuclear Physics Division, CERN.

I. INTRODUCTION

The theoretical background of neutrino experiments with high-energy machines has been given in the lectures of Professor Bernardini. I just want to recall some of the facts that render neutrino experiments possible with high-energy machines, and which determine the experimental problems one can study.

1. The cross-section for a neutrino to produce the elastic reaction[1,2]

$$\nu + n = \mu^- + p \qquad (1)$$

increases with neutrino energy[1] until it levels off (Fig. 1) at a level of about 10^{-38} cm^2 because of the limiting effect of the form factors of the weak interaction.

2. These form factors will cause a decrease of the differential cross-section when the momentum transferred to the nucleon is large, that is at large angles.

3. When the momentum transfer to the nucleon is small and the nucleon is bound in a nucleus, as is always the case in the detectors one can consider at present for neutrino experiments the differential cross-section is decreased by the effect of the Pauli principle in the nucleus[3].

4. If the weak interactions are mediated by an intermediate particle, which must be a charged boson of spin 1, this particle should be produced by the reaction

$$\nu \rightarrow W^+ + \mu^- \qquad (2)$$

if the neutrino energy E_ν is sufficient. The momentum balance of the reaction

$$q \approx M^2/2E_\nu \qquad (3)$$

is provided by the Coulomb field of a nucleus acting on the charge W^+ and μ^- [4]. M is the invariant mass of the system $W^+ + \mu^-$, which is mostly made up of the mass of the heavier W^+.

If for example the neutrino energy is 5 GeV and the mass M is 1 GeV, the necessary momentum transfer from the nucleus is only 100 MeV/c. Since the momentum transfer decreases with increasing neutrino energy, the cross-section for vector boson production increases very rapidly with increasing neutrino energy, and since only a semi-weak interaction is involved, the cross-section will rapidly become larger than the cross-section for ordinary neutrino reactions like (1).

The mass of the vector boson is known to be larger than the K-meson mass from the very existence of the K meson. The cross-section for producing it with neutrinos in the energy range available from present machines drops very rapidly with the mass.

5. The first high-energy neutrino experiment[5] in Brookhaven confirmed the theoretical belief that the neutrino, ν', associated in weak interactions with a muon is a different particle than the ordinary neutrino, ν, associated with an electron.

II. NEUTRINO SOURCES

The most abundantly produced of the secondary particles from high-energy interactions is the pion which by its dominant decay mode

$$\pi^+ \rightarrow \mu^+ + \nu' \qquad (4)$$

is a source of the μ neutrino. The average pion energy from a 25 GeV interaction is about 2 GeV, and since the neutrinos have energies from almost zero to a maximum of 42% of the pion energy, the average neutrino energy from this reaction is low - less than 1 GeV.

The decay distance of pions is about 55 m at a momentum of 1 GeV/c. To produce an intense neutrino flux, a free decay distance must be provided. In the CERN experiment this decay distance is 25 m.

In the decay of the pion the neutrino can receive a transverse momentum of up to 30 MeV/c. Particularly at low neutrino energies the neutrino beam will therefore have a considerably wider distribution than the parent pion beam.

The process (4) produces only μ neutrinos. Electron neutrinos are produced in the rare electronic decay of the pion

$$\pi^+ \rightarrow e^+ + \nu \qquad (5)$$

which, however, is only produced with a branching ratio of 10^{-4}. They are also produced in the muon decay

$$\mu^+ \rightarrow e^+ + \nu + \bar{\nu}' \qquad (6)$$

but the muon lifetime is too long for this reaction to contribute appreciably.

Secondary particles other than pions may also contribute to the neutrino flux, but the only important contribution comes from the K mesons, in the most frequent $K_{\mu 2}$ decay (60% probability)

$$K^+ \rightarrow \mu^+ + \nu' . \qquad (7)$$

In writing the reaction this way, it has been assumed that the neutrino associated with the muon in K decay is the same ν' as in π decay. This is, however, only an assumption. The identity, or non-identity of the neutrinos produced in different decay reactions can in principle only be proved by performing the inverse reactions with high-energy neutrinos of well defined origin. In the Brookhaven experiment a small fraction of the neutrino flux is caused by K decay. If as proposed by Bludman[6] and by Feinberg, Pais and Guersey[7] the roles of the two neutrinos are reversed in K meson, 5 electron events should have been expected, whereas no certain cases were observed.

Although the K meson is less abundantly produced in high-energy reactions, by a factor 5 for K^+, this is partly compensated by the shorter decay path, 7 m against 55 m. Another important feature is that K neutrinos can carry away up to 80% of the K meson energy as against 42% for the pion decay. Since the production spectra for K mesons and pions are similar and fall off rapidly at high energy, the neutrinos from K decay will dominate in the high-energy tail of the neutrino spectrum. They will be of great importance for the possibility of producing the vector boson with neutrinos from present day machines.

On the other hand the higher possible transverse momentum, 200 MeV/c in $K_{\mu 2}$ decay, will cause the neutrino beam to spread out more in angle than for π decay neutrinos of the same energy.

The smallness of the neutrino cross-sections makes it imperative to maximize the neutrino flux at the detector. The distance between source and detector is determined by the necessity to provide a sufficiently long decay path and to interpose shielding between the end of the decay

path and the detector. The thickness of the shielding is set by the maximum energy of the muons which have to be absorbed in it and can only be reduced by the use of heavy shielding materials. If the pion angular distribution is wide over an angular range corresponding to the neutrino angles with respect to the pions, it can be shown that the optimum is to make the decay path equal to the shielding thickness.

The Brookhaven experiment[1] had a calculated neutrino flux spectrum as shown by Fig. 2, normalized to 10^{11} protons interacting in the target. This flux spectrum would lead to an interaction rate of only a few events per day in 10 tons of material which was close to the value found in the experiment.

As long as the pion angular distribution is broad compared to the angles involved in the decay to neutrinos, intensity can be gained at the detector by a focusing of the pions beam before it decays. A device which is capable of focusing the pions over a wide range of angles of emission and of momenta to a nearly parallel beam, has been developed by van der Meer[8] at CERN. The principle of this device, called the neutrino horn, is shown in Fig. 3. A strong current of several hundred thousand amp generates a circular magnetic field in the volume between two cone-shaped conductors. The current is pulsed on at the same time as an extracted beam from the accelerator hits a narrow target on the axis of the cones. Particles which are emitted at an angle will pass through the inner conductor and will be bent towards the axis trajectory I, by the magnetic field to be re-emitted through the conical conductor with a much smaller angle to the axis than the original emission angle. With the CERN horn, 3 m long and with 300,000 amp, this type of focusing occurs at about 6 GeV/c momentum. Another type of focusing, effective at low momenta, is due to trajectories as the one denoted by II in Fig. 3. The particle makes a first reflection in the cylindrical part of the conductor and a second one in the conical part. If the emission angle is twice the angle of the cone, particles will come out parallel to the axis for a wide range of momenta.

Figure 4 shows the neutrino flux spectrum, calculated at 50 m distance from a target, equipped with a neutrino horn, assuming a decay path of 25 m. These parameters correspond to the experiment which is at present being prepared in CERN. With current in the horn, the spectrum shows two plateaus which correspond to the two momentum bands for which the horn focuses particles on the axis. The total neutrino flux is increased by a factor 7. The number of neutrino elastic interactions per ton per day of ideal running of the CERN proton synchrotron with $4 \cdot 10^{11}$ protons accelerated every 3 sec increases from 0.4 to 5.2. Since the low counting rate is always a problem in neutrino experiments, this increase is of great value.

Another important advantage of the horn is that it only selects one polarity of particles. If set for positive particles it will enhance only the neutrino component, whereas the anti-neutrinos are instead reduced, because negative particles are deflected away. With the flux from the horn it is thus possible to investigate separately neutrino and antineutrino interactions.

A quadrupole focusing system which also has been considered for increasing the neutrino flux does not have this feature since it focuses indiscriminately particles of both signs.

III. NEUTRINO DETECTORS

Even under the best conditions one can realize at present, the expected event rate per ton of sensitive material is only a few per day. The detector must therefore have a large sensitive mass. Another important requirement is the ability to reject background of cosmic rays or particles from the accelerator which manage to penetrate the shielding around the experiment.

Of present detectors, the bubble chamber, the Wilson cloud chamber and a combination of counters and spark chambers have been considered as detectors for neutrino reactions.

Bubble chambers have been made with volumes up to 500 l. and can be filled with a heavy liquid, such as freon CF_3Br to give a sensitive mass of the order of 1 ton. Since the bubble chamber cannot be triggered, it has to be exposed every burst, and to collect a reasonable number of neutrino events a very large number of photographs must be taken, most of which will be empty. The sensitive time of the bubble chamber is a few ms, short enough so that the background of cosmic rays is not very serious. With a magnetic field on the chamber, the momentum of the particles in the neutrino events can be determined, but with the heavy liquids which have to be used, the multiple scattering is large and the momentum accuracy limited to 10-20%. On the other hand, the short radiation length, 11 cm in freon, allows electrons and γ rays to be easily identified by the shower they generate. A rough measurement of the energy is possible from curvature and track length. With a sensitive mass of only a ton, many particles will leave the chamber without visible interaction, making it difficult to distinguish between muons and pions, except on a statistical basis.

The freon used in the bubble chamber contains no hydrogen but only complex nuclei. The neutrino events, produced in these nuclei, cannot be unambiguously reconstructed kinematically, since the energy of the incoming neutrino and the momentum and energy transfer to the nucleus are unknown. In the case of production of intermediate bosons, which decay into a lepton and a neutrino, energy and momentum are also carried away by the second unseen neutrino. Only in the case of decay in a charged and a neutral pion, which are both seen in the chamber, can the decay of the vector boson be reconstructed and its mass determined.

The big advantage of the bubble chamber lies in the high spatial resolution which for example would allow the study of the production of hyperons or K mesons with high-energy neutrinos. It is also of interest to study the weak coupling to resonance states, such as the excited nucleon states and two or three pion states as ρ, η and ω which are of importance for inelastic neutrino events in which one or several pions are produced.

It would be very interesting to study the more fundamental neutrino reactions in pure hydrogen or deuterium, in which also the kinematics would be better known. Since, however, liquid hydrogen has only $1/20$ the weight of freon, the event rate in even the largest hydrogen bubble chambers existing today is too low with present neutrino fluxes. An enormous bubble chamber of 14 m^3 would be needed to provide 1 ton hydrogen. Although probably technically feasible, such a chamber would be a long term project.

Scintillation counters, either liquid or plastic, can be made in large units and can involve several tons of material. The same is true for water Čerenkov counters, which have the desirable property of being directional so that they can discriminate against cosmic rays and background particles. Addition of a heavy salt, for example lead perchlorate, makes them specific detectors for high-energy γ rays and electrons which produce showers in the solution.

Counters have a time resolution of a few ns. This time resolution allows determination of the time of flight of the neutrinos if the time of production at the accelerator is known. In the accelerator, particles are accelerated by a high frequency voltage, only if they are in the correct phase with this voltage. At the CERN proton synchrotron, for example, the particles are bunched at the end of the acceleration in bunches of 10 ns width occurring at intervals of 95 ns. Because of this bunch structure the time of flight of the particles from target to detector, which is 200 ns for a 60 m distance, can be determined with a precision of $\pm$ 5 ns. The timing is a very powerful way of eliminating background of non-relativistic particles and of particles which have been able to penetrate to the detector by roundabout paths.

Good timing by counters will also essentially eliminate cosmic ray background in neutrino experiments. Taking, for example, the case of the CERN proton synchrotron operated with an external beam, 20 bunches of 10 ns width will be ejected every 3 sec, 30,000 times per day. During a twenty day experiment, neutrinos will be produced during a total time of only $20 \times 30{,}000 \cdot 20 \cdot 10^{-8} = 0.12$ sec.

About 100 cosmic ray muons will traverse a 10 m^2 set-up during this time and most of these can easily be rejected by shielding and the use of anti-coincidence counters. The number of neutrino events would be much higher.

Spark chambers. Although counters alone have been considered for neutrino experiments, the information they give on the neutrino events is very rough, since no visual picture is given of the event. They can, however, be used to advantage in a combination with spark chambers. The spark chamber has a sensitive time of 1 μsec and if triggered within this time after the event by a signal from the counters, it will complete the information from the counters with a visual display of the neutrino event. Both the Brookhaven experiment and the experiment now being prepared at CERN use large set-ups of counters and spark chambers. The spark chambers form the bulk of the mass of the set-up and provide most of the material in which the neutrino events occur. In the CERN set-up there are about 20 tons of effective mass in the form of spark chambers, made of aluminium or brass plates and only a few tons of counters, distributed to pick up the neutrino events.

Whereas the bubble chambers have to take a picture every burst of the machine, the spark chambers are only photographed when a possible neutrino event occurs and gives a signal in the counters.

The spark chamber samples the position of the particle trajectories only at discrete intervals where they traverse a spark gap and the picture of a spark chamber event will therefore be much cruder than for a bubble chamber. On the other hand, the larger size of the spark chamber and its high density gives a high stopping power. This allows the energy of particles to be determined from range up to energies above 1 GeV. This method will, of course, only be useful for muons. For other particles the total number of sparks gives a rough determination of the energy of the particle, in particular for electrons and γ rays which produce large showers. Figure 5 shows a beautiful picture of the two γ rays from a neutral pion, produced by charge exchange in a polythene scintillator target.

IV. THE BROOKHAVEN EXPERIMENT

The first experiment with high-energy neutrinos was performed at Brookhaven by a group of physicists from Columbia: Danby, Gaillard, Goulianos, Lederman, Mistry, Schwarz and Steinberger. This experiment used a 10 ton spark chamber, Fig. 6, of 2.5 cm thick aluminium plates, which was installed in a block house at an angle of 7° from a target in the AGS machine. The layout of the experiment is seen in Fig. 7. Thick iron sheets from an old American battle ship were used to shield the detector against muons. With 13.5 m of iron shielding, muons start to leak through when the energy of the AGS is above 15 GeV, and this was the energy at which the experiment was run.

The emphasis of the experiment was to:

i) demonstrate the existence of high-energy neutrino interactions, and measure the cross-section;

ii) check if the neutrinos from π decay are identical with those from β decay;

iii) search for signs of intermediate boson production.

Existence of high-energy neutrino events and measurements of the cross-sections

During the run the detector recorded 119 events which satisfied the selection criteria, and originated inside a fiducial region which excluded the borders of the set-up.

The 119 events could be subdivided into various classes, as follows.

Eighty-three events which showed a single straight track or at most a few extra sparks, probably evaporation prongs from the interaction. Of these, 34 had a visible momentum, if they were interpreted as muons, larger than 300 MeV/c. A few of these are shown in Fig. 8. This visible momentum is, however, only a minimum since all the tracks, except five, left the detector before stopping. The total detector has a stopping

power longitudinally of 700 MeV and sideways of only 300 MeV for minimum ionizing particles. Most of the conclusions of the experiment are based on the 34 events with a visible energy of more than 300 MeV/c. The class below 300 MeV/c contains most of the background of neutron interaction. Indeed, during the first half of the run when the shielding was not yet complete, many more short track events were observed than during the latter half.

Twenty-two events were of a more complicated character with more than one track, and all had a high energy release. Seven of these showed a visible energy of more than 1 GeV. Some of these are given in Fig. 9.

Finally, a class of eight events showed in general a single track with irregular structure, so that they are not likely to be due to muons. The first problem was to prove that the 34 single track events are not cosmic ray muons. A cosmic-ray muon from above which stops in the chamber, and stopping instead of a neutrino, will look as a neutrino-induced muon leaving the chamber upwards. A control experiment with the machine turned off showed that neutrino-like events were obtained at a rate of one per second. Since the detector was allowed to trigger only during a 3 μsec period every burst, the total effective time for the whole experiment which lasted $1.5 \cdot 10^6$ pulses was 5 sec. Only five of the 34 single track events could therefore be due to cosmic rays. Another test was the vertical distribution of the 34 events shown in Fig. 10. There is in fact a slight excess of events with a muon which appears to go upwards. However, the majority of the tracks are centred in the horizontal direction, as one should expect from neutrino-induced muons.

As the next problem, one should consider if the events could be caused by strongly interacting particles, mainly neutrons from the machine, which penetrate weak regions of the shielding. Because of the large interaction cross-sections, a very low flux of such particles could contribute to the event rate. The neutrons could not come from the direct line from the target where the shielding was very thick to stop

the muons, but would most probably penetrate from the side of the accelerator. The interactions should then show a marked anisotropy in their angular distribution in the horizontal direction. This was not the case. Furthermore the events are quite uniformly distributed in the chamber and there is no evidence for an attenuation, in spite of the fact that the neutron mean free path is small compared to the detector dimensions.

If the 34 - 5 = 29 events were charged pions produced in neutron interactions, one should expect half this number of neutral pions, which should give showers in the detector. These were not seen.

In the 34 single track events no clear cases of scattering or interactions are observed for a total track length of many times the nuclear interactions length. This indicates that the particles are muons.

A further control experiment to check that the events were due to neutrinos was to absorb the pions in an absorber close to the target, before they could decay. This reduced the event rate by a factor which agrees with what could be calculated from the decay length of pions and K mesons.

From these arguments it seems clear that at least the bulk of the 34 single track events and the 22 vertex events observed in the experiment are induced by neutrinos. The 29 single track events are probably examples of the reactions

$$\nu + n \rightarrow \mu^- + p \qquad (8a)$$

or

$$\bar{\nu} + p \rightarrow \mu^+ + n. \qquad (8b)$$

It should be remembered that the beam from the accelerator contains both negative and positive pions which will give rise to both neutrinos and antineutrinos.

At this stage the first important physics question comes in. Twenty-nine events were observed of reactions (8) with a muon produced. A priori one would expect a comparable number of events with an electron

produced if the neutrinos from $\pi - \mu$ decay were identical with neutrinos from β decay. The spectrum of the electrons should be very similar to that of the muons. Below 300 MeV/c it may be difficult to distinguish with certainty between an electron and a muon, since the electrons slow down rather than to produce a distinguishable shower. However, above 300 MeV/c, electrons are quite easy to distinguish from muons by the multiplication and scattering they suffer. This the Brookhaven group showed in a control experiment in a pure electron beam from the machine. The distribution of the number of sparks for a 400 MeV/c electron in the spark chamber is shown in Fig. 11. The only events which could possibly be electrons, judging from the appearance of the tracks, are six tracks with the spark distribution given in the lower part of Fig. 11. It is clear that if they are really electrons they must have an energy considerably below 400 MeV/c and there are no clear examples of an electron above 300 MeV as against 29 events with a muon. The conclusion must be that the electron production is strongly suppressed. The most natural conclusion is that the neutrinos from the dominant π-μ decay mode cannot produce electrons and are different from the neutrino in β decay. The six events which were observed and which could possibly be electrons were all observed in the first part of the run when the background conditions were known to be unsatisfactory and they could in fact all be due to neutron interactions.

If we identify the single track events with elastic neutrino reactions by the reaction (8a) and (8b), one can compare the observed rate with the theoretical calculations. The values of the weak interaction coupling constants at very small momentum transfers are quite well known from the study of decay processes. Virtually nothing is known experimentally of how the form factors for the weak interactions behave at high energies. In the neutrino energy range of the Brookhaven experiment, large momentum transfers will be quite common and the form factors will have a considerable influence on the cross-sections (see Fig. 1).

The weak interactions may be represented by four form factors if G-invariance is supposed to hold. Two of these apply to the vector interaction. The conserved vector current hypothesis which recently has received considerable experimental proof in the measurements on B^{12} and N^{12} and in the π^{+}-π^{0} decay, makes definite predictions for these form factors from the electromagnetic form factors. The form factors of the axial vector term are practically unknown. The main term has a larger value when coupling to the nucleon than to the lepton current by a factor 1.2, probably a renormalization effect. The second term, the induced pseudoscalar term, gives a contribution proportional to the lepton mass squared and can therefore be neglected for electrons, but enhances the muon production.

The theoretical total cross-sections for the elastic interactions, calculated by Lee and Yang, with these assumptions and neglecting the induced pseudoscalar term, are shown in Fig. 1. The difference between the neutrino and antineutrino interactions are due to the interference between the vector and axial terms in the interactions. If these cross-sections are folded together with the neutrino flux spectrum one calculates from the pion spectrum and the geometry of the experiment, one finds an expected number of 25 elastic events which compares very well with the 29 single track events actually found.

The theoretical value will, however, change considerably if other values for the form factors are assumed, or if one invokes the existence of a vector boson which mediates the weak interaction. If one, as previously, accepts the conserved vector current hypothesis, which defines the vector form factors, and neglects the pseudoscalar term, there are still two parameters, the mass of the vector boson and the characteristic length involved in the axial coupling to the nucleon. Variations of the latter between 1.6 and 0 f, and of the former between 500 and 1250 MeV give values for the expected rate ranging between 9 and 40 events. While the order of magnitude agreement of the Brookhaven experiment with theory is extremely satisfying, there are certainly extremely important questions concerning the form factors which must be settled by more detailed experiments.

66/NP/smg

An additional uncertainty comes from the influence of the induced pseudoscalar term on the result. While it was previously assumed on the basis of the then presumed strength of the coupling that this term will only give a 20% increase of the muon events with respect to the electron events, recent experimental results seem to indicate that the coupling is considerably stronger and the enhancement of the muon interactions therefore larger. Lapidus has pointed out that if the pseudoscalar term is sufficiently large the absence of electrons in the Brookhaven experiment may be due to an enhancement of the muon production by the pseudoscalar term, rather than the forbiddeness of the electron production if the two neutrinos are different. An objection against this argument is that a large pseudoscalar term will not only increase the muon-electron ratio but also the total cross-section. It therefore becomes difficult to reconciliate a sufficiently large pseudoscalar term with the good agreement between the observed and calculated event rate.

So far, we have only been concerned with the interpretation of the simple single track events, which were identified with elastic neutrino events. Events with two or more prongs may tentatively be identified with neutrino reactions where an additional pion is produced. These processes occur on free nucleons if the nucleon is left in an excited state or by formation of a pion-pion isobar in the pion cloud around the nucleon. In the aluminium nuclei, which are the target material of the spark chamber, pions may also be produced by reactions of the energetic recoil nucleon within the same nucleus. The inelastic reactions are therefore very complicated processes where the theoretical predictions are at present very vague. It is, however, not unreasonable that the inelastic cross-section in nuclei could be of the same order as the elastic, as indicated by the comparable number of single track and vertex events, 29 against 22.

Another fascinating interpretation of the vertex events is as the production and immediate decay of an intermediate vector boson, which has been proposed as mediator for the weak interactions. The vector boson is expected to decay to $(\mu + \nu)$, $(e + \nu)$, to two or more pions. If the

mass is sufficiently large, other decay modes with a K meson are possible. If there are two neutrinos, a vector boson is always produced together with a relatively low-energy muon, and the production and subsequent decay of the W would thus appear as a vertex of two or more particles, one of which is a muon, and the other a muon, an electron, or two or more pions. Among the 22 vertex events of the Brookhaven experiment there are several, in particular the three shown in Fig. 9, which would fit in with this interpretation. They can, however, equally well be inelastic events. The event rate depends very critically on the mass of the intermediate boson and drops from 20 expected events for a mass of 550 MeV to 2 events for 950 MeV.

V. THE CERN EXPERIMENT

I have treated rather completely the Brookhaven experiment which yielded a lot of very valuable information and has shown that experiments with high-energy neutrinos are feasible. However, the Brookhaven experiment has left many questions unanswered and it is the purpose of the experiment we prepare in CERN to attempt to answer them.

The CERN experiment has been prepared in parallel with the Brookhaven experiment during the last two years, and is scheduled to start in May of this year.

The proton beam is extracted from the CPS in a two μsec burst by a fast ejection system. Within the burst the beam is further bunched into 20 bunches of 10 ns width. I have previously pointed out the advantage of this bunching for rejection of cosmic ray and neutron background. The ejected beam is transported by a system of quadrupole lenses and bending magnet to the neutrino horn which I have described previously. The beam is focused on a thin tungsten rod target on the axis of the horn. The action of the horn focuses the pions of one side in a narrow beam which is allowed to decay in a 25 m long decay tunnel, Fig. 12. Between the end of this decay tunnel and the detector area is

a 25 m long iron shield, which removes the high-energy muons from the neutrino beam by energy loss. This iron shield, which involves about 4000 ton of iron, flares out towards the detector side so that muons cannot escape into the lighter concrete on the sides by multiple scattering during slowing down. The shielding around the decay tunnel also plays an important role in limiting the muon beam to the area which is covered by the iron shield.

Since the neutrino beam is not absorbed by the detector, several neutrino experiments can be set up behind each other in the same beam. In the CERN experiment we will have two main detectors, a heavy liquid bubble chamber and a spark chamber assembly.

The use of a bubble chamber with an effective mass of only about ½ ton is made feasible by the large neutrino flux, given by the extraction of the beam and the use of the neutrino horn. The expected rate in a 20 day run in the bubble chamber is about 50 elastic and a comparable number of inelastic events. While the statistics are too small to allow many quantitative results, these events will give the first detailed qualitative information on the neutrino-induced reactions at high energies.

The spark chamber set-up

The spark chamber and counter set-up which we intend to use is in many respects similar to the Brookhaven set-up. However, the effective mass is considerably larger, 20 tons of spark chamber, and the larger dimensions both in length and width allow particles of higher energy to be stopped and their energy determined by range. We also use thinner plates, on the average 0.75 cm, so as to have better space resolution. One of the 30 units which make up the set-up is seen in Fig. 13. The material in the region where the events are produced is either brass or alternating plates of brass and aluminium. As electrons and γ rays multiply quicker, a distinction between muon and electron for the question of the identity of the two neutrinos can be made more unambiguously in a brass-aluminium mixture than in pure aluminium.

With the increased neutrino flux due to the horn and the higher mass of the detector we expect a 20 day run to accumulate of the order of 500 to 1000 elastic neutrino events.

Two methods of introducing a magnetic field in the set-up are foreseen for the CERN neutrino experiment. The first which is being installed now uses a very large pair of Helmholz coils to produce a 3 kgauss field in the region behind a production region. A fraction of the particles produced in this region will traverse the magnetic field, where their curvature will be determined with a set of spark chambers. In addition a massive range chamber behind the magnetic field section will give range information and will also serve to identify the particle as a muon from the lack of interactions.

The second method mixes the magnetic field more intimately with the production and range region by the use of magnetized iron plates in between the spark chambers. Since this set-up is more compact, it allows the sign determination for a larger fraction of the events. However, the magnetic curvature in magnetized iron outweight the multiple scattering sufficiently only for particles which have traversed more than 300 g/cm^2 of iron and the method is only therefore applicable to high-energy muons. Fortunately in the case of neutrino interactions high-energy muons are the most common reaction products.

Problems to be investigated in the CERN neutrino experiment

It is obvious that the CERN neutrino experiment, like the Brookhaven neutrino experiment, will to a large extent be exploratory only. However, one can already see some of the problems which could be studied in the experiment.

1. One or two neutrinos

Although the Brookhaven experiment seems quite conclusive, there are still a few loopholes in the arguments, some of which I have discussed. The CERN spark chamber experiment should have about 10 times the event rate of the Brookhaven experiment and electrons should be more easily distinguishable because of the thinner plates and the admixture of brass plates in the set-up.

The bubble chamber will have an event rate comparable to that of the BNL spark chamber, but will have no triggering bias which could conceivably make the BNL set-up insensitive to low-energy electrons. It can therefore be hoped that the CERN experiment will patch up the remaining loopholes in the problem.

A related question, where the Brookhaven experiment is much less definite, is the question of the identities of neutrinos from K meson decays. Although these neutrinos could be a new set of neutrinos the simplest assumption would be that they are the same as the neutrinos from decay of ordinary particles. Bludman[6], and Feinberg, Gursey and Pais[7] have suggested that the K meson neutrinos are associated with muon and electron in the opposite way from the neutrinos in pion decay.

If this theory is true, K neutrinos which constitute about 10% of the neutrino flux, and which are mainly due to $K_{\mu 2}$ decay should give rise to a small number of neutrino events with an electron produced. These electrons should have an energy distribution which reflects the spectrum of the K neutrinos with a much higher mean energy than the pion neutrinos.

2. Intermediate vector boson

One of the most important aims of the experiment is the search for the production and subsequent decay of the intermediate boson, which can be produced by neutrinos in the Coulomb field of nucleons and nuclei, for neutrinos of sufficient energy. Figure 14 shows the cross-section per nucleon in iron for the production of vector bosons, assuming different masses, and in the same figure is plotted the neutrino spectrum we expect in our experiment. It is clear that only the high-energy tail of the neutrino spectrum, which is almost entirely due to K mesons, will contribute to the vector boson production. The rate depends very much on the mass. If the mass is 0.6 proton masses, close to the minimum value one can have, we will expect about 20 bosons produced per day, if the mass is one proton mass we expect 2, and at 1.4 proton masses we would be at the limit of observation where only a few events will be observed in the whole experiment. It should be

added that these figures are very uncertain since they depend on the details of K meson spectrum at high energies, which is only very sporadically known. Another team in CERN will, however, in the next few weeks carry out a comprehensive survey of the production spectra of K mesons in the momentum range of interest to the neutrino experiment.

The possibility of distinguishing vector boson production from other events will to a large extent depend on the details of the vector boson decay. In general the vector boson will carry off the major part of the neutrino energy leaving behind a low-energy negative muon. If the vector boson decays in a positive muon and a neutrino, and the positive muon gets a large part of the energy, its sign can be determined by the magnetic field of the spark chamber set-up and provide a good signature for vector boson decay. There are, however, some indications, from calculations made by Veltmann, that the vector boson gets polarized in the production process in such a way that it decays with the muon predominantly backwards, and thus with low energy in the lab system. If this is true the identification of the vector boson gets more difficult in the spark chamber, but easier in the bubble chamber.

The decay mode of the vector boson to an electron and a neutrino has the advantage that the background of ordinary neutrino events with electrons is small, since our beam contains mainly muon neutrinos. In the spark chamber the possibility to determine the sign drops out since the electron will quickly produce a shower. The most dangerous background is expected to be inelastic neutrino events in which a neutral pion is produced whose decay γ rays materialise in the same plate. Since the plate thickness is a fair fraction of the radiation length, the probability for this is not negligible. Many of these cases can be eliminated if the two γ rays give separate showers, but some will remain where the two showers superimpose, or one is very small.

In the bubble chamber the electron decay mode offers perhaps the most prominent possibility to detect the vector boson production since the high resolution and longer radiation length allows the sign to be determined and a discrimination made against the case of neutral pion production. However the rate of production will be sufficient for

the bubble chamber only if the mass of the W is low.

The decay modes of the W in two pions will be particularly prominent if the mass of the W happens to coincide with the mass of the ρ meson 740 MeV. In this case the production and decay of a W will look just as the production of a ρ meson in an inelastic neutrino interaction.

In principle a distinction could be made by the fact that the ρ resonance has a substantial width, 50-100 MeV, whereas the W meson is extremely narrow. Unfortunately, neither the bubble chamber nor the spark chamber will be able to determine the mass of the object to better than 20%, which is not good enough for this purpose. Instead one will have to argue the case of the W from the shape of the spectrum and perhaps also the charge distribution. The W made in a neutrino beam should always be positive. When ρ mesons are made in inelastic neutrino events, there should also be a positive excess, because they are always produced together with a negative muon, but this excess should not be so marked.

If evidence for the vector boson is found, it will be interesting to determine its mass. This can be done from the rate of vector boson production which is a very sensitive function of the mass. For the decay mode into a charged and neutral pion, the kinematics of the decay can be reconstructed to give a rough value of the mass. For the decay to a muon or lepton and a neutrino, this is not possible since the neutrino is not observed. Since, however, the theory of the production processes indicates that the vector boson is produced with low transverse momentum relative to the neutrino direction, the transverse momentum distribution of the decay lepton will be dominated by the kinematics of the decay process and may yield a value for the mass.

3. Elastic events

For the elastic events the Brookhaven experiment was limited to the determination of a rough total cross-section for a mixture of neutrinos and antineutrinos which agreed with theory.

In the CERN experiment, it would be of great interest to investigate the behaviour of the form factors of the weak interactions at large momentum transfers. The behaviour at small momentum transfers is not so interesting since it is known from other processes. In addition, neutrino reactions with complex nuclei, as opposed to hydrogen, are not very suitable for this problem, since at small transfer momenta the cross-sections are highly influenced by the Pauli exclusion principle and the Fermi momentum of the nucleus.

For momentum transfers beyond the Fermi momentum, say 300 MeV/c, however, the bound nucleons behave as if they were free and there is hope that neutrino experiments on complex nuclei can give information on the fundamental nucleon interaction. The Brookhaven experiment was not very well adapted to the study of interactions with large momentum transfers. The relatively small size of the experimental set-up allowed most of the muons produced in these events to escape before stopping, so that only their angular distribution, but not the energy distribution, could be determined. As this angular distribution is an average over the neutrino spectrum, large-angle events will be dominated by the events with low momentum transfer, produced by the more abundant low-energy neutrinos.

The main part of the CERN set-up is also of too low density to contain efficiently the muons produced in reactions with momentum transfers above 300 MeV/c. The low density is a consequence of the desire to have a high spatial resolution which has led us to use 5 mm thin plates in the production region. It is, however, intended to use a magnetized iron plate chamber behind the present production region which is compact enough to contain particles with transverse momenta up to 500 MeV/c. This chamber will consist of 5 cm iron plates magnetized to 18 kgauss, and separated by spark chambers and counters. The higher containment power of this more compact chamber would be at the expense of the spatial resolution and the information on the details of each event. However, for simple elastic neutrino events with muon production, this restriction can be accepted.

A very interesting problem which could be studied in this compact chamber would be the difference of the event rate for the two polarities of the neutrino horn, that is between neutrino and antineutrino

interactions. As the materials we use in the set-up contain approximately an equal number of neutrons and protons, this difference should be dominated by the interference term between axial and vector coupling which is responsible for the difference between the elementary neutrino and anti-neutrino interactions on nucleons. The complications of the Pauli principle and Fermi momentum should be the same in both cases. As we believe we know the behaviour of the vector form factors from the conserved vector current hypothesis, we could then deduce the behaviour of the axial form factors.

4. Inelastic processes

The study of the inelastic processes will certainly be a very important part of the experiment but the variety of processes which can occur will make this study more phenomenological than systematic. Even if the primary process on the individual nucleon is simple, leading for example to a $(3/2, 3/2)$ isobar resonance, the subsequent interaction of this isobar with the rest of the nucleus before the pion escapes makes a detailed treatment very difficult. The Fermi momentum of the target nucleon and the fact that the energy of the incoming neutrino is unknown will also make a kinematic reconstruction impossible.

A somewhat different class of inelastic events are those producing hyperons in the two body reactions with neutrinos

$$\nu + n \rightarrow \Sigma^+ + \mu^- \qquad (9)$$

or antineutrinos

$$\bar{\nu} + n \rightarrow \Sigma^- + \mu^+ \qquad (10a)$$

$$\bar{\nu} + p \rightarrow \Lambda^0 + \mu^+ \qquad (10b)$$

$$\bar{\nu} + p \rightarrow \Sigma^0 + \mu^+ . \qquad (10c)$$

K mesons can be produced in three body reactions

$$\nu + N \rightarrow N + \mu^- + K. \qquad (11)$$

To identify the strange particles a good spatial resolution is required and the bubble chamber is certainly the most suitable detector in this respect. Unfortunately, however, it must be expected that the strange

particle production in neutrino interactions will be reduced with respect to non-strange neutrino events by the same factor, about ten, that is found for the leptonic decays of the hyperons, and the rate will then be too small for the bubble chamber. The spark chamber set-up will not be able to identify Σ hyperons but could in favourable cases identify Λ^0 decays from reaction (10b) and (10c), and K^0 and K^+ decays from reaction (11).

* * *

REFERENCES

1. T.D. Lee and C.N. Yang, Phys.Rev.Letters 4, 307 (1960).

2. Y. Yamaguchi, CERN Int.Report 61-2, Progr.Theoret.Phys. (Kyoto) 6, 1117 (1960).

3. S.M. Berman, Proc.Int.Conf. on Theoret.Aspects of Very High Energy Phenomena, CERN (1961), p. 7 (CERN Int.Report 61-22).

4. T.D. Lee and C.N. Yang, Phys.Rev.Letters 7, 429 (1961).

5. G. Danby, J.M. Gaillard, K. Goulianos, L.M. Lederman, N. Mistry, M. Schwartz and J. Steinberger, Phys.Rev.Letters 9, 36 (1962).

6. S. Bludman, UCRL 9667.

7. G. Feinberg, F. Gursey and A. Pais, Phys.Rev.Letters 7, 208 (1961).

8. S. van der Meer, CERN Report 61-7.

DISCUSSION

Evans : Why does one not observe the recoil proton as well as the μ meson in $\nu + n \rightarrow \mu^- + p$?

Von Dardel : We define vertex events as those with the second track having more than four sparks. Hence, on this criterion we do not generally observe proton recoils.

Bott-Bodenhausen : Do you use spark chambers in a strong magnetic field at CERN?

Von Dardel : No. We place a magnetic field between the chambers.

Spitzer : How many bubble chamber pictures do you expect to take?

Von Dardel : 300,000; we can afford to take double exposures as most pictures will be blank.

Harmsen : Is there any interest in doing a similar experiment with ordinary machines? If yes, do you see any possible source for these high-energy neutrinos?

Von Dardel : Yes. One can use high-energy electrons, for example, from the projected accelerator at Stanford, when one would use the intermediate vector boson

$$e \rightarrow \gamma \rightarrow W^+ + W^-$$

$$W^+ \rightarrow e^+ + \nu$$

$$\rightarrow \mu^+ + \nu .$$

This seems to be the most efficient way but it also produces an equal number of neutrettos. One also gets a contamination of an ordinary neutretto beam with neutrinos from $\pi \rightarrow e + \nu$ and $K \rightarrow \pi + e + \nu$ but the reaction rate is very small, $\sim 10^{-4}$.

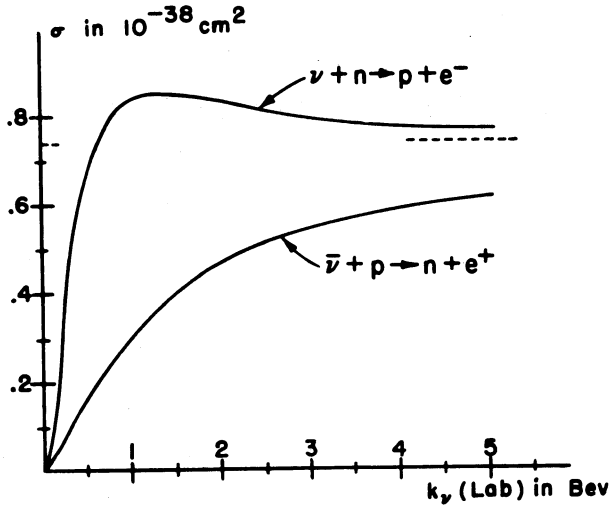

Fig. 1 Total cross section for neutrino interactions on free nucleons [1].

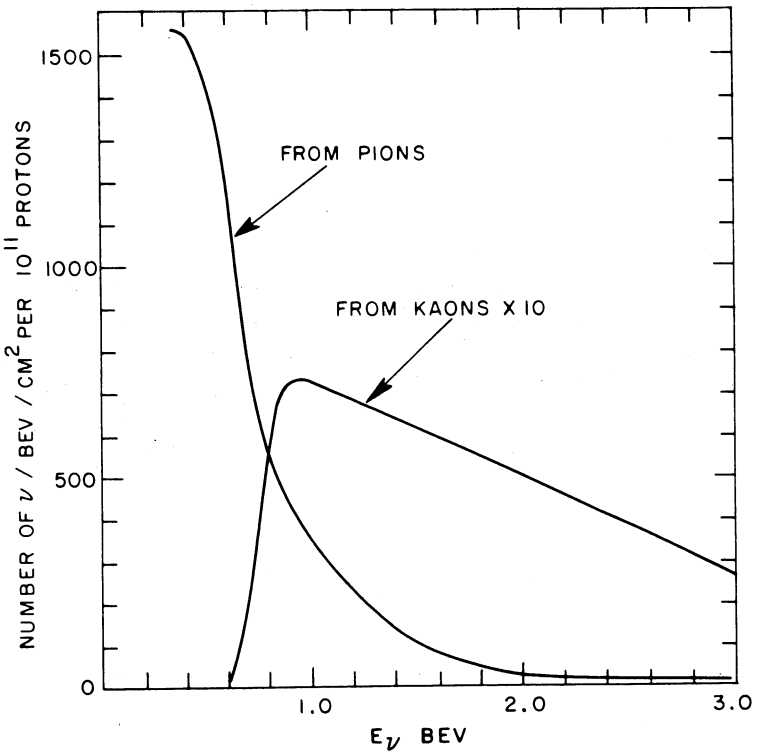

Fig. 2 Flux spectrum under the conditions of the Brookhaven neutrino experiment [5], Curve I : neutrinos from pion decay.

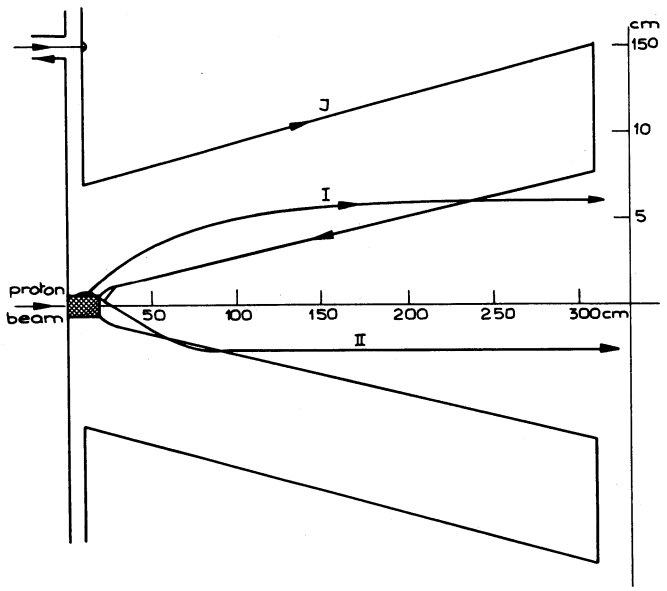

Fig. 3 Principle of the "neutrino horn" [8], and its focusing action on particles of high(I) and low momentum(II) .

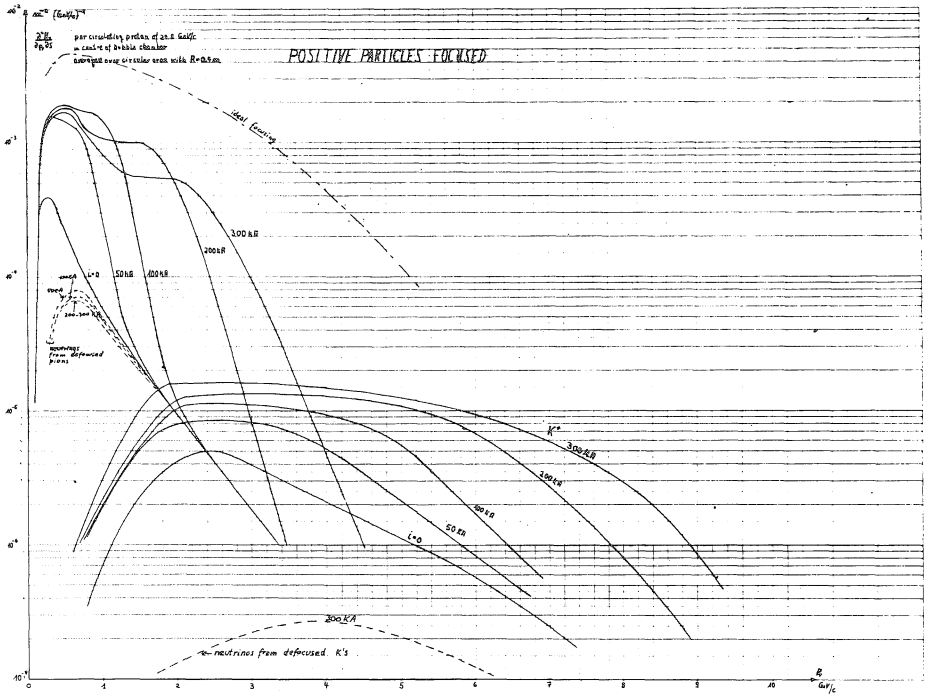

Fig. 4 Neutrino flux spectrum at 50 m distance for 25 m decay path, for 0, 10^5, 2×10^5 and 3×10^5 A current in the horn. If compared with fig. 2, the flux value should be multiplied by 10^7.

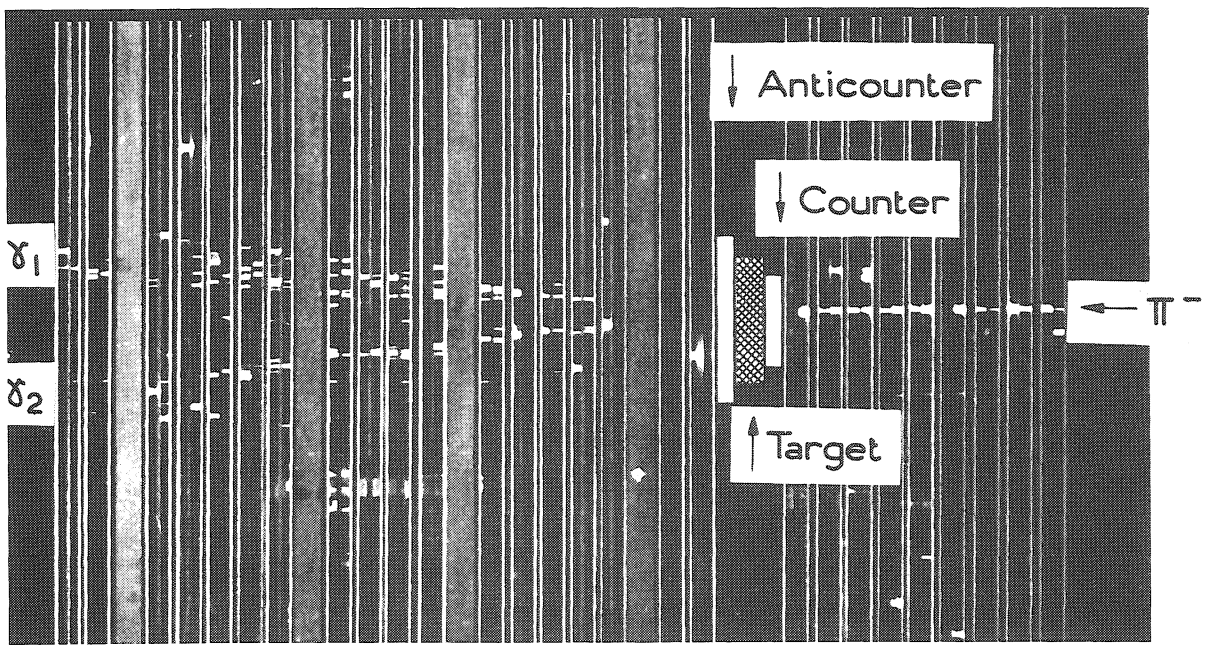

Fig. 5 Charge exchange reaction of π^- as seen in the spark chambers for the CERN neutrino experiment.

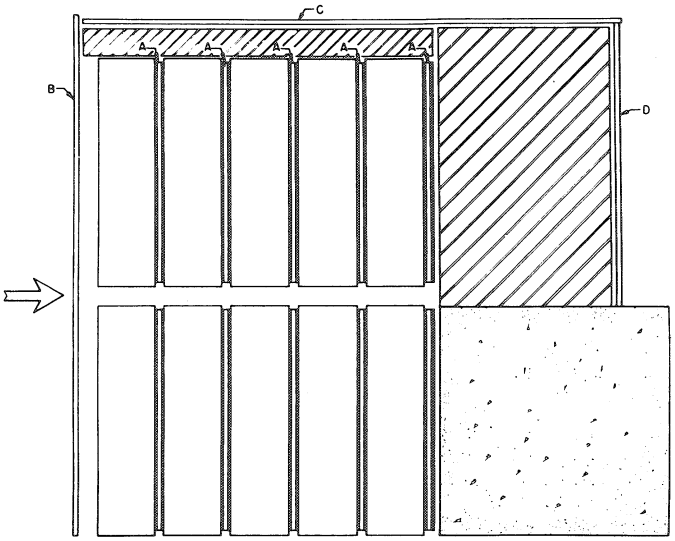

Fig. 6 Spark chamber set-up of the Brookhaven neutrino experiment.

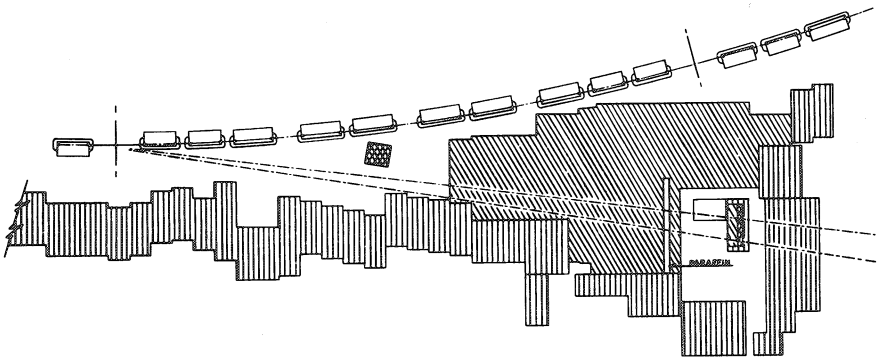

Fig. 7 Layout of the Brookhaven neutrino experiment.

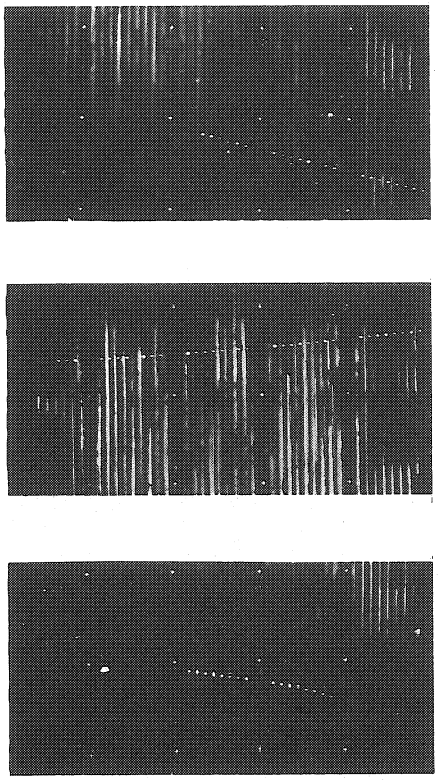

Fig. 8 "Single track" neutrino events in the Brookhaven experiment.

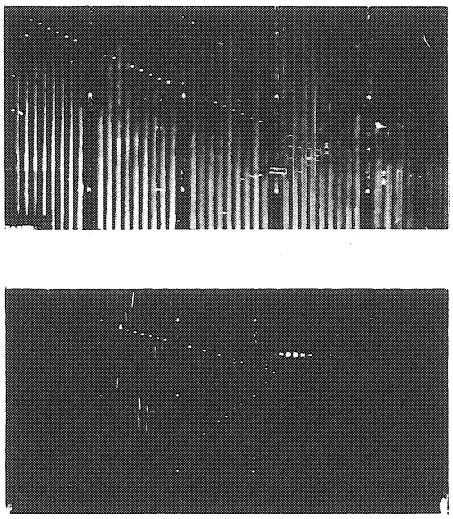

Fig. 9 "Vertex" events in the Brookhaven experiment. A possible interpretation is vector boson production with subsequent decay, according to the reactions

$$\nu^{\prime} \rightarrow W^{+} + \mu^{-}$$

$$\mu^{+} + \nu^{\prime} \qquad \text{(a)}$$

$$e^{-} + \nu \qquad \text{(b)}$$

$$\pi^{+} + \pi^{0} \qquad \text{(c)}$$

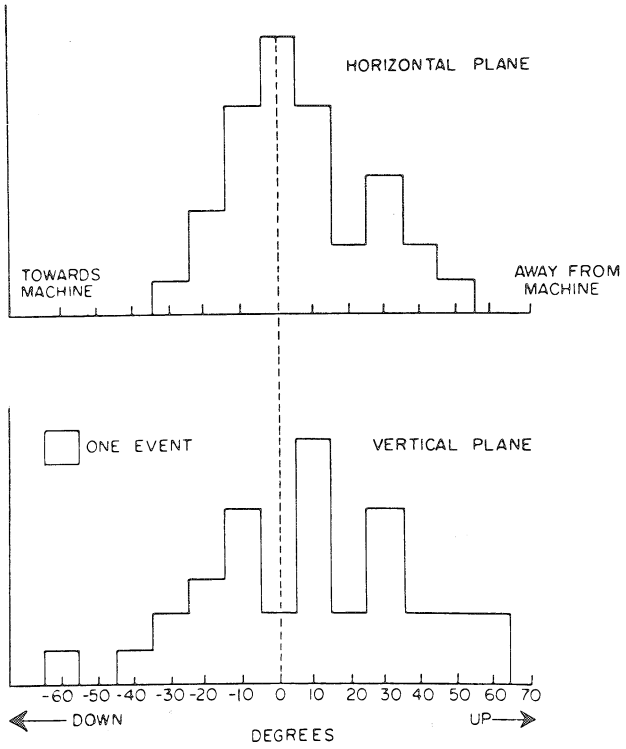

Fig. 10 Angular distribution of single track events in a horizontal and vertical plane around the neutrino direction.

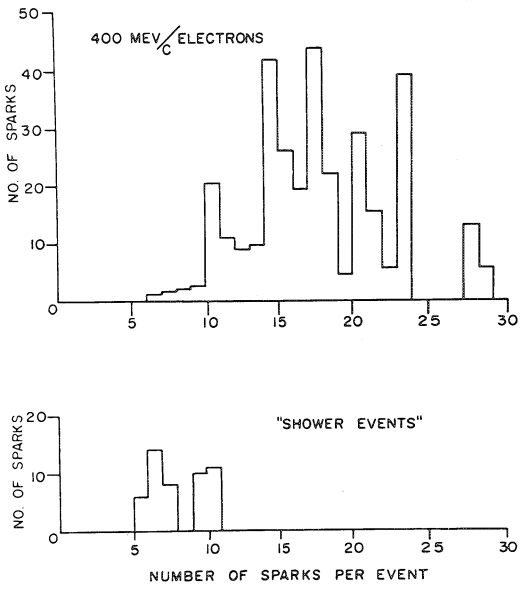

Fig. 11 Distribution of the number of sparks for 6 possible electron tracks of the neutrino experiment (bottom) compared with 400 MeV/c electrons in an external beam (top).

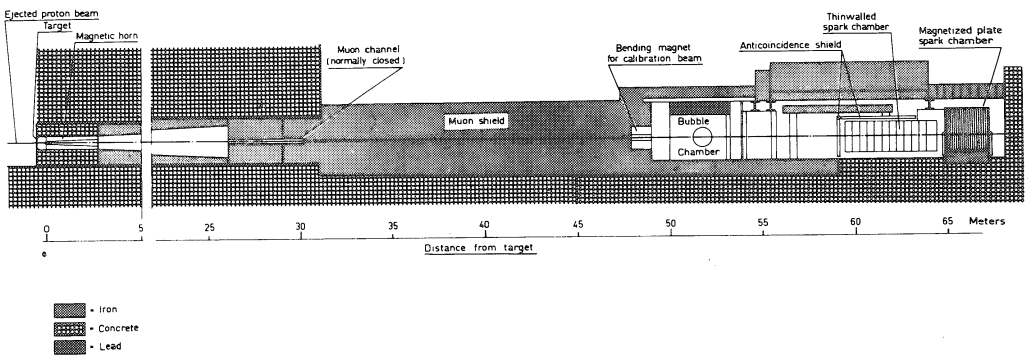

Fig. 12 Vertical cut through the planned CERN experiment showing decay tunnel, muon absorber, the detectors and the shielding around them.

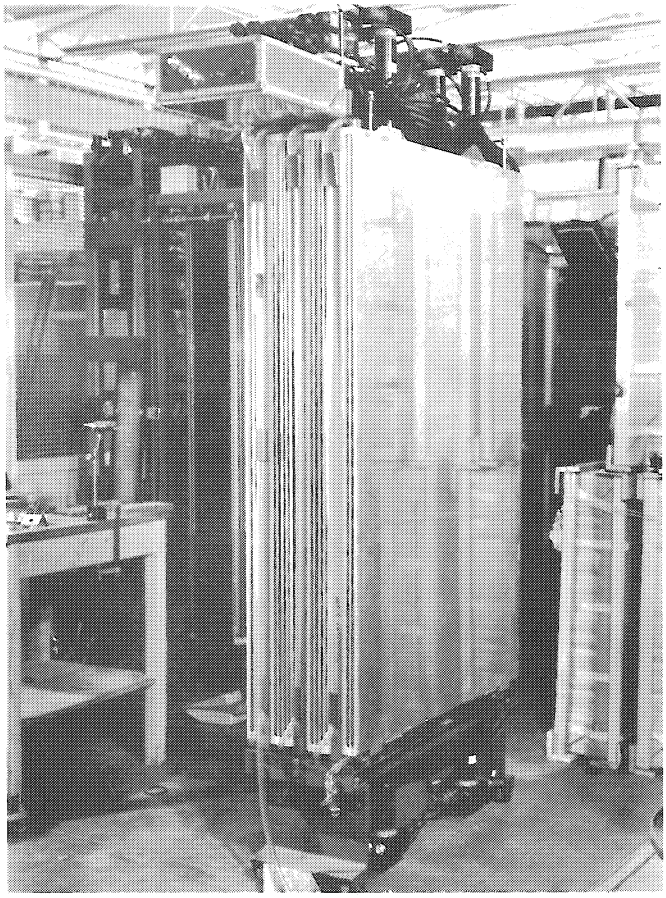

Fig. 13 Chariot carrying 9 two-gap spark chambers and two layers of scintillation counters for the CERN neutrino experiment. 30 of these units will be used in the experiment.

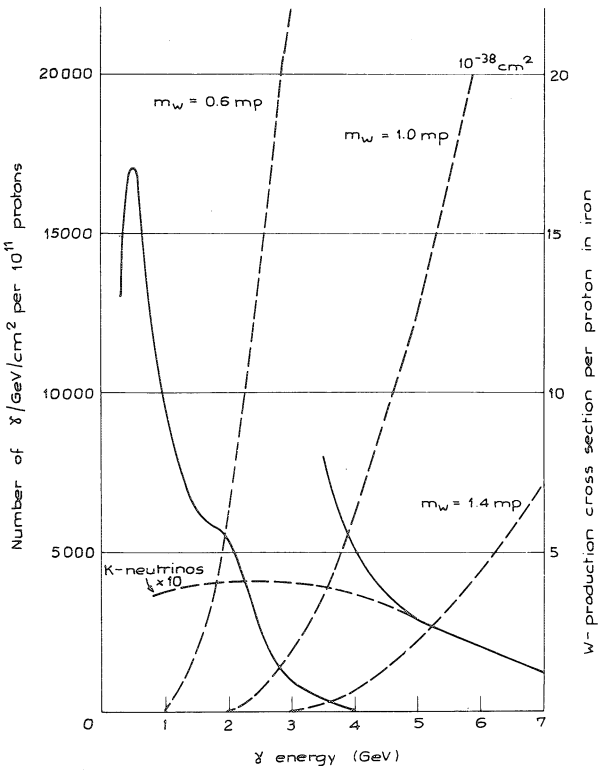

Fig. 14 Total cross section per nucleon for the production of intermediate bosons [4] by neutrinos in iron, as a function of neutrino energy for three values of the boson mass. (dotted curves). The full curves give the neutrino spectrum expected in the CERN neutrino experiment.

IV. EMULSION WORK IN THE SOVIET UNION

PART IV.1

SOME RESULTS AND PROBLEMS CONCERNING CURRENT DEVELOPMENT OF THE EMULSION METHOD

G.B. Zhdanov,
Lebedev Institute, Moscow.

I. INTRODUCTION

In my talk I intend to comment on certain work which seems to me to be of interest, performed by Soviet physicists using the emulsion method, over the last year. I do not intend to give a comprehensive and systematic account of the state of emulsion work in the Soviet Union, if only because that would call for a detailed comparison of our results with the progress achieved by foreign colleagues, and I should have to mention a great deal of information which was already well known to you. Although my account will necessarily be somewhat one-sided and unsystematic, I will try to deal with the following photo-emulsion subjects:

i) the application of photo-emulsions to the study of nuclear interactions at very high energies (over 10^{11} eV) in cosmic rays;

ii) photo-emulsion experiments on inelastic and elastic interactions at energies of the order of 10 GeV (and down to 1 GeV).

II. PHYSICS RESEARCH AT ENERGIES OF OVER 10^{11} eV

1. One of the major drawbacks to much research work concerning nuclear interactions in cosmic rays is the fact that the energy of the particle giving rise to the process of plural production of particles actually observed is not clearly known. At one time it was considered (and this is often still the case) that the angular distribution of the particles produced, especially if it is symmetric in a certain system

iii) the presence of showers (Group 1) which are different, on the contrary, by their comparatively high plurality and isotropic angular distribution; it is interesting to note that one of the cases of a similar type, studied in detail by us recently, was characterized by the fact that the effective mass of the target only slightly exceeded the mass of the π meson.

A comparison of the angular distribution (Fig. 3) and of the "population density" of groups 1, 2 and 3 shows that an increase in the degree of anisotropy is accompanied by a tendency to the formation of two maxima (this result was already known from the work of some Polish authors) and the considerable spread in the degree of anisotropy with constant plurality, is extremely difficult to explain by simple statistical fluctuations and should be interpreted rather as the consequence of the different degree of inelasticity of the interactions.

It is also interesting to examine (see Table 1) the coefficients of the pair correlations between the following four values which can be extracted from an analysis of the angular distribution:

$$X = \sigma_{1/2},\ Y = \lg n,\ Z = \lg \gamma_c,\ U = \Sigma \Theta_i^{-1}$$

(the last value is proportional to the total energy release to the charged particles when the transverse momentum is constant).

Table 1

r_{ik}	X	Y	Z	U
X	-	a) -0.3 b) ≈0	a) +0.1 b) -0.15	+0.2
Y	a) -0.3 b) ≈0	-	a) 0 b) -0.5	+0.3
Z	a) +0.1 b) -0.15	a) 0 b) -0.5	-	+0.3

Note: a) Coefficients of r_{xy}, r_{yz} and r_{xz} obtained after excluding group 6.
b) The same coefficients including group 6.

4. The importance of obtaining independent and sufficiently reliable information about the energy of the primary particle calls for the combination of the photoemulsion and the ionization methods. The first successful attempts to combine these methods were already reported by Grigorov and his colleagues (Moscow State University) at the Moscow Conference on cosmic rays in 1959.

Figure 4 is a diagram of such an experimental set-up, with transmission, suitable for the analysis of interactions at energies of $10^{13} - 10^{14}$ eV. The idea of the experiment is to use the ionization chambers on the one hand as indicators of very high-energy processes in one of the many photoemulsion layers, and on the other hand for an approximate estimate of the inelasticity coefficient of the interaction studied, according to the energy release in subsequent interactions occurring in the 200 g/cm^2 graphite layer.

By the use of a shower generator, situated at some distance from the photo-emulsions and consisting of an upper layer of 20 g/cm^2 graphite, one can study, by means of photo-emulsions, the angular and energy characteristics of γ quanta produced from carbon nuclei at energies above 10^{13} eV. One of the main questions is to determine the additional production processes (besides the formation of π^0 mesons).

Some technical details concerning the dimensions and efficiency of this installation are given below:

total area: 10 m^2 (NIKFI-R emulsions 100 μ thick);
number of ionization chambers: 215 (diameter 10 cm, length about 3 m);
number of hodoscope counters: 200, electron-photon cascade selection threshold - 2.10^{11} eV;
efficiency of cascade detection in the emulsion: ~ 70%;
expected transmission: of the order of 50 incident particles per month with an initial energy > 10^{13} eV.

In order to determine the energy of the electron-photon cascades, the emulsions are calibrated according to the individual cascades which have entered the ionization chamber. As a measure of energy, it was found convenient to use the radius of the circle containing the required number of particles in a cascade at a given depth of its development.

5. One of the questions which is important both from the point of view of method and that of physics is the comparison of nuclear interactions firstly between nucleons, secondly between nucleons and complex nuclei, and thirdly between two complex nuclei. For this purpose, comparisons of energy and angle distributions observed for secondary particles, and the corresponding calculations, were carried out by different authors for 9 GeV protons (Tolstov et al., Dubna; Zhdanov et al., Physics Institute, Moscow).

It was concluded that the intra-nuclear cascade model of successive interactions gave a satisfactory description of the main characteristics of the phenomenon. For energies of the order of 10^{11} eV, a similar conclusion can be drawn, although with a lesser degree of certainty, on the basis of the above-mentioned work by the Dobrotin and Slavatinskij group with a cloud chamber.

On the other hand, at still higher energies and particularly for the interaction of two complex nuclei, a method which seems likely to give considerably better results is the hydrodynamic method of examining the processes occurring in a single tube of nuclear matter. Such was the conclusion drawn in 1961 in particular by Loktionov, a junior colleague of Professor Takibaev at Alma Ata. He analysed the angular distribution of a great number of showers studied both in the Alma Ata and in other laboratories, including about 40 events due to α particles with an energy of over 10^{12} eV. Two of Loktionov's main results were that, for nucleus-nucleus interactions, the growth of the multiplicity with the energy is faster and that of the degree of anisotropy (see Fig. 5) slower than for nucleon-nucleon (or similar) interactions.

6. In order to understand the mechanism of the interactions taking place, in addition to the distribution of secondary particles according to spatial angles Θ, the analysis of the distribution according to azimuthal angles φ is also of outstanding interest. In particular, the discovery of anisotropy in the distribution according to φ could provide important evidence in favour of the participation of intermediate states with high momentum.

A methodological difficulty arises, however, from the absence of physically separate directions for individual events. An interesting method of strict statistical analysis which by-passes this difficulty was evolved and used in the laboratory of Professor Azimov (Tashkent). Another equally strict method, which was at the same time considerably simpler, was used by Professor Gurevich's group (Moscow). Studying the distribution according to $\Delta\varphi$ angles for all kinds of pairs of particles, two members of this laboratory, Mishakov and Nikolskij, analysed 78 events in cosmic rays (at energies of $10^{10} - 10^{13}$ eV) and about 400 9 GeV proton interactions. In an overwhelming number of cases there was no indication of azimuthal anisotropy, although for low multiplicity ($n_s = 2, 4$) allowance should be made for an azimuthal anticorrelation of the particles which is already perceptible, and which is apparently due to the law of momentum conservation.

7. For the use of photo-emulsions for studying very high processes in cosmic rays and also for investigation of the radiation zones of the earth, it would be very useful to learn to control the sensitivity of emulsions in time. An interesting but fruitless attempt to use a strong pulsed electric field ($> 10^6$ V/cm) for this purpose was made in 1962 at the Lebedev Physics Institute (FIAN), by a group of junior colleagues of Professor Alikhanyan. Submitting ordinary thin layer (30 μ) emulsions to the action of a simultaneous light ($\sim$ 30 μsec) and electric pulse with a peak voltage of 110 kV for a 150 μ gap, these physicists established the absence of any perceptible sensitivity variation where the electric field was applied.

On the other hand, a positive result which appears quite normal was obtained in the same year by Samoglovich et al., using the method of varying the concentration of hydrogen ions (pH). It was found that for NIKFI-R emulsions, a partially irreversible reduction of the density of the tracks of relativistic protons and electrons (and also of slow protons) takes place when the pH falls below 2 - 3. Immersion in an acid solution (to modify the pH) could be carried out either during or after the irradiation.

Some measuring characteristics of the apparatus are given below:

i) the lower limit of momentum measurement is determined by the inertness of the tracking device and is about 300 MeV/c; the upper limit is connected with the background of the tracking and counting equipment (of the order of 0.06 μ) which is generally lower than the background of the emulsion itself;

ii) the lower limit of grain density of tracks which can be followed is about 20/100 μ and the results of the measurement of this density depend to a certain extent on the width of the working (centring) area, and therefore on the degree of inertness of tracking along OY;

iii) the error due to the apparatus in the counting of the total number of clusters is usually found to be 1.5 - 2 times lower than the statistical error due to ionization fluctuations;

iv) the normal speed for reliable measurements is 32 μsec which, for a double measurement, represents about 1 cm/10 min; the main limitation of the operating efficiency of the machine is connected with the non-automatic character of the auxiliary operations (the discovery of a given track in the field of vision and its alignment along the axis OX);

v) the resolution (width of the analysing channels) for measurements of length of gaps and clusters is 0.2 μ.

The efficiency of measurement of momentum and relative ionization attained in practice (for tracks of about 1 cm long) is at present 4 tracks for a seven-hour shift (the machine being worked by one experienced operator). The characteristic length distribution curves for gaps under different working conditions (over a length of 1 cm) together with the corresponding visual measurement data (over a 1 mm section) are shown in Fig. 7. Table 2 gives an example of machine time distribution for a five-day working period.

Table 2

Operation	Time taken	
	hours	% of total time
1. Search for given tracks	4.5	14
2. Positioning of tracks along the axis OX	3.5	11
3. Triple measurements over a length of 17.5 cm (including entry in the working record)	19	57
4. Inspection, overhaul and shutdown	6	18

2. The measurement of the angular distribution of the particles is also generally an operation calling for a great deal of work.

For this work our Leningrad physicists and engineers designed and built a specialized semi-automatic microscope, type MIGE-I. This microscope records the current track co-ordinates on magnetic tape, and they are then calculated in a special computer according to a standard programme. Using this instrument about 500 tracks per day can be measured with an accuracy of $\sim 1°$, which represents a saving by a factor of about 10. In various work recently published this apparatus was used for the study of angular correlation between heavy fragments ($Z = 4 - 7$) and black tracks from fission events caused by 9 GeV protons.

Equipment for automatic along-the-track or area scanning of emulsions has not yet been developed. The first of these operations can be carried out fast enough (up to 5 m per day), even by hand, on a standard Soviet microscope MBI-9, which can be used to scan tracks easily in any desired direction, at any point of the photo-emulsion layer. In order to compete successfully with this fast method (which was first introduced at the Joint Institute by Podgoretskij and Bannik), an automatic device would have to carry out the tracking at a speed of the order of 1 mm/sec.

3. A well-known and very unfortunate drawback of the photo-emulsion method is the difficulty of distinguishing elementary interactions with one nucleon. Some progress in this respect has been made by the Emulsion Group of the Lebedev Physics Institute. Statistical analysis of the angular and momentum distribution showed that the selection of events according to the criterion $N_b \leq 1$, $N_g \leq 1$ (according to the number of black and grey tracks) sorts out a group of events comprising at least 80% of single-nucleon interactions. A more efficient method of selection of individual events, based on the calculation of the total square of the mass, M_e^2, of all the observed particles, was worked out at Dubna by Podgoretskij et al. The method is based on the fact that the influence of the binding of the nucleons in the nucleus leads to a negative value of M_e^2, the regions $M_e^2 < 0$ and $M_e^2 > 0$ being separated by a fairly pronounced dip when $M_e^2 = 0$.

4. When seeking the events with which we are concerned along the track of the primary particle, and especially by area scanning (the latter takes place particularly when studying elastic scattering by means of perpendicular irradiation), a problem which becomes of great importance is that of obtaining satisfactory scanning efficiency or at least a sufficiently accurate and reliable method of determining it. For this purpose, repeated scanning is usually used but often without taking into account the dependence of the efficiency on the type of event and on the conditions under which it was observed in the emulsion layer, as well as on the subjective characteristics of the observer which vary with time.

These two factors were subjected to a close analysis in a recent paper by Tolstov and Sokslov (Dubna Joint Institute). They proposed a new method based on the study of the results of triple scanning which constitutes above all an experimental check of the hypothesis of constant efficiency. This method consists of comparing the number of events m_i observed during simple scanning with the number

$$m_i' = m_{ij} \frac{m_{ik}}{m_{ijk}}$$

calculated from the data of two double and one triple scanning operation. When m_i' is found to be much smaller than m_i, it is necessary to use the following formula in order to discover the actual number of events:

$$n = \frac{\Sigma m_i \, m_{jk}}{\underbrace{2m_{123}}_{A}} - \sqrt{A^2 - \frac{2m_1 m_2 m_3}{m_{123}}}$$

and to evaluate the error from

$$\frac{\delta n}{\sqrt{n}} = \sqrt{1 - \left(\frac{1 - \bar{\epsilon}}{\bar{\epsilon}}\right)^3}$$

where $\bar{\epsilon}$ is the mean efficiency for the three scanning operations.

5. In conclusion, mention must be made of the accurate measurement of the ionizing capacity of the particles. These measurements require calibration data relating to tracks of particles of the required kind and energy in the same range, which are also formed under the same irradiation conditions as the tracks being measured. It is only under such conditions that ionization measurements with an accuracy of the order of 2% can be carried out.

There is an additional difficulty in the case of electrons whose energy may change sharply (due to Bremsstrahlung). Neglect of this point may substantially mask the actual dependence of the ionization on the momentum of the particles.

Experiments performed during the last two years by the Emulsion Group of the Physics Institute, taking into account the requirements mentioned above, led to the discovery of an interesting effect, namely an ionization decrease of about 6% at energies of over 200 mc^2 (in NIKFI-R and ILFORD-G5 emulsions) which agrees well with theoretical forecasts, taking into account radiative corrections (see Fig. 8).

* * *

BIBLIOGRAPHY

1. G.B. Zhdanov, E.A. Zamyalova, M.I. Tretyakova and M.N. Shcherbakova, Suppl. No. 2, Nuovo Cimento 81, 726 (1958).

2. N.L. Grigorov, V.V. Guseva, N.A. Dobrotin et al. Papers of the International Conference on Cosmic Rays, pub. USSR Academy of Science, Moscow 1960, Vol. 1, p. 140.

3. K.I. Alekseeva, L.L. Gabuniya, Den Pkhen Su, G.B. Zhdanov and M.I. Tretyakova, JETP 43, 783 (1962).

4. N.L. Grigorov, M.A. Kondrateva, A.I. Saveleva, V.A. Sobinyakov A.V. Povgurskaya and V.Ya. Shestoperov, Papers of the International Conference on Cosmic Rays, pub. USSR Academy of Science, Moscow 1960, Vol. 1, p. 122.

5. V.S. Barashenkov, V.M. Maltsev and E.K. Mikhul, preprint UNRI D-597, Dubna 1960. K.I. Alekseeva, G.B. Zhdanov, E.A. Zamgalova, M.I. Tretyakova and M.N. Shcherbakova, JETP 40, 1625 (1961). A.A. Loktionov, Papers of the Nuclear Physics Institute, Academy of Science, Kazakstan SSR 5, 34 (1962).

6. V.M. Chudakov, JETP 40, 156 (1961). A.P. Mishakova and B.A. Nikolskij, JETP 43, 1213 (1962).

7. M.A. Babalov, B.A. Dolgoshein, B.I. Puchkov and F.R. Sosnin, PTE No. 5, 178 (1962). D.M. Samojlovich, E.S. Barinova and I.V. Ardashev, Preprint IAE-305 (1962).

8. N.L. Grigorov and I.D. Rapoport "Ionization calorimeter for measuring the energy of cosmic ray particles by means of emulsion stacks", Bulletin of Inventions No. 6 (1962).

9. A.E. Voronkov, L.V. Sukhov, I.V. Shtranikh et al. PTE No. 2, 63 (1961); No. 1, 42 (1962). A.E. Voronkov, G.B. Zhdanov and L.V. Sukhov, Report to the 4th International Colloquium on Nuclear Photography, Munich 1962.

10. F.G. Lepekhin and M.M. Makarov, JETP 44, 68 (1963); B.P. Bannik and M.I. Podgoretskij, PTE No. 3, 36 (1960).

11. D.K. Kopylova, V.B. Lyubimov, M.I. Podgoretskij and E. Trka, Joint Institute for Nuclear Research, Preprint No. 1186, Dubna 1963.

12. K.D. Tolstov and S.N. Sokolov, Joint Institute for Nuclear Research, Preprint 1-1085, Dubna 1962.

13. G.B. Zhdanov, M.I. Tretyakova, V.P. Tsytovich and M.N. Shcherbakova, JETP 43, 342 (1962).

5666/NP/smg

DISCUSSION

Bott-Bodenhausen : Can you give me some reference about the automatic measuring-machine?

Zhdanov : The construction is described in the Journal for instruments and technique No. 2, 63 (1961) and in No. 1, 42 (1962) by Voronkov et al. Unfortunately this is in Russian but it is available at CERN. The application-efficiency is described in the Proceedings of the Fourth International Conference on Corpuscular Photography, Munich 1962, p. 447 (in English).

Bott-Bodenhausen : Are there experiments on automatic scanning-machines?

Zhdanov : The searching of a surface is technically more complicated than following a track, and even for scanning along the track you would need a speed of at least 1 mm per second to compete with visual methods. Until now there is no experience of this type.

O'Ceallaigh : Would it not be better to measure the mean gap length instead of blob-counting, because the physical development may cause a change in blob-density up to 1 or 2%? Your machine would measure this.

Zhdanov : Yes.

O'Ceallaigh : There exist different measurements of the energy-loss of particles, for example by Stiller (as reported at the Munich conference) of electrons of a γ value in the region of 200 to 1,500, and by our group at Dublin, up to about $\gamma = 600$, which do not show the drop at high energies. Stiller himself does nct exclude the

O'Ceallaigh (cont.) : possibility that, at the second exposure, at Cornell, the stack might not have been at room temperature, and consequently the sensitivity might have been lower; but this could have the tendency to bring his results into agreement with yours. The Ilford G5 seemed to follow the same curve as the one you show, whereas the other emulsions yielded a plateau-value = 1.14 min.

Zhdanov : We also were rather confused about this discrepancy, but all other groups did not attain our accuracy, except Stiller et al. who had the same statistical weight. For G5 emulsion, the average of the values at high energies is the same in Stiller's work as in ours, but not the shape of the curve; we found a tremendous discrepancy for the NIKFI-R emulsion perhaps because it was not developed in the proper way. However, the main objection is, as mentioned, the difference in sensitivity between the calibration with π mesons and the irradiation with electrons. The measurements will be continued.
(Further details of the work of Professor Zhdanov's group on this problem are given in the Proceedings of the Fourth International Conference on Corpuscular Photography, Munich, 1962, p. 558. The authors are K.L. Alekseyeva, G.B. Zhdanov, M.I. Tretyakova, V.N. Zytovich and M.N. Shcherbakova. Ed.)

O'Ceallaigh : What was the method you used to estimate the energy of the electrons?

Zhdanov : We measured the scattering of the tracks, and only used those parts of the track where over a considerable length there was no change of density visible.

O'Ceallaigh : How could you achieve this accuracy at a γ value up to 2,000?

/NP/smg

Zhdanov : In our experiment the scattering was quite precise.

O'Ceallaigh : Again a question concerning the energy-loss curve. The important feature of your experiment is the contemporaneity of the proton tracks and those of the electrons. This is a defect of the other experiments. Nevertheless, the point could be checked by using beams of electrons of known momentum from electron accelerators.

Evans : a) Are there any plans to put the emulsion plus calorimeter experiment on a satellite?
b) What sort of exposures or experiments have occurred at Dubna in the past year?

Zhdanov : We plan to fly emulsions on satellites, but there is a great competition for experiments on satellites. I can only mention some of the experiments carried out at Dubna. The study of elastic scattering: exposure of stacks to study the inelastic scattering of proton and π mesons, each by many groups. The experiments are compared with the theory of peripherial collisions, which is worked out by the theoreticians of our institute. There was a good agreement in the first approximation and we shall continue.

Lock : The reports of the Dubna Photo-Emulsion Committee give complete lists of experiments with emulsions that have been done and that are planned. We have copies of these reports at CERN which we have had translated into English and French.

Bott-Bodenhausen : Are there experiments in the USSR with emulsions in pulsed magnetic fields?

Zhdanov : There have been some trials with magnetic fields of about 200,000 Oe, which are under construction.

* * *

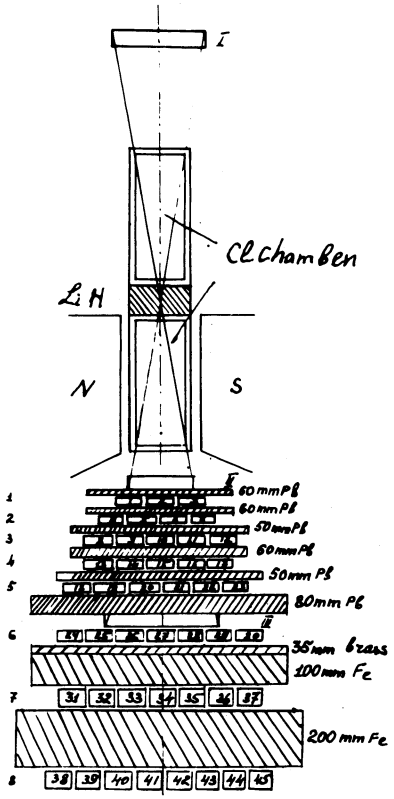

Fig. 1 Set-up for the study of high energy (10^{11}-10^{12} eV) nuclear interactions by the cloud chamber method with ionization calorimeters.

The figure shows : two cloud chambers (K. B.), Li H filter, 3 groups of counters (I-III), and rows of ionization chambers (1-8) with lead, brass and iron interlayers.

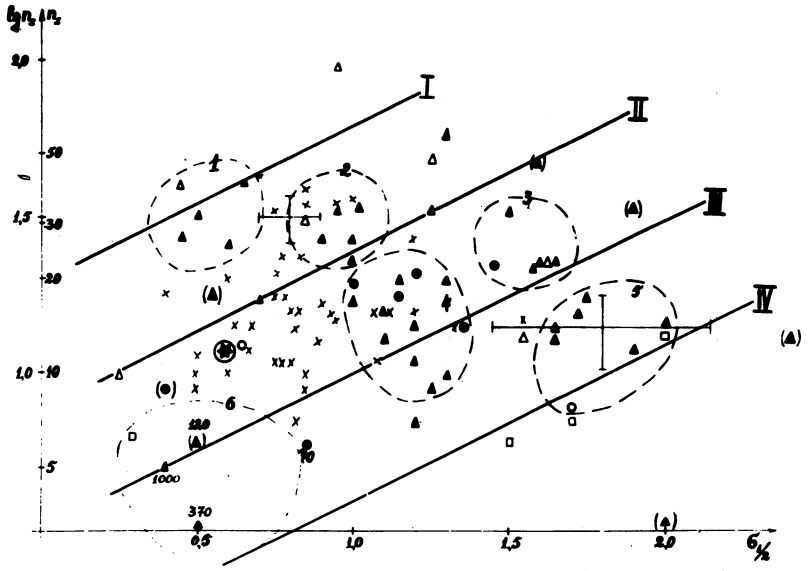

Fig. 2 Distribution according to the number of charged particles (n_s) and degree of anisotropy (σ 1/2 - half-width of the angular distribution in the logarithmic scale) for events discovered by the area scanning method (X) and the method of inverse continuation of electron cascades (Δ , 0). The signs ($\square$) represent events connected with the interaction of secondary particles.

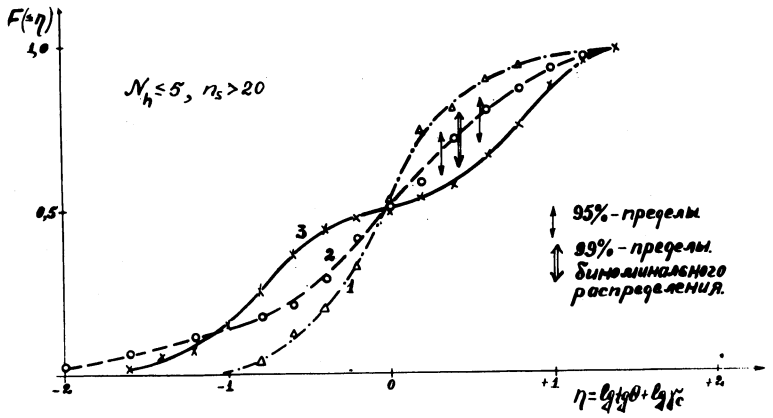

Fig. 3 Mean values of integral angular distribution of secondary particles, for groups of events 1, 2, 3 (see fig. 2). The arrows show the confidence limits for fluctuations governed by binomial distribution for a given total number of particles in a group.

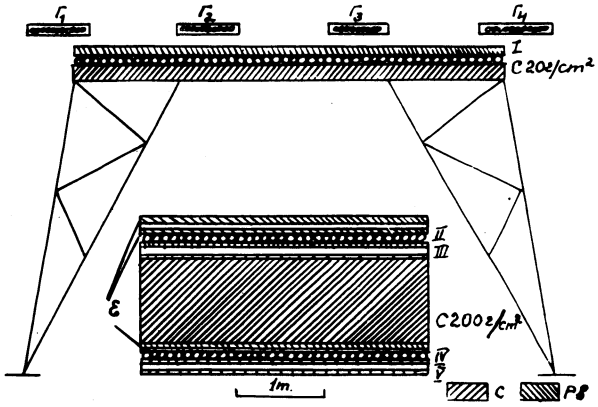

Fig. 4 Set-up for the study of very high energy (10^{13} - 10^{14} eV) nuclear interactions by the "controlled" photo-emulsion method. The drawing shows emulsion layers (ε), rows of ionization chambers (I-V) and hodoscope counters (Γ_1 - Γ_4) and also graphite and lead filters.

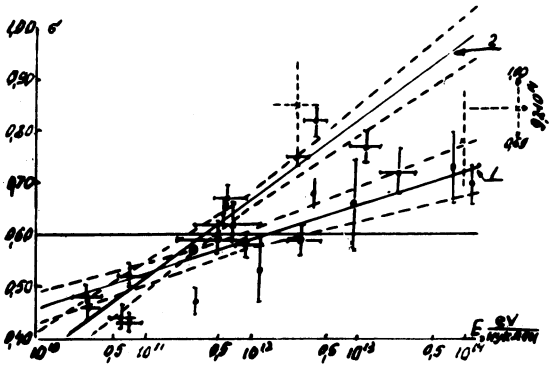

Fig. 5 The dependence of the degree of anisotropy on the energy of the interacting particles :

1) for interactions between alpha particles and heavy nuclei of the emulsion,

2) for showers of the nucleon-nucleon type.

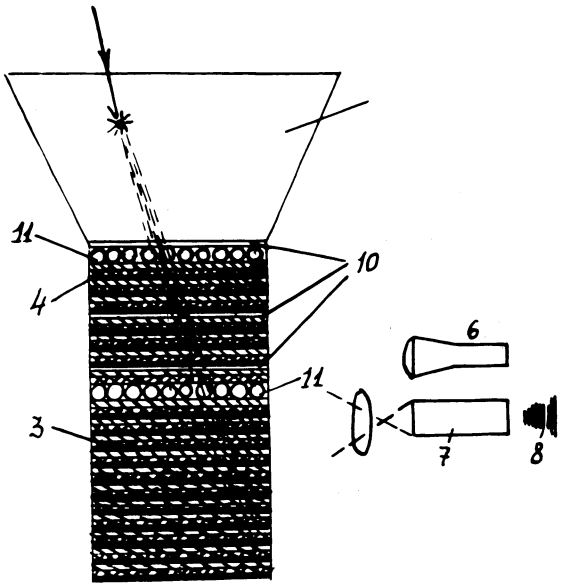

Fig. 6 Combination of an emulsion stack (1) with plastic scintillators (4), filters (3) and spark chambers (10) for efficient discovery of primary nuclear interactions and determination of the energy of the electronic cascades. (6-8) electronic optical and photographic devices.

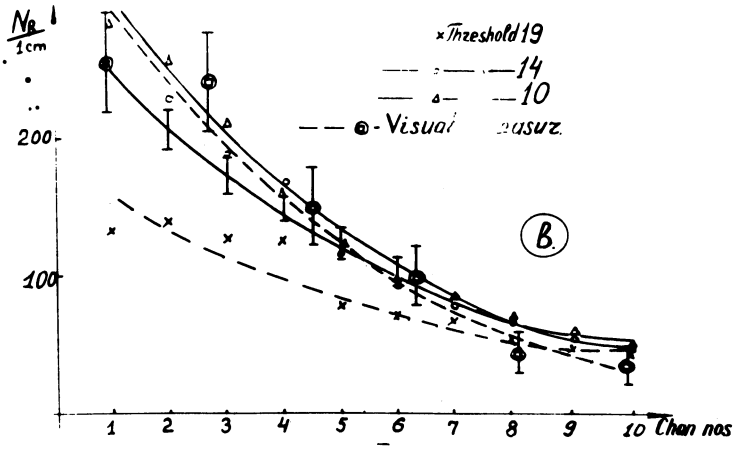

Fig. 7 Distribution according to gap length on tracks of primary protons (20 BeV) obtained by the visual method (over a length of 1 mm) and automatically, for different values of the threshold voltage separating the working pulse from the background.

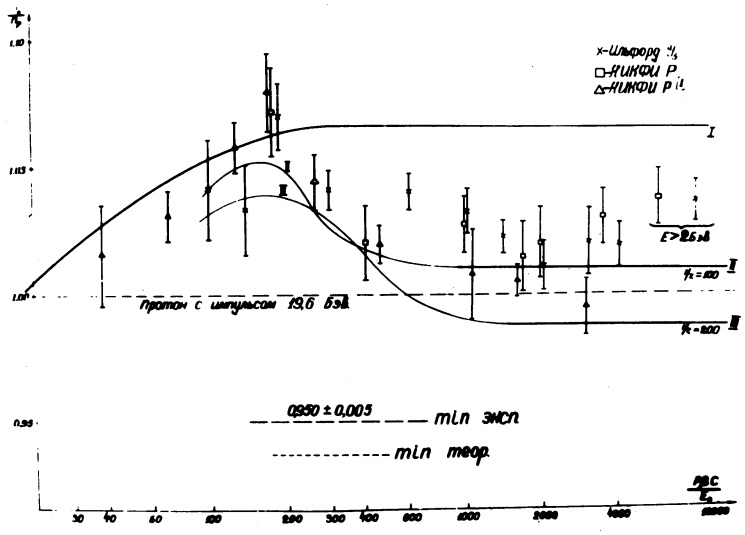

Fig. 8 The dependence of the density of clusters on the energy for electrons (the density of proton tracks of about 20 BeV is taken as a unit of reference).

The calculation curves correspond to :

I - usual perturbation theory (in the first order)

II - III - calculations by V. N. Tsytovich, taking into account radiative corrections for different values of the parameter 1/3.

V. HYPERFRAGMENTS

PART V.1

THE STRONG AND WEAK INTERACTIONS OF BOUND Λ PARTICLES*)

R.H. Dalitz,

The Enrico Fermi Institute for Nuclear Studies and Department of Physics, The University of Chicago, Chicago, Illinois.

I. THE NUCLEAR INTERACTIONS OF THE Λ PARTICLE

1. The s-wave Λ-N interaction

The binding of Λ particles to the s-shell nuclei H^2, H^3, He^3 and He^4 is due dominantly to the s-wave Λ-N interactions V_S for the singlet (S = 0) and triplet (S = 1) configurations. From the spin determinations for ${}_\Lambda H^3 (J = \frac{1}{2})$ and for ${}_\Lambda H^4$ (J = 0), we know that the singlet interaction V_0 is more attractive than the triplet interaction V_1. Our knowledge of their strengths depends on quantitative calculations on the structure of these light hypernuclei, as discussed below. However, the conclusion that the triplet interaction V_1 is attractive depends on rather qualitative considerations. The mean Λ-N attraction in ${}_\Lambda H^3$ is given by $\frac{1}{4}(3V_0 + V_1)$, dominated by the singlet interaction; hence calculations on ${}_\Lambda H^3$ alone provide a lower limit on the strength of V_0. In ${}_\Lambda He^5$, on the other hand, the mean Λ-N attraction $\frac{1}{4}(3V_1 + V_0)$ arises dominantly from the triplet interaction; owing to its small weighting, the singlet interaction cannot provide sufficient attraction to account for the ${}_\Lambda He^5$ binding and we must conclude that V_1 is also attractive.

In order to estimate the strength of the Λ-N interaction, we must make a definite assumption about its range. We shall assume that this interaction has the same intrinsic range (1.5 f) as a Yukawa potential of range parameter $(2m_\pi)^{-1}$. This corresponds to the assumption that the

*) This paper was also presented at the Hyperfragment Conference.

Λ-N potential arises dominantly from the exchange of pions; charge symmetry for the Λ particle (which has isospin I = 0) forbids one pion exchange, but the two-pion-exchange potential is allowed and is expected to be strong, in view of our current belief (based on the existence of a $p_{3/2}$ π-Λ resonance analogous to the π-N resonance, for example) that the $\pi\Sigma\Lambda$ coupling has strength comparable with that of the pion-nucleon coupling. This value for the intrinsic range is quite close to the values obtained for the Yukawa potentials which are equivalent (in the sense of having the same zero-energy scattering length a_s and effective range r_s) to the meson-theoretic Λ-N potentials calculated recently by de Swart and Iddings[1]. In fact, in view of the low binding energies of the light hypernuclei, it is reasonable to expect that these will not be greatly sensitive to the details of the potentials V_0 and V_1, but that they will be determined primarily by the low-energy scattering parameters, (a_0, r_0) and (a_1, r_1), of these potentials. As we shall see, the detailed calculations which have been made to date (but always with central potentials) do bear out this expectation.

$_{\Lambda}H^3$ is the lightest hypernucleus, with Λ-d separation energy $B_\Lambda = 0.21 \pm 0.2$ MeV, and is known to be a singlet state, with isospin I = 0 and spin J = ½. This npΛ system is sufficiently simple to allow quite detailed and accurate variational calculations, even with hard-core potentials. For its space wave-function, Downs, Smith and Truong[2] have recently used a ten-parameter trial function,

$$\psi = f(r_{\Lambda n})\, f(r_{\Lambda p})\, g(r_{np}), \tag{1}$$

where f,g both have the general form,

$$\left\{\left[\exp[-\alpha(r-d)] - \exp[-\beta(r-d)]\right] + x\left[\exp[-\mu(r-d)] - \exp[-\nu(r-d)]\right]\right\}. \tag{2}$$

This calculation used a Λ-N potential of the exponential form

$$V_{\Lambda N}(r) = \bar{U} \exp[-3.54(r-d)/(b-2d)], \qquad r \geq d \tag{3}$$

outside the hard core radius d. The intrinsic range is given by b = 1.5 f. For d = 0.4 f, their result was $\bar{U}$ = 1144 MeV, which corresponds to a mean well-depth parameter $\bar{s}$ = 0.810. The scattering length which corresponds to this mean Λ-N potential is $\bar{a}$ = - 1.82 f. Calculations were also made for d = 0.2 f and 0.6 f, leading to scattering lengths $\bar{a}$ = - 1.75 f and - 2.11 f, respectively. It is also of interest to compare these results with the value $\bar{a}$ = - 1.55 f which was obtained in an earlier calculation[3] of comparable complexity, for Yukawa potentials of the same intrinsic range, without hard cores. These results illustrate the insensitivity of the low-energy parameters obtained (for fixed intrinsic range) for the mean potential to the shape assumed for this potential. We may also compare this result of Downs et al. with that from their earlier calculation[2] using a four-parameter trial function of the form (1), with f,g of the form (2) with x = 0, which gave $\bar{U}$ = 1202 MeV. The more elaborate trial function led only to 4.8% improvement in the value obtained for $\bar{U}$, so that we may assume their final value to be rather close (better than 1%) to the true value.

Muller[4] has also made calculations on ${}_{\Lambda}H^{3}$ for exponential hard-core potentials, using an eight-parameter trial function of the form (1). He assumed a potential of greater intrinsic range, of the form $\bar{U}\exp[-2.38(r-d)]$ outside hard-core radius d, and obtained $\bar{U}$ = 228.2 MeV. The corresponding calculation of Downs et al.[2], for potential shape $\bar{U}\exp[-2.36(r-d)]$, gave $\bar{U}$ = 226.1 MeV, so that their results are in good agreement. The scattering length for this potential is $\bar{a}$ = - 2.7 f; we note that the scattering length obtained does increase with the potential range assumed, as is reasonable.

For ${}_{\Lambda}He^{5}$, it is a reasonable assumption to neglect the distortion of the He^{4} core by the presence of the Λ particle, in view of the tight binding of He^{4}. Since the form of He^{4} is known from electron-scattering experiments, the strength of the mean Λ-N potential in ${}_{\Lambda}He^{5}$ may be deduced directly, for an assumed Λ-N potential shape without hard core. This calculation was done quite early[5] for Λ-N potentials of Gaussian form, and was combined with the results of calculations for ${}_{\Lambda}H^{3}$ to give the results shown in the first column

of Table 1. For later reference, we quote here the volume integrals of the singlet and triplet potentials obtained by this way: $\bar{V}_0 = 386$ MeV f^3, $\bar{V}_1 = 170$ MeV f^3. The errors quoted in the Table are those derived from the uncertainties in the B_Λ values and in the radius of He^4.

With hard-core potential shapes, calculations have been made for $_\Lambda He^5$ and $_\Lambda H^4$ (with charge symmetry, $_\Lambda He^4$ is the mirror hypernucleus to $_\Lambda H^4$, with the same structure and the same B_Λ value, as is consistent with the data) by Dietrich et al.[6] and by Gutsch[7], using a method proposed by Mang and Wild[8] for light nuclei. This method takes into account accurately the two-body correlations in these light nuclei, rather in the spirit of the Brueckner method as developed for the discussion of nuclear matter, although the detailed justification of the method for these light nuclei depends on quite different physical factors (essentially on the large spacing of the one-particle states for the oscillator potential determined self-consistently) than does its justification (the Pauli principle and the high Fermi momentum) for the problem of nuclear matter. To date, these calculations have used square-well potentials of width (b-2d) outside hard-core radius d; the results available for d = 0.2 f and d = 0.4 f, with intrinsic range b = 1.484 f, are given in Table 1. It is of interest to note the insensitivity of the conclusion to the hard-core radius assumed; for orientation, we remark that, for d = 0, the increase from $a_0 = 2.4$ f to $a_0 = 4.2$ f requires an increase by only 10% in the potential strength of V_0. For d = 0.4 f, the scattering length a_0 corresponds to a well-depth parameter s = 0.8 for the $^1S_0$ potential, so that there is no reason to expect a bound state for the Λ-N system.

Dietrich et al.[6] and Gutsch[7] have also made calculations for $_\Lambda H^3$, using the same method. For d = 0.4 f, Gutsch finds that the observed B_Λ requires a mean well-depth $\bar{V}_3 = 170$ MeV for the outer square-well potential; the value $\frac{1}{4}(3V_0 + V_1)$ given by the potentials V_0 and V_1 obtained from the discussion of $_\Lambda H^4$ and $_\Lambda He^5$ is 168.0 MeV. The scattering length corresponding to this value $\bar{V}_3$ is $\bar{a} = 2.5$ f. This is appreciably larger than the value (2.0 f) found from the variational calculations mentioned

above, and corresponds to a well-depth parameter about 12% too large; this is probably due to the fact that the Mang-Wild method is least accurate for small binding energies, as it does not give a correct account of the asymptotic region (which is of particular importance for small B_Λ). However, the internal comparisions between all of these calculations for the s-shell hypernuclei are rather satisfactory, in view of their approximate nature and the range of potential forms which have been used.

Finally, we consider whether there exists a J = 1 particle-stable state for the hypernuclei ${}_\Lambda H^{4*}$ and ${}_\Lambda He^{4*}$. This question is of great interest in view of its bearing on the interpretation of the ${}_\Lambda H^4$ and ${}_\Lambda He^4$ hypernuclei observed following $K^- - He^4$ capture events, whether these are produced directly (which would imply that the KΛ parity is odd) or whether they result from γ decay of such directly-produced excited states, with direct production of the ground state hypernuclei being forbidden. The situation is summarized in Table 1. The calculations[3,15] for d = 0 (corrected to the He^3 r.m.s. radius recently measured by Hofstadter and Collard) do indicate the existence of a bound state with $B_\Lambda^* \approx 1.3$ MeV, corresponding to a well-depth parameter of about 1.25 for the J = 1 configuration. The more recent calculations[6,7] carried out for hard-core potentials do not allow the existence of a J = 1 bound state. The attraction predicted for the J = 1 configuration actually decreases with increasing hard-core radius, the well-depth parameter of the $\Lambda - He^3$ attraction being only 0.83 in this state for d = 0.4 F. Further calculations along these lines for outer potential shapes more realistic than the square well, and which can be compared directly with the more accurate variational calculations on the ${}_\Lambda H^3$ system, would be rather desirable at this point.

The interpretation of these potentials V_0 and V_1, together with the data available on the ratio $R = (\Sigma^0 n)/(\Lambda n)$ for $\Sigma^- p$ capture from rest, has been extensively discussed in terms of the pion-hyperon interactions $\Sigma\Sigma\pi$ and $\Sigma\Lambda\pi$ by de Swart and Iddings[1]. Their calculations are based on a two-channel approach, in which the ΛN and ΣN channels are treated on the same footing in view of the relatively small mass difference $(m_\Sigma - m_\Lambda) \approx 80$ MeV. We confine our attention here to their essential conclusions for the case of

even $\Sigma\Lambda$ parity. The $^1S_0$ potential depends primarily on the coupling $f_{\Sigma\Lambda}$ and its strength requires that $f_{\Sigma\Lambda}$ be comparable in magnitude with the pion-nucleon coupling f_{NN}. The $^3S_1$ potential strength and the ratio R both depend quite strongly on $f_{\Sigma\Sigma}$ and an adequate fit to all three data requires $f_{\Sigma\Sigma} \approx 0.1$, taking the hard-core radius to be d = 0.5 f, as required for the corresponding NN potentials.

For small $f_{\Sigma\Sigma}$, the coupling between the ΛN and ΣN channels is not of major importance in the $^1S_0$ state, and the dominant interaction is the two-pion exchange potential in the ΛN channel, which depends only on the $\Sigma\Lambda\pi$ coupling. In the $^2S_1$ state, the one-pion exchange potential linking ΛN and ΣN channels is very strong and of the tensor form; there is a strong $f_{\Sigma\Sigma}$ dependence both because of the importance of the $\Sigma\Sigma\pi$ coupling in the ΣN channel and because $f_{\Sigma\Sigma}$ contributes to the fourth-order potential V(ΛN,ΣN) which interferes with the strong one-pion exchange term in this potential. However, the low-energy ΛN scattering wave-function does not have a large D-state, so that the tensor component of the effective ΛN potential is expected to be of relatively minor importance, in contrast with the situation for the NN system.

2. The s-wave Λ-Λ interaction

Very recently Danysz et al.[9] have reported the first example of a double Λ hypernucleus, for which the most probable interpretation is $_{\Lambda\Lambda}Be^{10}$, with separation energy $B_{\Lambda\Lambda} = 17.5 \pm 0.5$ MeV relative to $\Lambda + \Lambda + Be^8$(g.s.). Since $B_\Lambda = 6.5 \pm 0.15$ MeV $_\Lambda Be^9$, $B_{\Lambda\Lambda}$ exceeds $2B_\Lambda(Be^9)$ by 4.5 ± 0.6 MeV, so that we conclude that the Λ-Λ interaction is attractive. Since both particles are in the ground s-orbit relative to the nuclear core, the Pauli principle requires that their spins be coupled in the singlet configuration, so that $B_{\Lambda\Lambda}$ is determined predominantly by the $^1S_0$ Λ-Λ potential.

An estimate of the Λ-Λ potential strength may be obtained using a simple product wave-function[10],

$$\psi = \varphi(|\underline{r}_1 - \underline{R}|)\ \varphi(|\underline{r}_2 - \underline{R}|)\ (u_1 v_2 - v_1 u_2)/\sqrt{2}\,, \qquad (4)$$

where $\underline{R}$ denotes the c.m. position of the Be^8 core. If $E_\Lambda(\varphi)$ denotes the separation energy of ${}_\Lambda Be^9$ [relative to $\Lambda + Be^8$(g.s.)] calculated for the wave-function φ, then

$$-B_{\Lambda\Lambda} \geq -2E_\Lambda(\varphi) + \langle V_{\Lambda\Lambda} \rangle . \qquad (5)$$

We take the potential $V_{\Lambda\Lambda}$ to be of Gaussian form $-\bar{v}_{\Lambda\Lambda}(\lambda/\pi)^{3/2} \times \exp(-\lambda r^2)$, with $\lambda = 2.0604/b^2$ and intrinsic range $b = 1.5$ f corresponding to the process of two-pion exchange. If φ is taken to be the wave-function for ${}_\Lambda Be^9$, then $-\langle V_{\Lambda\Lambda} \rangle$ can be identified with $(B_{\Lambda\Lambda} - 2B_\Lambda) = 4.5 \pm 0.6$ MeV, which leads to a first estimate 520 ± 70 MeV f^3 for the volume integral $\bar{v}_{\Lambda\Lambda}$ of the ${}^1S_0$ Λ-Λ potential. However, this estimate is considerably too large, since, owing to the additional binding energy, the wave-function φ appropriate to ${}_{\Lambda\Lambda} Be^{10}$ will actually fall off much more rapidly with r than φ for ${}_\Lambda Be^9$. To allow for this, we vary the form of φ, using the inequality (5) as a variational principle for $\bar{v}_{\Lambda\Lambda}$. The form

$$\varphi(r) = N\,[\exp(-ar^2) + y \exp(-cr^2)] \qquad (6)$$

provides a good fit to the ${}_\Lambda Be^9$ wave-function for $a = 0.25\ f^{-2}$, $c = 0.07\ f^{-2}$ and $y = 0.33$, the Λ-Be^8 potential being represented by a shell-model form with strength adjusted to fit the observed B_Λ value. The effect of interest is roughly represented by decreasing y; the minimum occurs for $y = 0.15$, leading to the improved estimate,

$$\bar{v}_{\Lambda\Lambda} = 440 \pm 60\ \text{MeV}\ f^3 . \qquad (7)$$

Further improvements to this estimate are still necessary, with improved wave-functions which take into account:

i) the possibility of strong spatial correlations between the two Λ particles;

ii) the distortion of the nuclear core by the presence of two strongly bound Λ particles.

The inclusion of these effects may be expected to lower our estimate for $\bar{v}_{\Lambda\Lambda}$ further, but certainly not by more than the error quoted in Eq. (7).

As pointed out by Danysz et al.[9], there is possibly an alternative interpretation for this event as ${}_{\Lambda\Lambda}Be^{11}$ with separation energy 19.0 ± 0.6 MeV relative to $\Lambda + \Lambda + Be^9$. For ${}_{\Lambda}Be^{10}$, $B_\Lambda = 7.9 \pm 0.4$ MeV, but only the spin-average $\Lambda - Be^9$ interaction is effective in ${}_{\Lambda\Lambda}Be^{11}$, since the Λ spins are in the singlet configuration. Using intermediate coupling wave-functions for Be^9, the spin dependent term in B_Λ is $0.32\langle\Delta\rangle$, where $\langle\Delta\rangle$ is an appropriate expectation value of the spin-dependent part of the $\Lambda - N$ interaction which has the value 1.8 ± 0.4 MeV for neighbouring hypernuclei, as discussed in Section III. Hence the quantity $(B_{\Lambda\Lambda} - 2\bar{B}_\Lambda)$ has the value $[19.0 - 2(7.9 - 0.6)] = 4.4 \pm 1.0$ MeV, quite comparable with the value used above for ${}_{\Lambda\Lambda}Be^{10}$, so that our estimate (7) of $\bar{v}_{\Lambda\Lambda}$ would not be appreciably modified if the alternative interpretation ${}_{\Lambda\Lambda}Be^{11}$ were adopted.

As for the $\Lambda - N$ potential, the long-range part of the $\Lambda - \Lambda$ potential arises from two pion exchange. For even $\Sigma\Lambda$ parity, the ${}^1S_0$ $\Lambda - \Lambda$ interaction arises dominantly from the two-pion exchange potential in the $\Lambda\Lambda$ channel, since the potential coupling the $\Lambda\Lambda$ and $\Sigma\Sigma$ channels is relatively weak. The reason for this is essentially the same as for the $\Lambda - N$ case, namely:

a) for pseudoscalar mesons, the one-pion exchange potential is known to be quite weak;

b) the two-pion contribution to $V(\Lambda\Lambda - \Sigma\Sigma)$ is necessarily proportional to $f^2_{\Sigma\Sigma}$, which appears to be a relatively small coupling parameter.

The structure of the two-pion contribution to $V(\Lambda\Lambda,\Lambda\Lambda)$ is the same as that for $V(\Lambda N,\Lambda N)$, except for the additional factor $f^2_{\Sigma\Lambda}/f^2_{NN}$. Hence, if the same hard-core radius is assumed for the $\Lambda - \Lambda$ and $\Lambda - N$ interactions, the comparison of the values $\bar{v}_{\Lambda\Lambda} = 440$ MeV f^3 indicates that $f_{\Sigma\Lambda} \approx f_{NN}$ quite closely.

3. Binding energies for the p-shell hypernuclei

On the basis of a shell-model representation for the core nuclei, Lawson and Rotenberg[11] and Iwao[12] have proposed the following expression:

$$B_\Lambda = C + N_p \langle \bar{V} \rangle + \alpha_N \langle \Delta \rangle \qquad (8)$$

for the binding energies of hypernuclei with nuclear cores belonging to the 1p shell. In this expression N_p denotes the number of p-shell nucleons, and $\langle \bar{V} \rangle$, $\langle \Delta \rangle$ denote the expectation values of $\frac{1}{4}(3V_1 + V_0)$ and $(V_0 - V_1)$ respectively between the Λ-particle wave-function and the wave-function of a p-shell nucleon. The coefficient α_N depends on the spin of the hypernuclear state and on the details of the structure of the core nucleus; values of α_N have been calculated by Dalitz and Soper[13] using intermediate coupling wave-functions for the core nuclei and including the admixture of excited nuclear states where these are of significance. Generally speaking, the values of α_N are close to those for L-S coupling at the beginning of the p-shell, for A < 9, and close to those for j-j coupling for A > 9. For j-j coupling, the value of α_N is

$$\alpha_N = -\frac{1}{4}\left[1 - \frac{\ell(\ell+1) - \frac{3}{4}}{j(j+1)}\right]\left[J(J+1) - J_N(J_N+1) - \frac{3}{4}\right]. \qquad (9)$$

We note here that the result established empirically for ${}_\Lambda H^3$, ${}_\Lambda H^4$ and ${}_\Lambda Li^8$ [14] that the ground-state hypernuclear spin value is $|(J_N - \frac{1}{2})|$ is not expected to be a general rule. For example, C^{13} belongs to the $p_{1/2}$ shell, so that $j = \frac{1}{2}$, $\ell = 1$, $J_N = \frac{1}{2}$, and the coefficient α_N has the values $+\frac{1}{12}$ for $J = 1$, $-\frac{1}{4}$ for $J = 0$. Hence spin $J = 1$ is expected to hold for the ground state of ${}_\Lambda C^{14}$ and ${}_\Lambda N^{14}$, contrary to the above rule. With $J = 1$, the two-body decays ${}_\Lambda C^{14} \to \pi^- + N^{14}(J = 1+)$ and ${}_\Lambda N^{14} \to \pi^- + O^{14}(J = 0+)$ are both allowed through the dominant s-interaction. However, if $J = 0$ held for the $({}_\Lambda C^{14}, {}_\Lambda N^{14})$ doublet, the two-body decay ${}_\Lambda N^{14} \to \pi^- + O^{14}$ would be forbidden for the s-interaction, although still allowed through the p-interaction (about 10 times weaker). Since O^{14} has

no known particle-stable excited states, this means that there can be no confusion from ($\pi^- + O^{14*}$) modes, and the two-body decay of $_\Lambda N^{14}$ would be quite rare; for J = 0, the two-body decay $_\Lambda C^{14} \to \pi^- + N^{14}$ is allowed through the s-interaction.

The derivation of expression (8) is based essentially on a variational estimate for B_Λ, in which the same trial function is used to describe the Λ-nucleus relative motion for all the p-shell hypernuclei. The wave-functions directly calculated do not deviate far from such a mean wave-function, for as the B_Λ value increases and the tail of the wave-function falls off more rapidly, so also does the radius of the Λ-nucleus potential increase, partly compensating this effect. The constant term C then results from the kinetic energy terms and the interaction of the Λ particle with the s-shell nucleons.

For hypernuclei whose core nuclei are spinless, expression (8) gives a linear relation between B_Λ and N_p. For the systems $_\Lambda He^5 (B_\Lambda = 3.1 \pm 0.05$ MeV), $_\Lambda Be^7 (B_\Lambda = 4.9 \pm 0.5$ MeV), $_\Lambda Be^9 (B_\Lambda = 6.5 \pm 0.15$ MeV) and $_\Lambda C^{13} = 10.6 \pm 0.4$ MeV), this linear relation is well satisfied, with C = 3.1 ± 0.05 MeV and $\langle \bar{V} \rangle = 0.90 \pm 0.04$ MeV. This value of $\langle \bar{V} \rangle$ is in good agreement with the value directly calculated[15] from the s-wave Λ-N potentials (without hard core) discussed in Section I.

The spin-dependent term $\langle \Delta \rangle$ can be estimated in four reliable cases, from $_\Lambda Li^7 (B_\Lambda = 5.52 \pm 0.45$ MeV), $_\Lambda Li^8$ and $_\Lambda Be^8 (\bar{B}_\Lambda = 6.50 \pm 0.25$ MeV), $_\Lambda Li^9 (B_\Lambda = 8.0 \pm 0.3$ MeV), and $_\Lambda B^{12} (B_\Lambda = 10.5 \pm 0.2$ MeV). The comparison with the expression (8) is given in Table 2. In the $_\Lambda Be^7 - _\Lambda Li^7$ comparison, it is clear that $\Delta B_\Lambda = \langle \Delta \rangle$ cannot exceed 0.9(± 0.1) MeV, otherwise $_\Lambda Be^7$ would not be particle-stable. The value expected for $\langle \Delta \rangle$ on the basis of our knowledge of the Λ-N s-wave potentials is about 0.85 MeV, not incompatible with this value for A = 7, especially when the mean wave-function assumed in (8) is replaced by the more diffuse wave-function appropriate to the low B_Λ values for these systems. On the other hand, the large difference $\Delta B_\Lambda = 1.5$ MeV between $_\Lambda Be^9$ and $_\Lambda Li^9$ requires a correspondingly large value for $\langle \Delta \rangle$, not really consistent with this estimate for $\langle \Delta \rangle$. Indeed, the values of $\langle \Delta \rangle$ given in Table 2 show a

steady increase as N_p increases through the p-shell, roughly in proportion with N_p. The reason for this behaviour of the B_Λ values is not yet known. Possibly it reflects the inadequacies of the approximations made in the derivation of the expression (8), or perhaps it reflects properties of the Λ-N forces (for example, the effect of a spin-orbit term) which have not yet been taken into account here.

At this point, accurate and reliable B_Λ values for further hypernuclear species in this p-shell region would be of great interest, to explore further the dependence of B_Λ on the spin and structure of the core nucleus. In order for such events to represent a useful addition to the present data, it is essential that they allow a unique and reliable identification of the species, either from analysis of its production process or from its decay process, or both.

II. THE DECAY INTERACTIONS OF THE Λ PARTICLE

1. The mesic decay processes

It is well known that, owing to the low momentum (100 MeV/c) of the proton resulting from Λ decay at rest, the rate of π^- decay of a Λ particle in nuclear matter is generally reduced as a result of the Pauli principle, since a large fraction of the final states which can be reached by the final proton are already occupied. This effect is already quite large in ${}_\Lambda He^5$, where the π^- decay rate is reduced by a factor of about 0.37; in ${}_\Lambda C^{13}$, the calculated reduction factor is about 0.14.

It is perhaps less well known that in the lightest hypernuclei, the effect of the Pauli principle can lead to an enhancement of the decay rate in suitable circumstances, namely if the spin configuration and the decay interaction are such that the final proton is necessarily emitted into a final state which satisfies the symmetry requirements of the Pauli principle. For example, in ${}_\Lambda H^4 \rightarrow \pi^- + He^4$ decay with J = 0 for

$_{\Lambda}H^4$, the s-interaction for Λ decay is spin-independent, so that the final proton is necessarily s-wave and in the spin configuration appropriate to He^4, and the decay rate for this transition is enhanced by almost a factor 2 (the space wave-functions do not overlap precisely) as a result of the antisymmetrization appropriate for a final state with two protons.

These same effects hold also for the π^0 decay modes, of course. Thus, with J = 0 for $_{\Lambda}He^4$, the rate for π^0 decay through the s_0 interaction is enhanced, whereas the rate for π^0 decay through the p_0 interaction is strongly suppressed; the rate for π^- decay of $_{\Lambda}He^4$ is also strongly suppressed, by a factor about 0.35, since there are already two s-wave protons present in the initial state. Hence the π^0/π^- ratio in $_{\Lambda}He^4$ decay is strongly sensitive to the p_0/s_0 ratio in $\Lambda \to n + \pi^0$ decay. For free Λ decay, the π^0/π^- ratio is very close to 0.5; for $_{\Lambda}He^4$ decay Block et al.[16] have observed the π^0/π^- ratio to be 2.0 ± 0.3. From this striking result, Block et al. have been able to deduce that the π^0 mode of Λ decay is dominantly through the s_0-channel, with $p_0^2/(p_0^2 + s_0^2) = 0.23 \pm 0.16$, in agreement with expectation (0.12 ± 0.03) from the $\Delta I = \frac{1}{2}$ rule.

2. The non-mesic de-excitation of the Λ particle

For bound Λ particles, the presence of nucleons allows the weak interactions

$$\Lambda + p \to n + p \qquad (10a)$$

$$\Lambda + n \to n + n \qquad (10b)$$

to become effective, releasing the full energy difference of about 176 MeV between the Λ particle and nucleon. This weak interaction can scarcely be investigated without appeal to studies of Λ-hypernuclear decay, and rather little is known of its detailed properties at this time.

These processes (10) represent the only strangeness-changing weak interaction which is readily accessible to observation and which involves four strongly-interacting fermions*). With our present views on the nature of weak interactions, it is natural to expect the existence of a primary four-fermion interaction (10a). The validity of the $\Delta I = \frac{1}{2}$ rule for strangeness-changing weak interactions then requires also the existence of a primary interaction of the form (10b), although there is no direct evidence for a neutral weak interaction current (in fact, there is very strong evidence against neutral leptonic currents of strength comparable with the charged currents for leptons). In this view, it is natural to regard the $\Lambda \to N + \pi$ decay interactions as secondary in character since they can occur as a consequence of these four-fermion interactions; this connection is illustrated explicitly in Fig. 1, which depicts one sequence of processes by which the interaction (10a) can give rise to $\Lambda \to p + \pi^-$ decay. Since this four-fermion interaction involves four strongly-interacting particles, mesonic corrections may be expected to distort the form of the interaction quite strongly from the (V-A) form which the current-current theory would predict. This is illustrated in Fig. 2, which shows a series of processes contributing to the physically-observed interaction (10a). The terms (a) and (b) show the primary interactions (10a) derived from the charged and neutral currents, in turn, the vertices shown being distorted from their primary forms by the usual vertex corrections. The remaining graphs (c) - (f) show corrections which involve the exchange of various mesonic systems between the strangeness-changing and strangeness-conserving currents; the relation between these graphs and the primary interaction may be seen by analysing each ($\Lambda \to N +$ meson) vertex in the manner of Fig. 1. The terms (c) and (d) are well known, from their discussion by Karplus and Ruderman[24]) who recognized the importance of their contribution if the Λ spin were large and used its comparison with the experimental data to argue against

*) The strangeness-conserving weak interaction $n + p \to n + p$ is expected to exist if the current-current hypothesis of Feynman and Gell-Mann [Phys.Rev. 109, 193 (1958)] holds valid. This weak interaction is expected to produce parity-violating effects of very small amplitude in nuclear forces and the properties of nuclear states, some of which have been quantitatively estimated by Blin-Stoyle and co-workers.

the possibility of spin $\geq 3/2$ for the Λ particle. Now that $j_\Lambda = 1/2$ is well established and the $\Lambda \to N + \pi$ interaction is known to be dominantly s-wave, there is no reason to believe that these Karplus-Ruderman terms contribute dominantly to the observed process $\Lambda + N \to N + N$; these terms must be taken together with a large number of other mesonic correction terms, of which several are given explicitly in Fig. 2.

Rather little is known at present concerning the properties of this weak interaction:

$$\Lambda + N \to N + N . \tag{11}$$

The simplest properties of interest are its <u>charge-dependence</u> and its <u>spin-dependence</u>. For bound Λ particles this interaction will dominantly occur for ΛN s-states, in view of the relatively low Λ-N relative momenta to be expected in hypernuclei. The final nucleon momentum for ΛN de-excitation at rest is about $q = 400$ MeV/c, so we shall simplify the discussion by using the non-relativistic form for the matrix-elements. For Λp capture from an s-state configuration the general form of the matrix-element is

$$\begin{aligned} M(\Lambda p \to np) = {} & a_p P_o + b_p P_1 + \frac{3}{\sqrt{8}}\, c_p (\underline{\sigma}_Y \cdot \underline{q}\,\underline{\sigma}_N \cdot \underline{q} - \tfrac{1}{3}\underline{\sigma}_Y \cdot \underline{\sigma}_N q^2)/M^2 \\ & + \sqrt{\frac{3}{8}}\, d_p (\underline{\sigma}_Y + \underline{\sigma}_N) \cdot \underline{q}/M + e_p (\underline{\sigma}_Y - \underline{\sigma}_N) \cdot \underline{q} P_o/2M \\ & + \sqrt{3}\, f_p (\underline{\sigma}_Y - \underline{\sigma}_N) \cdot \underline{q} P_1/M , \end{aligned} \tag{12}$$

where $P_o = (3 + \underline{\sigma}_Y \cdot \underline{\sigma}_N)/4$ and $P_1 = (1 - \underline{\sigma}_Y \cdot \underline{\sigma}_N)/4$ denote the singlet and triplet spin projection operators, $\underline{\sigma}_Y$ denotes the Λ or n spin and $\underline{\sigma}_N$ here denotes the proton spin. In this expression the terms a_p and e_p denote the $^1S_0$ transition amplitudes leading to the $^1S_0$ and $^3P_0$ final states, respectively, and the terms b_p, c_p, d_p and f_p denote the $^3S_1$ transition amplitudes leading to the $^3S_1, ^3D_1, ^3P_1$ and $^1P_1$ final states. For Λn capture the corresponding form is

$$M(\Lambda n \to nn) = a_n P_o + \sqrt{\frac{3}{8}}\, d_n (\underline{\sigma}_Y + \underline{\sigma}_N) \cdot \underline{q}/M + e_n (\underline{\sigma}_Y - \underline{\sigma}_N) \cdot \underline{q} P_o/2M \tag{13}$$

where $\underline{\sigma}_Y$ here denotes the spin of the Λ particle and either of the final neutrons and $\underline{\sigma}_N$ denotes the spin of the other neutron. Terms of the form b, c and f are absent here, as they lead to final states which are forbidden for the n-n system. If the $\Delta I = \frac{1}{2}$ rule holds then we have in addition the following equalities:

$$a_n = \sqrt{2}\, a_p, \quad d_n = \sqrt{2}\, d_p, \quad e_n = \sqrt{2}\, e_p . \tag{14}$$

We note that the transitions a, b and c conserve parity, whereas the transitions d, e and f reverse the parity of the state. If time-reversal invariance holds then the phases of each of these amplitudes may be determined from the known NN scattering phases by the use of Watson's theorem. Obviously the determination of all these parameters, and the test of the equalities (14), will require polarization experiments involving the measurement of the longitudinal polarization of the fast n and p emitted from unpolarized hypernuclei (or the angular distribution of the fast nucleons from non-mesic decay of polarized hypernuclei), and of the polarization correlation coefficients for the fast (np) and (nn) pairs emitted in non-mesic decay of hypernuclei. These polarization coefficients could also be measured for initial ΛN states of definite spin by selecting the appropriate light hypernuclei (cf. below). Such experiments will be difficult to carry out and to interpret and lie far in the future.

In principle, for the calculation of non-mesic decay rates for hypernuclei, matrix-elements of the forms (12) and (13) should be used for each of the nucleons and evaluated between the initial hypernuclear wave-function and the final nuclear states. Here, we shall consider instead a simplified calculation for the non-mesic decay rates which treats the Λ de-excitation by different nucleons as incoherent. This approximation is not strictly valid, because, owing to the identity of the neutrons and of the protons, the same final state can generally be reached through capture on any one of the nucleons; however, because of the large energy release, it is rather likely that these interference effects will generally be small and will tend to cancel out in the total de-excitation rates, summed over all final states.

Let us denote by R_{NS} the $\Lambda N \to NN$ transition rate, when the ΛN system is in an s-state of total spin S, for unit density of nucleons of type N at the Λ position. The non-mesic decay rate for a given hypernucleus is then given by the expression

$$R_{n.m.} = \bar{R}({}_{\Lambda}Z^{A+1})\ \rho_A\,,$$

$$= \bar{R}({}_{\Lambda}Z^{A+1})\ A \int \psi_\Lambda^2\ \rho_N(\underline{r})\, d_3 r\,, \qquad (15)$$

where ρ_A is the mean density of nucleons at the Λ position, $\rho_N(\underline{r})$ being the nucleon density at position $\underline{r}$ and ψ_Λ the wave-function for the Λ nucleus relative motion and $\bar{R}$ is the spin and charge average of the R_{NS} which is appropriate to the hypernucleus considered. In terms of the amplitudes (12) and (13), these quantities R_{NS} are given by

$$R_{p0} = |a_p|^2 + |e_p|^2 (q/M)^2\,, \qquad (16a)$$

$$R_{p1} = |b_p|^2 + |c_p|^2 (q/m)^4 + |d_p|^2 (q/M)^2 + |f_p|^2 (q/M)^2\,, \qquad (16b)$$

$$R_{n0} = [|a_n|^2 + |e_n|^2 (q/M)^2]\,, \qquad (16c)$$

$$R_{n1} = |d_n|^2 (q/M)^2\,. \qquad (16d)$$

In the last expressions R_{nS}, we have taken into account the symmetry requirements of the final state and the identity of the two final neutrons. If the $\Delta I = \frac{1}{2}$ rule holds, the equalities (14) lead to the predictions

$$R_{p0} = \tfrac{1}{2} R_{n0}\,, \qquad (17a)$$

$$R_{p1} \geq \tfrac{1}{2} R_{n1}\,. \qquad (17b)$$

The quantity most readily measured is the ratio Q = (non-mesic/π^--mesic). Here, we shall not include π^0- mesonic decay events[25] among the non-mesic decay rate, for the π^0-mesonic events normally give an exceedingly small star with a visible energy release of at most several

MeV and would very frequently be overlooked, whereas the non-mesic decay events involve a large energy release. For $_{\Lambda}He$ hypernuclei in emulsion, estimates of this ratio have been reported as follows: $Q = 2.3 \pm 1.0$ by Fry[17], $1.5(\pm 0.4) \leq Q \leq 2.8$ by Silverstein[18] and $Q \geq 1.1 \pm 0.5$ by Schlein[19], whose non-mesic decay rate includes only two-prong events. For $_{\Lambda}He^4$, Block et al.[16] have obtained a rather accurate value, $Q = 0.52 \pm 0.10$. About 80% of the π^- decays of $_{\Lambda}He$ in emulsion are due to $_{\Lambda}He^5$ decay; adopting the value $Q = 1.5$ for $_{\Lambda}He$, the correction for admixture of $_{\Lambda}He^4$ non-mesic decay events leads to the estimate $Q = 1.8$ for $_{\Lambda}He^5$. On this basis, it is then possible to estimate Q for some of the heavier hypernuclei. This involves an estimate of $R_{n.m.}$ from Eq. (15), using the value $\rho_4 = 0.038\ f^{-3}$ for $_{\Lambda}He^5$ and corresponding calculated values ρ_A for the hypernuclei of interest, together with an estimate of the π^- decay rate $R(\pi^-)$ using the completeness-relation method[20]. For example, for $_{\Lambda}He^5$, the calculated value of $R(\pi^-)$ is $0.25\ \Gamma_\Lambda$, where $1/\Gamma_\Lambda$ denotes the free Λ lifetime, so that our estimate of Q and the above value for ρ_4 lead to the estimate

$$\begin{aligned} \bar{R}(_{\Lambda}He^5) &= \tfrac{1}{8}(3R_{pl} + R_{po} + 3R_n + R_{no}) \\ &= (1.8)\ (0.25)\ \Gamma_\Lambda/(0.038) = 12(\pm 3)\ \Gamma_\Lambda, \end{aligned} \tag{18}$$

where the error quoted represents only the statistical uncertainty on Q. With this value for $\bar{R}$, estimates have been made for Q for $_{\Lambda}Li^7$ (neglecting the spin-dependence of R_{NS}), $_{\Lambda}Be^9$ and $_{\Lambda}C^{13}$, as given in Table 3. The rapid rise in Q with increasing A is due primarily to the rapidly increasing suppression of the π^- decay process by the Pauli principle. However, the non-mesic decay rate does increase from $0.45\ \Gamma_\Lambda$ for $_{\Lambda}He^5$, through $1.5\ \Gamma_\Lambda$ for $_{\Lambda}C^{13}$, to a value of $2.0\ \Gamma_\Lambda$ for a very heavy hypernucleus (say $A \approx 100$). Several independent estimates of $R(\pi^-)$ we have made for a hypernucleus of mass number $A \approx 100$, including pion re-absorption effects, lead to values about $0.015\ \Gamma_\Lambda$, and therefore to a large value $Q \approx 130$. We conclude that the decay lifetime of a heavy hypernucleus ($A \approx 100$) may be expected to be essentially independent of A, with the value $\approx 1.2 \times 10^{-10}$ sec.

The evidence on the charge dependence of the non-mesic process appears somewhat contradictory at first sight. For ${}_{\Lambda}He^4$, Block et al.[16] have classified non-mesic decay events with a recoil proton of momentum exceeding 250 MeV/c as due to Λp capture, leading to the estimate $(\Lambda p)/(\Lambda n) = 2.2 \pm 0.8$. Since ${}_{\Lambda}He^4$ has J = 0, this corresponds to the ratio

$$\frac{(3R_{p1} + R_{po})/2}{R_{no}} = 2.2(\pm\ 0.8)\,. \qquad (19)$$

On the other hand, for spallation hyperfragments following high-energy K^- interactions in emulsion, for which typically $A \approx 70$, Beniston[21] and Lagnaux[22] have compared the observed proton spectrum with those predicted by a Monte Carlo calculation for (Λp) and (Λn) capture processes, and have concluded that, in these heavy hypernuclei, the (Λn) capture process is the dominant non-mesic decay process. The ratio $(\Lambda n)/[(\Lambda n) + (\Lambda p)]$ obtained by Beniston was $\gamma = 0.8 \pm 0.1$, and by Lagnaux $\gamma = 0.65 \pm 0.1$, the difference between these values being due, at least in part, to the differing assumptions made about the spatial distribution of the Λ particle. To continue, we shall adopt the value $\gamma = 0.7$, so that

$$\frac{3R_{p1} + R_{po}}{3R_{n1} + R_{no}} = \left(\frac{1}{\gamma} - 1\right) \approx 0.4\,. \qquad (20)$$

From this ratio and the value of Eq. (19), we can conclude the value $3R_{n1} + R_{no} = 69(\pm\ 20)\ \Gamma_{\Lambda}$ to be used below. The striking difference between the $(\Lambda p)/(\Lambda n)$ ratios observed for ${}_{\Lambda}He^4$ and for heavy hypernuclei can be understood quite simply if the (Λn) de-excitation process has a strong spin-dependence, with

$$R_{no}/R_{n1} \approx 0.3\,, \qquad (21)$$

the non-mesic (Λn) decay interaction being significantly weaker in the singlet configuration.

The remaining information to be discussed consists of the non-mesic rates for ${}_{\Lambda}He^4$ and ${}_{\Lambda}H^4$, for which the nucleon density ρ_3 is 0.019 f^{-3}.

For ${}_{\Lambda}He^4$, the calculated suppression[20] of $R(\pi^-)$ to 0.26 Γ_Λ, and the above value $Q = 0.52 \pm 0.10$, lead to

$$3R_{p1} + R_{po} + 2R_{no} = 41(\pm 10)\ \Gamma_\Lambda . \qquad (22)$$

From Eqs. (18), (21) and (22) we conclude that $R_{n1} = 21(\pm 7)\ \Gamma_\Lambda$, $R_{no} = 6(\pm 2)\ \Gamma_\Lambda$ and $(3R_{p1} + R_{po}) = 28(\pm 8)\ \Gamma_\Lambda$. For ${}_{\Lambda}H^4$, the π^- decay rate $R(\pi^-)$ has been calculated[20] to be 0.74 Γ_Λ, and the non-mesic rate is given by

$$0.31(\pm 0.06) \geq (0.019)\ (R_{po} + 3R_{n1} + R_{no})/6 \geq 0.22(\pm 0.06), \qquad (23)$$

using the above values for $(3R_{n1} + R_{no})$ and the requirement $0 \leq R_{po} \leq 28(\pm 8)\ \Gamma_\Lambda$. On this basis, the ratio Q for ${}_{\Lambda}H^4$ is expected to lie between 0.29(± 0.08) and 0.42(± 0.08). In the experiment of Block et al.[16], 120(± 11) ${}_{\Lambda}H^4 \to \pi^-$ events were seen. From the number of ${}_{\Lambda}He^4$ production events and from charge independence, it was concluded that the total number of ${}_{\Lambda}H^4$ production events was 163 ± 10. From the π^0/π^- ratio (2.5 ± 0.5) observed for ${}_{\Lambda}He^4$ decay, and from the prediction of the $\Delta I = \frac{1}{2}$ rule that[20]

$$\frac{\pi^0}{\pi^-}\ ({}_{\Lambda}He^4) \times \frac{\pi^0}{\pi^-}\ ({}_{\Lambda}H^4) = \frac{1}{4}, \qquad (24)$$

we may estimate the number of ${}_{\Lambda}H^4 \to \pi^0$ events as 12 ± 1. The remainder of the events, amounting to 31 ± 15, must be attributed to non-mesic decay processes; this leads to the ratio $Q = 0.26 \pm 0.13$, which is not at all in disagreement with the value predicted above.

This small fraction of ${}_{\Lambda}H^4$ decay events which proceed through the non-mesic mode may not be easy to identify in the helium bubble chamber experiment, especially because of the confusion possible with slow Σ^- hyperons following $K^- - He^4$ capture which come to rest and interact to give

a one-prong star. If we assume [for lack of other knowledge*)] that the Λp capture interaction is spin independent, i.e. $R_{po} = R_{p1}$, then R_{po} has the value 7(± 2) Γ_Λ and the (Λp)/(Λn) ratio predicted for $_\Lambda H^4$ has the value $2R_{po}/(3R_{n1} + R_{no}) = 14(\pm 2)/69\ (\pm 20) = 0.2(\pm 0.06)$, so that only six non-mesic $_\Lambda H^4$ decay events are expected to occur with a fast proton (say ≳ 250 MeV/c) in the experiment of Block et al.[16]. However, the majority of the (Λn) capture events are expected to give a visible prong. Some indication on this can be obtained from the $\pi^- + He^4$ interaction studies of Bortolani et al.[23], which also proceeds through two-nucleon emission with a comparable energy release (≈ 140 MeV). Of 356 π^- interactions at rest in a helium chamber, only 23 gave no visible track; since the primary capture interaction $\pi^- + p + n \to n + n$ is believed to account for at least ¾ of these capture events (the remainder being due to the $\pi^- + p + p \to n + p$ interaction), we may estimate**) that not more than 9% of the (Λn) de-excitation events for $_\Lambda H^4$ will give no visible track. Although the separation of the $_\Lambda H^4$ non-mesic decay events is a difficult task, a value of the (Λp)/(π^--mesic) ratio for $_\Lambda H^4$, or even an upper limit on this would be very valuable in providing a limit on R_{po}, and therefore a direct indication of the spin dependence for the (Λp) de-excitation process.

---

*) With the $\Delta I = \frac{1}{2}$ rule for the ΛN → NN process, the value $R_{no} = 6(\pm 2)\ \Gamma_\Lambda$ and Eq. (17a) would require $R_{po} = 3.0(\pm 1.0\ \Gamma_\Lambda)$, an appreciably smaller value than that assumed here. With this value the (Λp)/(Λn) ratio for $_\Lambda H^4$ would be 0.08(± 0.04), which would predict only two non-mesic $_\Lambda H^4$ with a fast proton in this experiment. We may note here that these spin-dependences for the Λn and Λp processes are quite at variance with a simple (V-A) form for the ΛN → NN interaction; in the non-relativistic limit, the first term (a_0) of (5.4) would be dominant, and the ratio R_{po}/R_{p1} would be predicted to be exceedingly large.

**) We should emphasize here that the Λn → nn interaction may have quite different spin dependence from the $\pi^- pn \to nn$ interaction, in which case this proportion might well turn out to be larger than this estimate. For example, H^3 production is found to occur in 22% of $\pi^- - He^4$ capture events; this appears to be a particular feature of the ($\pi^- pn$) and ($\pi^- pp$) capture amplitudes. There is certainly no reason to expect the (Λn) and (Λp) capture amplitudes to have a similar spin and charge dependence, and it is quite unlikely that the mode $H^3 + n$ will prove to be as abundant in $_\Lambda H^4$ non-mesic decay.

5666/NP/smg

REFERENCES

1. J. de Swart and C. Iddings, Phys.Rev. 128, 2810 (1962); Phys.Rev. 130, 319 (1963).

2. B. Downs, D. Smith and T. Truong, Phys.Rev. 129, 2730 (1963); also private communications (1963).

3. B. Downs and R. Dalitz, Phys.Rev. 114, 593 (1959).

4. D. Muller, Untersuchunger zum Dreikorperproblem der Kernphysik, (Heidelberg, 1962).

5. R. Dalitz and B. Downs, Phys.Rev. 111, 967 (1958).

6. K. Dietrich, R. Folk and H. Mang, Proc.Rutherford Jubilee Int.Conf. (Heywood, London, 1961), p. 165.

7. U. Gutsch, University of Frankfurt (private communication, 1963).

8. H. Mang and W. Wild. Z.Phys. 154, 182 (1959).

9. M. Danysz, K. Garbowska, J. Pniewski, T. Pniewski, J. Zakrewski, E. Fletcher, J. Lemonne, P. Renard, J. Sacton, D. O'Sullivan, L.P. Shah, A. Thompson, P. Allen, Sr. M. Heeran, A. Montwill, J.E. Allen, M.J. Beniston, D.H. Davis, D.A. Garbutt, V.A. Bull, R.C. Kumar and P.V. March, Phys.Rev.Letters, to be published (1963).

10. R.H. Dalitz, Phys.Letters, to be published (1963).

11. R.D. Lawson and M. Rotenberg, Nuovo Cimento 17, 449 (1960).

12. S. Iwao, Nuovo Cimento 17, 491 (1961).

13. R.H. Dalitz and J. Soper, report in preparation (1963).

14. R.H. Dalitz, Nucl.Phys. 41, 78 (1963).

15. R.H. Dalitz, Proc.Rutherford Jubilee Int.Conf. (Heywood, London, 1962), p. 103.

16. M.M. Block, R. Gessaroli, J. Kopelman, S. Ratti, M. Schneeberger, L. Grimellini, T. Kikuchi, L. Lendinara, L. Monari, W. Becker and E. Harth, Hyperfragment studies in the helium bubble chamber, Proc.Int.Con.on Hyperfragments (CERN, 1963).

17. W.F. Fry, Ann.Revs.Nucl.Sci.

5666/NP/smg

18. E. Silverstein, Suppl.Nuovo Cimento 10, 41 (1959).

19. P. Schlein, Phys.Rev.Letters 2, 220 (1959).

20. R.H. Dalitz and L.S. Liu, Phys.Rev. 116, 1312 (1959).

21. M.J. Beniston, University of Chicago, private communication (1963).

22. J.P. Lagnaux, Université Libre de Bruxelles, Brussels (1963).

23. M.V. Bortolani, L. Lendinara and L. Monari, Nuovo Cimento 25, 603 (1962).

24. M. Ruderman and R. Karplus, Phys.Rev. 76, 1458 (1949); see also F. Cerulus, Nuovo Cimento 5, 1685 (1957) and R.H. Dalitz, Rev.Mod.Phys. 31, 823 (1959).

25. R. Ammar, Nuovo Cimento 14, 1226 (1959).

* * *

5666/NP/smg

Table 1

Hard core radius d	d = 0.0 f (Gaussian shape)	d = 0.2 f (square well)	d = 0.4 f (square well)
a_0 (f)	$-2.4^{+1.2}_{-0.6}$	$-4.2^{+3.0}_{-1.3}$	-4.5
a_1 (f)	-0.5 ± 0.1	-0.55 ± 0.05	-0.6
Notes	obtained from ΛH^3 and ΛHe^5 (Refs. 3,5)	obtained from ΛH^4 and ΛHe^5 (Ref. 6)	obtained from ΛH^4 and ΛHe^5 (Ref. 7)
Existence of J = 1 excited state ΛH^{4*}?	$B_\Lambda^* \approx 1.3$ MeV ($s^* = 1.25$)	Not bound ($s^* = 0.90$)	Not bound ($s^* = 0.83$)

Table 2

Hypernuclei compared	ΔB_Λ (MeV)	Estimate from Eq. (8)†	Value of $\langle\Delta\rangle$
$_\Lambda Be^7 - {}_\Lambda Li^7$	0.6 ± 0.5 (≤ 0.9)	$0.98 \langle\Delta\rangle$	$\langle\Delta\rangle = 0.6 \pm 0.5$ MeV
$_\Lambda Be^8 - {}_\Lambda Be^9$	0.0 ± 0.3	$0.59 \langle\Delta\rangle - \langle\bar{V}\rangle$	$\langle\Delta\rangle = 1.5 \pm 0.5$ MeV
$_\Lambda Be^9 - {}_\Lambda Li^9$	1.50 ± 0.3	$0.70 \langle\Delta\rangle$	$\langle\Delta\rangle = 2.1 \pm 0.4$ MeV
$_\Lambda B^{12} - {}_\Lambda C^{13}$	-0.10 ± 0.4	$0.28 \langle\Delta\rangle - \langle\bar{V}\rangle$	$\langle\Delta\rangle = 2.7 \pm 1.3$ MeV

†) The coefficients α_N used here are those computed from intermediate coupling nuclear wave-functions constructed by J. Soper.

Table 3

$Q = (\text{non-mesic})/(\pi^-\text{-mesic})$

Hypernucleus	${}_{\Lambda}H^4$	${}_{\Lambda}He^4$	${}_{\Lambda}He^5$	${}_{\Lambda}Li^7$	${}_{\Lambda}Be^9$	${}_{\Lambda}C^{13}$	${}_{\Lambda}Ag^{109}$
Q =	0.15	0.5	1.8	2.7	6.2	11.3	130

The underlined entries represent the empirical values for Q; the other entries are calculated values based on the entry for ${}_{\Lambda}He^5$.

DISCUSSION

Zakrzewski : Could you tell us a little more about these calculations of Beniston, in particular what sort of nuclei have been calculated for? Has he taken into account any secondary processes which may occur?

Dalitz : The calculations use the Monte Carlo method and take into account secondary collision processes using standard cross-sections. The nuclei that were considered here are the residual hyperfragment left after fast K^- interactions, so that they have 'Z' around 30 to 40. All the data used for comparison comes from these fast K^- interactions. These calculations do depend a little bit on the form used for the nucleon momentum distribution in the nucleus. However, the general conclusion that there are too few fast protons for equal Λn and Λp stimulation seems to remain unchanged whatever assumption you make about the spectrum.

Zakrzewski : Has he made any comparison with the experimental data?

Dalitz : The number $(\Lambda n)/(\Lambda p) = 4$ was derived from comparison with the experiment. This is a preliminary number but Beniston has made calculations on a number of different assumptions and always comes out with a value of about four and so that is what I have written down here. I do not know what other values people have obtained in other experiments and I would be interested if anyone has any comment on this ratio.

Renard : In Brussels also such a Monte Carlo calculation has been done with a Fermi gas model and it seems that this value is lower than four and stands somewhere between one and two.

Dalitz : It would be interesting to compare your Monte Carlo calculation in detail with that of Beniston for I am not clear what the reasons for the difference are likely to be. Reducing the

Dalitz (cont.) : value of $(\Lambda n)/(\Lambda p)$ does not change very much in my discussion except that if I reduce this ratio by a factor of two, then I will not necessarily disagree with Block any more about the ${}_{\Lambda}H^{4}$ non-mesic rate.

Pniewski : Could you say anything about the ratio of the non-mesonic to mesonic decay for the double hyperfragment; I mean for the second Λ^{o} in the double hyperfragment. It should probably be different.

Dalitz : I do not think it should differ very much from that for a single Λ particle and the same core nucleus. Essentially the point is that each Λ^{o} particle decays independently of the other Λ^{o} particle. The wave function of the first is not very much different from the wave function of the other Λ particle. Take ${}_{\Lambda\Lambda}B^{10}$ for example. The wave function of each Λ particle in this system is not very much different from the wave function of the Λ particle in ${}_{\Lambda}Be^{9}$ system. So the non-mesonic and mesonic rates are going to be rather comparable with the situation for ${}_{\Lambda}Be^{9}$. If anything, I would expect that the Λ wave functions in ${}_{\Lambda\Lambda}Be^{10}$ might be somewhat more compact than the Λ wave function for ${}_{\Lambda}Be^{9}$, owing to the higher binding per Λ particle. This would mean that the non-mesic rate would be increased a little and the mesic decay rate decreased a little, so that the ratio non-mesic/(π^{-}-mesic) would be a little greater in ${}_{\Lambda\Lambda}Be^{10}$ than for ${}_{\Lambda}Be^{9}$.

Zakrzewski : I would like to make one remark with respect to the determination of the non-mesonic to mesonic ratio for heavy hyperfragments, namely the problem of biases in identification. This is a very serious problem and the losses may be such that they just enhance some kinds of decay and if you use this sample of decays to determine this ratio, you can come to quite different results depending on the type of selection criterion you have accepted.

Dalitz : In the selection criterion used here only hyperfragments which give moderately energetic protons (energy greater than 20 MeV) are used. Beniston's considerations are based only on the form of the spectrum for the fastest proton and so I am not clear how the bias will affect his arguments.

Levi-Setti : I would like to add at this point some information about the calculation of Beniston. It is a Monte Carlo calculation for 2,000 events induced by proton stimulation and for about 4,000 events induced by neutron stimulation. The energy spectra of the protons emitted are remarkably different. The comparison with the experimental data is then made for proton energies above 30 MeV. The average Z and A has been taken as 34 and 79; however, other test runs have been done for a certain range of mass values without changing too much the results. Also B was assumed to be 25 MeV and the calculations have been done for various values of the nucleon radius r_0 (1.25 to 1.4 f). The likelihood function has been built for the fit. The likelihood function shows a very sharp peak for a fraction of neutron stimulation of about 0.78. The peak is full from a rapid drop to 0, so that at least all neutron stimulation is certainly excluded by many standard deviations. For the other details about the calculation of internuclear cascade, I think that the method followed is very similar to the one which has been used by Metropolis and collaborators in an analogous Monte Carlo calculation for protons in the several hundred MeV region and also for π^- capture.

Hoogland : What would be the effect on the calculation of the $(\Lambda n)/(\Lambda p)$ ratio in the case of heavy hyperfragments if α particle clusters were assumed to exist in the nucleus?

Dalitz : First, as far as the calculation is concerned you have to modify the momentum spectrum which you use for the nucleons. I think both the Chicago and Brussels calculations have simply used Fermi gas distributions. Now it is true that the clusters give a momentum distribution with a fairly long tail and I think that this is required anyway from what one knows experimentally about the momentum spectrum in a nucleus. What this change would do to these Monte Carlo calculations, I cannot estimate off-hand, but I think this is a point which is rather desirable to look into because higher momenta for the capturing nucleon would in fact give a greater spread in the proton spectrum and this would already act in a direction to reduce the number of faster protons. However, I do not really think this would affect the comparison with experiment very strongly. It would probably act in the direction of reducing the ratio from four but how far I do not know.

* * *

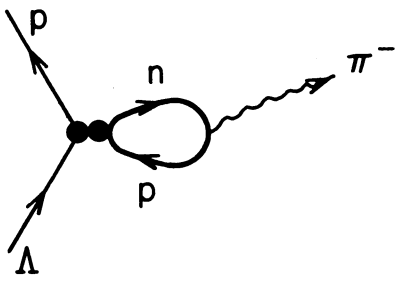

Fig. 1. The Decay $\Lambda \rightarrow p + \pi^-$ as a consequence of the Four-fermion Weak Interaction. (5.1a)

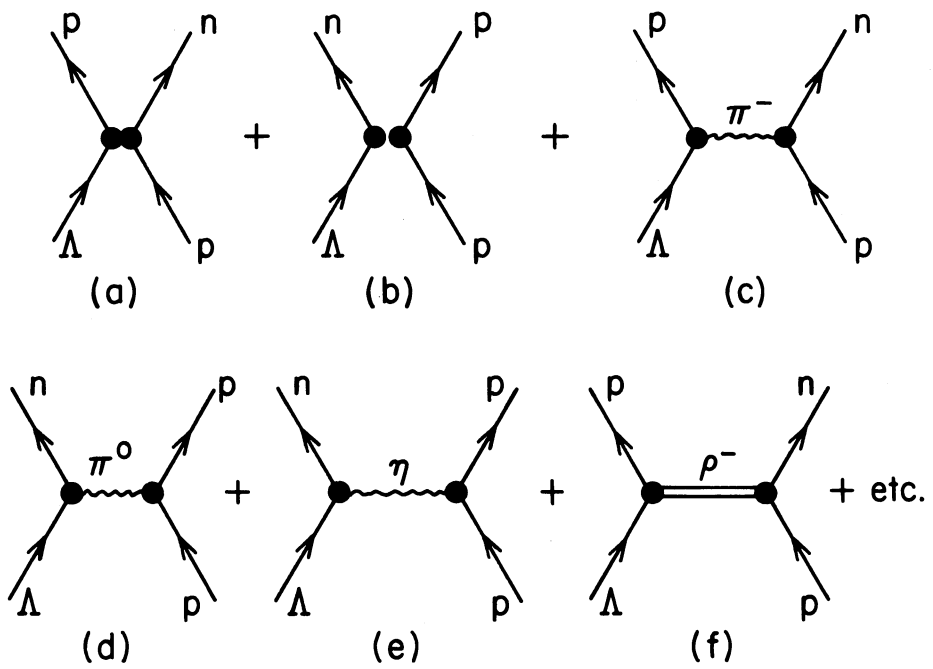

Fig. 2. Contributions to the Process $\Lambda + p \rightarrow n + p$.

HYPERNUCLEI*)

PART V.2

R. Levi-Setti,
Enrico Fermi Institute, University of Chicago.

I. BASIC DEFINITIONS AND NOMENCLATURE

Λ hypernucleus: a hyperon bound to a nuclear core

$$(\Lambda + H^2) \rightarrow {}_{\Lambda}H^3$$

$$(\Lambda + H^3) \rightarrow {}_{\Lambda}H^4 \text{, etc.}$$

The nuclear core need not be a stable nucleus; examples of hypernuclei in which the core in its ground state is a nuclear resonant state are e.g. $(\Lambda + Be^8) \rightarrow {}_{\Lambda}Be^9$, where ordinary Be^8 would disintegrate $Be^{8*} \rightarrow 2He^4 + 0.1$ MeV. Occasionally the Λ-nucleon attraction provides sufficient binding to form hypernuclei out of a completely unbound core, e.g. $(\Lambda + Be^6) \rightarrow {}_{\Lambda}Be^7$ where ordinarily $Be^{6*} \rightarrow 2p + He^4 + 1.4$ MeV.

The Λ-binding energy B_Λ is defined as usual from

$$ {}_{\Lambda}(A,Z) = (A-1,Z) + \Lambda - B_\Lambda \qquad (1)$$

and can be measured, since ${}_{\Lambda}(A,Z) \rightarrow \Sigma_{ij}(A_i,Z_j) + Q$

$$B_\Lambda = Q_o - Q, \text{ where } Q_o = (A-1,Z) + \Lambda - \Sigma_{ij}(A_i,Z_j). \qquad (2)$$

Hypernuclear disintegrations in which $\Lambda \rightarrow \begin{matrix}\pi^- + p \\ \pi^o + n\end{matrix}$ are called <u>mesonic</u> decays; those where $\Lambda + n,p \rightarrow n + n,p$ are called <u>non-mesonic</u> decays. Common abbreviations for decay modes are

$(\pi - r)$ e.g. ${}_{\Lambda}H^3 \rightarrow \pi^- + He^3$, ${}_{\Lambda}Li^7 \rightarrow \pi^- + Be^7$, etc.,

$(\pi - p - r)$ e.g. ${}_{\Lambda}He^5 \rightarrow \pi^- + p + He^4$, etc.,

$(\pi - n - r)$ e.g. ${}_{\Lambda}H^4 \rightarrow \pi^- + n + He^3$, ${}_{\Lambda}Li^9 \rightarrow \pi^- + n + Be^8$, etc.

---

*) This paper was also presented at the Hyperfragment Conference.

Note that Q_0 for (π,p,r) decays is always $Q_\Lambda = 37.58$ MeV. B_Λ can be measured best from mesonic or mesic decays in view of the low energy release, usually in the range 25 - 55 MeV. For non-mesic decays $Q \approx 176 \text{ MeV} - B_\Lambda$.

II. OBSERVATION AND IDENTIFICATION OF HYPERNUCLEI

Although hyperfragments can originate any time a Λ is created within a nucleus, and therefore from reactions such as

$$\pi^- + p \rightarrow \Lambda + K^o, \quad p + p \rightarrow \Lambda + K^+ + p, \text{ etc.} \tag{3}$$

the most copious source of h.f. are K^- induced reactions in nuclear matter, where the elementary reactions are

$$K^- + n,p \rightarrow \Lambda + \pi^{-,o}. \tag{4}$$

The reason is obvious; while reactions of type (3) have a high threshold and small cross-section, reactions of type (4) are exothermic and occur very frequently. The big step of creating strangeness is separated, in Eq. (4), from that of producing h.f.'s. Typical production rates of h.f.'s from K^- absorbed at rest in light nuclei are $\sim 2 - 5\%$. In the processes of <u>production</u>, <u>survival</u> and <u>decay</u> of a hyperfragment we find the means of observation and identification of particular hypernuclear species. It would be desirable, of course, to be able to compare the observables on the three steps simultaneously. This is, however, seldom possible.

1. <u>Identification at production</u>

Identification at production is particularly reliable in two-body reactions

$$K^- + He^4 \rightarrow \begin{matrix} {}_\Lambda He^4 + \pi^- \\ {}_\Lambda H^4 + \pi^o \end{matrix}. \tag{5}$$

These reactions are obviously exclusive domain of the He bubble chamber. Similar reactions have been observed in nuclear emulsion, such as:

$$K^- + C^{12} \rightarrow {}_\Lambda B^{12} + \pi^0$$
$$\Sigma^- + C^{12} \rightarrow {}_\Lambda B^{12} + n\,. \qquad (6)$$

Fig.1

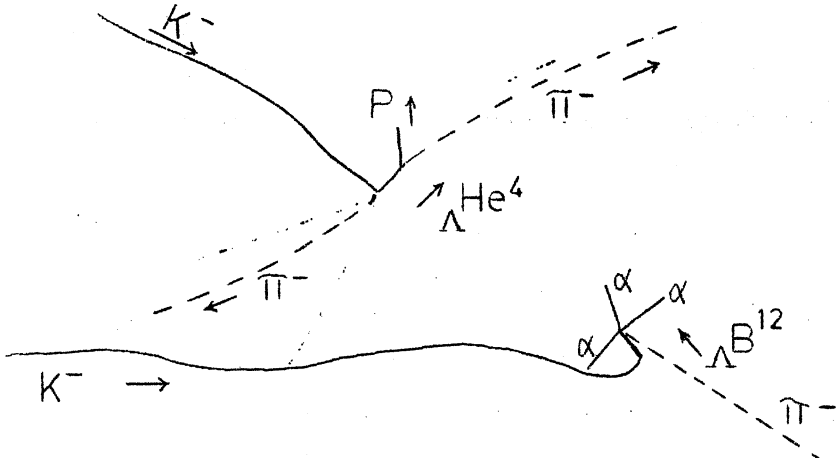

In this case, however, the uncertainty as to the target nucleus detracts from the evidence. The requirements of energy and momentum balance can only be checked approximately in Eq. (6), where the only observable of the production process is a very short (~ 4 μm) h.f. track. Hopefully, reactions such as in lithium-loaded emulsion should yield an independent clear-cut identification at production

$$K^- + Li^7 \rightarrow \begin{matrix} {}_\Lambda Li^7 + \pi^- \\ {}_\Lambda He^7 + \pi^0 \end{matrix}\,. \qquad (7)$$

Occasionally it is possible to obtain a satisfactory energy, momentum, charge and mass balance of more complicated production reactions in nuclear emulsion. Very seldom, however, is such information independent from that supplied by the decay process. This method is in all cases a very powerful tool; very likely the only method to give a reliable identification of relatively heavy hypernuclei. As we shall see, some decay modes (π - r) of heavy hypernuclei become completely non-characteristic and a combined analysis of production and decay reaction is called for, e.g.

$$K^- + O^{16} \rightarrow {}_\Lambda C^{14} + 2H^1 + \pi^-\,; \quad {}_\Lambda C^{14} \rightarrow \pi^- + N^{14}\,. \qquad (8)$$

Related remark — The use of small emulsion stacks for h.f. work prevents, in general, the observation of the production pion in its entire range, and its sign determination. On the other hand, at this stage in h.f. work, this information is quite fundamental.

2. Identification during survival

Hyperfragments can be identified during their survival namely from measurements on the h.f. track itself. If the h.f. comes to rest and it has sufficient range, any of the conventional means of determining mass and charge in emulsion apply. Thus, direct mass measurements can occasionally identify ${}_{\Lambda}H^{3}$ and ${}_{\Lambda}H^{4}$ when several millimeters of track are available. Z determinations usually require more than ~ 50 μm of h.f. track to be reliable. Thickness measurements in various ways, as well as gap-length measurements have been used. A direct determination of Z often determines the identity of a h.f., when its decay offers certain alternatives, e.g. for ${}_{\Lambda}H^{4}$, ${}_{\Lambda}He^{4}$, when in the $\pi - p - r$ mode of decay the recoil has a very short range, insufficient for direct distinction from range-momentum curves. Identification from h.f. decay is still the most widely attained.

3. Identification at decay

A blind approach to this problem is that of feeding input data, such as ranges and angles into a computer programmed to try all permutations of prong identities until a good fit is obtained. Then, amongst the output reactions, one chooses the one which yields the lowest momentum unbalance ΔP. Although this procedure is necessary for the analysis of complicated decays, it may often hide some relevant information. Thus, a few remarks are in order.

$(\pi - r)$ events

The pion momentum uniquely determines the recoil momentum and comparison with P - R curves immediately identifies the event. This is true, of course, for recoils which are long enough to afford discrimination.

In order to improve the fit, collinearity may be imposed, when justified. The direction of the recoil is, in fact, seldom well defined, in particular its dip angle. One can obtain a better recoil range estimate by measuring its projected range, and inferring its dip angle from the knowledge of the π direction.

Note This is a procedure which should be used with caution. There is a point in measuring accurately ΔP and deviations from collinearity even for species as common and typical as ${}_{\Lambda}H^{4} \rightarrow \pi^{-} + He^{4}$. In fact, if species such as ${}_{\Lambda}H^{5}$, ${}_{\Lambda}H^{6}$ should exist, their decays

$$ {}_{\Lambda}H^{5} \rightarrow \pi^{-} + n + He^{4}, \quad {}_{\Lambda}H^{6} \rightarrow \pi^{-} + 2n + He^{4} \qquad (9) $$

could very well simulate ${}_{\Lambda}H^{4} \rightarrow \pi^{-} + He^{4}$, with some departure from collinearity. Furthermore, a decay

$$ {}_{\Lambda}H^{6} \rightarrow He^{6} + \pi^{-} \qquad (10) $$

would look like an anomalous π - r decay of ${}_{\Lambda}H^{4}$, with a recoil somewhat shorter ($\sim 5.4\ \mu m$) than usual ($8.1\ \mu m$).

Some of the possible pitfalls in identifying π - r events are worth mentioning. Even ${}_{\Lambda}H^{3} \rightarrow \pi^{-} + He^{3}$ is not exempt from simulators. In fact,

$$ {}_{\Lambda}Li^{9} \rightarrow \pi^{-} + n + 2He^{4} \qquad (11) $$

can occur in a configuration similar to ${}_{\Lambda}H^{3}$ (π - r). In such a case, however, the h.f. track should tell the difference unless too short (as usually the case for ${}_{\Lambda}Li^{9}$). The real difficulties arise from π - r decays of heavier species, when the discriminating power of the recoil range is lost (as well as the possibility of ascertaining collinearity!). The trouble begins very soon. We are very likely unable to tell the difference between

$$ {}_{\Lambda}He^{6} \rightarrow \pi^{-} + Li^{6} \quad \text{(if it exists)}, $$

and

$$ {}_{\Lambda}Li^{7} \rightarrow \pi^{-} + Be^{7} . \qquad (12) $$

Both decays yield (or are expected to) π ranges of $\sim$ 2.2 cm and recoil ranges in the neighbourhood of 2 μm. If $_{\Lambda}He^{8}$ should exist, its decay

$$_{\Lambda}He^{8} \rightarrow \pi^{-} + n + Li^{7} \qquad (13)$$

would have an overwhelming chance of being confused with

$$_{\Lambda}He^{7} \rightarrow \pi^{-} + Li^{7} . \qquad (14)$$

From $_{\Lambda}Be^{10}$ on, all recoils have a range of 1 μm or less. On the other hand, the π ranges from many different species overlap. The properties of the recoils may then help, like their β decay

See fig. 2

$$_{\Lambda}B^{11} \rightarrow \pi^{-} + C^{11}, \text{ recoil } \beta^{+}, \text{ range } \sim 2.07 \text{ cm}$$

$$_{\Lambda}Be^{10} \rightarrow \pi^{-} + B^{10}, \text{ recoil stable, } \pi \text{ range } \sim 2.0 \text{ cm}. \qquad (15)$$

The failure to observe the decay β will automatically involve misidentification. Even when the recoil is unstable like Li^{8}, a pitfall is open. Take

See fig. 3

$$_{\Lambda}Be^{8} \rightarrow \pi^{-} + B^{8}, \; B^{8} \rightarrow \beta^{+} + \nu + Be^{8*}, \; Be^{8*} \rightarrow 2He^{4}. \qquad (16)$$

If the β^{+} were overlooked, the event may be interpreted in a very complicated way, perhaps even as

$$_{\Lambda}Li^{9} \rightarrow \pi^{-} + n + 2He^{4} . \qquad (17)$$

The same would hold for a hypothetical decay

$$_{\Lambda}He^{8} \rightarrow \pi^{-} + Li^{8} . \qquad (18)$$

All this is further complicated by the possibility that heavy recoils be emitted in excited states, or that the hypernucleus decays from an isomeric state. For these reasons, identifications based on $\pi - r$ events of heavy h.f. should always be taken with great caution and in general are <u>not</u> as clear-cut as those based on other all-charged decay modes. The importance of a combined analysis <u>production-decay</u> vertices for these events cannot be stressed any further.

($\pi - p - r$) events

After checking for consistency with coplanarity, it is, in general, useful to impose coplanarity by inferring the recoil direction from that of the resultant momentum $\vec{P}_{\pi p} = \vec{P}_{\pi} + \vec{P}_{p}$. Next it is useful to plot $|\vec{P}_{\pi p}|$ versus the corrected recoil range R_{rec}. Range momentum curves can be constructed experimentally in this way for various isotopes. Errors and anomalies can easily be spotted. Below certain recoil ranges it becomes impossible to discriminate among neighbouring isotopes. Thus, below ~ 3 μm, it becomes meaningless to accept a discrimination between He^3 and He^4. Problem cases of this type are frequently encountered for all species, ${}_{\Lambda}H^3$, ${}_{\Lambda}H^4$, ${}_{\Lambda}He^4$, ${}_{\Lambda}He^5$, ${}_{\Lambda}Li^7$, etc. For the lighter species, however, a good fraction of the events yield recoils in the sensitive region. For the heavier species, <u>problem cases</u> become the rule because the recoil ranges, usually very short, become increasingly insensitive to the momentum $\vec{P}_{\pi p}$. Obviously in this region, one cannot even assess that the decay is indeed of the $\pi - p - r$ type, nor that neutrons are emitted. Analysis in conjunction with the production kinematics becomes once more crucial. In discussing $\pi - p - r$ events of even the lighter hypernuclei, one should bear in mind that the recoil co-ordinates in the P-R plot have considerable spread. In certain regions

See fig. 4

of the plot, in particular when an abundant species ($_{\Lambda}He^5$) is next to a less abundant one ($_{\Lambda}He^4$) some overlap of the distributions will always occur, so that some contamination of one species with another may be present. With increased statistics one can attempt to <u>purify</u> a collection of events of a given species by imposing a progressively increasing <u>range cut-off</u> on the recoil in order to accept events only in a region of the (P-R) plots where no overlap can occur.

<u>Remark</u> A procedure as outlined above is the only method to eliminate from a sample of a given species possible contaminations. Such contaminations introduce <u>systematic</u> biases in the determination of, for example, binding energies. The addition of small or large samples of identified h.f. to the world statistics becomes a <u>worthless</u> proposition if only B_{Λ}'s or worse, $\bar{B}_{\Lambda}$'s are given. The raw data are instead needed in order to attempt an elimination of the intrinsic, systematic errors due to contamination.

Again, some features of the recoil may help, when the recoil itself is too short. For example, in the decay

Fig. 5

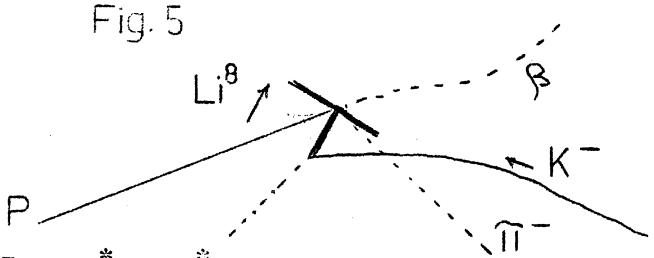

$$_{\Lambda}Li^9 \rightarrow \pi^- + p + Li^8,\ Li^8 \rightarrow \beta^- + \bar{\nu} + Be^{8*},\ Be^{8*} \rightarrow 2He^4; \qquad (19)$$

watch out, however, for the very similar decay

$$_{\Lambda}B^9 \rightarrow \pi^- + p + B^8,\ B^8 \rightarrow \beta^+ + \nu + Be^{8*},\ Be^{8*} \rightarrow 2He^4. \qquad (20)$$

Incidentally, the range energy curves obtained from h.f. recoil in nuclear emulsion are quite certainly the best available in the approximate range 2 - 40 μm.

(π - n - r) and complex decays

These events are best analysed with computer programmes. However, the following example illustrates some auxiliary method to improve the over-all reliability in the identification of a certain class of events.

The decay

$$_{\Lambda}Li^{9} \rightarrow \pi^{-} + n + 2He^{4} \qquad (21)$$

may easily be confused with

$$_{\Lambda}Li^{8} \rightarrow \pi^{-} + 2He^{4} \qquad (22)$$

when the neutron momentum is $|\vec{P}_n| \leq 40$ MeV/c. The ΔP distribution for three-body charged decays, in fact, extends up to this approximate value, due to measurement errors. If the energy release Q is plotted against the missing momentum P_n (or ΔP), a separation between $_{\Lambda}Li^{8}$ and $_{\Lambda}Li^{9}$ can be achieved on an entire body of events, and some statistical method may be used to cut off a possible contamination of $_{\Lambda}Li^{8}$ events amongst $_{\Lambda}Li^{9}$.

See fig. 6

A general comment is required concerning all decays involving neutron emission, when considering B_{Λ}. Such events will yield <u>systematically</u> underestimates of B_{Λ}. In fact, while the momentum unbalance ΔP, due to exp. errors is neglected in decays involving only charged particles, ΔP will contribute to the estimate of the neutron momentum, as

$$(P_n)_{exp} = (P_n)_{true} + \frac{(\Delta P)^2}{3(P_n)_{true}}. \qquad (23)$$

Thus, the neutron energy will be overestimated, and so will Q, giving a corresponding underestimate of B_{Λ}. Of course, this effect will be felt at small ($P_n \approx \Delta P$) neutron momenta and is in general small. However, since average B_{Λ}'s for some species, or even individual decay modes, have errors (statistical) smaller than 0.1 MeV, even an effect of this kind should not be neglected. Whenever possible, it may be best to base binding energy estimates on decay modes involving charged particles only.

4. Identification on the basis of B_Λ

This is the last remedy, resort to which is obviously very dangerous. It is difficult, of course, to assess the extent to which it is practiced. To some extent it is always used, if nothing else, when one rejects an identification leading to a negative B_Λ. It should be realized, however, that an identity, giving a B_Λ in agreement with a known value is by no means an identification. Pitfalls may be wide open when a species is "expected" to have a certain B_Λ, and an event is attributed to that species on this basis. This is particularly the case with $(\pi - r)$ events, where the interpolated B_Λ is the only basis on which to predict the configuration. The only situation in which this approach seems justified is encountered in the determination of branching ratios between various decay modes of a certain species, e.g. the separation between the $(\pi - p - r)$ decays of ${}_\Lambda H^3$ and ${}_\Lambda H^4$, when the recoil is invisible. Careless use of this method will, on the other hand, produce non-Gaussian distributions of B_Λ, will cut off interesting tails, and will hide possible splittings in B_Λ due to excited initial or final states.

5. Experiments with known target nuclei

Some have been mentioned previously. It may be that even accurate B_Λ estimates may be obtained from the measurement of the π range following

$$K^- + (A,Z) \rightarrow {}_\Lambda(A,Z) + \pi^- + Q \qquad (24)$$

where $Q = B_\Lambda - B_n + 176$ MeV, and B_n is the binding of the last neutron in (A,Z). This approach carries the identification at production to its logical extreme, that of producing particular h.f. species. It may be valuable for $A \gtrsim 8 - 10$. It offers the advantage that techniques other than nuclear emulsion may be used advantageously, such as bubble chambers, spark chambers, etc.

III. INFORMATION DERIVED FROM HYPERNUCLEAR PROPERTIES

What does one learn from the study of hypernuclei, study which is based so far on a sample of perhaps 2000 mesic decays analysed in nuclear emulsion and several hundreds in the He bubble chamber? Several basic answers have been given to properties of the strong and weak interaction of the Λ hyperon with nucleons, as well as to intrinsic questions regarding strange particles properly.

A brief summary of the main results is the following.

1. Strong Λ - n interaction

a) The Λ-nucleon interaction is charge symmetric as substantiated by the well-established existence of hypernuclear charge multiplets. Such multiplets correspond to those for the nuclear cores since the Λ has isospin T = 0.

b) The Λ-nucleon interaction is strong with coupling constant of the order of unity. This follows from an analysis of the Λ-binding energies for light hypernuclei. A measure of this strength is given (following Dalitz) by the volume integral of a Λ-nucleon central potential of appropriate shape for a particular spin state S. In these terms one can compare the Λ - n to the n - n interaction, e.g.

$$^3S_1 \; n-p \text{ volume integral } U \approx 1400 \text{ MeV f}^3$$

$$^1S_0 \; \Lambda-p \text{ volume integral } U \approx 380 \text{ MeV f}^3.$$

Since the range of Λ-nucleon force is much shorter (at least two π exchange) than that of the n-n force, the over-all Λ - n binding is weaker than the corresponding nucleon-nucleon binding, even though the interactions have comparable strengths[1]. Alternatively, the interaction can be described in terms of singlet and triplet scattering lengths. (See Dalitz, following lecture.)

c) <u>The Λ-nucleon interaction is strongly spin-dependent</u>. This follows from an analysis of both the Λ-binding energies and the direct determination of the spin of several hypernuclei ($_{\Lambda}H^3$, $_{\Lambda}H^4$, $_{\Lambda}Li^8$). Indirect information stems also from the measurement of hypernuclear lifetimes. The $^1S_0$ Λ-n interaction is more attractive than that in the $^3S_1$ state, opposite to the nucleon-nucleon case[2].

For the sake of illustration, recall that the Fermi scattering lengths are, for:

n - p	Λ - p (See Dalitz, next lecture).
$a_s = -2.34 \times 10^{-12}$ cm	$a_s \approx -2.4 \times 10^{-13}$ cm
$a_t = 0.52 \times 10^{-12}$ cm	$a_t \approx -0.6 \times 10^{-13}$ cm

Fig. 7

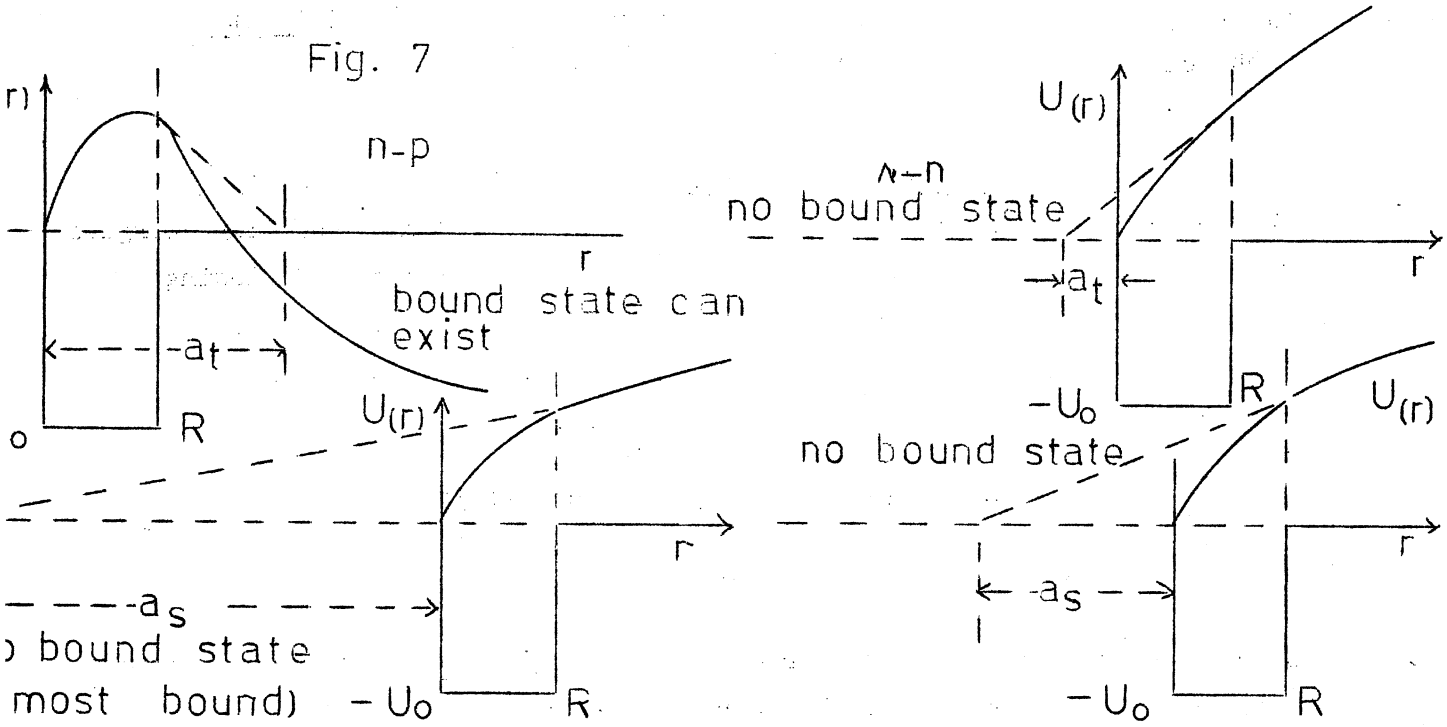

d) <u>The well-depth experienced by a Λ particle in nuclear matter is ≃ 30 MeV</u>. This result stems from the determination of B_{Λ} for heavy hypernuclei as well as from theoretical calculations.

e) <u>The K^- is a pseudoscalar particle</u>. This follows the study of the reaction $K^- + He^4 \rightarrow {}_{\Lambda}H^4 + \pi^0$ in the He bubble chamber, knowing that $J(_{\Lambda}H^4) = 0$.

2. Weak Λ - n interaction

a) Several checks of the validity of the $|\Delta T| = \frac{1}{2}$ rule in Λ-pionic decay modes have been given from the study of branching ratios in the decay modes of some light hypernuclei. Perhaps the most significant result is the determination of the ratio p_o/s_o between the p- and s-wave amplitudes in Λ-decay via the π^o mode obtained by the He bubble chamber group. The prediction of the $|\Delta T| = \frac{1}{2}$ rule, that $p_o/s_o = p/s$ seems well satisfied.

b) Information on the strength of the weak interaction leading to $\Lambda + n \rightarrow n + n$. This is obtained from the branching ratios non-mesic/mesic for the decay modes of individual hypernuclear species. Very little is known on this subject. One would like to know whether, for instance, this interaction is spin-dependent or not.

3. Nuclear physics

A variety of final state interaction effects can be found in hypernuclear decays. Typical examples ${}_{\Lambda}He^5 \rightarrow \pi^- + Li^{5*}$; $Li^{5*} \rightarrow p + He^4$ ($P_{3/2}$ resonance dominant) ${}_{\Lambda}Li^8 \rightarrow \pi^- + Be^{8*}$; $Be^{8*} \rightarrow \pi^- + 2He^4$ (0^+, 2^+ intermediate states present). These properties, as we shall see, may be very useful for specific purposes, like spin determination. Occasionally, new information on low energy nuclear physics problems may be gained as a by-product.

We will now try to justify some of the above results by presenting the evidence in some detail.

IV. Λ BINDING ENERGIES

The enclosed tabulation contains up-to-date averages of B_Λ for established species. When relevant, $\bar{B}_\Lambda$ are given separately for the most abundant decay modes of the same species. Several features are exhibited by a plot of B_Λ versus mass number A.

See fig.8

These are:

i) the presence of charge multiplets reflecting the isospin structure of the core nuclei;

ii) an over-all monotonic increase of B_Λ as a function of A;

iii) a discrete structure within the multiplets which is to be attributed to spin-dependent effects.

$_\Lambda H^3$ is the lightest hypernucleus known. It is attributed T = 0 since there is no evidence for the other members of a T = 1 state, $_\Lambda n^3$ and $_\Lambda He^3$. Its B_Λ is very small, (0.31 ± 0.15) MeV and the B_Λ distribution for this species is rather broad, somewhat more than expected from range-straggling alone.

See fig.9

$_{\Lambda}H^4$, $_{\Lambda}He^4$ are mirror hypernuclei ($T = 1/2$) and have very similar B_Λ's (2.14 ± 0.08) MeV and (2.47 ± 0.09) MeV respectively as required from charge symmetry. One may comment that these values, due to the small errors, are almost in disagreement. The $\bar{B}_\Lambda$ determination of $_{\Lambda}H^4$ requires some more detailed investigation. As can be seen from Table 1, $\pi - r$ events yield for $\bar{B}_\Lambda$ the value (2.40 ± 0.12) MeV, very close to $_{\Lambda}He^4$. n events give a very low $\bar{B}_\Lambda$, (1.75 ± 0.1_) MeV and perhaps should not be included in the average for the reasons discussed above. Finally, ($\pi - p - r$) events for which $\bar{B}_\Lambda$ = (2.00 ± 0.14) MeV could contain a contamination of $_{\Lambda}H^3$ which would lower $\bar{B}_\Lambda$. On the other hand, $_{\Lambda}He^4$ could well contain a contamination of $_{\Lambda}He^5$, which would increase $\bar{B}_\Lambda$, in the sense of emphasizing a difference between $_{\Lambda}H^4$ and $_{\Lambda}He^4$ which may not be real at all. The one way to improve the situation here is not a mere increase in statistics, but a more severe selection of the events as pointed out in the section on identification problems.

The B_Λ distribution for the $\pi - r$ decays of $_{\Lambda}H^4$ is somewhat skew at the higher end. This could be due on one side to the inclusion of events in which the long pion (4 cm) may have lost energy in undetected interactions. On the other hand, a contamination of still hypothetical decays:

$$_{\Lambda}H^5 \rightarrow \pi^- + n + He^4, \quad _{\Lambda}H^6 \rightarrow \pi^- + 2n + He^4 \tag{25}$$

cannot be ruled out and should perhaps be kept in mind.

$_{\Lambda}He^5$. It is the most abundant hypernucleus. It decays essentially by the $\pi - p - r$ mode only. Its $\bar{B}_\Lambda$, (3.10 ± 0.05) MeV, is the best known and the B_Λ distribution is the closer to a Gaussian than any of the others.

($_{\Lambda}He^6$, $_{\Lambda}Li^6$). No clear cut evidence for the existence of these hypernuclei has been reported, nor the large number of $_{\Lambda}He^5$ giving decays also compatible with

$$_{\Lambda}He^6 \rightarrow \pi^- + p + n + He^4 \tag{26}$$

is a valid argument to support the existence of ${}_{\Lambda}He^{6}$. The decay

$$ {}_{\Lambda}He^{6} \rightarrow \pi^{-} + H^{3} + H^{3}, \quad Q_o = 26.44 \text{ MeV} \tag{27} $$

would provide good evidence.

See fig. 10

${}_{\Lambda}He^{7}$, ${}_{\Lambda}Li^{7}$, ${}_{\Lambda}Be^{7}$. ${}_{\Lambda}Li^{7}$ has T = 0 while ${}_{\Lambda}He^{7}$ and ${}_{\Lambda}Be^{7}$ are members of a T = 1 state. The B_{Λ} for ${}_{\Lambda}Li^{7}$ is well-established, (5.52 ± 0.12) MeV from decays other than π^{-}r. Only two examples of ${}_{\Lambda}Be^{7}$ are known, yielding $\bar{B}_{\Lambda}$ = (4.9 ± 0.5) MeV while for ${}_{\Lambda}He^{7}$ an average of 14 B_{Λ} values would give $\bar{B}_{\Lambda}$ = (3.96 ± 0.24) MeV.

See fig. 11

Two effects are present here. On one side, the $\bar{B}_\Lambda$ of ${}_\Lambda Li^7$ is higher than either of the $\bar{B}_\Lambda$ of ${}_\Lambda He^7$ or ${}_\Lambda Be^7$, and this can be understood in terms of the spin dependence of the Λ-nucleon interaction. On the other side, the $\bar{B}_\Lambda$'s for ${}_\Lambda He^7$ and ${}_\Lambda Be^7$ which should be identical, are indeed in disagreement. A suggestion made by Danysz and Pniewski[3], is the following. ${}_\Lambda He^7$ may decay from an isomeric state (He^6 has a level at 1.6 MeV in the continuum) and the observed B_Λ distribution may contain, in fact, two groups of B_Λ's. That this should be the case is substantiated by the very existence of ${}_\Lambda Be^7$. In fact, the condition for the stability of ${}_\Lambda Be^7$ against break up

$$ {}_\Lambda Be^7 \rightarrow 2p + {}_\Lambda He^5 , \tag{28} $$

is that its B_Λ be greater than 4.5 MeV. Thus even with only two ${}_\Lambda Be^7$ events, we know that $B_\Lambda({}_\Lambda Be^7)$ must exceed 4.5 MeV. From charge symmetry one would then expect that the ground state ${}_\Lambda He^7$ should have B_Λ also > 4.5 MeV. Thus, considerable interest is attached to an increase in the statistics of ${}_\Lambda He^7$ events. At present it is difficult to detect a splitting in the B_Λ distribution. The reasons to expect such splitting are, however, plausible, as will be further illustrated by Dalitz (these lectures).

${}_\Lambda Li^8$, ${}_\Lambda Be^8$. Another well-established pair of mirror hypernuclei. Their $\bar{B}_\Lambda$'s are in very close agreement.

See fig.12

$_{\Lambda}Li^{9}$, $_{\Lambda}Be^{9}$, (B^{9}). The binding energy of $_{\Lambda}Li^{9}$ (T = 1) is about 1.5 MeV greater than that of $_{\Lambda}Be^{9}$ (T = 0). This is of course a point of great interest because if this difference is to be attributed to spin dependence only, it may be incompatible with the results from the mass 7 hypernuclei. Unfortunately the B_{Λ} distribution for $_{\Lambda}Li^{9}$ is not one of the most satisfactory. $_{\Lambda}B^{9}$ has never been reported. Its decay (π - p - r) could be confused, as remarked before, with that of $_{\Lambda}Li^{9}$. This misidentification would not, however, affect the observed large difference in B_{Λ} between the T = 0 and T = 1 states. For heavier species, the plot shows how little is known. The spread σ of the B_{Λ} distributions is shown as a function of Q in the following plot. The over-all monotonic increase of B_{Λ} versus A can be understood in a rather simple way. The Λ particle, not obeying the Pauli principle in a single Λ hypernucleus, occupies the lowest s state. Thus, no saturation effects are expected until the Λ will reach the bottom of the potential well, for a very heavy hypernucleus.

See fig. 13

As the radius R of the region of interaction increases, with increasing A, the Λ will progressively "sink" to a lower energy state in the well. This can be seen as follows. Consider for simplicity the Λ in a square potential well of depth $U(r) = -D_{\Lambda}$, radius R.

Fig. 14

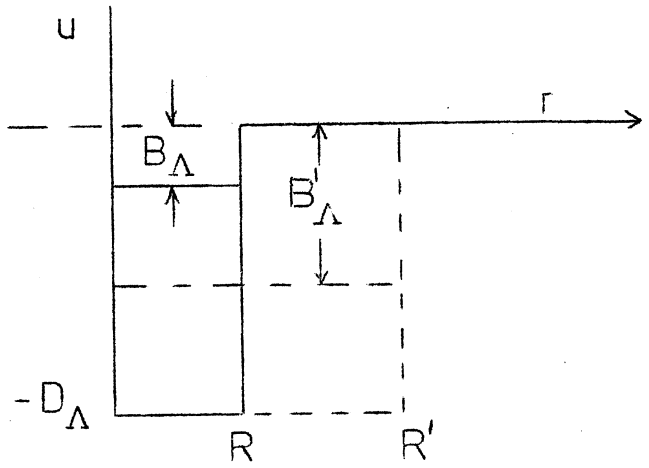

The standard solution of the Schrödinger equation for this problem, after matching the wave functions at the boundary R is:

$$K \cot KR = -\gamma, \text{ or } \sqrt{\frac{2M}{\hbar^2}(D_\Lambda - B_\Lambda)} \cot \sqrt{\frac{2M}{\hbar^2}(D_\Lambda - B_\Lambda)}\, R = -\sqrt{\frac{2M}{\hbar^2} B_\Lambda} \qquad (29)$$

$$\cot \sqrt{\frac{2M}{\hbar^2}(D_\Lambda - B_\Lambda)}\, R = -\sqrt{\frac{B_\Lambda}{D_\Lambda - B_\Lambda}}\,. \qquad (30)$$

One can now find approximate solutions for convenient asymptotic cases. Take for example $B_\Lambda \approx D_\Lambda$, then

$$\sqrt{\frac{2M}{\hbar^2}(D_\Lambda - B_\Lambda)}\, R \approx \pi; \quad B_\Lambda \approx D_\Lambda - \frac{\pi^2\hbar^2}{2M_\Lambda r_o^2 A^{2/3}}\,. \qquad (31)$$

Equation (31) expresses explicitely how B_Λ depends on A for heavy hypernuclei. This equation suggests a method for the determination of D_Λ. In fact, a plot of B_Λ versus $A^{-2/3}$ for heavy hypernuclei should be, in the zeroth approximation, a linear plot. Extrapolation to $A \to \infty$ will give a value for D_Λ. This has indeed been accomplished at least partially from the knowledge of an upper limit of B_Λ for hypernuclei in the mass range $60 < A < 100$. The result[4] is that $D_\Lambda \lesssim 30$ MeV. The upper limit of B_Λ for $60 < A < 100$ hypernuclei was obtained from the upper limit in the energy release of mesic and non-mesic disintegrations of "spallation hyperfragments".

See fig.15

An attempt is being made at present to obtain a lower limit of B_Λ for bromine hypernuclei following the measurement of the energy release in the reaction at rest

$$K^- + Br^{79} \rightarrow {}_\Lambda Br^{79} + \pi^- , \qquad (32)$$

if such a reaction is found to occur to the ground state or some low lying state of ${}_\Lambda Br^{79}$. This study is made in a large CF_3Br bubble chamber where K^- mesons have been brought to rest. Even when B_Λ for heavy hypernuclei is known more accurately, the crude linear extrapolation to D_Λ will have to be improved, making use of a better approximation of Eq. (31). This will take into account a more realistic shape for the potential and indications are (Dalitz) that the correct functional dependence of B_Λ versus $A^{-2/3}$ is not linear but possesses some curvature (the slope increases slightly with A).

V. THE SPINS OF Λ HYPERNUCLEI

Spin assignments have been obtained so far for ${}_{\Lambda}H^{3}$, ${}_{\Lambda}H^{4}$, and ${}_{\Lambda}Li^{8}$. The spin of species with spinless core, such as ${}_{\Lambda}He^{5}$ can be inferred as being equal to the Λ spin, $J = \frac{1}{2}$. We can distinguish several approaches to this problem.

i) Determination by direct methods. It implies the production or selection of an aligned sample of hypernuclei. It is based on the study of angular correlations of the decay products with respect to some axis of quantization.

ii) Determination from branching ratios of different decay modes. Conservation of angular momentum may favour certain final states over others.

iii) More indirect approaches, e.g. based on hypernuclear lifetimes. These are, however, not independent of (ii).

Take, for example, ${}_{\Lambda}H^{4}$. A direct spin determination has been obtained by the He bubble chamber group from a study of the sequence of reactions

$$K^{-} + He^{4} \rightarrow {}_{\Lambda}H^{4} + \pi^{0}; \quad {}_{\Lambda}H^{4} \rightarrow \pi^{-} + He^{4} . \tag{33}$$

All particles in these reactions are spinless except possibly ${}_{\Lambda}H^{4}$ which can have at the most $J = 0$ or 1. If ${}_{\Lambda}H^{4}$ has $J = 0$, the decay ${}_{\Lambda}H^{4} \rightarrow \pi^{-} + He^{4}$ is then necessarily isotropic. Note that in such a case, since the orbital angular momentum ℓ in the initial state must equal the orbital angular momentum L in the final state, the observation of Eq. (33) implies that the intrinsic parity $\omega_{K} = \omega_{\pi} = -1$ or ($\omega_{\Lambda} = +1$ by convention) that the K is pseudoscalar. Consider now the case of $J = 1$, and K^{-} capture from an s-orbital (there are good arguments in favour of this assumption)[5]. Then $L = 1$ in the final state which implies that $\omega_{K} = +1$, a scalar K meson. As to the angular distribution in the decay of ${}_{\Lambda}H^{4}$, take the direction of ${}_{\Lambda}H^{4}$ as the axis Z of quantization. Only the projection $J_{Z} = m({}_{\Lambda}H^{4}) = 0$ is allowed in the final state.

This, in turn, implies that in the rest system of π, He^4, $\ell_\pi = 1$, $m_\pi = 0$. Then the angular distribution is characterized by the spherical harmonic $Y_1^0(\Theta)$ only and $P(\Theta) \propto \cos^2\Theta$. The exp. distribution found by Block et al.[6] is isotropic, strongly suggesting that $J({}_\Lambda H^4) = 0$ and that the K is pseudoscalar. Prior to this direct determination, $J = 0$ for ${}_\Lambda H^4$ had already been assigned as a result of an emulsion experiment.

Fig. 16

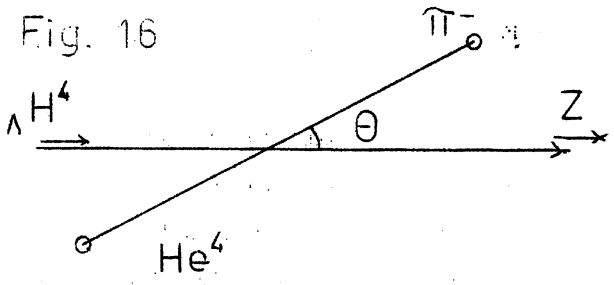

Fig. 17

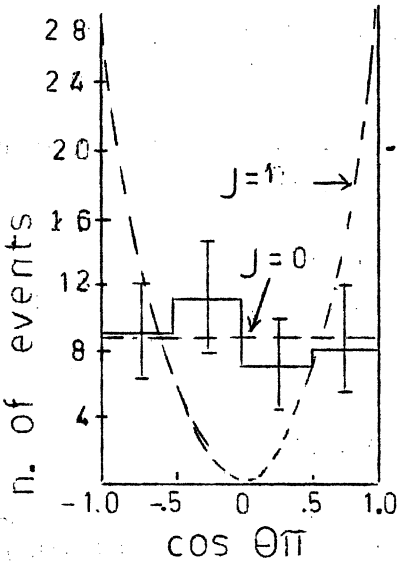

The spin assignment in question follows:

a) the original argument given by Dalitz[7] and also Dalitz and Liu[8] which relates the branching ratio $R_4 = \frac{\pi^- + He^4}{\text{all modes}}$ to the spin J and to the p/s ratio in Λ decay;

b) an exp. determination of R_4 in nuclear emulsion[9];

c) the accurate determination of the p/s ratio in Λ decay by Beall et al.[10] and by Cronin et al.[11].

The argument in its essence is the following: the decay $\Lambda \to \pi^- + p$ violates parity conservation and can proceed through both

s- and p-wave pion emission (see Dalitz, following lecture). Since the decay ${}_{\Lambda}H^4 \rightarrow \pi^- + He^4$ involves spinless particles in the final state, the spin J of ${}_{\Lambda}H^4$ equals the orbital angular momentum L in the final state.

See fig. 18

Thus, if $J({}_{\Lambda}H^4) = 0$, the π - r decay will be favoured if s-wave pion emission predominates in Λ decay, being forbidden for zero s-wave amplitude. Conversely, $J({}_{\Lambda}H^4) = 1$, the π - r decay is forbidden for zero p-wave amplitude and enhanced otherwise.

The experimental value of R_4 found in emulsion is 0.67 ± 0.06. This combined with the value $\frac{p^2}{(s)^2 + (p)^2} = 0.11 \pm 0.03$, and on the basis of the curves calculated by Dalitz and Liu, clearly determines $J({}_{\Lambda}H^4) = 0$. A more recent determination of R_4 has recently been reported by the He bubble chamber group. Their value, 0.68 ± 0.04, is in substantial agreement with that mentioned above.

By an entirely similar reasoning $J = \frac{1}{2}$ has been assigned to ${}_{\Lambda}H^{3\,12)}$.

Both angular correlation among the decay products and branching ratios among different final states have enabled a determination of the spin of ${}_{\Lambda}Li^8$. This is the first hypernucleus of the nuclear p-shell for

which such information is available. The ground state of Li^7 has $J = 3/2$ while the first excited state of 0.475 MeV has $J = 1/2$. The Λ can couple to form ${}_{\Lambda}Li^8$ to either of these states so that a priori the spin of ${}_{\Lambda}Li^8$ could be 0^-, 1^- or 2^-. The solution of the problem hinges on evidence that the dominant decay

$$ {}_{\Lambda}Li^8 \rightarrow \pi^- + 2He^4 \qquad (34) $$

indeed proceeds through intermediate Be^{8*} states

$$ {}_{\Lambda}Li^8 \rightarrow \pi^- + Be^{8*}; \quad Be^{8*} \rightarrow 2He^4 . \qquad (35) $$

The information on the spin is derived from:

i) the existence of transitions to discrete Be^{8*} states and a comparison of the observed with the predicted partial rates for particular final states[13];

ii) the study of the angular correlation between the π^- direction and the $2He^4$ direction in their centre of mass.

Values of E_{rel} and $\cos\Theta$ have been calculated for about 43 events[14]. A plot of E_{rel} shows a remarkable grouping of events for E_{rel} values of ~ 0.1 MeV, ~ 3 MeV and ~ 17 MeV corresponding to all known levels of Be^{8*}.

See fig. 19

A very small continuum background seems to contribute. The theoretical predictions by Dalitz are based on the following assumptions (simplified here).

a) The Λ-decay interaction is dominantly s interaction and therefore has odd parity. Thus, any transition via π^- emission to a final state of <u>even</u> parity [like the 0^+, 2^+ (T = 0), 2^+ (T = 1) levels detected here] requires ℓ_π = odd. Very likely only ℓ_π = 1 contributes significantly.

b) The continuum in the E_{rel} distributions is neglected.

c) The calculations are based on appropriate intermediate-complying nuclear wave functions.

The predictions and the expt. results can be summarized as follows.

		Theory	Expt.
If $J = 2^-$	i)	Very small transition rate to Be^{8*} (2^+, 3.0 MeV) or $P(\Theta) \approx \sin^2\Theta$ for (2^+) events	Very large
	ii)	Ratio $\frac{2^+,(T=1) \text{ at } 17 \text{ MeV}}{2^+,(T=0) \quad 3 \text{ MeV}} \sim 4.5$	4/32
If $J = 1^-$	i)	$\frac{2^+(T=0)\ 3.0 \text{ MeV}}{0^+(T=0)\ 0.09 \text{ MeV}} \rightarrow 2.7 - 6.4$	32/5
	ii)	$\frac{2^+(T=1)\ 17 \text{ MeV}}{2^+(T=0)\ 3 \text{ MeV}} \sim 0$	4/32
	iii)	$P(\Theta) \approx 1 + 3\cos^2\Theta$ for (2^+) events	Consistent

Fig. 20

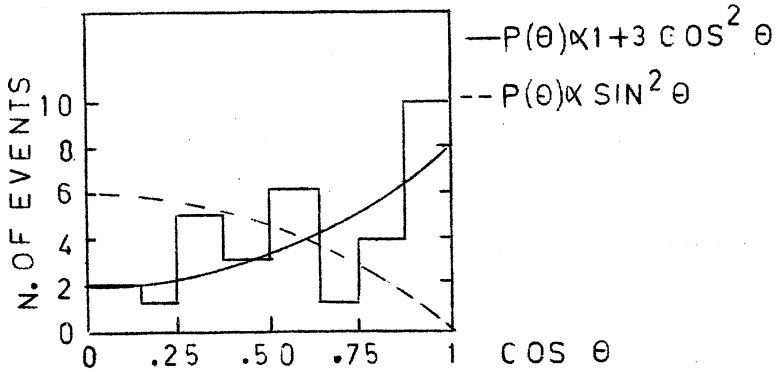

5666/NP/smg

	Theory	Expt.
If $J = 0^-$	Transitions to 0^+, 2^+ states forbidden by angular momentum conservation	Both observed

In conclusion the over-all evidence favours $J = 1$ for ${}_{\Lambda}Li^8$. This shows that even in the p-shell hypernuclei, as well as in the s-shell ones like ${}_{\Lambda}H^3$, ${}_{\Lambda}H^4$,

$$J(HF) = |(J_i - \tfrac{1}{2})|$$

where J_i = spin of the core in its ground state. Purely as an exercise, a calculation of the angular correlation in ${}_{\Lambda}Li^8$ decay, assuming $\ell_\pi = 1$ is appended. This is valid for transitions to the 2^+, 3.0 MeV state of Be^{8*}.

As mentioned previously, the study of hypernuclear lifetimes provides us with another check on the spin assignments. Lifetime estimates of some significance are available for ${}_{\Lambda}H^3$ and ${}_{\Lambda}H^4$. For ${}_{\Lambda}He$ hypernuclei some data have been collected; for heavier hypernuclei no information is available at all. Dalitz and Rajasekharan[15] have shown that if ${}_{\Lambda}H^3$ has spin $J = \tfrac{1}{2}$, the total decay rate is enhanced considerably. A similar situation occurs if $J({}_{\Lambda}H^4) = 0$. This can be understood qualitatively as due to the fact that if $J({}_{\Lambda}H^3) = \tfrac{1}{2}$ and $J({}_{\Lambda}H^4) = 0$, the s-channel decay is enhanced by both the Pauli principle, since it leads predominantly to allowed spin configurations, and by the energetic $(\pi^- + He^3)$ and $(\pi^- + He^4)$ final states respectively. A good estimate of the ${}_{\Lambda}H^3$ lifetime is available from the He bubble chamber group experiment[16]. An estimate of the lifetime of ${}_{\Lambda}H^4$ has been reported by Crayton et al.[17] from an emulsion experiment.

A comparison of the theoretical expectation with the experimental data is given in the following table.

$\tau({}_{\Lambda}H^3)$	$J = 1/2$	$J = 3/2$
Theory ($\tau_{\Lambda} = 2.35 \times 10^{-10}$ sec)	$(1.79 \pm 0.10) \times 10^{-10}$ sec	$(2.40 \pm 0.03) \times 10^{-10}$ sec
Exp.	$(1.05^{+\ 0.20}_{-\ 0.18}) \times 10^{-10}$ sec	(36 events of which 29 in flight)

$\tau({}_{\Lambda}H^4)$	$J = 0$	$J = 1$
Theory	1.5×10^{-10} sec	$> 2.7 \times 10^{-10}$ sec
Exp.	$(1.2^{+\ 0.6}_{-\ 0.3}) \times 10^{-10}$ sec	(52 π - r events of which 9 in flight)

The predicted enhancement of the total decay rate for the Λ - n anti-parallel spin orientation has been observed. As a matter of fact the enhancements seem to be even greater than expected at least for ${}_{\Lambda}H^3$, and this may have to be explained.

Examples of ${}_{\Lambda}H^4$ decays in emulsion by the π - r mode are shown:

Fig. 21

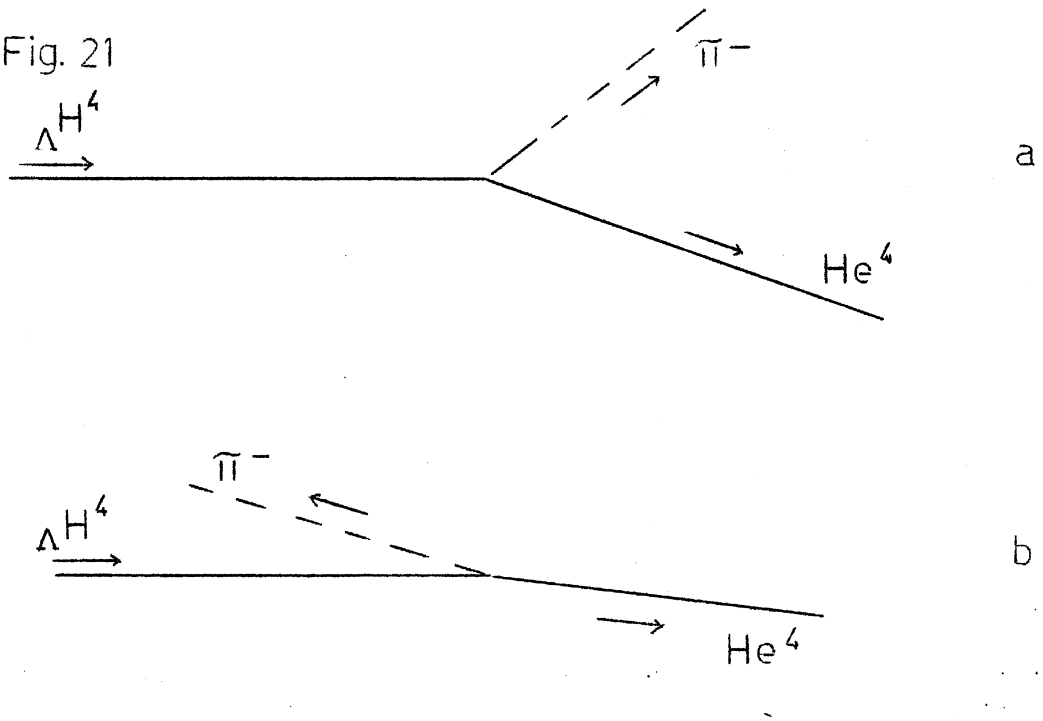

In a recent study by Ammar et al.[18] out of 99 π^- mesic decay of ${}_{\Lambda}He^{4,5}$ five were found to occur in flight. This yields $\tau({}_{\Lambda}He^{4,5}) = (1.2^{+\ 1.0}_{-\ 0.4}) \times 10^{-10}$ sec. A result in substantial agreement[19] based on 51 ${}_{\Lambda}He$ events of which only four in flight, is again $\tau({}_{\Lambda}He^{4,5}) = (1.4^{+\ 1.8}_{-\ 0.5}) \times 10^{-10}$ sec.

* * *

REFERENCES

1. R.H. Dalitz and B.W. Downs, Phys.Rev. 111, 967 (1958).
2. R.H. Dalitz, The nuclear interaction of the hyperons, Bangalore Lectures, EFINS 62-9.
3. M. Danysz and J. Pniewski, Phys.Letters 1, 142 (1962).
4. D.H. Davis, R. Levi-Setti, M. Raymund, O. Skjeggestad, G. Tomasini, J. Lemonne, P. Renard and J. Sacton, Phys.Rev.Letters 9, 464 (1962).
5. T.B. Day and G.A. Snow, Phys.Rev.Letters 2, 59 (1959).
6. M.M. Block, L. Lendinara and L. Monari, Int.Conf.on High-Energy Phys., CERN 1962. p. 371.
7. R.H. Dalitz, Phys.Rev. 112, 605 (1958).
8. R.H. Dalitz and L. Liu, Phys.Rev. 116, 1312 (1959).
9. R.G. Ammar, R. Levi-Setti, W.E. Slater, S. Limentani P.E. Schlein and P.M. Steinberg, Nuovo Cimento 19, 20 (1961).
10. E.F. Beall, B. Cork, D. Keefe, P.G. Murphy and W.A. Wenzel, Phys.Rev. Letters 8, 75 (1962).
11. J.W. Cronin, Bull.Am.Phys.Soc. 7, 68 (1962).
12. M.M. Block, C. Meltzer, S. Ratti, L. Grimellini, T. Kikuchi, L. Lendinara and L. Monari, Int.Conf.on High-Energy Phys., CERN 1962, p. 458; R.G. Ammar et al. NUPHYS 62104 - in press.

66/NP/smg

13. R.H. Dalitz, Nucl.Phys. 41, 78 (1963).

14. D.H. Davis, R. Levi-Setti and M. Raymund, Nucl.Phys. - in press, EFINS 62-48.

15. R.H. Dalitz and G. Rajasekharan, Phys.Letters 1, 58 (1962).

16. M.M. Block, C. Meltzer, S. Ratti, L. Grimellini, T. Kikuchi, L. Lendinara and L. Monari, Int.Conf.on High-Energy Phys., CERN 1962, p. 458 and Hyperfragment Conference 1963.

17. N. Crayton, D.H. Davis, R. Levi-Setti, M. Raymund, O. Skjeggestad, G. Tomasini, R.G. Ammar, L. Choy, W. Dunn, M. Holland, J.H. Roberts and E.N. Shipley, Int.Conf.on High-Energy Phys., CERN 1962, p. 460.

18. R.G. Ammar et al., Phys.Letters - in press - NUPHYS 62105.

19. Y.W. Kang, N. Kwak, J. Schneps and P.A. Smith, Hyperfragment Conference 1963.

* * *

5666/NP/smg

APPENDIX

Angular correlation in the decay $_{\Lambda}Li^{8} \rightarrow \pi^{-} + Be^{8}$

$$_{\Lambda}Li^{8} \rightarrow \pi^{-} + Be^{8}$$

$$J \rightarrow 1 \quad 0 \quad 2$$

Fig. 22

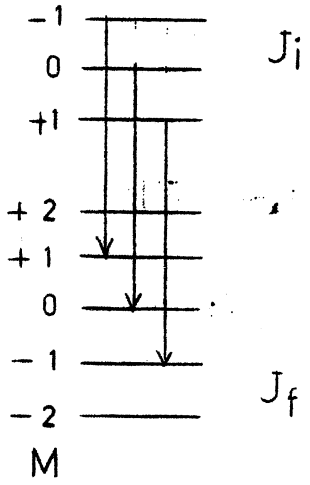

Fig. 23

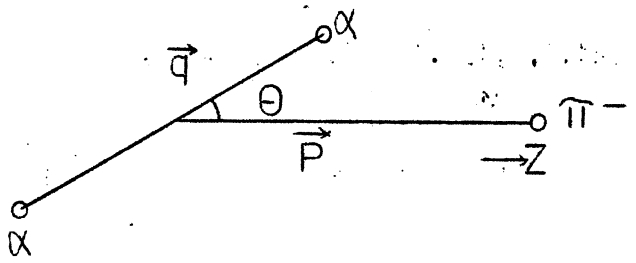

Take $\ell_{\pi} = 1$

$$\omega(\Theta) = \sum_{\ell_p \ell_q} |C(\ell_p, m_p, \ell_q, m_q | J, m)\ Y^{m_p}_{\ell_p}(\hat{p})\ Y^{m_q}_{\ell_q}(\hat{q})|^2$$

$$\cos \Theta_p = 1 \quad \cos \Theta_q = \cos \Theta$$

$$Y^{m_p}_{\ell_p}(1) = 0 \qquad Y^{o}_{\ell_p}(1) = 1$$

566/NP/smg

$$\omega(\Theta) \sim \sum_{\ell_p \ell_q} |C(\ell_p, o, \ell_q, m_q | j, m)\ Y_{\ell_q}^{m_q}(\cos\Theta)|^2$$

$$\ell_p = 1, \quad \ell_q = 2, \quad j = 1, \quad \Delta m_j = 0$$

$$\omega(\Theta) \sim \Sigma |\langle 1,0,2,M | 1,M\rangle\ Y_2^M(\cos\Theta)|^2$$

$$M = m = m_q$$

$$M = m_p + m_q$$

$$\omega(\Theta) \sim |\langle 1,0,2,1 | 1,1\rangle\ Y_2^1|^2 + |\langle 1,0,2,0 | 1,0\rangle |Y_2^0|^2 + |\langle 1,0,2,-1 | 1,-1\rangle\ Y_2^{-1}|^2$$

$$\langle 1,0,2,1 | 1,1\rangle = \left[\frac{(j+M)(j+M+9)}{(2j+1)\ (2j+2)} \right]^{1/2} = \sqrt{\tfrac{1}{2}} \quad \begin{matrix} J = j+1 \\ 2 \quad\ 1 \end{matrix}$$

$$\langle 1,0,2,0 | 1,0\rangle = \left[\frac{(j-M+1)(j+M+1)}{(2j+1)(2j+2)} \right]^{1/2} = \sqrt{\tfrac{2}{3}}$$

$$\langle 1,0,2,-1 | 1,-1\rangle = \left[\frac{(j-M)(j-M+1)}{(2j+1)(2j+2)} \right]^{1/2} = \sqrt{\tfrac{1}{2}}$$

$$Y_2^0 = \sqrt{\frac{5}{16\pi}}\ (3\cos^2\Theta - 1)$$

$$Y_2^{\pm 1} = \mp \sqrt{\frac{15}{8\pi}} \sin\Theta \cos\Theta\ e^{\pm i\varphi}$$

$$Y_2^{\pm 2} = \sqrt{\frac{15}{32\pi}} \sin^2\Theta\ e^{\pm 2i\varphi}$$

$$\omega(\Theta) = 2\,\frac{1}{2}\,\frac{15}{8}\,\sin^2\Theta\cos^2\Theta + \frac{2}{3}\,\frac{5}{16}\,(9\cos^4\Theta - 6\cos^2\Theta + 1) =$$

$$\frac{15}{8}\sin^2\Theta\cos^2\Theta + \frac{15}{8}\cos^4\Theta - \frac{30}{24}\cos^2\Theta + \frac{5}{24} = \frac{5}{24}\,(1 + 3\cos^2\Theta)\,.$$

Case $2 \to 2$

$$\omega(\Theta) = 2\left|\langle 1,0,2,2|2,2\rangle\, Y_2^2\right|^2 + 2\left|\langle 1,0,2,1|2,1\rangle\, Y_2^1\right|^2$$
$$+ \left|\langle 1,0,2,0|2,0\rangle\, Y_2^0\right|^2 \to \sim \sin^2\Theta\,.$$

* * *

5666/NP/smg

Table 1

Binding energies from uniquely identified mesonic decays†)
March, 1963

Identity	Decay mode	$\bar{B}_\Lambda$ (MeV)	σ_{av} *) (MeV)	σ (MeV)	No. of events
$_\Lambda H^3$	π - r	0.38	0.24	1.05 ± 0.16	20
	all other	0.27	0.19	0.80 ± 0.15	18
	total	0.31	0.15	-	38
$_\Lambda H^4$	π - r	2.40	0.12	0.99 ± 0.10	62
	n	1.75	0.18	0.82 ± 0.13	20
	all other	2.00	0.14	0.71 ± 0.10	27
	total	2.14	0.08	-	109
$_\Lambda He^4$	all	2.47	0.09	0.61 ± 0.008	48
$_\Lambda He^5$	all	3.10	0.05	0.57 ± 0.04	147
$_\Lambda He^7$	all	3.96	-	0.9 ± 0.2	14
$_\Lambda Li^9$	π - r	5.51	-	1.0 ± 0.3	9
	all other	5.52	0.12	0.45 ± 0.08	16
$_\Lambda Li^8$	all	6.65	0.15	1.06 ± 0.12	44
$_\Lambda Li^9$	π - r	6.9	0.8	inferred	1
	all other	8.01	0.29	-	9
$_\Lambda Be^7$	all	4.9	0.5	inferred	2
$_\Lambda Be^8$	all	6.35	0.30	inferred	4
$_\Lambda Be^9$	all	6.50	0.16	0.30 ± 0.06	10
$_\Lambda Be^{10}$	π - r	9.48	-	1.0 ± 0.4	4
	all other	8.36	0.6	inferred	1
$_\Lambda B^{10}$	π - r	10.0	-	1.0 ± 0.3	6
$_\Lambda B^{11}$	π - r	10.0	-	0.6 ± 0.2	4
	all other	9.9	0.6	inferred	1
$_\Lambda B^{12}$	all	10.50	0.18	0.6 ± 0.15	8
$_\Lambda C^{13}$	π - r	10.6	0.4	inferred	2
$_\Lambda C^{14}$	π - r	13.2	0.7	inferred	1
$_\Lambda N^{14}$	π - r	11.7	0.5	inferred	1

*) Possible systematic errors (± 0.2 MeV) have not been included.

†) Computed from the data contained in the enclosed references.

5666/NP/smg

REFERENCES to Table 1

R.G. Ammar, R. Levi-Setti, W.E. Slater, S. Limentani, P.E. Schlein and P.H. Steinberg, Nuovo Cimento 15, 181 (1960).

R.G. Ammar, R. Levi-Setti, W.E. Slater, S. Limentani, P.E. Schlein and P.H. Steinberg, Nuovo Cimento 19, 20 (1961).

P.E. Schlein and W.E. Slater, Nuovo Cimento 21, 213 (1961).

R. Levi-Setti, W.E. Slater and V.L. Telegdi, Nuovo Cimento 10, 68 (1958); contains previous literature.

S. Mora and I. Ortalli, Nuovo Cimento 12, 635 (1959).

G.C. Deka, Nuovo Cimento 14, 1217 (1959).

S. Lokanathan, D.K. Robinson and S.J. St. Lorant, Proc.Roy.Soc.(London) A254, 470 (1960).

J. Sacton, Nuovo Cimento 15, 110 (1960).

J. Tietge, Nucl.Phys. 20, 227 (1960).

M. Taher-Zadeh, Nuovo Cimento 17, 980 (1960).

M.M. Nikolić, Nucl.Phys. 21, 595 (1961).

Y. Prakash, P.H. Steinberg, D.A. Chandler and R.J. Prem, Nuovo Cimento 21, 235 (1961).

M.J. Beniston and D.H. Davis, Phil.Mag. 7, 2119 (1962) and private communication.

N. Crayton, R. Levi-Setti, M. Raymund, O. Skjeggestad, D. Abeledo, R.G. Ammar, J.H. Roberts and E.N. Shipley, Rev.Mod.Phys. 34, 186 (1962).

W. Gajewski, J. Pniewski, T. Pniewski and S. Popov (to be published), quoted in J. Pniewski and M. Danysz, Phys.Letters 1, 142 (1962); 1 $_{\Lambda}He^{7}$ event.

A.A. Varfolomev, R.I. Gerasimova and L.A. Karpova, Soviet Phys.Doklady 1, 579 (1956), DAN 110, 758 (1956); 1 $_{\Lambda}He^{7}$ event.

S.J. St. Lorant, private communication, 1 $_{\Lambda}Be^{7}$ event.

R.G. Ammar, M. Holland, J.H. Roberts and E.N. Shipley, Nuovo Cimento 27, 769 (1963); 1 $_{\Lambda}Be^{7}$ event.

5/NP/smg

D.J. Prowse, Bull.Am.Phys.Soc. II, 7, 297 (1962), and private communication June 1962; 1 $_{\Lambda}N^{14}$ event.

A.Z. Ismail, I. Kenyon, A. Key, S. Lokanathan and Y. Prakash, Nuovo Cimento 27, 1228 (1963); 3 $_{\Lambda}He^{7}$, 1 $_{\Lambda}Li^{7}$, 1 $_{\Lambda}Li^{8}$ and 2 $_{\Lambda}B^{12}$ events.

R.G. Ammar, L. Choy, W. Dunn, M. Holland, J.H. Roberts, E.N. Shipley, N. Crayton, D.H. Davis, R. Levi-Setti, M. Raymund, O. Skjeggestad and G. Tomasini, Nuovo Cimento 27, 1078 (1963).

D.H. Davis, R. Levi-Setti and M. Raymund, Nucl.Phys. 41, 73 (1963).

* * *

5666/NP/smg

DISCUSSION

Rao : I would like to know why the lighter of the decay products of the hyperfragments is generally taken as a π^- meson.

Levi-Setti : We can say that the so-called π meson is indeed a π^- meson in perhaps 60% of the cases because we do observe a σ star, a capture star which can only be characteristic of π^- mesons and not of captured μ^- mesons, for instance. Of course, there are a large number of cases in which the π^- stops without producing any visible star and then the question is open if that particle is indeed a pion or not. In general in the large majority of cases one has obtained a satisfactory momentum balance for such identification and with this evidence one is satisfied with the interpretation of it being a pion. One would expect that if the particle was indeed, for instance, a μ meson, this would lead to noticeable anomalies in the decay. This, of course, suggests that it may be worth while to actually measure the mass of the particle which is emitted when this leads to a so-called ρ ending. A further consideration is that, as we know, μ^- at rest in emulsion β decay in a sizeable fraction of the cases so that if indeed a μ^- is emitted one would very much like to see the decay electron to support this conclusion.

Spitzer : Is there any success in the search for π^0 mesic decays, and why, if you count these decays among the mesic decays, is there no correction in the production rate of the mesic hyperfragments for the unseen π^0 mesic decays?

Levi-Setti : π^0 mesic decays have been occasionally observed in emulsion. In two or three examples Dalitz pairs have been observed. There has been a systematic analysis made in Chicago of π^0

Levi-Setti (cont.) : decays by measuring those events in which only a recoil was visible. This turned out in the identification of a number of two-body decays of ${}_{\Lambda}He^{4}$ by the π^{0} mode. I would like, however, to say that it is a lost cause to try to do any work on π^{0} decays in emulsion. I think that the He bubble chamber has given exceedingly good results on π^{0} modes for ${}_{\Lambda}H$ and ${}_{\Lambda}He$, certainly more reliably than could ever be achieved in emulsion. For π^{0} decays of heavier species, of course, the emulsion would be the only way, but in view of the difficulties encountered even in the π^{-}-mesic decays (if you take away the pion, you observe only a blob), I would say that in general, they would be undetected.

Hoogland : There exists some different range momentum curves and you showed the Wilkins' normalized curves. I know that different groups are using them and I think that for a rather heavy fragment this can give rise to some differences in interpretation of the hyperfragments. Does there exist some normalization in the use of these curves?

Levi-Setti : The slide I have shown is an old slide of several years ago. Now we use the Barkas heavy ion range-energy curves. To some extent if you have a large body of events, this becomes somewhat irrelevant because you can actually obtain a best fit to an empirical range-energy curve for He^{4} and from that derive the curve for the other isotopes. In all cases there is a good normalization point which one can obtain from the π-r decays of ${}_{\Lambda}H^{4}$. Any experimental curve for He^{4} will have to intercept this calibration point.

Renard : What is the situation about the experimental difference in binding energy of ${}_{\Lambda}H^{4}$ and ${}_{\Lambda}He^{4}$?

Levi-Setti : Taking the ${}_{\Lambda}H^{4}$ π-r modes the binding energy is 2.40, to be compared with ${}_{\Lambda}He^{4}$ for which the average binding is 2.47 MeV. (See Table 1.)

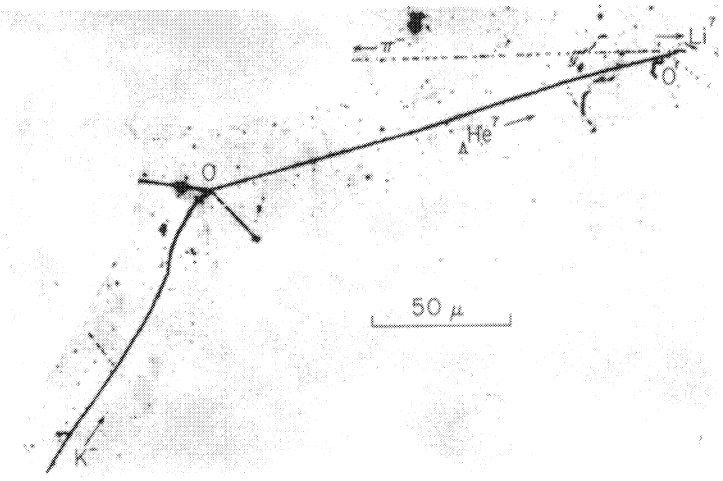

Fig. 2. Example of $_\Lambda He^7 \rightarrow Li^7 + \pi^-$

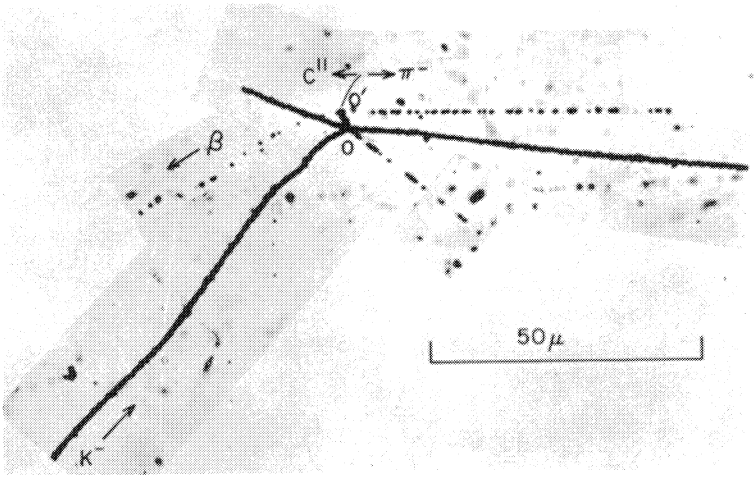

Fig. 3. Example of $_\Lambda B^{11} \rightarrow \bar{\pi} + C^{11} + \beta^+$

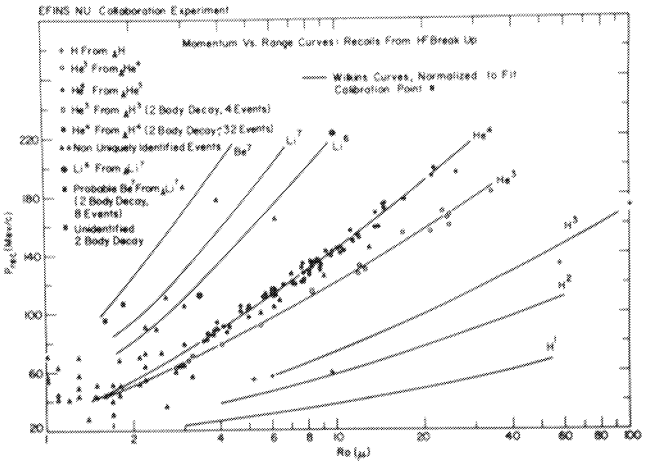

Fig. 4. Plot of recoil momentum against range.

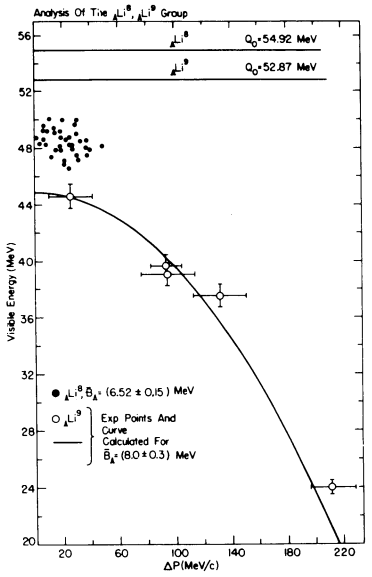

Fig. 6. Energy release Q versus missing momentum (Δ P) for Li^8 and Li^9 events.

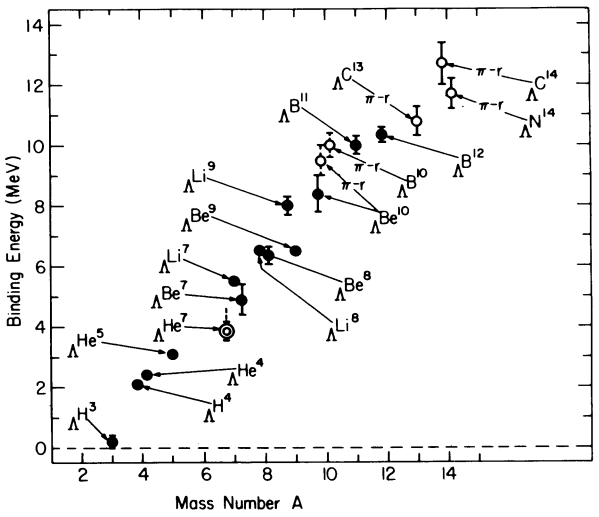

Fig. 8. Binding energy versus Mass Number.

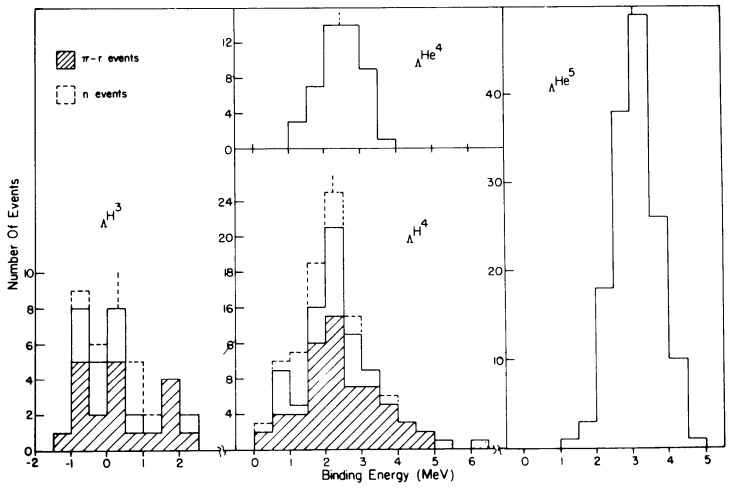

Fig. 9. Binding energies of $_\Lambda H^3$, $_\Lambda He^4$, $_\Lambda H^4$ and $_\Lambda He^5$.

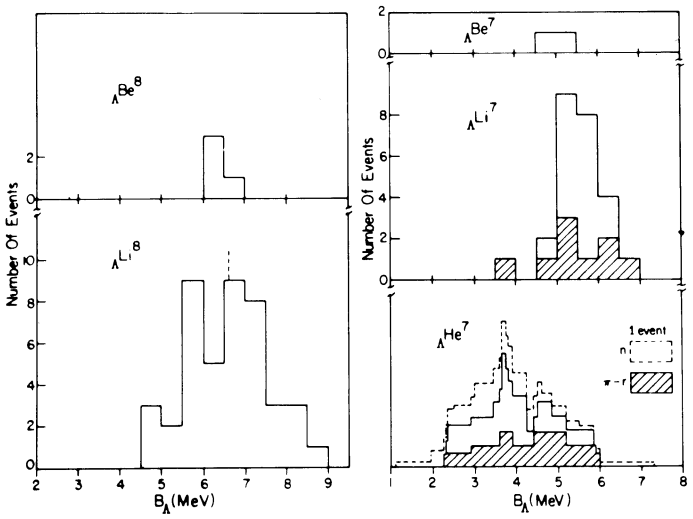

Fig. 10. Binding energies of $_{\Lambda}Be^{7}$, $_{\Lambda}Li^{7}$, $_{\Lambda}He^{7}$, $_{\Lambda}Be^{8}$ and $_{\Lambda}Li^{8}$

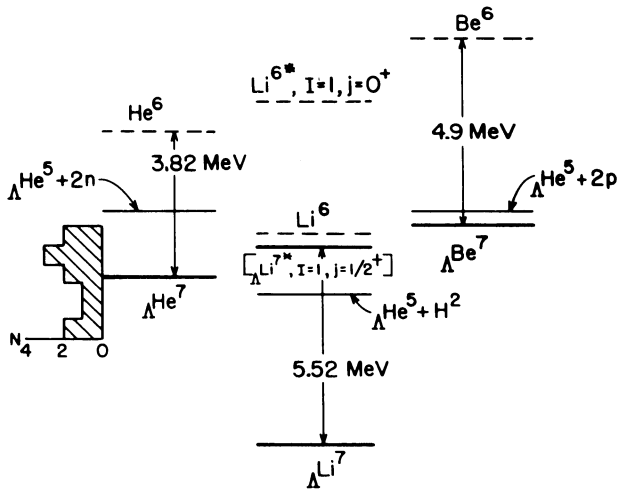

Fig. 11. Energy level diagram.

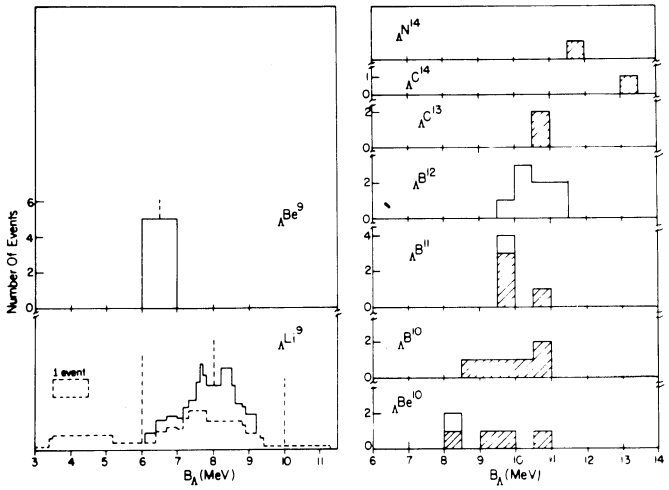

Fig. 12. Binding energies of Li, Be, B, C, and H hypernuelei.

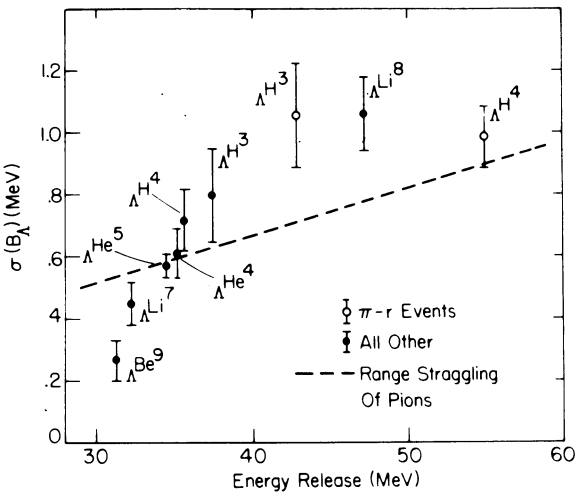

Fig. 13. Spread σ of B_Λ distributions as a function of the energy release Q.

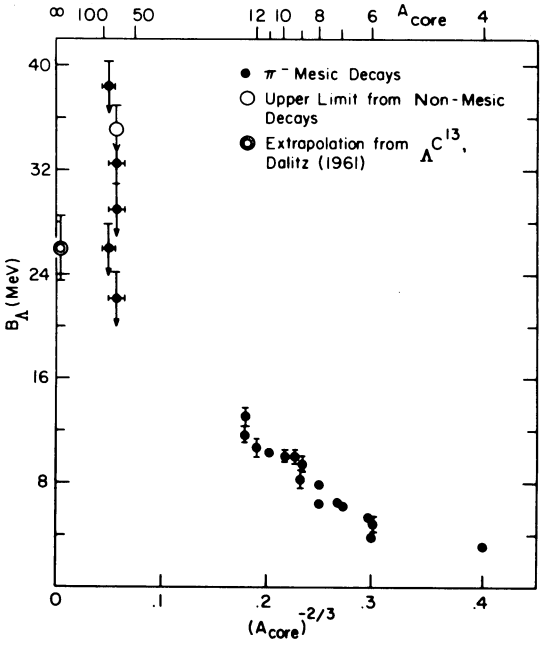

Fig. 15. B_Λ versus $A^{-2/3}$.

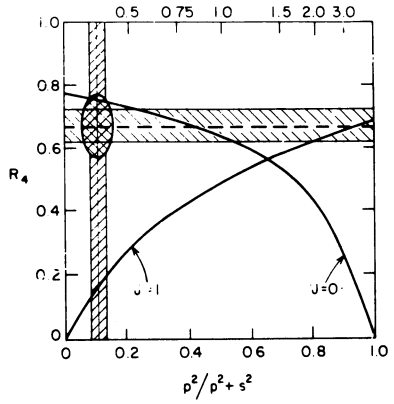

Fig. 18. The branching ratio R = $(He^4 + \pi^-)$/(all π^- modes) for $_\Lambda H^4$ decay is compared with the calculated ratios for $_\Lambda H^4$ spin J = 0 and J = 1, and with the measured value $p^2/(p^2 + s^2) = 0{,}11 \pm 0{,}03$.

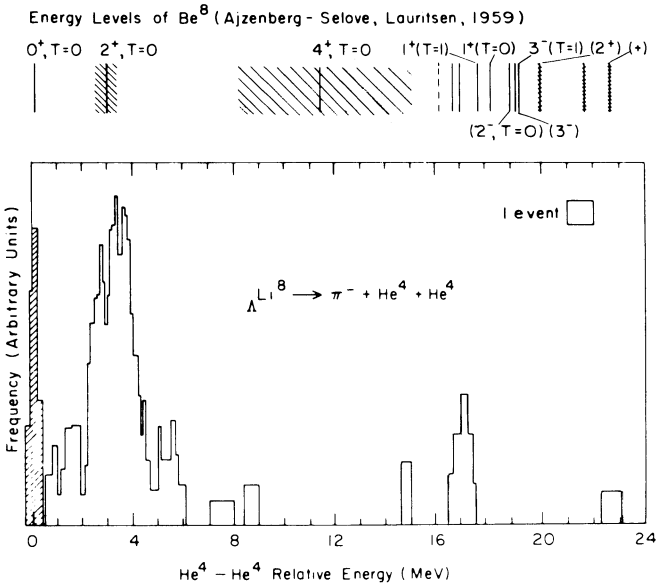

Fig. 19. Plot of He^4 - He^4 relative energy for $Li^8 \rightarrow \pi^- + He^4 + He^4$.

VI. AFTER-DINNER TALK

AFTER-DINNER TALK

G. Bernardini,

Istituto di Fisica "Guglielmo Marconi",
Università degli Studi, Rome.

I found myself in a position of complete lack of inspiration when I was preparing this speech. This is a very serious matter, you know, because in the dinner speeches which have been given in the last ten years (and looking for inspiration, I read many of them) everything has been said! All correlations between physics and the whole aspect of mankind have been considered - science and sociology, science and history, science and philosophy, science and religion, science and politics, everything! I must say that in the end I was slightly embarrassed because my impression was that these people, consciously or unconsciously, tried to convince everybody that physicists are very important people. This I think is true, completely true, but to advertise so much is a little bit embarrassing. I then reconsidered what I could say and the only answer I found was the following: if you don't mind, tonight I shall speak on physics as a personal matter; what physics means for a man like me.

Well, I have to justify this statement. When I was a young man and very fond of oriental philosophies, mainly to be very charming with girls, I was deeply interested in Confucius, Buddha, and so on. Unfortunately, I do not remember too much of this broad culture. Evidently it was not very deeply absorbed. However, I still remember a statement by Buddha. He said: "I cannot teach anything, I can tell only how I lived". This, after all, is not so modest, but he was Buddha. I do not pretend to be in that position, but frankly I want

to say that when I decided to be a physicist it was merely by chance. I was pushed into physics by the fluctuation of life, and actually for many years I very much regretted this decision. I thought that I could have been good at painting or medicine or anything else but not at physics; probably I was right. However, after 20 years of physics, if I were again in the position to choose, I would choose to have this kind of life. I will now try to explain why.

It is very simple. Culture has many meanings. Going in the directions I mentioned before, it has a great sociological value. To me it also has a very personal aspect. Culture is one of the strong forces which I have within myself to have a decent life and to be a civil man. This is very simple. I have my own definition of culture which I believe is common to all of us. Culture is essentially the possibility of having within ourselves the tools with which to re-build, to some extent, the spiritual experiences of great men who have lived before us. When you are listening to a record, when you are reading a poem, you just do not do anything else. In the limits of your culture you are pushed by this great man (who, fortunately for you, lived in an earlier era) to that level in which he was capable to live with your very modest forces. Well, physics, and usually science, is one of the best kinds of culture, and I would like to make a series of brief statements as to why I believe that this is a kind of culture which in this respect is better than many others.

Something like 20 years ago I read a book by Aldons Huxley entitled "Two or Three Graces" where he described a lady who had three lovers. One was very profoundly versed in literature, one in poetry, and the third in painting. All very artistic activities and this lady, according to whichever lover she was entertaining, was also very clever at painting, or literature, or poetry. I do not suppose that this is a true story, but it is something which one may consider possible in a so-called humanistic culture. Humanistic culture is a very serious

business but it can be understood in different ways at different levels and be a source of self-deception. You could believe to understand it rightly and actually you just live on the surface of it. Because it is irrational, you have no measure of this connection between you and these great minds. You may claim to have established a contact with a kindred spirit or to have broken now and then the painful sense of loneliness which we all must feel. In parenthesis, this power to overcome our isolation is to me one of the main aspects of the humanistic culture. The culture you acquire enables you to alleviate the sad moments in which you are not strong enough to tolerate your loneliness. However, reading a poem or listening to a record now and then (if you are not a poet or a musician, in other words, if you are afflicted as I am, by all the superficiality of an amateur) leaves you with a sense of instability which may be worse than the loneliness.

In science such self-deception is not possible. The culture of science has the very satisfying feature that it does not give you the illusion that you understand, if you do not. It gives you disquiet up to the point in which you start to understand; and when you start to understand you are entitled to feel that you have established a contact with another mind, which is extremely pleasant.

There are other aspects of science. You are allowed to be irrational because also science starts from free flights of imagination. However, this cannot stand for ever. Irrationality is allowed at the beginning but finally you have to keep yourself systematically under control because you approach something which may be very limited but has to be communicated to others in rational terms and has to be consistent with what is already known. You may go a step further and make this approach the basis of your ethics, as far as you can. Then you may feel that if you are not born an honest man (very few are those born honest) you can still behave as an honest man, because you are rational, consistent with yourself, and as responsible as you may be of your

actions and their consequences. After all I am inclined to believe that the real basis of morality is to be consistent with oneself, and science is master in teaching this attitude. Well for all these reasons I will not now change my decision, the decision that I took 30 years ago and purely by chance.

Now I am an old man and there is another problem for me, which is to teach to others the fondness for this kind of culture. This is not so simple. Physics has changed a lot in the course of my life. Probably you could teach others as well as I can or better. You are all very young; however, I would like to tell you that I consider that besides the ambitions that you have, that you must have, for a scientific career, it is also very important for you to consider yourselves responsible for the spreading of this culture, as a personal richness that can be given to everybody.

* * *

566/NP/smg

APPENDIX

LIST OF PARTICIPANTS

APPENDIX

LIST OF PARTICIPANTS

Lecturers	Addresses
Bernardini, G.	Istituto di Fisica "G. Marconi" Università degli Studi, Piazzale delle Scienze 5, Rome.
Dalitz, R.H. *)	Enrico Fermi Institute for Nuclear Studies, University of Chicago, Chicago, Illinois.
von Dardel, G.	NP Division, CERN, Geneva 23.
Ekspong, A.G.	Kungl Universitetet, Fysiska Institutionen, Vanadisvägen 9, Stockholm.
Hagedorn, R.H.	Th Division, CERN, Geneva 23.
van Hove, L.	Th Division, CERN, Geneva 23.
Levi-Setti, R. **)	Enrico Fermi Institute for Nuclear Studies, University of Chicago, Chicago, Illinois.
Wetherell, A.	NP Division, CERN, Geneva 23.
Zhdanov, G.B.	Lebedev Physical Institute of the Academy of Sciences, Lenin Prospect 53, Moscow.

* * *

*) Now at the Clarendon Laboratory, University of Oxford, Oxford.

**) At CERN for the academic year 1963-64.

Students

Country	Name	Address
AUSTRIA	Kellner, G.	Institut für Theoretische Physik der Universität Wien, Boltzmanngasse 5, Vienna.
BELGIUM	Renard, P.	Service de Physique nucléaire, Université Libre de Bruxelles, 50 Av. F.D. Roosevelt, Brussels.
EIRE	Heeran, M. Sr.	Physics Department, University College, Dublin 2.
	O'Ceallaigh, C.	Institute for Advanced Studies, 5 Merrion Square, Dublin.
	Thompson, A.	Institute for Advanced Studies, 5 Merrion Square, Dublin.
FRANCE	Augerat,	Faculté des Sciences, Laboratoire de Physique nucléaire, 34 Avenue Carnot, Clermont-Ferrand, Puy-de-Dôme.
	Bartholin, F.	Institut de Physique nucléaire, 1 Rue Raulin, Lyon.
	Bauman, G.	Laboratoire de Physique Corpusculaire, Centre de Recherches nucléaires, Strasbourg-Cronenbourg.
	Burdet, A. Mrs.	Institut de Physique nucléaire, 1 Rue Raulin, Lyon.
	Cotteron, J.	Laboratoire de Physique, 1 Rue Victor Cousin, Paris V.
	Gardes, J.	Faculté des Sciences, Laboratoire de Physique nucléaire, 34 Avenue Carnot, Clermont-Ferrand, Puy-de-Dôme.
	Gerber, J.P.	Laboratoire de Physique Corpusculaire, Centre de Recherches nucléaires, Strasbourg-Cronenbourg.

Country	Name	Address
FRANCE (cont.)	Patou, C. Miss	Laboratoire de Physique nucléaire, Faculté des Sciences, Caen.
	Quebert,	Laboratoire de Physique nucléaire, Bordeaux.
	Tinland, B.	Institut de Physique nucléaire, 1 Rue Raulin, Lyon.
W. GERMANY	Bott-Bodenhausen, M.	Max-Planck-Institut für Physik, Föhringer Ring 6, Munich 23.
	Cuevas, J.E.	II Physikalisches Staatsinstitut, Luruper Chaussee 149, Hamburg-Bahrenfeld.
	Diaz, J.	II Institut für Experimentalphysik, Luruper Chaussee 149, Hamburg-Bahrenfeld.
	Drieschner, M.	Max-Planck-Institut für Physik, Föhringer Ring 6, Munich 23.
	Harmsen, D.	II Institut für Experimentalphysik, Luruper Chaussee 149, Hamburg-Bahrenfeld.
	Lorenz, E.	Max-Planck-Institut für Physik, Föhringer Ring 6, Munich 23.
	Manz, A.	Max-Planck-Institut für Physik, Föhringer Ring 6, Munich 23.
	Spitzer, H.	II Institut für Experimentalphysik, Physikalisches Staatsinstitut, Luruper Chaussee 149, Hamburg-Bahrenfeld.
INDIA	Rao, N.K.	Tata Institute of Fundamental Research, Colaba, Bombay 5.
ITALY	Cartacci, A.M. Miss	Istituto di Fisica dell'Università, Via S. Leonardo 71, Florence.
	Lamborizio, C. Miss	Department of Physics, University of Parma, Via d'Azeglio 85, Parma.

Country	Name	Address
ITALY (cont.)	Pelosi, V.	Istituto Nazionale di Fisica Nucleare, Via Ponzio 16, Milan.
	Sassi, E. Miss	Istituto Nazionale di Fisica Nucleare del C.N.R.N., Mostra d'Oltremare, Naples.
	Sichirollo, A. Miss	Istituto Nazionale di Fisica Nucleare, Via Ponzio 16, Milan.
JUGOSLAVIA	Popov, S.	Institut de Physique, Faculté des Sciences, Studentski Trg. 3, Belgrade.
NETHERLANDS	Bosgra, S.J.	Zeeman Laboratorium, Plantage Muidergracht 4, Amsterdam.
	Hoogland, W.	Zeeman Laboratorium, Plantage Muidergracht 4, Amsterdam.
PAKISTAN	Shaukat, M.A.	Atomic Energy Centre, Ferozepur Road, P.O. Box 658, Lahore.
POLAND	Gajewski, W.	Uniwersytet Fizyki Doswiadczalnej, Hoza 69, Warsaw.
SPAIN	Llosa, R.	Department of Physics, University of Valencia, Valencia.
SWEDEN	Andersson, B.	Institutionen för Fysik, University of Lund, Lund.
	Carlson, P.	Institute of Physics, University of Stockholm, Vanadisvägen 9, Stockholm Va.
	Danielsson, O.	Department of Physics, University of Stockholm, Vanadisvägen 9, Stockholm Va.
	Otterlund, I.	Institutionen för Fysik, University of Lund, Lund.

Country	Name	Address
SWITZERLAND	Schneeberger, R.	Physikalisches Institut der Universität, Länggastrasse 7, Berne.
UNITED KINGDOM	Bishara, L.B. Miss	Department of Physics, University College, Gower Street, London, W.C.1.
	Briggs, G.A.	Department of Physics, Science Laboratories, South Road, Durham.
	Finney, P.J.	N.I.R.N.S., Rutherford High-Energy Laboratory, Chilton, Didcot, Berks.
	Fletcher, E. Miss	Department of Physics, University of Bristol, Royal Fort, Bristol 8.
	Garbutt, D.A.	Department of Physics, University College, Gower Street, London, W.C.1.
	Glass, C.N.	Physics Department, University of Bristol, Royal Fort, Bristol 8.
	Green, K.	Department of Physics, University of Bristol, Royal Fort, Bristol 8.
	Ismail, A.Z.M.	Department of Nuclear Physics, University of Oxford, Oxford.
	Keereetaveep, J. Miss	Department of Physics, University of Bristol, Royal Fort, Bristol 8.
	Key, A.W.	The Clarendon Laboratory, Parks Road, Oxford.
	Khan, N.A.	Department of Physics, Science Laboratories, South Road, Durham.
	Kitchen, C.A.	Department of Physics, Science Laboratories, South Road, Durham.
	Tolun, P. Miss	Department of Physics, University of Bristol, Royal Fort, Bristol 8.
	Yaseen, M.	Department of Physics, Westfield College, Hampstead, London, N.W.3.

Country	Name	Address
USA	Dyer, J.N.	Naval Postgraduate School, Monterey, California.
CERN	Dahl-Jensen, E.	NP Division, CERN, Geneva 23.
	Doble, N.T.	NP Division, CERN, Geneva 23.
	Scheuing, V.	NP Division, CERN, Geneva 23.

* * *